Fakultät für
Mathematik, Informatik
und Naturwissenschaften

RWTH AACHEN UNIVERSITY

„Dual Remote C–H Functionalization Using Aryl Sulfonium Salts & Applications of Ruthenium η^6–Arene Complexes“

Von der Fakultät für Mathematik, Informatik und Naturwissenschaften der RWTH Aachen University zur Erlangung des akademischen Grades eines Doktors der Naturwissenschaften genehmigte Dissertation

Vorgelegt von

Aboubakr Hamad, M.Sc.

aus

Qena, Ägypten

Berichter: Prof. Dr. Tobias Ritter
Prof. Dr. Carsten Bolm
Prof. Dr. Sonja Herres-Pawlis

Tag der mündlichen Prüfung: 23.06.2025

Diese Dissertation ist auf den Internetseiten der Universitätsbibliopthek online verfügbar

Dissertation advisor: Prof. Dr. Tobias Ritter Aboubakr Hamad

Summary

In this thesis, advanced strategies for regioselective aromatic C–H functionalization via the formation of aryl sulfonium salts and transition metal catalysis were explored. Additionally, catalytic and stoichiometric π-arene activation, using ruthenium phenoxo complexes, was explored. The work is divided into two sections:

Double C–H Functionalization Using Aryl Sulfonium Salts

Methods for site-selective C–H functionalization provide a powerful approach to increase the structural complexity of organic compounds. Significant efforts have been devoted to developing novel strategies for the directed and selective functionalization of C–H bonds. For example, iridium-catalyzed borylation of arenes has become a valuable tool in modern organic synthesis. However, its selectivity is determined mainly by substitution patterns or the presence of specific directing groups. On the other hand, aromatic C–H functionalization via thianthrenation reaction offers excellent *para*-selectivity for mono-substituted arenes independent of the presence of a directing group. However, the thianthrenation reaction is limited to the functionalization of a single position on the arene.

The first section of this thesis presents an approach to regioselective double C–H functionalization. A sulfoxide-tethered to a directing group was employed in the synthesis of aryl sulfonium salts via electrophilic aromatic substitution (S_EAr). Subsequently, the directing group was used in directed C–H functionalization, where oxidative Heck coupling was achieved. Afterwards, the sulfonium moiety served as a linchpin for subsequent Sonogashira coupling. The reaction conditions were optimized, and the reaction demonstrated regioselective double C–H functionalization of simple arenes.

Applications of Ruthenium η^6–Arene Complexes with Phenoxo Ligands

π-Arene activation through facial coordination to a transition metal significantly changes the electronic properties of the coordinated arene from an electron-rich to an electron-poor arene. This ‘‘umpolung’’ of arene reactivity has been utilized with various rhodium and ruthenium complexes to facilitate otherwise unattainable transformations without η^6–arene coordination to a transition metal. Various ruthenium complexes rely on cyclopentadienyl (Cp) ancillary ligands,

which exhibit low arene exchange rates. Consequently, the slow arene exchange associated with Cp-supported ruthenium complexes has resulted in limited reactivity.

The second section of this work explored the reactivity of ruthenium phenoxo complexes in the hydrolysis of fluoroarenes, deoxyfluorination, and catalytic decarboxylation reactions. Ruthenium phenoxo complexes were synthesized and evaluated for their reactivity with aryl fluorides, phenols and phenylacetic acid derivatives. Key findings include:

Hydrolysis of Fluoroarenes: Stoichiometric conversion of facially coordinated fluoroarenes to phenols was achieved, though the reaction was limited to simple substrates and required elevated temperatures and long reaction times.

Benzylic Decarboxylation: Catalytic decarboxylation of phenylacetic acid derivatives proceeded efficiently via π-arene activation, but the methodology was not applicable to substrates with strong donor groups or increased steric hindrance.

Mechanistic studies offered insights into the reaction pathways. For example, the involvement of η^6–coordinated intermediates in decarboxylation and hydrolysis reactions were established. The reactivity trends observed in ruthenium-catalyzed transformations provided a deeper understanding of metal-arene chemistry and expanded the utility of these complexes in organic synthesis.

Overall, this thesis demonstrates the potential of transition-metal catalysis and tailored intermediates in enabling selective C–H functionalization. Additionally, the second part has shown potential application for π-arene activation using ruthenium supported by phenoxo ligands. The findings contribute to advancing efficient synthetic methodologies, addressing challenges in the activation and transformation of inert bonds.

Dissertation advisor: Prof. Dr. Tobias Ritter Aboubakr Hamad

Zusammenfassung

In dieser Arbeit werden fortschrittliche Strategien zur regioselektiven C–H-Funktionalisierung mittels Sulfoniumsalz-basierter Methoden und Übergangsmetallkatalyse untersucht. Ein weiterer Schwerpunkt liegt auf der π-Aren-Aktivierung durch Phenoxo-Ligand-Ruthenium η^6–Komplexe und deren Anwendung in der organischen Synthese. Diese Arbeit gliedert sich in zwei Hauptteile:

Doppelte C–H-Funktionalisierung durch Aryl-Sulfoniumsalzen

Methoden für die selektive C–H-Funktionalisierung eröffnen den Zugang zu einer breiten Palette an Molekülstrukturen und somit zu molekularer Diversität. Umfangreiche Forschungsarbeiten wurden durchgeführt, um neue Methoden für die direkte und selektive Funktionalisierung inaktiver C–H-Bindungen zu entwickeln. Zum Beispiel hat sich die Iridium-katalysierte Borylierung von Arenen als wertvolles Werkzeug in der modernen organischen Synthese etabliert, wobei die Selektivität jedoch stark von Substitutionsmustern oder spezifischen dirigierenden Gruppen abhängt. Im Gegensatz dazu bietet die Thianthrenierung eine ausgezeichnete *para*-Selektivität, ist jedoch auf die Funktionalisierung einer einzigen Position des Arylrings beschränkt.

Im ersten Teil dieser Arbeit wird ein neuartiger Ansatz zur regioselektiven doppelten C–H-Funktionalisierung vorgestellt. Aryl-Sulfoniumsalze, die aus einem speziell entwickelten Sulfoxid mit angehängter dirigierender Gruppe abgeleitet wurden, wurden durch die Aktivierung des Sulfoxids mittels elektrophiler aromatischer Substitution (SEAr) synthetisiert. Anschließend diente die dirigierende Gruppe an der Sulfonium-Einheit, zur dirigierten C–H-Funktionalisierung. Das Sulfonium-Salz fungierte darüber hinaus als vielseitiger Verbindungspunkt für nachfolgende Sonogashira-Kupplungen. Die Studie optimierte die Reaktionsbedingungen und demonstrierte eine selektive Funktionalisierung einfacher Arene. Die Methode zeigte jedoch Einschränkungen bei komplexeren Substraten, bei denen Nebenreaktionen auftraten.

Anwendungen von Ruthenium η^6–Aren-Komplexen mit Phenoxo-Liganden

Die Aktivierung von π-Arenen durch die η^6–Koordination eines Arenes an ein Übergangsmetall verändert die elektronischen Eigenschaften des komplexierten Arenes signifikant. Diese ‘‘umpolung’’ der Reaktivität wurde mit verschiedenen Rhodium- und Rutheniumkomplexen genutzt, um Transformationen zu ermöglichen, die ohne η^6–Koordination nicht erreichbar wären.

Die meisten dieser Komplexe basieren auf Cyclopentadienyl-Liganden, die jedoch langsamere Aren-Austauschraten aufweisen, was die Reaktivität dieser Systeme einschränkt.

Der zweite Teil dieser Arbeit untersucht das Potenzial von Ruthenium η^6–Aren-Komplexen in Hydrolyse-, Deoxyfluorinierungs- und katalytischen Decarboxylierungsreaktionen. Hierfür wurden Rutheniumkomplexe mit Phenoxo-Liganden synthetisiert und hinsichtlich ihrer Reaktivität mit Arylfluoriden und Phenylessigsäurederivaten getestet. Zu den zentralen Ergebnissen gehören:

Hydrolyse von Fluorarenen: Die stöchiometrische Umwandlung von Fluorarenen zu Phenolen wurde erreicht, jedoch war die Reaktion auf einfache Substrate beschränkt und erforderte hohe Temperaturen sowie lange Reaktionszeiten.

Benzylische Decarboxylierung: Die katalytische Decarboxylierung von Phenylessigsäure-derivaten konnte durch verlief effizient über die π-Aren-Aktivierung erreicht werden, war jedoch bei Substraten mit starken Donorgruppen oder erhöhter sterischer Hinderung nicht erfolgreich.

Mechanistische Studien, einschließlich Kontrollreaktionen und spektroskopischer Analysen, lieferten wertvolle Einblicke in die Reaktionsmechanismen. Zum Beispiel konnte die Beteiligung η^6–koordinierter Intermediate an Decarboxylierungs- und Hydrolysereaktionen nachgewiesen werden. Die beobachteten Reaktivitätstrends in Ruthenium-katalysierten Transformationen tragen zu einem erweiterten Verständnis der Metall-Aren-Chemie bei und ermöglichen neue Anwendungsbereiche dieser Komplexe in der organischen Synthese.

Insgesamt zeigt diese Dissertation das Potenzial der Übergangsmetallkatalyse und maßgeschneiderter Intermediate für die selektive C–H-Funktionalisierung. Darüber hinaus wurden im zweiten Teil Anwendungen der π–Aren-Aktivierung durch Ruthenium-Komplexe mit Phenoxo-Liganden demonstriert. Die Ergebnisse leisten einen Beitrag zur Weiterentwicklung nachhaltiger und effizienter synthetischer Methoden und bieten Ansätze zur Überwindung der Herausforderungen bei der Aktivierung und Umwandlung inaktiver Bindungen.

Acknowledgments

First and foremost, I would like to express my heartfelt gratitude to Prof. Dr. Tobias Ritter for giving me the opportunity to pursue my PhD studies at the Max-Planck-Institut für Kohlenforschung. His guidance, expertise, support, and patience have been instrumental in overcoming scientific challenges throughout this journey. I deeply appreciate his encouragement to always strive for excellence, significantly enriching my personal and professional growth. I am also profoundly thankful to Prof. Dr. Carsten Bolm and Prof. Dr. Sonja Herris-Pawlis for their willingness to serve as examiners and for making the conclusion of this PhD possible.

I extend my warmest thanks to my family for their unwavering emotional support throughout this journey. My family has been my pillar of strength, always standing by me and encouraging me during the most challenging times. And a special thanks to my father and to my mother, for their emotional support.

I would also like to thank my friends and colleagues who made my time in Mülheim so memorable. Working alongside Michal Mrozowicz, Tim Schulte, Javier-Mateos Lopez, Philipp Hartmann, Moritz Hommrich, Beatrice Lansbergen and Pia Münstermann has been a privilege, and their camaraderie, insights, and collaboration have made the research environment both enjoyable and inspiring.

Finally, I am grateful to the Max-Planck-Institut für Kohlenforschung for providing an excellent research environment and resources, and to all those who contributed to this remarkable chapter of my life, directly or indirectly.

Notes and Abbreviations

In this thesis, the chemical compounds are given as numbers in bold print that are assigned in the schemes and charts. The references are labeled as superscript numbers and are listed in sequential order in the section “References”. The following abbreviations were used in the writing of the thesis.

Ac	acetyl
Ac-Gly-OH	*N*-acetylglycine
Alk	Alkyl
Ar	Aryl
B_2pin_2	Bis(pinacolato)diboron
cb-DBT	4-(2-cyanobenzyl)dibenzothiphene
CP	cyclopentadienyl
DCE	Dichloroethane
DCM	dichloromethane
DG	Directing group
DIPEA	*N,N*-diisopropylethylamine
dppf	1,1′-bis(diphenylphosphino)ferrocene
EDG	Electron-donating group
EI	Electron impact ionization
equiv.	Number of chemical equivalents
ESI	Electrospray ionization
EWG	Electron-withdrawing group
GC−MS	Gas chromatography−Mass spectrometer
HFIP	1,1,1,3,3,3-hexafluoroisopropanol
HOTf	Triflic acid
HRMS	High-resolution mass spectrometry
L	Ligand
LC−MS	Liquid chromatography−Mass spectrometer
Lit.	Literature
LMCT	Ligand-metal charge transfer
m/z	mass/charge
MPAA	Mono-protected amino acid
Me	methyl

Ms_2O	methanesulfonic acid anhydride
n-Bu	n-butyl
n.d.	not detected
NMR	Nuclear Magnetic Resonance
$^{-}NTf_2$	Bis((trifluoromethyl)sulfonyl)amide
^{-}OTf	Trifluoromethanesulfonate
Ph	phenyl
ppm	parts per million
r.t.	room temperature
RDS	Rate Determining Step
S_EAr	Electrophilic aromatic substitution
SET	Single Electron Transfer
S_NAr	Nucleophilic aromatic substitution
TBAF	Tetrabutylammonium fluoride
TBAOMs	tetrabutylammonium mesylate
Tf_2O	Triflic anhydride
TFA	Trifluoroacetic acid
TFAA	Trifluoroacetic acid anhydride
TLC	Thin Layer Chromatography

Table of Contents

Note

Portions of this thesis have been taken, with permission, from the following publication: Aboubakr Hamad[#], Michał Mrozowicz[#], Yuanhao Xie, Tobias Ritter*. 'Regioselective Double C–H Functionalization of Arenes via Aryl Thianthrenium Salt Analogues'. *Synlett* **2024**, 35, 1028–1032.

Portions of this thesis were taken from the following publication: Tim Schulte, Zikuan Wang, Chen-Chen Li, Aboubakr Hamad, Felix Waldbach, Julius Pampel, Roland Petzold, Markus Leutzsch, Fritz Bahns, Tobias Ritter*. 'Ruthenium Phenoxo Complexes: An Isolobal Ligand to Cp with Improved Properties'. *J. Am. Chem. Soc.* **2024**, 146, 15825−1583.

Chapter (1)

Site-Selective Aromatic C–H Functionalization

1.1 Introduction

Site-selective C−H functionalization methods are powerful in organic synthesis, through which quick access to molecular diversity is achieved. The synthesis of intricate aromatic molecules or novel drug candidates poses a fundamental challenge due to the inherent difficulty in achieving selective synthesis.[1–3] For instance, the diversification of an arene relies largely on classical electrophilic aromatic substitution S_EAr. However, the S_EAr reactions are often less selective, unless there is a specific directing group existing or certain substitution patterns.[4] Bromo and boryl functional groups are highly valued in organic chemistry, yet introducing them selectively, particularly without directing groups or specific substitution patterns, remains a significant challenge.[1,4–6] Thianthrenation reaction has allowed selective C−H functionalization of arenes with a superior selectivity in comparison to all existing methods.[3]

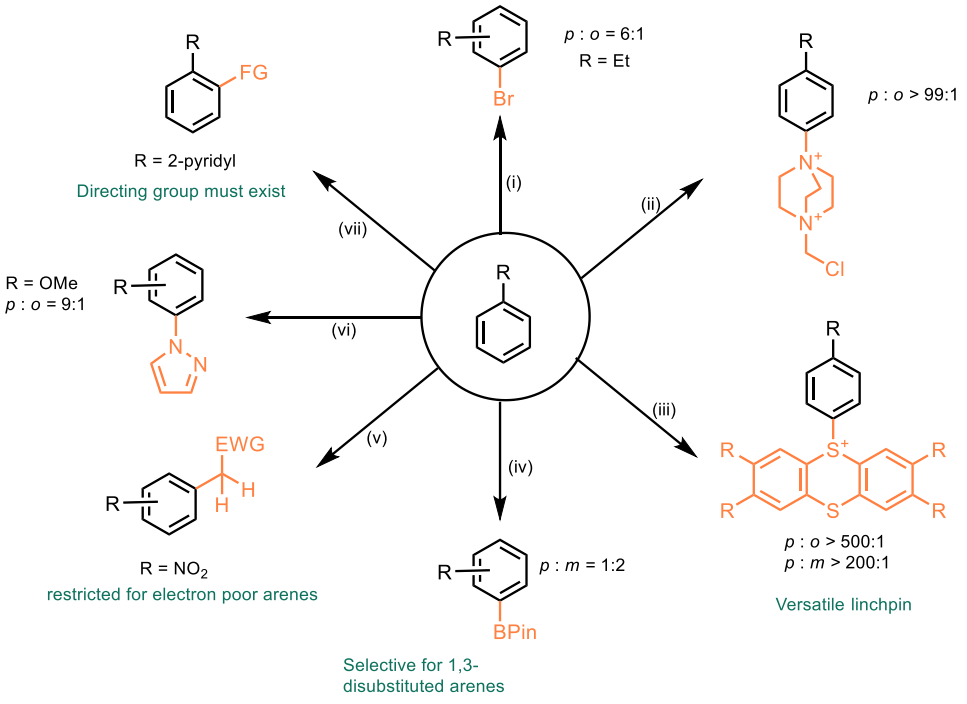

Scheme 1. Schematic illustration for various reactions for C−H functionalization of arenes. (i) Bromination of ethylbenzene using Br_2 as brominating agent. (ii) Aromatic C–H TEDAylation via addition elimination of radical cation. (iii) *para* selective C–H Thianthrenation of ethylbenzene using TFAA and $HBF_4.Et_2O$ in DCM. (iv) Iridium catalyzed borylation of ethylbenzene. (v) Vicarious Nucleophilic Substitution (VNS) of nitrobenzene. (vi) Selective C–H amination via photoredox catalysis. (vii) Transition metal-catalyzed C−H of phenylephrine.

Leveraging site-selective functionalization of remote C−H bonds is potent for accessing molecular diversity.[7–9] However, achieving selectivity is challenging in the presence of multiple non-equivalent C−H bonds.[6,10–14] While classical electrophilic aromatic substitution reactions are governed by substituents on the aromatic ring, approaches using transition metals or hydrogen bonding organocatalysis offer avenues for achieving selectivity by forming substituent-catalyst intermediates that guide electrophiles to *ortho* or *meta* positions.[15] In this intricate landscape of organic synthesis, the development of reaction methodologies that enable control over regio-selectivity at a late stage represents a critical frontier in advancing chemical synthesis and expanding the scope of accessible molecular structures.[1,3,5,7] Recent advancements in late-stage functionalization reactions have provided efficient pathways to diversify complex molecules.[1,5,13] Despite these strides, achieving site-selective C–H functionalization remains challenging. However, the aromatic C–H thianthrenation reaction, developed by Ritter et al., offers promising avenues for selective C–H functionalization of arenes, particularly at the *para*-position.[6,16,17]

Classical C–H functionalization methods of arenes

1.1.1 Electrophilic Aromatic Substitution (S_EAr)

Electrophilic aromatic substitution (S_EAr) is a widely used and useful reaction in organic synthesis.[4,15] The reaction starts with the attack of an electron-rich arene on an electrophile, which in turn results in the formation of a cationic intermediate known as Pfeiffer-Wizinger intermediate [18-20] or Wheland intermediate.[21]

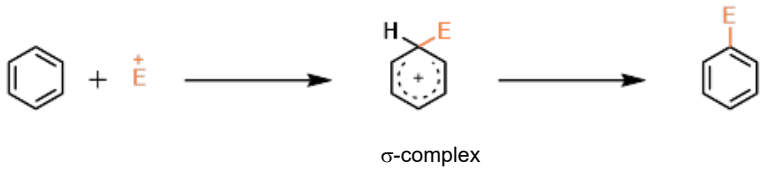

Scheme 2. Schematic depiction of sigma complex formation in a benzene ring.

Based on the experimental results based on the kinetic isotope effect of the deuterated and tritiated aromatics, together with the confirmed cationic intermediate, it has been accepted that the reaction mechanism entails two steps (Scheme 2).[22,23] Dewar demonstrated that S_EAr can proceed, in addition to the sigma complex, via the formation of a π-complex, which plays a significant role in the reaction (Scheme 3).[24] Expectedly, in S_EAr, studies have shown that when the π-complex represents the highest-energy transition state, no primary kinetic isotope effect is

observed. Evidently, in the nitration of perdeuteriobenzene, an inverse secondary isotope effect ($k_H/k_D \approx 0.89$) was observed, supporting the π-complex transition-state model.[22]

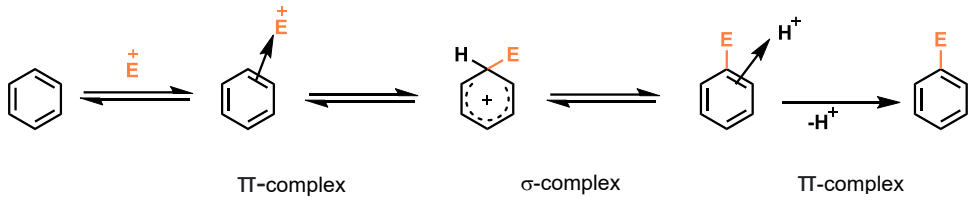

Scheme 3. Schematic illustration of Dewar's mechanism showing the formation of π-complex in a benzene ring.

Despite the numerous classical S_EAr reactions developed and used to functionalize aromatic molecules, efficient chemical methods capable of achieving site-selective aromatic substitution remain needed.[25–28] Substitutes are classified into two categories based on the type of substituents in the aromatic ring: *ortho* and *para*-directing or *meta*-directing. The Friedel-Crafts acylation reaction has been developed as a *para*-selective reaction for certain arenes.[22,23,28,29] For instance, Gattermann and Koch developed a Friedel-Crafts-type formylation reaction that nearly yields *para*-substituted toluene. However, this reaction is not applicable to ethers and phenols.[22,30] Despite the effect of the substituent and the presence of a suitable directing group, several intermediates are observed in most S_EAr reactions, resulting in a mixture of all three constitutional isomers (Scheme 4).[29]

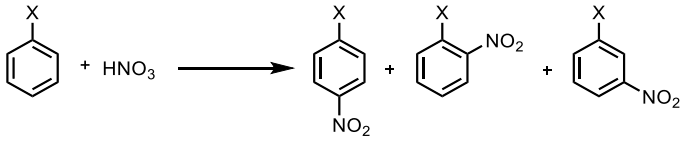

Scheme 4. Schematic illustration of the nitration of a mono-substituted arene.

1.1.2 Vicarious Nucleophilic Substitution (VNS)

Polish chemists Mieczysław Mąkosza and Jerzy Winiarski introduced a specific type of nucleophilic aromatic substitution, vicarious nucleophilic substitution (VNS), by which aromatic C−H functionalization is achieved where a nucleophile replaces a hydrogen atom on the aromatic ring, rather than leaving groups typically encountered in S_NAr.[31,32] However, VNS is highly dependent on the reactivity of the arene, restricting selective C−H functionalization to certain classes of aromatic molecules.[33] The S_NAr substitution reaction initiates with the attack of a nucleophile in polar solvents. The reaction is generally depicted as the rate-limiting formation of a Meisenheimer complex, σ-complex[34,35] or π-complex,[36] proposed as reaction

intermediates.[23,37–39] Conversely, VNS reaction is typically encountered with electron-deficient arenes, typically nitroarenes, particularly involving nucleophiles that result in alkylated arenes. The new substituent can occupy either *ortho* or *para* positions, reversing the usual *meta*-selectivity observed with such compounds under electrophilic substitution. Carbon nucleophiles, possessing an electron-withdrawing group and a leaving group, are ideal where the nucleophile attacks the aromatic ring, and the excess base facilitates elimination to form an exocyclic double bond, which is subsequently protonated under acidic conditions, restoring aromaticity (Scheme 5).[31,32]

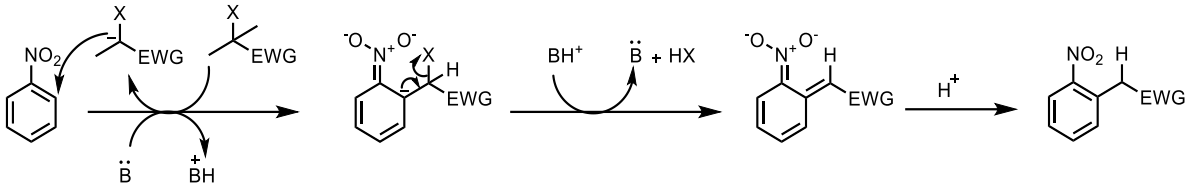

Scheme 5. Schematic illustration of VNS reaction of nitrobenzene.

Since the Meisenheimer complex forms at a high endergonic level in S_NAr reactions, it's challenging to introduce different nucleophiles to different aromatic compounds.[14,27,30,31] Additionally, an electron-withdrawing group in the *ortho* or *para* position is required to stabilize the Meisenheimer complex.[41] Therefore, for the *ortho* and *para* substitution reactions, scientists have invoked steric effects to disable or reduce the substitution in the ortho position.[38,40]

Recent Methods for Aromatic C−H Functionalization

1.1.2 Radical Substitution Reactions of Aromatic Compounds

Developing new reaction methodologies that can selectively functionalize molecules regardless of the presence of specific directing groups is a significant challenge in organic chemistry.[42–48] The direct replacement of C–H bonds with new C−C, C−N, or C−O bonds and the achievement of site-selectivity represent a promising research field in organic synthesis.[25,47] Francesco Minisci introduced alkyl residues via radical substitution reaction to heteroaromatic compounds, where nucleophilic radicals enabled the selective alkylation of protonated heteroarenes (Scheme 6).[49]

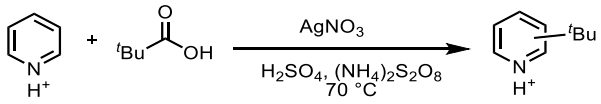

Scheme 6. Schematic illustration of radical substitution via Minisci reaction.

Recently, various radical aromatic substitution reactions were developed by which electron-rich arenes are functionalized.[2,50] Nicewicz and his co-workers have developed a strategy for the direct C−H amination of electron-rich aromatics utilizing Fukuzumi's highly oxidizing acridinium catalyst. In this strategy, 2,2,6,6-(tetramethyl piperidine-1-yl)oxyl (TEMPO) is used to abstract from the adduct, which results in rearomatization(Scheme 7).[50,51]

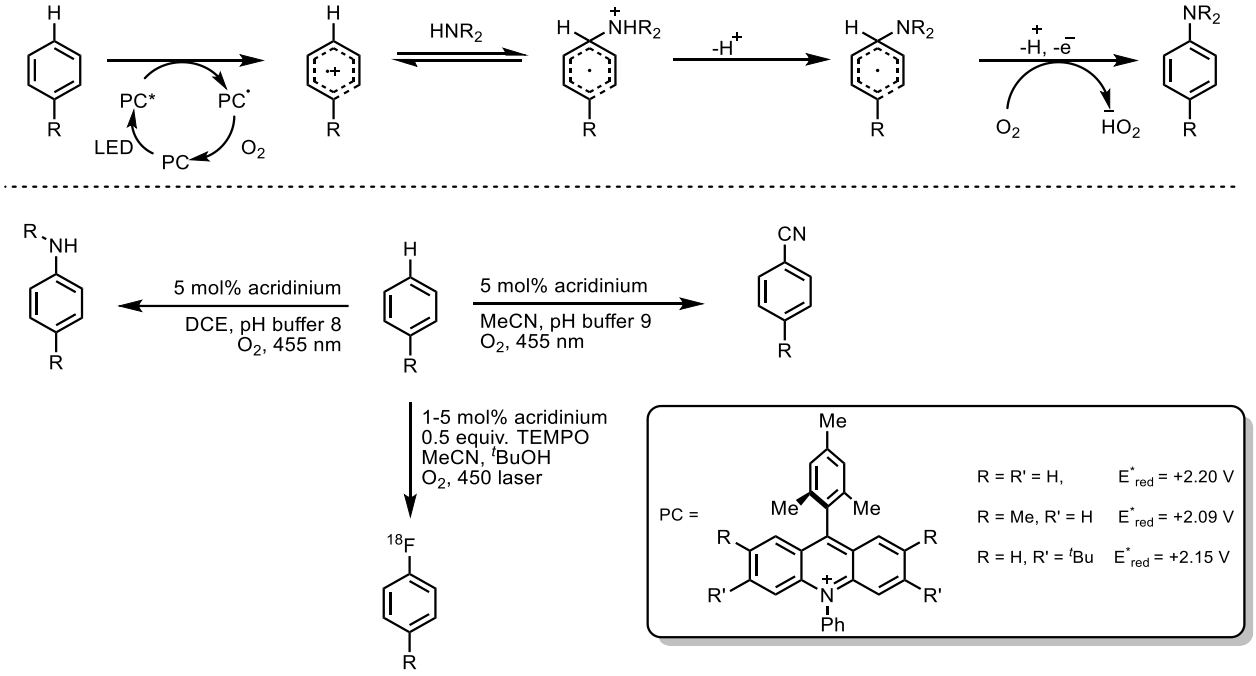

Scheme 7. Schematic illustration of photoredox-catalyzed aromatic C–H functionalization reactions.

Alternatively, direct oxygen streaming traps the radical intermediate to form a cyclohexadienyl peroxyl radical, which undergoes intramolecular elimination to yield the desired amine and a hydroxyperoxyl radical while additional oxygen regenerates the catalyst. (Scheme 7). The utility of photoredox catalysis was further exploited, resulting in the development of numerous reactions using different nucleophiles, including cyanide,[52] primary amine[53] and radio-fluoride (Scheme 7).[54,55] Ritter and coworkers recently developed a site elective aromatic substitution using a highly electrophilic radical. The dicationic radical, $TEDA^{2+\bullet}$ (TEDA = *N*-(chloromethyl)triethylenediamine), engaged in electrophilic aromatic substitution, through which *N*-aryl-*N'*-chloromethyldiazoniabicyclo[2.2.2]octane salts which are converted into aryl piperazines in one pot. The reaction is catalyzed by two different catalysts, $Ru(bipy)_3(PF_6)_2$ and palladium catalyst, to afford highly *para*-selective Ar-TEDA salts (Scheme 8).[2]

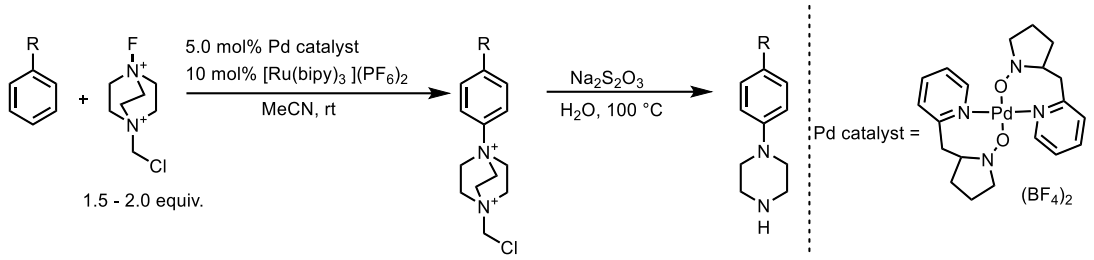

Scheme 8. Schematic illustration of *para*-selective synthesis of aryl piperazines.

1.1.3 Chemoselective Directed Aromatic C−H Functionalization

Developing methods for directly converting unactivated C–H bonds into C–O, C–X, C–N, and C–C bonds remain a significant challenge in organic chemistry.[17] Mild and selective transformations of this nature will likely have extensive applications, including synthesizing pharmaceuticals, natural products, agrochemicals, and feedstock chemicals. Traditional methods for forming these functional groups typically require pre-functionalized starting materials to achieve both reactivity and selectivity.[56] The presence of a suitable directing group enables chemoselective C–H activation of arenes.

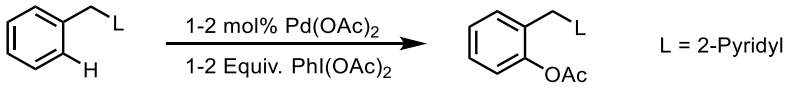

Scheme 9. Chemoselective aromatic C–H acetoxylation of phenylpyridine.

Various arenes containing a directing group, such as pyridine, azobenzene, pyrazole, and imine derivatives, were selectively used in the C–H activation to form the corresponding esters, ethers, and aryl-halides under mild conditions (Scheme 9).[57] The C–H activation reactions for aromatic molecules containing directing groups, such as the pyridyl substituent in 2-phenylpyridine, consistently direct electrophilic palladation to the *ortho* position of the pyridine substituent via a concerted metalation-deprotonation (CMD) pathway.[58] This strategy is utilized in C–C, C–O, C–N, and C–X bond-formation reactions.[57–59] Overcoming this requirement will enhance atom economy and improve the overall efficiency of multistep synthetic sequences.[5,17] In the last decade, Yu and his co-workers have developed a strategy to introduce a directing group to molecules containing specific functional groups such as benzylic alcohols and phenylacetic acid derivatives. The development of Yu's approach started with the removable nitrile template (T) that presumably works due to the weak 'end-on' interaction between the linear nitrile group and the metal center.[1] This strategy was initially used to functionalize benzylic alcohols after attaching

the nitrile template to the alcohol functional group, through which remote C–H bonds, typically in the *meta*-position, are olefinated (Scheme. 10).[60]

Reaction design for remote C–H functionalization:

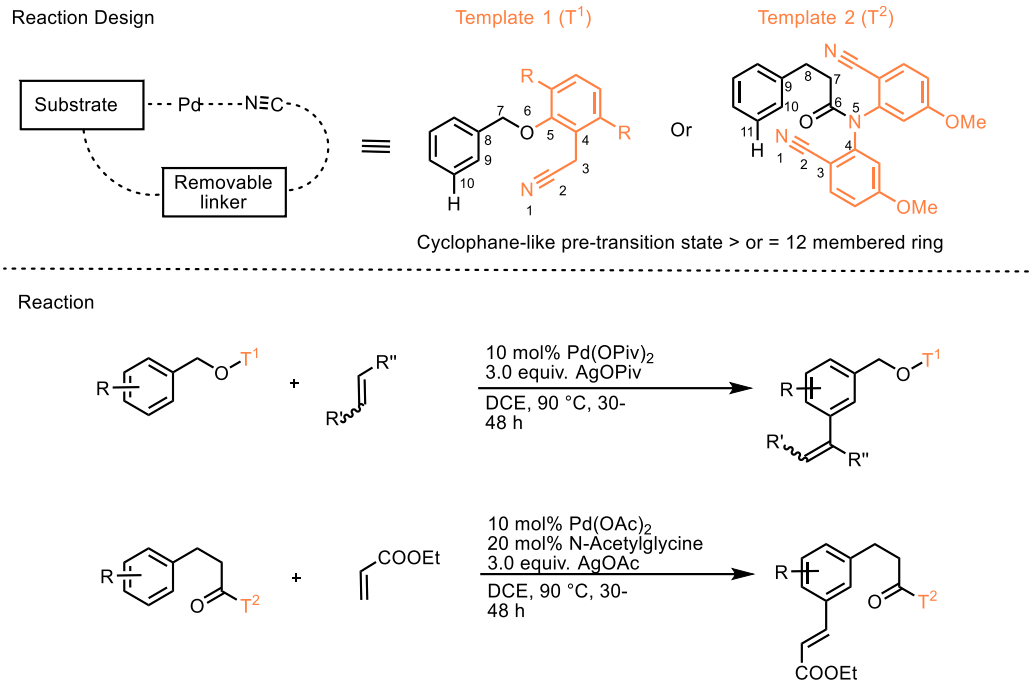

Scheme 10. Template-assisted remote C–H activation of hydrocinammic acids and toluene derivatives.

The *meta*-C–H activation proceeds via a cyclophane-like pre-transition state which is less affected by the coordination geometry. Furthermore, the developed template bypasses *ortho*-directing effects and steric biases, making it widely applicable to hydrocinnamic acid and benzylic alcohol derivatives.[60,61] Furthermore, various templates for an expanded scope of different benzylic alcohol derivatives have been developed along with a variety of different transformations, among which are arylation,[62] cyanation,[63] hydroxylation,[64] silylation,[65] deuteration,[66,67] and allylation (Scheme 11).[68] Beyond *meta* C–H activation, harnessing the distance and geometry-guided template, Maiti and his co-workers have developed a new template by which *para* selectivity is achieved (Scheme 12a).[69] Yu and his co-workers conducted further research, which has achieved *para*-selective C–H functionalization of electron-deficient benzoic acid derivatives (Scheme 12b).[70] In order to achieve catalyst-controlled selective C–H activation, it was established that the use of readily available mono-*N*-protected amino acids (MPAA) is crucial for a better reaction outcome.[16]

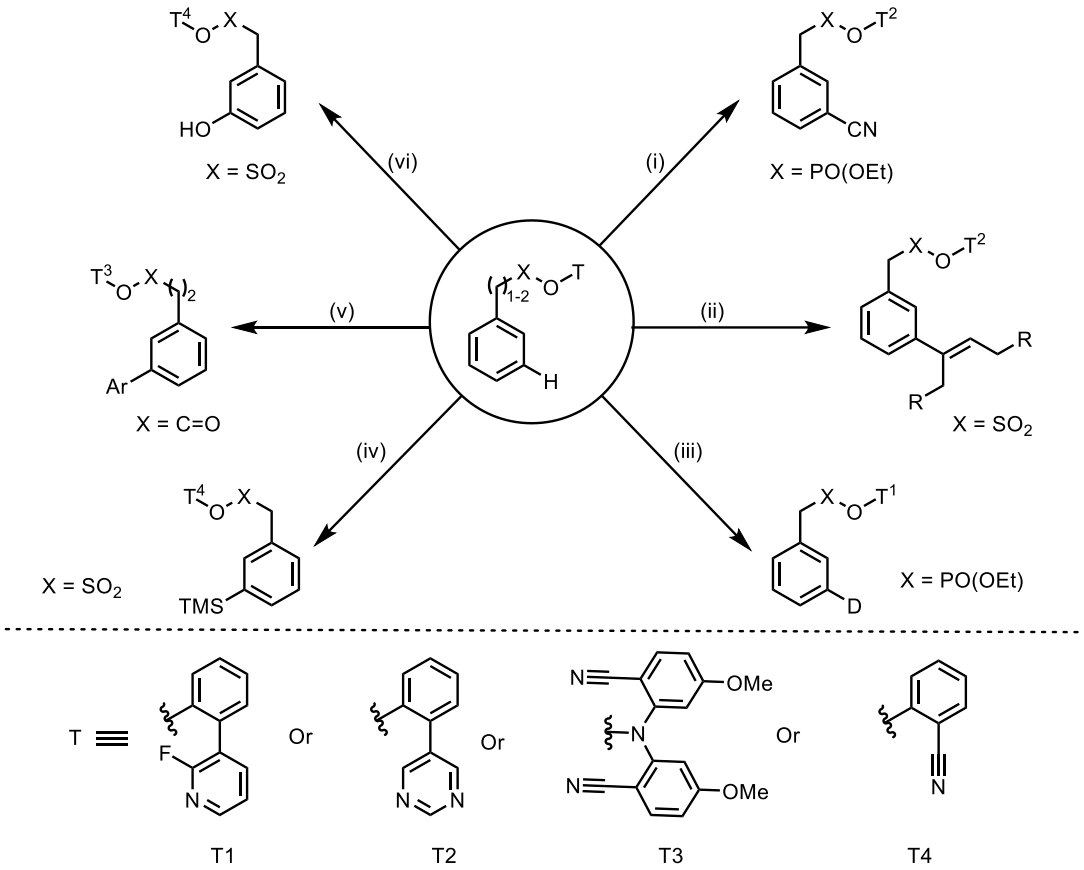

Scheme 11. Palladium-catalyzed *meta* C–H functionalization of arenes using removable templates. (i) 10 mol% $Pd(OAc)_2$, 20 mol% Ac-Gly-OH, 1.5 equiv. CuCN, 3.0 equiv. Ag_2CO_3, HFIP, 80 °C, 30 h. (ii) 10 mol% $Pd(OAc)_2$, 20 mol% Ac-Nle-OH, 2.0 equiv. CuF_2, 3.0 equiv. Ag_2CO_3, MeCN, 90 °C, 24 h. (iii) 10 mol% $Pd(OAc)_2$, 20 mol% Ac-Gly-OH, CD_3COOD, 110 °C, 24 h. (iv) 10 mol% $Pd(OAc)_2$, 20 mol% Ac-Gly-OH, 3.0 equiv. Ag_2CO_3, 1.2 equiv. $(Me_3Si)_2$, Na_2SO_4, HFIP, 80 °C, 30 h. (v) 10 mol% $Pd(OAc)_2$, 20 mol% Ac-Gly-OH, 3.0 equiv. Ar-BPin, 2.0 equiv. Ag_2CO_3, 2.0 equiv.CsF, 3.0 equiv. TBAP-PF_6, HFIP, 90 °C, 24 h. (vi) 10 mol% $Pd(OAc)_2$, 20 mol% Boc-Ala-OH, 4.0 equiv. $PhI(OAc)_2$, 3.0 equiv. Ag_2CO_3, HFIP, 70 °C, 24 h.

The use of MPAA ligands has shown improvements in reaction yields, times, and higher regio- and enantioselectivity.[16,71] DFT calculations and MS analysis were used to examine the reaction mechanism of amino acid-assisted distant C–H bond activation.[16] The role of the MPAA ligands was revealed, and a CMD mechanism was confirmed in which the basic N-protecting group of the anionic amidated ligand contributes to the deprotonation of the C–H bond. Yu and his co-workers have also provided experimental support for the production of monomeric Pd(MPAA) complexes.[16] Quick progress has been made in creating strategies to overcome barriers and encourage C–H functionalization, one of which is the frequent use of 1,1,1,3,3,3-hexafluoroisopropanol (HFIP).[1]

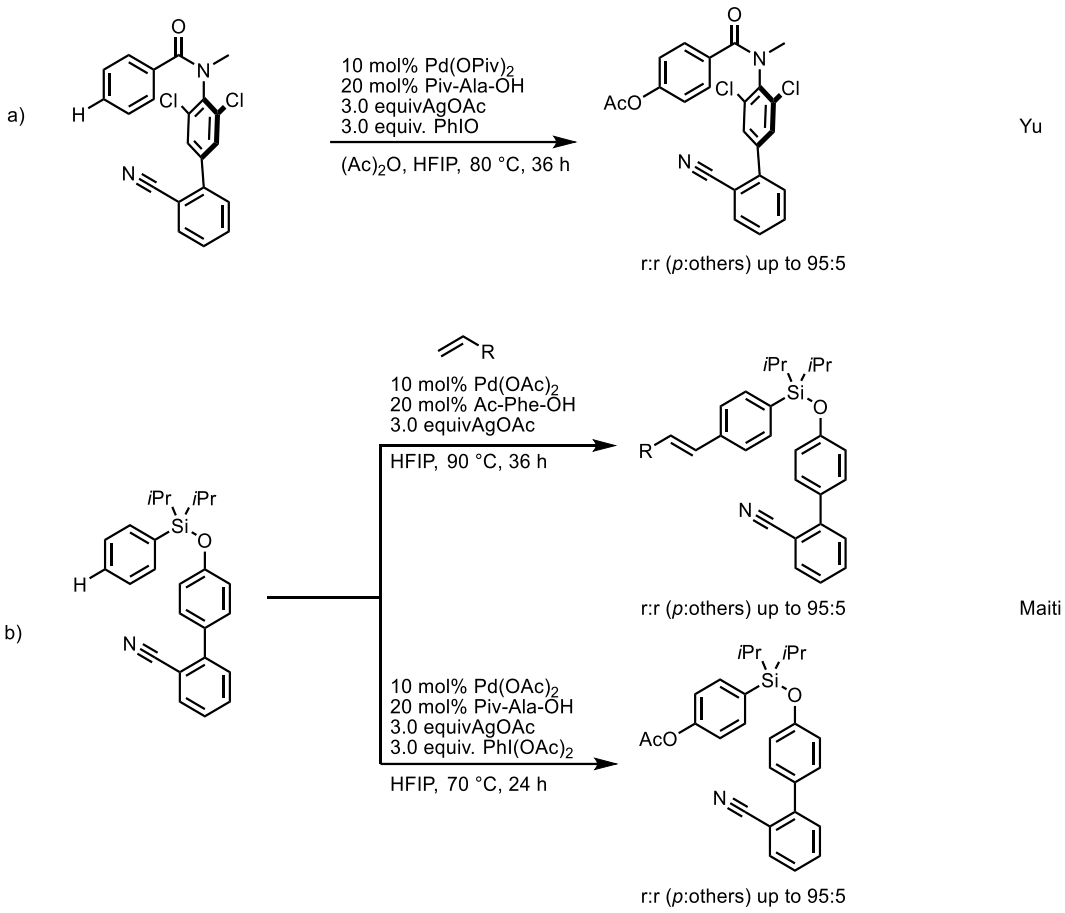

Scheme 12. *Para*-selective C–H functionalization using distance and geometry-guided templates.

The ability of HFIP to form hydrogen bonds with the substrate enhances the reactivity of these methods. Furthermore, by stabilizing macrocyclic pre-transition states, this enhanced coordinating medium enhances the selectivity and reactivity of these transitions.[72–75] Moreover, HFIP functions as a potent ligand to coordinate with the metal catalyst and increase the catalyst's efficiency.[76] Additionally, the application of HFIP in a few metal-free and metal-catalyzed C–H functionalization reactions has increased its significance in organic synthesis.[73–76]

1.1.4 Transition Metal Catalyzed Non-Directed C–H Functionalization

Cost-effective diversifications of feedstock and fine chemicals can be achieved synthetically through methods such as site-predictable and chemoselective C–H bond functionalization processes.[77] Numerous catalysts based on transition metals have surfaced to activate and functionalize C–H bonds selectively. Regio- and chemoselectivity problems appeared when applied to complex compounds with a high functional group diversity.[77,78] Electrophilic metalation strategy for aromatic C–H functionalization is used extensively in research as a short pathway

enabling direct derivatization of target molecules.[6] Organoboron compounds are used extensively in synthesis due to the versatility of the boryl substituent in different cross-coupling reactions. Hartwig and his co-workers developed a mild borylation method of arenes catalyzed by iridium and substituted bipyridine ligands (Scheme 13).[11]

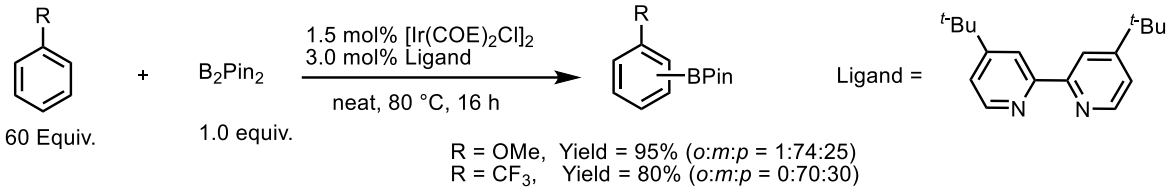

Scheme 13. Schematic illustration of Hartwig's iridium-catalyzed borylation of arenes.

However, this reaction's drawback is that it forms different constitutional isomers for some arenes, especially mono-substituted arenes.[11] The reactivity has been further tuned to achieve *ortho*,[79] *para*[80] and *meta*[81] selective borylation but only for certain classes of aromatic compounds (Scheme 14). Additionally, more in-depth control experiments and computational analyses showed that this transition from iridium bis(boryl) complex to iridium tris(boryl) complex results in an unprecedented Bpin shift, which in turn controls the remote selectivity.[81] On the other hand, bidentate bipyridine or phenanthroline ligands were reported as effective ligands for achieving C–H borylation. As a result, the *meta* and/or *para* positions become competitively functionalized. It was observed that the modification to the bipyridine ligand, specifically the addition of a trifluoromethyl substituent at position 5, can completely alter the regioselectivity of the borylation process of aromatic amides, thereby facilitating the synthesis of various *ortho*- borylated arenes.[79] Using bipyridine derivatives to synthesize different iridium catalysts, *para*-C–H borylations of tetraalkylammonium sulfates and sulfamates have been accomplished. The substituents on the bipyridine ligands and the length of the alkyl groups in the tetraalkylammonium cations can alter selectivity. It is suggested that ion pairing, in which the cation's alkyl groups protect the *meta*-C–H bonds in the counteranions, explains *para*-selectivity. Superior selectivity was obtained with the 4,4′-dimethoxy-2,2′-bipyridine ligand.[80,82]

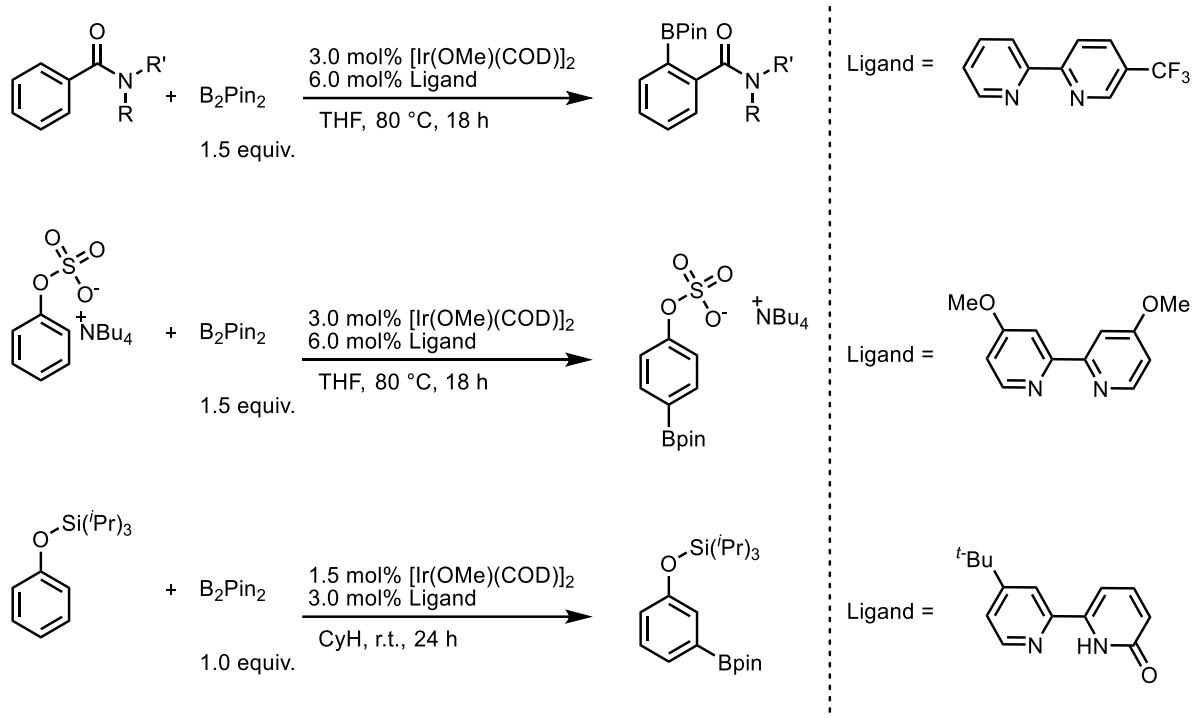

Scheme 14. Schematic illustration of different selective iridium-catalyzed borylation reactions.

1.1.5 Late-Stage Aromatic C−H Functionalization via Thianthrenation

Thianthrene sulfoxide was assessed and employed previously to create arylthianthrenium salts of electron-rich arenes such as anisole. The corresponding arylthianthrenium salts were suggested to be produced using the thianthrenium radical cation generated as the reaction proceeds.[83,84] Despite the thianthrenation step being known, the selectivity and the reaction's utility, especially in the late-stage, were not investigated due to the challenges of the reaction using substrates with several functional groups such as pyridines,[85] amines[86] and alcohols.[87] Recently, Ritter and his co-workers have developed the reaction further by adding a proper acid anhydride and weak acid to generate an electrophilic species that selectively reacts with a large scope of aromatic molecules in the late-stage, producing the corresponding aryl sulfonium salt.[1]

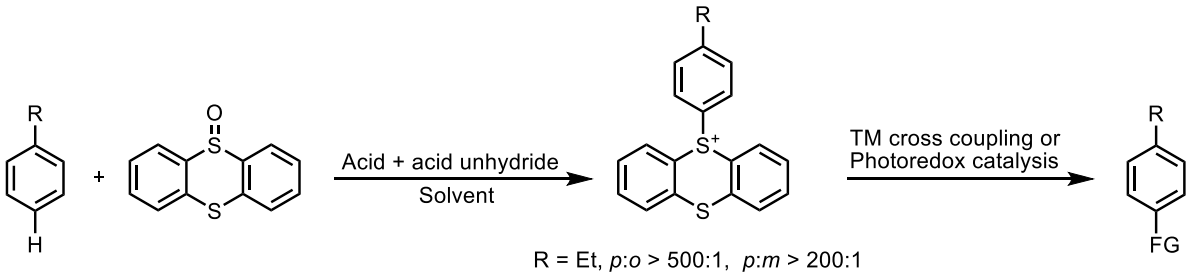

Scheme 15. Schematic illustration of the C–H functionalization via thianthrenation.

Similarly to aryl halides and aryl pseudohalides, the thianthrenium moiety serves as a versatie linchpin and can be substituted with various desired functional groups via transition metal cross-coupling reactions or photoredox catalysis (Scheme 15).[3]

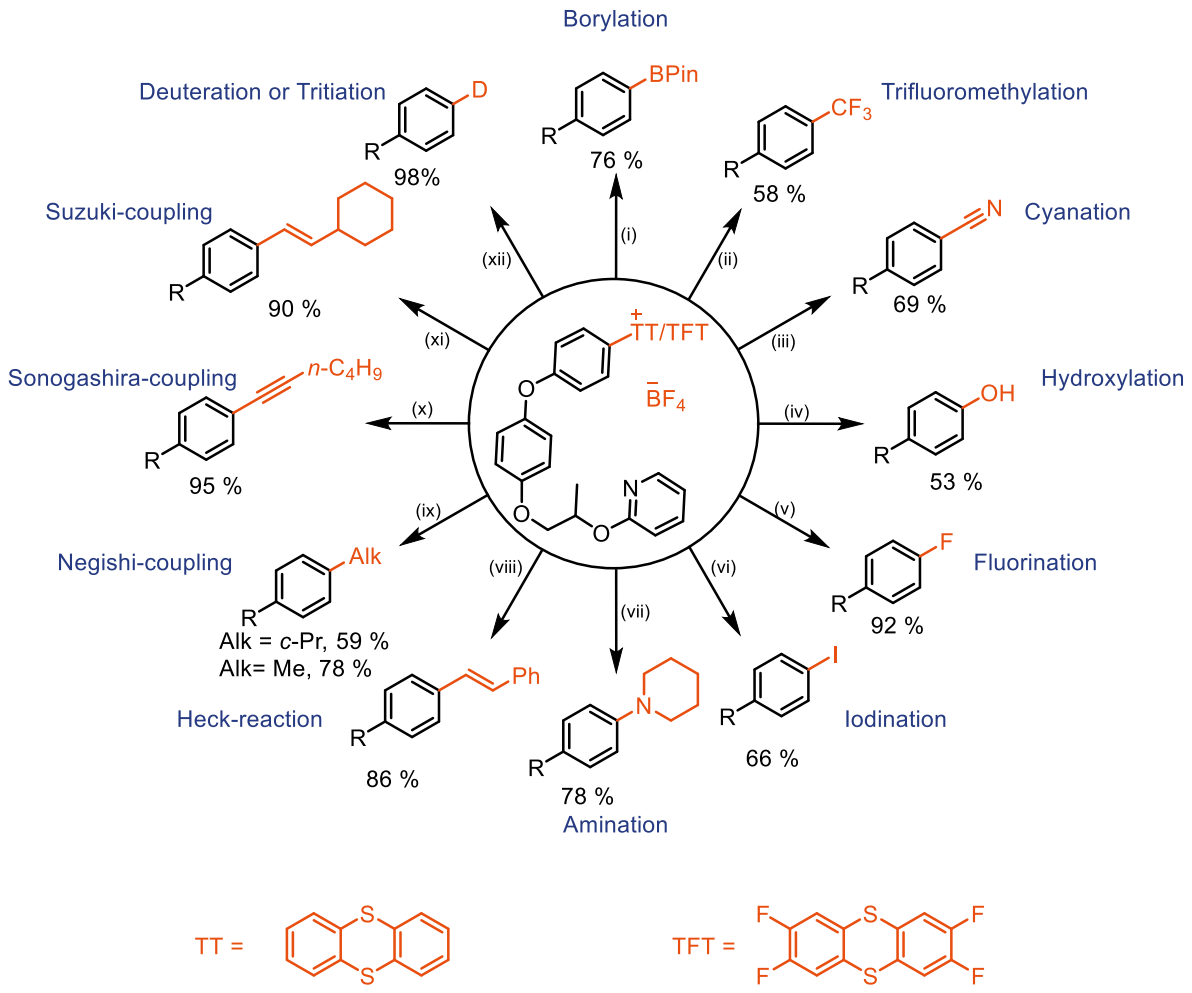

Scheme 16. *Ipso*-substitution of pyriproxyfen thanithrenium salt. (i) B_2Pin_2 (2.5 equiv.), pyridine (5.0 equiv.), LED. (ii) CuSCN (1.5 equiv.), CsF (2.0 equiv), $TMSCF_3$ (1.5 equiv.) in DMF (c=0.3 m) at 23 °C for 30 min, followed by addition of aryl (tetrafluoro)thianthrenium salts (0.2–0.3 mmol), $Ru(bipy)_3(PF_6)_2$ (2 mol %) in MeCN (c=0.2 m), blue LED, 30 °C, 3 h. (iii) NBu_4CN (2.5 equiv.), $Cu(MeCN)_4BF_4$ (1.2 equiv.), LED. (iv) $[Ir[dF(CF_3)ppy]_2(dtbpy)PF_6]$ (1 mol %), dimethylglyoxime (10 mol %), Cu_2O (0.8 equiv), MeCN/H_2O (10/3, v/v), blue LED (34 W), 30 °C, 16 h. (v) CsF (1.2 equiv.), $[Cu(MeCN)_4]BF_4$ (1.5 equiv.), $[Ir[dF(CF_3)ppy]_2(dtbpy)PF_6]$ (1 mol%), acetone (0.1 or 0.2 M), LED (68 W), 30 °C, 20 h.(vi) LiI (10 equiv.), $Cu(MeCN)_4BF_4$ (1.0 equiv.), MeCN/DMSO (3/2), LED. (vii) 2.0 mol% $NiCl_2{\cdot}6H_2O$ or $NiBr_2{\cdot}$diglyme, 2.0 equiv. piperidine. (viii) Pd(OAc)2 (9.0 mol%), PPh3 (15 mol%), styrene (2.0 equiv.), NEt_3 (3.0 equiv.), DMF, 100 °C. (ix) c-PrZnBr or MeZnCl (3.0 equiv.), $Pd(PPh_3)_2Cl_2$, KOAc (6.0 equiv.), THF, 50 °C. (x) 1-hexyne (2.0 equiv.), CuI (20 mol%), $Pd(dppf)Cl_2$, *N*-methylmorpholine (2.0 equiv.), dioxane, 40 °C. (xi) Cyclohexylvinylboronic acid (2.0 equiv.), K_2CO_3 (4.0 equiv.), $Pd(dppf)Cl_2$, EtOH, 50 °C. (xii) a: $(Pd[(PtBu_3)]_2$, 1 mol%), THF (0.1 M or 0.2 M), $^2H_2$ (1 atm, about 5 equiv.), 23 °C, 12 h.

The synthetic utility of the thianthrenation reaction relies not only on the ability to functionalize arenes at late-stage but also on its unusual *para*-selectivity for mono-substituted arenes. The

selectivity of the thianthrenation reaction is notably superior to halogenation or borylation reactions. The origin of selectivity is attributed to steric and electronic properties. The high value of the reaction rate constant ($\rho = -11$) indicates a highly developed positive charge in the C–S bond transition state, favoring *ortho* and *para* positions over the *meta* position. The *ortho* position is unfavored due to steric effects, which leads to functionalizing the most electron-rich position, which is not sterically hindered.[3,88] The reaction proceeds via the activation of sulfoxide under acidic conditions with an anhydride to generate the active species, trifluoroacetylthianthrenium cation, which reacts with the most electron-rich C–H bond of a given arene.[88] Aryl thianthrenium salts are used in cross-coupling reactions, where the thianthrenium moiety serves as an electrophilic linchpin that can be substituted with various functional groups (Scheme 16). Similarly to aryl halides, aryl thianthrenium salts were used in various reactions such as Sonogashira, Suzuki, Heck, and Negishi cross-coupling.[3] Additionally, the versatility of the thianthrenium moiety was harnessed in photoredox catalysis while numerous strategies were applied to develop reactions such as borylation, cyanation, chlorination,[3,89] hydroxylation,[90] trifluoromethylation,[91] fluorination,[92] and carbon-heteroatom cross-coupling (Scheme 16).[93, 94] In addition to the numerous applications of the reaction, it was observed that the thianthrenyl leaving group exhibits weaker coordination affinity to palladium catalysts compared to conventional leaving groups. The thianthrenyl group's weak coordination ability was used to achieve selective hydrogenolysis of arenes. This feature was used in the tritiation and deuteration of aryl thianthrenium salts, which demonstrates a significant advantage over aryl halides, as such transformations are not yet achievable with the latter using homogenous catalysis.[95] Aryl thianthrenium salts are proven to be superior to aryl halides, which primarily rely on heterogeneous catalysis, which often results in the unwanted reduction of other functional groups, especially for complex molecules.[96]

1.2. Objective

This project aims to develop a new linchpin that can be selectively introduced to arenes via electrophilic aromatic substitution. The developed linchpin is tethered to a directing group and shall be used in transition metal-catalyzed C–H activation. A new analog of thianthrene S-sulfoxide tethered to a directing group shall be developed to achieve this goal. The developed sulfoxide shall be used to synthesize different aryl sulfonium salts with high site-selectivity. Therefore, the reaction conditions for synthesizing aryl sulfonium salts shall be tested and optimized, and the selectivity must be comparable to the selectivity of the thianthrenation reaction. Subsequently, the synthesized aryl sulfonium salts shall be tested to develop directed C–H functionalization based on the directing group tethered to the sulfonium moiety, and the possible transformations shall be optimized. Afterwards, the attached linchpin must be *ipso*-substituted to deliver selectively difunctionalized arenes.

1.3 Results and Discussions

Parts of this chapter are adapted, with permission, from our published work in Synlett in collaboration with Michal Mrozowicz. The concept of thianthrene-like linchpins with directing groups was proposed by the author. All experimental results involving aryl sulfonium salts and their derivatives presented in this work were conducted by the author.[97]

1.3.1 Design of the reagent

To achieve similar reactivity to the thianthrenation reaction, the initially proposed reagent targeted minimal structural perturbation of thianthrene. Replacing a carbon atom with a nitrogen atom results in azathianthrene; however, the given structure has two sulfur atoms, which are susceptible to oxidation. In addition to the low selectivity oxidation of the sulfur atoms, the activated sulfoxide might be engaged in acyl transfer from one sulfur atom to another, forming different constitutional isomers. To circumvent this problem, azaphenoxathiin was proposed as a potential reagent; however, the coordination of a transition metal to the nitrogen atom becomes challenging due to the lack of nucleophilicity of the directing group because of its existence near a positively charged sulfur atom. Based on the pioneering work from Yu and his co-workers (Chapter 1.2.3), the separation of the directing group from the thianthrene-like structure was suggested to overcome the lack of nucleophilicity of the coordinating group via avoiding the mesomeric influence of the aromatic dibenzothiophene moiety. Upon the coordination of the directing group to the palladium catalyst, it forms macropalladacycle which is engaged in the C–H activation process. (Scheme 17).

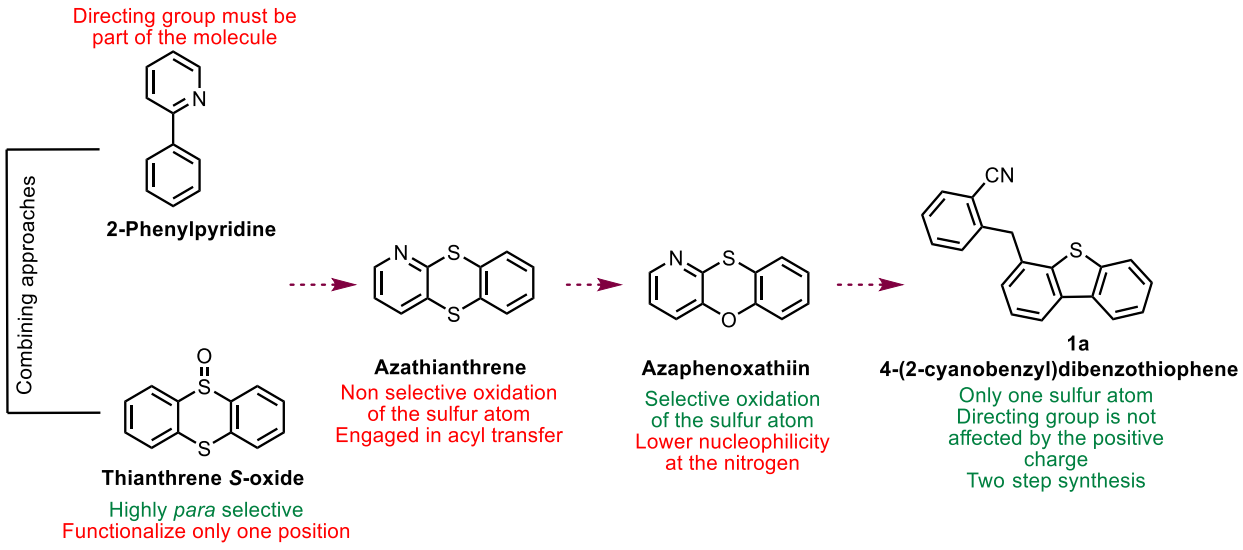

Scheme 17. Design of the reagent for double C–H functionalization.

The synthesis of the desired reagent **1b** was achieved in good yields in two steps via conventional Suzuki coupling followed by oxidation. The coupling of the dibezothiophen-4-ylboronic acid and 2-cyanobenzyl bromide to yielded **1a**, which was subsequently converted to the corresponding sulfoxide **1b** by oxidation. Using the same protocol as dibenzothiophene, the dibenzothiophene derivative **1a** was oxidized to the corresponding sulfoxide (Scheme 18) using hydrogen peroxide in an acidic medium. The yield of the oxidation step was increased from good to quantitative yield with a minor modification to the process. It was found that the oxidation reaction is sensitive to temperature, and over-oxidation was observed when the temperature rises above 0 °C.

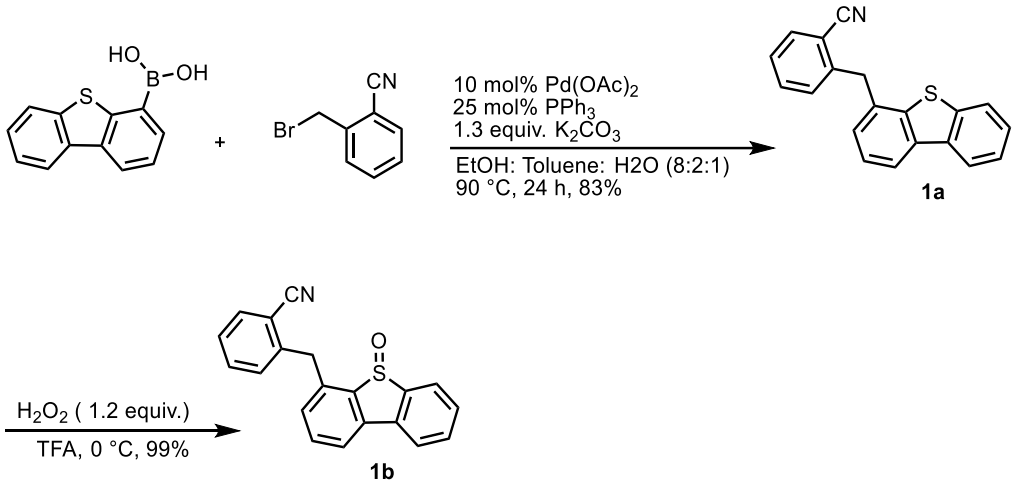

Scheme 18. Design of the reagent for double C–H functionalization.

To prevent further oxidation from **1b** to the corresponding sulfone, peroxide was thus added to a suspension of **1a** at 0 °C. Furthermore, the product must be extracted directly after the reaction was quenched at 0 °C.

Utility of the reagent

To assess the utility of the synthesized reagent **1b**, reactions to synthesize different aryl sulfonium salts using different arenes. Afterwards, the synthesized sulfonium salts were used to achieve directed C–H functionalization using transition metal catalysis. After the two C–H functionalization steps, the sulfonium moiety *ipso*-substituted with an alkyne via Negishi coupling.

1.3.2 First C–H functionalization step (Synthesis of aryl sulfonium salts)

Optimization of the Reaction Condition:

Several chemical reagents were studied to optimize the dibenzothiophenylation step to

synthesize aryl sulfonium salts. Using **1b** as a limiting reagent, the dibenzothiophenylation reaction conditions were optimized using fluorobenzene **2a** as a model substrate.

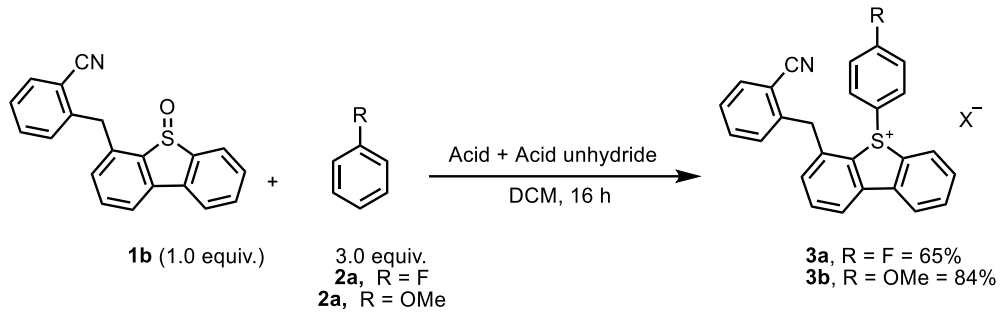

Scheme 19. Schematic illustration of the general dibenzothiophenylation reaction.

Table 1. Optimization of the dibenzothiophenylation reaction conditions of substrates **2a**.

Entry	Arene	Anhydride	Acid	Solvent	Temperature	Yield%
1	**2a**	TFAA	HBF_4	MeCN	25 °C	25
2	**2a**	TFAA	HBF_4	MeCN	0 °C	29
3	**2a**	TFAA	HBF_4	MeCN	−40 °C	26
4	**2a**	Tf_2O	TFA	MeCN	−40 °C	40
5	**2a**	TFAA	HOTf	MeCN	−40 °C	38
6	**2a**	TFAA	HOTf	MeCN	−40 °C	35
7	**2a**	Tf_2O	TFA	CH_2Cl_2	−78 °C	55
8	**2a**	Tf_2O	HOTf	CH_2Cl_2	−40 °C	51
9	**2a**	Tf_2O	HOTf	CH_2Cl_2	−40 °C	59
10	**2a**	TFAA	-	CH_2Cl_2	−50 °C	65
11	**2b**	Tf_2O	HOTf	CH_2Cl_2	−50 °C	50
12	**2b**	TFAA	HOTf	CH_2Cl_2	−15 °C	84

The reaction was found to be temperature-sensitive, and higher temperatures increased the ratio of the byproduct. An acid was added to the reaction mixture to synthesize the sulfonium salt of anisole **2b**, which increased the yield; however, the selectivity was low. Furthermore, as the optimization (Table 1) illustrates, the choice of the anhydride and or/the acid was crucial for both conversion and selectivity. It was observed that the addition of strong acid is required to activate the reagent. Additionally, adding one extra equivalent of the acid resulted in enhanced yields, possibly because one equivalent was consumed to protonate the cyano group of the reagent. The purification of sulfonium salts was achieved by column chromatography.

1.3.3 Remote C–H Functionalization and Subsequent Sulfonium *Ipso*-substitution

Different palladium-mediated C–H activation strategies were attempted to utilize the synthesized sulfonium salts (Scheme 19) to selectively functionalize arenes in two positions. Under different reaction conditions, only directed C–H olefination of the *ortho*-position was successful. At the same time, palladium acetate was used as a precatalyst and *N*-acetylglycine was used as a ligand. It was observed that the reaction is sensitive to the solvent of choice, oxidant, base, ligand, and olefin.

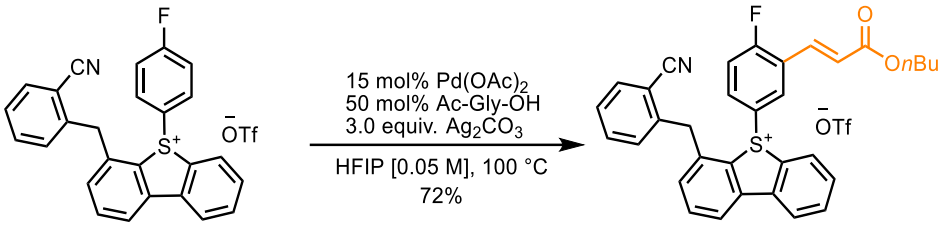

Scheme 20. Schematic illustration of the directed olefination reaction of fluorobenzene-derived sulfonium salt.

Table 3. Optimization of the olefination reaction.

Entry	Change in reaction conditions	Conversion [%]
1	0.50 M concentration	17
2	0.25 M Concentration	35
3	0.10 M concentration	53
4	0.05 M concentration	72
5	Additional equivalent of BQ	65

Table 3 (continued). Optimization of the olefination reaction.

	Change in reaction conditions	Conversion [%]
6	Additional equivalent of Ag_2O	60
7	Additional equivalent of AgF	55
8	Additional equivalent of K_2CO_3	51
9	Additional equivalent of Pyridine	n.d.
10	Additional equivalent of Lutidine	n.d.
11	Additional equivalent of triethyl amine	n.d.
12	Isopropanol instead of HFIP	n.d.
13	DCE instead of HFIP	11
14	TFE instead of HFIP	12
15	Dioxane instead of HFIP	n.d.
16	MeCN instead of HFIP	n.d.
17	Ac-Phe-OH instead of Ac-Gly-OH	28
18	Boc-Gly-OH instead of Ac-Gly-OH	n.d.
19	Ac-Ala-OH instead of Ac-Gly-OH	31
20	Ac-ßAla-OH instead of Ac-Gly-OH	26
21	*N*-acetyl-4-aminobutyric acid instead of Ac-Gly-OH	n.d.
22	Methyl acrylate instead of n-butyl acrylate	19
23	Etylacrylate instead of n-butyl acrylate	29
24	$PdCl_2$ instead of $Pd(OAc)_2$	63
25	$Pd(OPiv)_2$ instead of $Pd(OAc)_2$	69

The conversion of the aryl sulfonium salts to the corresponding olefinated aryl sulfonium salts was calculated via ^{1}H-NMR using the integration of the dibromemethane peak as the internal standard versus the integration of the olefinic C–H bond. For a successful olefination of the aryl sulfonium salts, it was found that HFIP is the solvent of choice to achieve C–H activation. On the other hand, replacement with TFE or DCE results in lower yields, while other solvents, such as DCM and acetonitrile, lead to no reactivity. The dual role of silver carbonate as an oxidant and a base showed better conversion while adding other organic or inorganic oxidants showed lower yields. The concentration of the reaction played an essential role in obtaining better yields. On the other hand, the change of the used precatalyst did not severely influence the reaction while $Pd(OAc)_2$ gave the highest yield. The reaction yielded a mixture of starting material and product, inseparable from each other via flash column chromatography. Thus, the reaction mixture was filtered through a Ceilte pad to remove the inorganics, and the reaction mixture was dried and subsequently used without further purification.

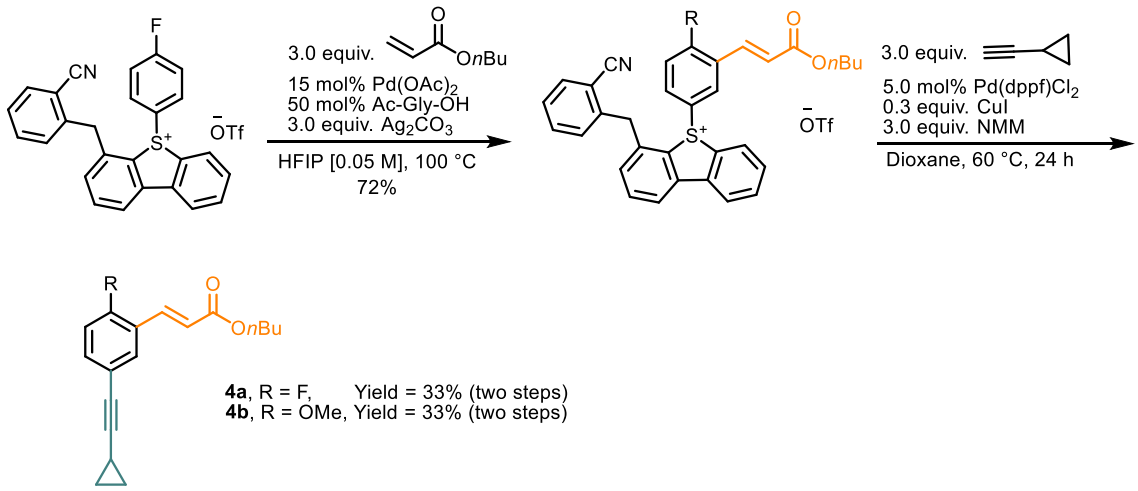

Scheme 21. Regioselective double C–H functionalization.

To achieve *ipso*-substitution of the olefinated aryl sulfonium salts, the sulfonium moiety was replaced by cyclopropylacetelene via conventional Sonogashira coupling (Scheme 21). The two steps delivered regioselective double C–H functionalization of the original arene independent of a directing group.

1.3.4 Limitation of the method

According to the results, the developed method for sequential C–H functionalization showed proof of concept. Moreover, the method resulted in the development of sulfoxide, which was used

successfully in the *para*-selective synthesis of aryl sulfonium salts. The first C–H functionalization is possible via this strategy for different simple arenes. However, the selectivity of the first C–H functionalization step is lower in comparison with the thianthrenation reaction.

The subsequent directed C–H olefination reaction was limited to mono-substituted sulfonium salts of simple arenes, where it was not possible to isolate and characterize the desired product from the reaction mixture using column chromatography. Although the TLC analysis of the reaction mixture showed only one single spot, the product formation was measured and detected ^{1}H-NMR and LC-MS analyses of the reaction mixture. The results showed the formation of the desired product (mono-olefinated sulfonium salt) as well as other byproducts.

Due to the difficult separation of the mono-olefinated product from the reaction mixture, polar inorganics and insoluble particles were removed by filtration. Subsequently, the mixture was directly used in the Sonogashira coupling with cyclopropylacetelene. The reaction was conducted under standard reaction conditions analogous to thianthrenium salts.[97] it was observed that changing the cyclopropyl acetylene to another alkyne, such as trimethylsilyl acetylene, led to undesired reactivates, and the desired product was not obtained. The Sonogashira coupling of olefinated sulfonium salts **3a'** and **3b'** delivered the desired product in acceptable yields.

1.5 Conclusion

In conclusion, this project has demonstrated the possibility of activating remote C–H bonds sequentially through two distinct mechanisms. The desired reagent was designed to have a sulfoxide functional group and a directing group. The designed sulfoxide was used in selective C–H activation via electrophilic aromatic substitution, forming aryl sulfonium salts. The tethered directing group was used in the C–H olefination of the synthesized sulfonium salts was successfully achieved for simple arenes, though its applicability was limited to these substrates. Furthermore, the *ipso*-substitution of the olefinated sulfonium salts was accomplished for simple arenes, whereas this transformation proved challenging for more structurally complex molecules.

Chapter (2)

Transition Metal η^6– Arene Complexes in Catalysis, Defluorohydroxylation and Deoxyfluorination

2.1 Introduction

Aromatic compounds, upon π-coordination to a metal center, exhibit a shift in the chemical and electronic properties of the corresponding arene. As a result of the facial coordination of the arene to the metal center, the coordinated arene becomes more electron deficient, which in turn leads to an increased acidity of the corresponding aromatic and benzylic C–H bonds.[98] This class of complexes was discovered by Fischer discovered in 1955.[99] The application of η^6–arene complexes has become an interesting research field. The facial coordination of arenes to transition metals facilitates various transformations that are not possible without coordinating to a metal center.[99,100] Nucleophilic aromatic substitution (S_NAr), deprotonation followed by a subsequent reaction, and electrophile oxidative addition are facilitated when electron-rich substrates are facially bound to transition metals.[100–103] Research has shown that some arenes and transition metals exhibit reversible π-complexation.[100–102] As a result, the stoichiometric transformation of a coordinated arene complex can be adapted to a catalytic process in relation to the ML_n core. This appealing possibility necessitates a balance between the reactivity of the coordinated arene and the exchange of the coordinated arene product with the reactant arene.[98] The strength of the transition metal-arene π-bond varies significantly, from strong, as in ruthenium complexes, to relatively weak, as reported for silver complexes.[104] This diversity in stability enables the use of arene complexes for various applications. Facially coordinated arenes can stabilize metals in catalytically active species, making them efficient catalysts for many processes, among which hydrogenation,[105,106] C–H activation[107–109] and olefin metathesis.[110,111] In contrast, weakly coordinated arenes can be substituted by different ligands, allowing such complexes to be used as starting molecules in organometallic synthesis.[112,113]

2.1.1 Reactivity of η^6–Arene Complexes

The π-coordination of an arene to transition metal affects its electronic properties, which results in higher stability of cations, anions, and radicals formed at the coordinated arene.[114] The η^6–arene coordination alters its properties from a nucleophile to an electrophile, consistent with the decreased pK_a of its aromatic and benzylic protons (Figure 1).[98,115] Due to the electrophilicity of

the coordinated arene, nucleophilic attack on the arene is facilitated and becomes possible with higher stereoselectivity. The remarkable stereoselectivity is attributed to the blocked face of the arene face coordinated to the metal center, which results in one face, opposite to the metal being attacked by a nucleophile. On the other hand, the site selectivity in the coordinated arene is controlled by the substituent effect.[98,114]

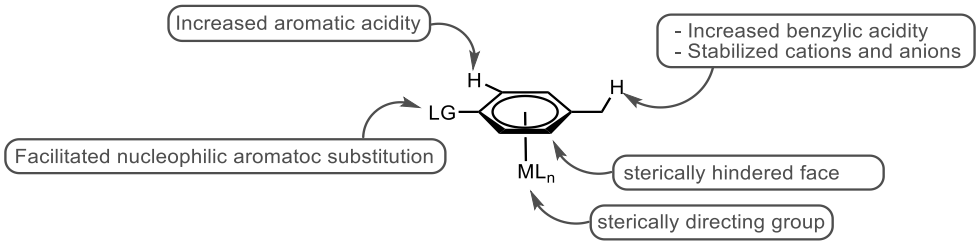

Figure 1. The electronic change of an arene upon η^6– coordination to a metal central atom.

2.1.2 Nucleophilic Aromatic Substitution of η^6– coordinated arenes

The η^6–coordination of arenes to transition metals results in higher electron density flowing from the ligand to the metal center, which increases the electrophile nature of the coordinated arenes.[100,114] Moreover, various nucleophiles have been used in organic synthesis to react with different π-arene complexes. In this type of coordination, nucleophilic attack occurs on the ligand, the arene, instead of the metal center since it is either electronically saturated, sterically hindered, or both.[114] The reactions of nucleophiles with different π-arene complexes such as (arene)$Cr(CO)_3$, (arene)$Fe(CO)_3$, and (arene)$Mn(CO)_3$ deliver unprecedented arene reactivity. This reactivity has been studied extensively and is used in various useful syntheses. This class of π-arene complexes has been used in organic synthesis, where the used nucleophile, upon reaction with the arene complex results in a substitution reaction on the aromatic ring. Alternatively, the used nucleophile may undergo an irreversible nucleophilic addition which results in de-aromatization of the arene (Scheme 22).[116]

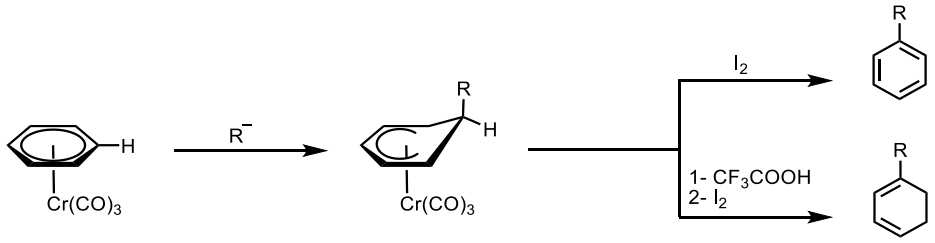

Scheme 22. S_NAr versus nucleophilic addition of different nucleophiles on $(C_6H_6)Cr(CO)_3$. Unreactive nucleophiles: $(CO_2R)_2CHLi$, MeMgBr, Me_2CuLi and CH_2=CHLi. Reactive nucleophiles: PhLi, $PhSCH_2Li$ and *t*BuLi

The developed nucleophilic addition reactions and nucleophilic aromatic substitution reactions were achieved using a stoichiometric amount of the transition metal.[117,118] Transition metals, including ruthenium and iron, were used in the synthesis of π-arene complexes. The nucleophilic attack on π-arene complexes such as Ar-Ru^{+}Cp* and Ar-Fe^{+}Cp occurs on the arene, not the cyclopentadienyl ligand.[118,119] Pearson and coworkers harnessed the reactivity of π-arene complexes in the synthesis of diphenyl ethers, which is challenging in the case of complex natural products, such as vancomycin (Scheme 23).[120,121]

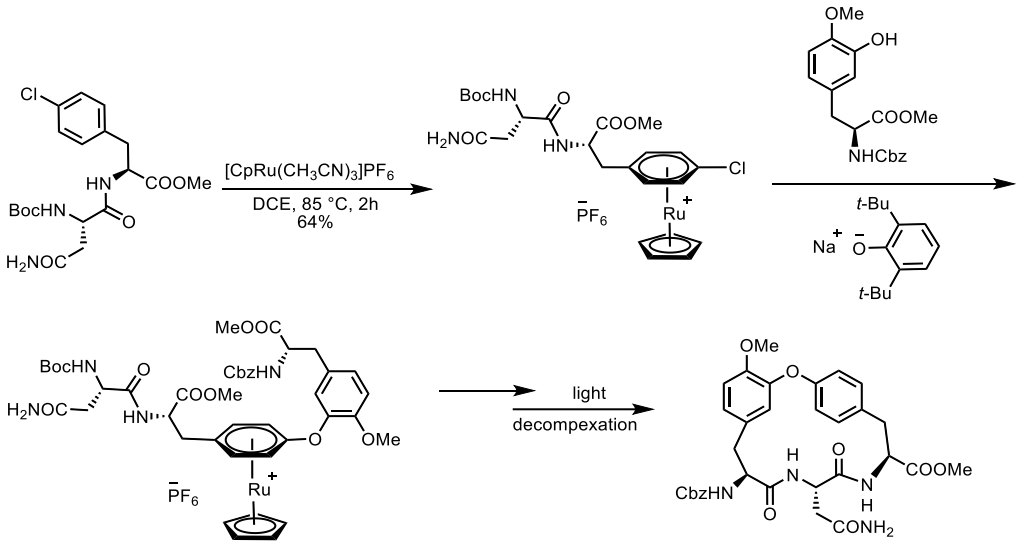

Scheme 23. Application of ruthenium η^6–arene complexes in the synthesis of Vancomycin.

The η^6–coordination of arenes to transition metals is recognized as a method that facilitates nucleophilic aromatic substitution chemistry, where the nucleophilic attack occurs on the aromatic π-system which is not possible before the coordination to the metal center.[120, 121] The C–H bond activation via a nucleophilic attack on π-arene complexes is well established where different complexes. Different η^6–arene complexes were synthesized via complexation with [Cr(CO)$_3$], [Mn(CO)$_3$]$^{+}$, [FeCp]$^{+}$, [RuCp]$^{+}$ or [IrCp*]$^{2+}$ precursors where it was found that the C–H bond activation is often kinetically preferred over the C–X bond activation.[122] Strong nucleophiles, such as carbanions, generate stable η^5-cyclohexadienyl adducts through irreversible nucleophilic attack, which can subsequently can be oxidized to yield C–H-functionalized products. The reactivity of π-arene complexes was used to develop C–H oxygenation of arenes using recoverable stoichiometric iridium complex. The method showed a selective nucleophilic attack on the C–H bond followed by oxidation, reversing the role of an arene from a nucleophile to an electrophile(Scheme 24a).[123]

The utility of π-arene complexes as suitable electrophiles was demonstrated in the stereoselective synthesis of valuable molecules such as acetoxytubipofuran. In this synthesis, the nucleophilic addition of vinyllithium, followed by the oxidation of the metal center through the addition of iodomethane, leads to a migratory insertion of one of the CO ligands to the methyl group to form an acetyl ligand, which migrates subsequently to the endo face. The formed product acts as a nucleophile and reacts with additional iodomethane, and the metal center is subsequently oxidized to release the adduct for the upcoming synthetic steps (Scheme 24b).[124]

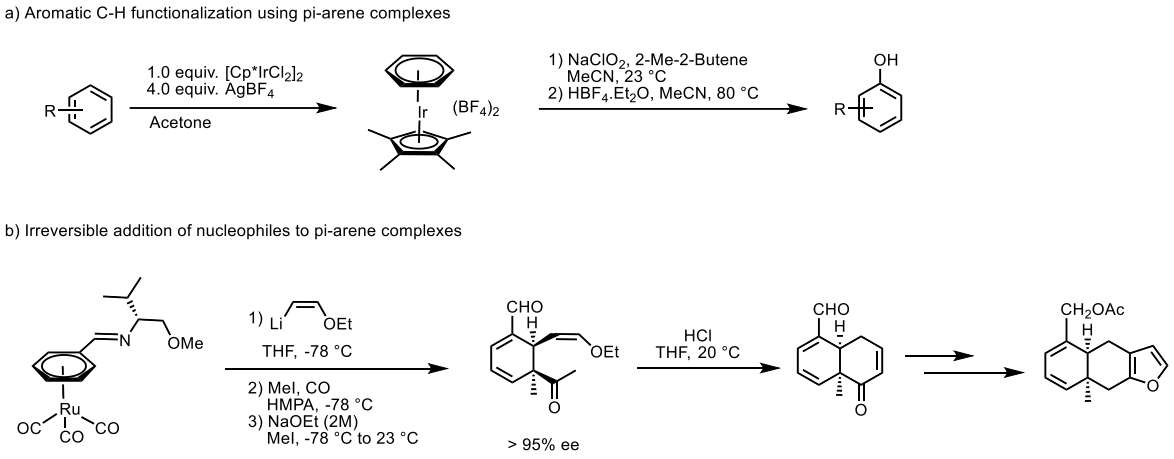

Scheme 24. Applications of η^6–arene complexes in C–H activation and stereo-selective synthesis.

The stereochemistry for the nucleophilic addition reactions was enhanced using chiral auxiliaries, chiral nucleophiles such as Evan's enolates, amino acids, or chiral ligands.[125–129]

2.1.3 Catalytic Applications of η^6–Arene Complexes

π-Coordination of arenes to transition metals alters their electronic properties from nucleophiles to electrophiles facilitating reactions that would not be achieved otherwise.[98,101] To use such reactivity in catalysis, the reactivity of the coordinated arene must be in balance with the exchange of the coordinated arene with another equivalent of the reactant arene.[98] The arene exchange mechanism was initially understood as a sequence of steps where the η^6–coordinated arene dissociates to η^4–coordinated arene and then to η^2–coordinated arene while the reactant arene coordinates to the metal center.[130] In 1984, Houghton and Voyle reported the first example of a catalytic reaction. The developed reaction enabled the cyclization of several derivatives of 3-(2-fluorophenyl)-propanol to the corresponding chroman via intramolecular nucleophilic substitution catalyzed by forming η^6–coordinated fluoroarenes (Scheme 25).[131] The relatively long reaction time and the limited substrate scope decreased the reaction's utility.

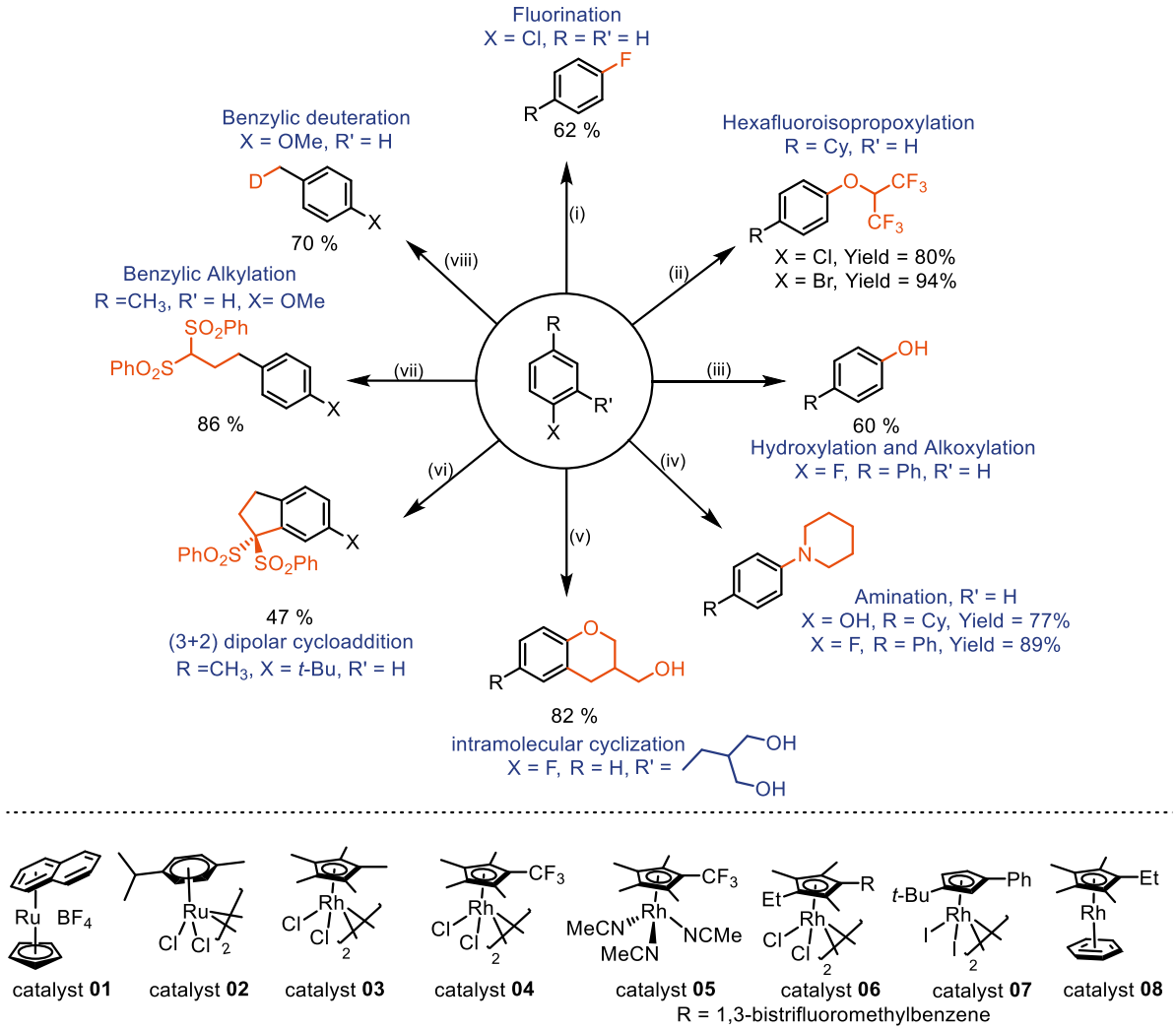

Scheme 25. Schematic illustration of catalytic π-arene activation reactions via η^6–coordination to transition metals. (i) Chlorobenzene (1.0 equiv.), catalyst **01** (10 mol%), CsF (2.0 equiv.), DMF, 140 °C, 14 days. (ii) Haloarene (1.0 equiv.), catalyst **04** (2.5 mol%), AgNTf (10 mol%), HFIP (10 equiv.), 80 °C. (iii) Fluoroarene (1.0 equiv.), catalyst **03** (2.5 mol%), AgOTf (10 mol%), H_2O (3.0 equiv.), THF, 150 °C. (iv) a- Phenol (1.0 equiv), catalyst **07** (2.5 mol%), Na_2CO_3 (10 mol%), Morpholine (3.0 equiv.), heptane, 120 °C, 24 h. b- Fluoroarene (1.0 equiv.), catalyst **02** (2.5 mol%), $AgPF_6$ (10 mol%), Ligand = $Ph_2P(C_2H_4OCH_3)$ (12 mol%), Morpholine (1.1 equiv.), 4 A° MS, 1,4-dioxane, 100 °C. (v) Fluoroalcohol (1.0 equiv.), catalyst **08** (0.1 equiv.), acetone (1.7 mL), nitromethane (8.7 mL), 80 °C, 6 h. (vi) Toluene derivative (1.0 equiv.), 1,1-bis(phenylsulfonyl)ethylene (3.0 equiv.), catalyst **07** (3.0 mol%), $AgBF_4$ (12 mol%), HFIP, 100 °C. (vii) Toluene derivative (1.0 equiv.), 1,1-bis(phenylsulfonyl)ethylene (1.1 equiv.), catalyst **07** (2.5 mol%), $AgPF_6$ (10 mol%), HFIP, 120 °c. (viii) Arene (1.0 equiv.), catalyst **05** (2.5 mol%), $AgNTf_2$ (10 mol%), Li_3PO_4 (10 mol%), acetone-*d6*, 120 °C.

Further attempts to achieve catalytic S_NAr reaction of aryl halides using ruthenium based catalyst instead of rhodium showed that it is possible to achieve catalytic amination of aryl chlorides. However, the reaction time must be extended up to 14 days, which comes at the expense of the substrate scope.[132] To harness such reactivity in catalysis, Shi and coworkers developed Ru/hemilabile-ligand-catalyzed nucleophilic amination (S_NAr) of aryl fluorides.[133] Shifting from ruthenium to rhodium, different rhodium catalysts were synthesized with different derivatives of

the Cp ligand. The synthesized rhodium complexes were used to achieve various transformations via π-arene activation. Recently, rhodium catalysts have been used in the amination of phenols, benzylic deuteration, dehydrogenative (3+2) cycloaddition of toluene derivatives, hydroxylation, alkoxylation of fluoroarenes and the hexafluoroisopropoxylation of aryl chlorides and aryl bromides (Scheme 25).[134–139] Despite the recent achievements, the utility of most of these reactions is limited due to slow arene exchange rates when a Cp or Cp* ligand is used, which necessitates high reaction temperatures that frequently exceed 120 °C, limiting the substrate scope. Transition metal complexes having ligands other than Cp derivatives have been reported to have a faster arene exchange. However, those complexes are less electrophilic, making them unsuitable for catalytic applications requiring an electrophilic arene.[140] Therefore, it is highly desirable to synthesize complexes based on new ligands that activate the coordinated arene similarly to ruthenium Cp complexes while possessing a fast arene exchange rate. Beyond ruthenium and rhodium, catalytic amounts of nickel complex, supported with an NHC ligand, were employed in π-arene activation where hydrogenolysis of aryl ethers was achieved.[141,142] A similar protocol was developed for the cross-coupling of aryl fluorides with amines in the presence of *t*-BuONa.[143] In general, substituents that increase arene's reactivity often reduce its capacity to undergo arene exchange, and achieving this precise balance is critical to enhancing a catalyst's turnover. Another issue complicating the arene exchange step is the displacement of the aromatic product with the starting material, which is frequently hampered by their relative thermodynamic stability. With both concerns in mind, careful consideration of substrates and ways for triggering arene exchange in stable complexes are required.[98]

2.1.4 Applications of η^6–Arene Complexes in Deoxyfluorination of Phenols

Fluorinated chemicals account for over 20% of the drug market, despite their scarce natural abundance.[141] Therefore, fluorination of aromatic molecules has attracted attention in medicinal chemistry, pharmaceutical industry, agriculture, and positron emission tomography (PET) as tracers.[144–147] PET is a non-invasive imaging technology utilized extensively in illness diagnosis and drug development.[148,149] The radiopharmaceutical industry relies heavily on ^{18}F-labeled medications due to the convenience of radioactive fluorine's half-life ($t_{1/2}$ = 109.8 min.).[150] Furthermore, producing ^{18}F-labeled molecules for PET utilizing simple and practical procedures is difficult.[149] Fluorination of aromatic pharmaceutical compounds plays an important role in PET, due to the fact that fluorine can be used as a hydrogen bioisoester. Hence, there is a need for simple and efficient methods to label complex drug molecules for clinical use.[151] When an ^{18}F-labeled medicine is ingested, the drug's disposition and certain biochemical transformations can

be traced, which is widely used in various applications such as cancer diagnoses, neuroimaging, and glycolysis studies.[152,153] Electrophilic fluorination involves the reaction of a nucleophilic carbon center with an electrophilic fluorinating agent such as *N*-fluoro-*o*-benzenedisulfonimide (NFOBS), *N*-fluorobenzenesulfonimide (NFSI), or Selectfluor (F-TEDA-PF_6).[154] However, this approach is rarely employed in organic synthesis due to its low selectivity.[154–156] In contrast, nucleophilic fluorination is often challenging due to the lower nucleophilicity of hydrated fluoride anions, which are less basic, while dry fluorides are highly basic nucleophiles.[157] Recently, chemoselective fluorination methods have been developed using transition metals, one of which is the silver-catalyzed late-stage fluorination of aryl stannanes.[155,158] This transformation enables selective fluorination of aryl stannanes, which are synthesized from the corresponding phenols, including natural products like estrone, strychnine, and polypeptides, using silver triflate and F-TEDA-PF_6.[155,158] The proposed mechanism involves transmetalation, oxidative addition of fluoride, and reductive elimination of silver to produce aryl fluorides (Scheme 26).[155]

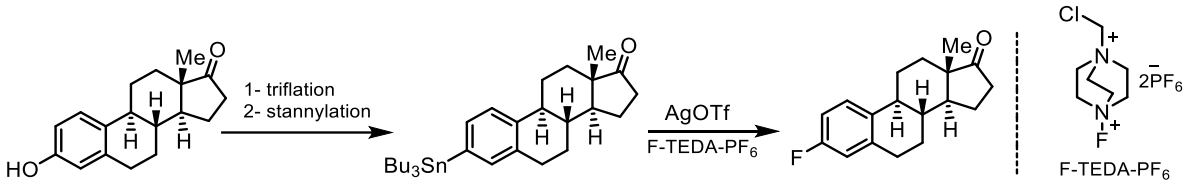

Scheme 26. Schematic illustration for the silver-mediated deoxyfluorination of estrone.

PhenoFluor is a powerful deoxyfluorinating reagent for phenols, demonstrated by a broad substrate scope and high functional group tolerance. The reaction proceeds via concerted nucleophilic aromatic substitution (CS_NAr) mechanism, where a neutral four-membered ring transition state is formed during the reaction (Scheme 27).[159–161] Despite the broad scope and the applicability of PhenoFluor in deoxyfluorination, electron-rich arenes remain challenging for radiofluorination. Therefore, the utility of this reaction in radiolabeling, specifically with radioactive fluoride, remains limited to phenols with electron-withdrawing substituents. To overcome this problem, a ruthenium-mediated deoxyfluorination reaction was developed to deoxyfluorinate electron-rich phenols. Electron-rich phenols were activated via facial coordination to ruthenium forming η^6–complexes where ‘‘umpolung’’ of the arene reactivity was achieved. The formed complexes were deoxyfluorinated, and subsequently, a decomplexation step was required to release the corresponding aryl fluorides. The reaction demonstrated an expanded substrate scope and exhibited good functional group tolerance (Scheme 27).[162] Moreover, following the same protocol, the coordination of tyrosine to ruthenium forms a stable complex that was used in

the synthesis of peptides. Subsequently, the deoxyfluorination of the tyrosine moiety of the synthesized peptides was successfully carried out to deliver ^{18}F-labeled peptides.[163,164]

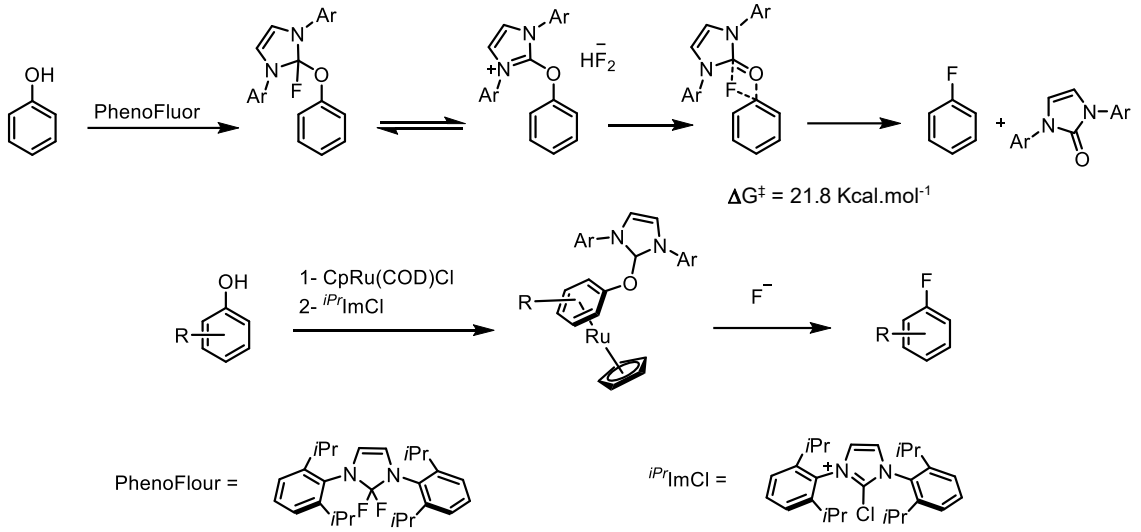

Scheme 27. Deoxyfluorination of phenols via CS_NAr mechanism.

Besides the importance of ruthenium complexes in radiolabeling, the same class of complexes was used in the hydrolysis of lignin ester as well as in the synthesis of various cytotoxic organometallics.[165,166]

2.1.5 Chemical Pathways for Decarboxylation

Carboxylic acids are abundant and stable feedstock of high synthetic utility. Upon a decarboxylative reaction, carbon dioxide is released as an easy-to-remove byproduct.[167] Hammick discovered that α-picolinic acid can be thermally decarboxylated upon heating to form an intermediate that reacts further with strong electrophiles such as ketones or aldehydes.[168–170] The Hammick intermediate was proposed as pyridine ylidene; however, recent studies proved that a carbene intermediate is formed which reacts with strong electrophiles faster than hydrogen transfer occurs (Scheme 28).[171,172] The reaction is limited to carboxylic acids possessing an α-nitrogen atom, such as α-picolinic acid derivatives and the α-carboxylic acids of quinoline and isoquinoline.[173]

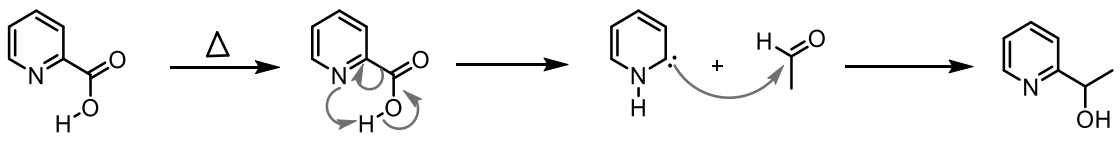

Scheme 28. Schematic illustration for the Hammick reaction of α-picolinic acid.

Protodecarboxylation is the simplest method by which a carboxylic group is replaced by a hydrogen atom. This strategy was widely used for simple carboxylic acids and in the synthesis of certain natural products.[109,174–176] In addition to classical protodecarboxylation, other hydrogen isotopes were used to label molecules.[177–179] Another approach was developed by Kochi and co-workers using silver persulfate to decarboxylate aliphatic carboxylic acids via a radical pathway.[180–182] However, due to the harsh reaction conditions, the scope of the developed reactions is limited to simple carboxylic acids. Therefore, various transition metal-catalyzed reactions were developed to achieve C(sp^2)−COOH decarboxylation. For instance, the decarboxylation of benzoic acid derivatives was achieved using different transition metal complexes such as copper,[62,183–187] palladium,[188] silver[183,185] or gold.[189–191]

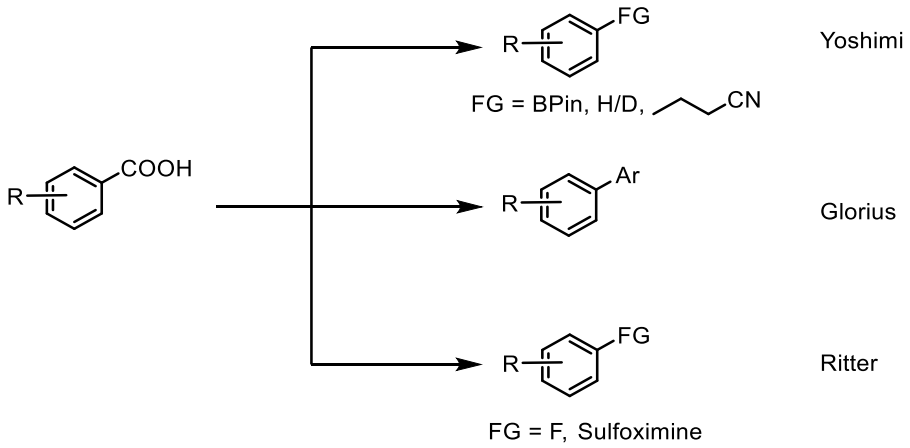

Scheme 29. Recent decarboxylative strategies involving aryl radical intermediates. (i) a- Borylation: Benzoic acid (1.0 equiv.), B_2Pin_2 (5.0 equiv.), photocatalyst (0.5 equiv.), MeCN:H_2O = 8:1, blue LED (405 nm, 18 W), 6 h, 30 °C. b- Protodecarboxylation or deuteration: Benzoic acid (1.0 equiv.), NaOH (1.0 equiv.), photocatalyst: Biphenyl (0.25 equiv.) and 1,4-dicyanonaphthalene (0.25 equiv.), MeCN:H_2O = 8:1 or CD_3CN:H_2O = 8:1 blue LED (405 nm, 18 W), 3 h, 30 °C. c- Cyanoalkylation: Benzoic acid (1.0 equiv.), cyanoethylene (5.0 equiv.), NaOH (1.0 equiv.), photocatalyst (0.5 equiv.), MeCN:H_2O = 9:1 blue LED (405 nm, 18 W), 3 h, 30 °C.

Despite the achievements, those methods are not widely applicable in organic synthesis due to the harsh conditions that lead to the formation of side products, especially for complex molecules. Recently, Ritter, Yoshimi, and Glorius developed light-mediated decarboxylative strategies by which aryl radical species are generated under mild conditions that can be subsequently trapped yielding decarboxylated functionalized arene from benzoic acid (Scheme 29).[192–194] For protodecarboxylation, Barton developed a strategy for carboxylic group deletion involving two steps via converting the carboxylic acid into the corresponding thiohydroxamate ester (Scheme 30) and subsequently radical decarboxylation via photo- or thermal cleavage was achieved followed by the abstraction of a hydrogen atom.[195,196] Following Barton's redox ester's protodecarboxylation strategy, efficient and cost-effective reactions were developed where

decarboxylation was achieved under mild conditions.[197] Baran developed redox-active esters that can be decarboxylated under mild conditions with less toxic, less odorous side products and more stable esters compared to Barton's method.[198] Subsequently, based on NHPI redox-active esters, several strategies for decarboxylation were developed with a broader substrate scope and a higher functional group tolerance (Scheme 30).[199–204]

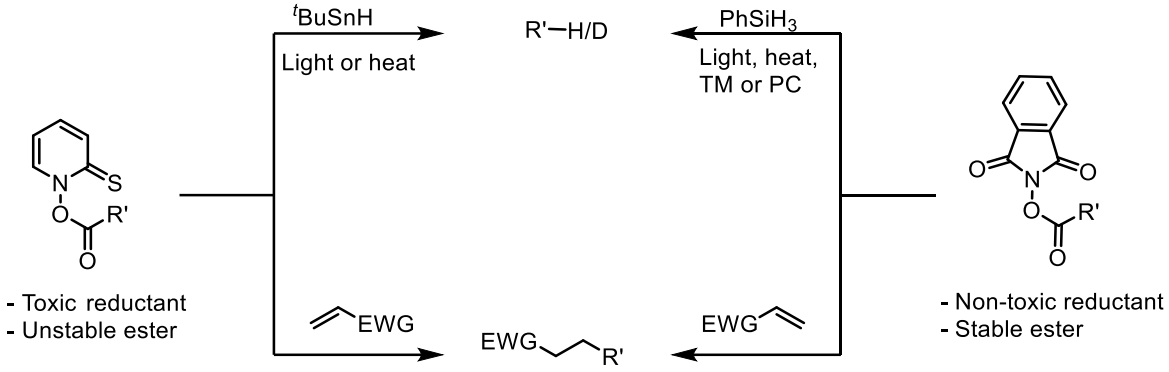

Scheme 30. Comparison between Barton's redox-active esters to Baran's redox-active esters.

Despite the examples and modifications of the achieved decarboxylation reactions via redox-active esters, those methods usually require an additional step for the activation of the carboxylic acids, in addition to the need for a high number of equivalents of the hydrogen donors. To overcome this impracticality, Nicewicz developed a photocatalytic protodecarboxylation strategy using acridinium as a highly reductive photoredox catalyst ($E_{1/2}$>2 vs SCE) in its excited state. Despite the ability of the acridinium photocatalyst to drive radical decarboxylation, the extremely oxidizing nature of its excited state results in low selectivity oxidation in the presence of other oxidatively-labile functional groups, such as electron-rich arenes, and olefins, limiting the scope of this method to simple and/or highly activated carboxylic acid.[205–209] Recently, West and co-workers developed a chemoselective decarboxylative protonation using Earth-abundant iron photocatalysis. The developed technique uses a synergistic combination of iron and hydrogen atom transfer catalysts, eliminating the need for expensive photoredox catalysts, toxic hydrogen atom sources, high temperatures, powerful oxidants, and pre-activation of acid substrates.[210]

2.2 Objective

The synthesis of radiolabeled aryl fluorides from non-radioactive aryl fluorides is a challenge in organic synthesis. This project aims to convert aryl fluorides into radioactively labeled ^{18}F-aryl fluorides using η^6–ruthenium complexes. The process shall begin with the activation of aryl fluorides via facial coordination to ruthenium complexes. Different ruthenium complexes with different phenoxo ligands shall be tested and evaluated regarding their ability to coordinate with aryl fluorides. Once coordination is achieved, the coordinated fluoroarenes shall be converted to the corresponding phenols without decomplexation under suitable reaction conditions. The next step involves deoxyfluorination of the phenol moiety of the synthesized complexes. The last step is the subsequent detachment of the arene from the ruthenium complex through suitable decomplexation conditions. To optimize these processes, various deoxyfluorination strategies shall be tested, and reaction conditions shall be optimized to shorten the reaction time. Additionally, the decomplexation step shall be optimized to minimize reaction time.

2.3 Results and Discussion

Parts of this chapter are adapted, with permission, from our published work in the Journal of the American Chemical Society. [214] *The concept of arene exchange using ruthenium phenoxo complexes and its application in catalysis was developed by Tim Schulte. The catalytic decarboxylation reaction of phenylacetic acid derivatives using ruthenium was discovered and optimized by the author. All experimental results involving the synthesis of ruthenium complexes presented in this work were conducted by the author, except for compounds* ***5a–d****, which were synthesized and reported by Tim Schulte.*[214]

The η^6–coordination of an electron-rich arene to ruthenium induces an ‘‘umpolung’’ of its reactivity, effectively transforming it from a nucleophilic to an electrophilic species.[100,114] This reactivity was explored using ruthenium complexes supported by phenoxo ancillary ligands, aiming to facilitate the hydrolysis of fluoroarenes to their corresponding phenols. Additionally, the potential for catalytic activation of benzylic C–H bonds was investigated as a complementary aspect of this study.

2.3.1 Hydrolysis of fluoroarenes

To achieve stoichiometric coordination of fluoroarenes to ruthenium via arene exchange and to convert the coordinated aryl fluorides to phenols, a series of ruthenium phenoxo complexes were synthesized and evaluated (scheme 31).

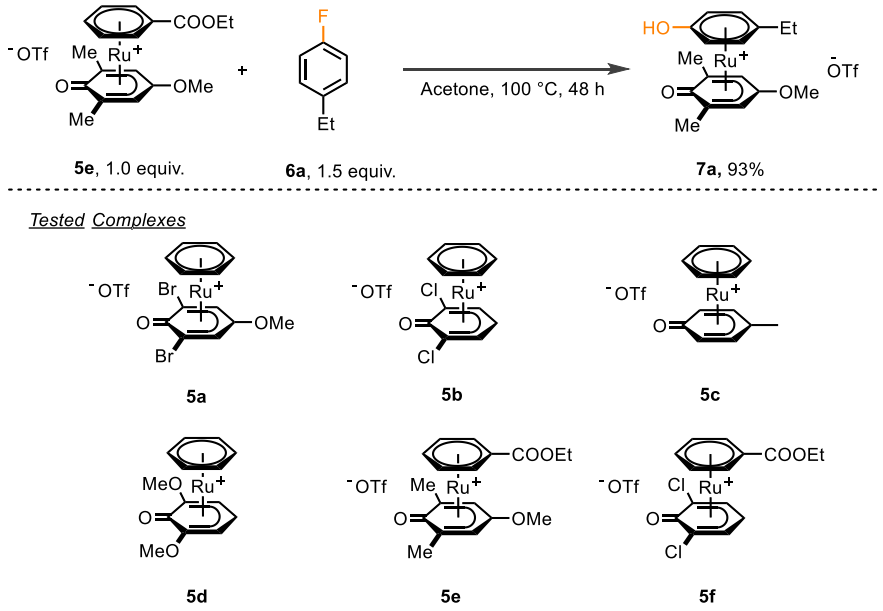

Scheme 31. Complexation of of 4-ethylfluorobenzene followed by hydrolysis of the C–F bond in acetone.

Table 4. Optimization of the arene exchange reaction and hydrolysis of the C–F bond.

Entry	Change in reaction conditions	Yield [%]
1	Dioxane instead of acetone	72
2	DCE instead of acetone	84
3	THF instead of acetone	17
4	Acetonitrile instead of acetone	n.d.[a]
5	DMF instead of acetone	n.d.[a]
6	Methanol instead of acetone	n.d.[a]
7	Additional equivalent of TBAOMs	24
8	Complex **5a** instead of **5e**	decomposition[b]
9	Complex **5b** instead of **5e**	decomposition[b]
10	Complex **5c** instead of **5e**	decomposition[b]
11	Complex **5d** instead of **5e**	decomposition[b]
12	Complex **5f** instead of **5e**	decomposition[b]

[a]the desired product was not detected via NMR spectroscopy or MS spectroscopy. [b]The reaction was incomplete, and the starting complex and the desired product were not obtained; however, the starting complex was detected in the reaction mixture, where it was not fully decomposed.

The main challenge involved the coordination of the desired fluoroarenes to ruthenium and the subsequent conversion of the C–F bond to a C–OH bond. Despite complexes **5a** and **5b** being known to have faster arene exchange, attempts to use them stoichiometrically were not successful where the reaction was not complete which made separation of the desired complex from the starting material not possible. Notably, the reaction demonstrated improved efficiency when complex **5e** was employed, with 4-ethylfluorobenzene **2c** serving as the model substrate (Scheme 31). The high yield is likely attributed to the change of the leaving group from benzene to ethyl benzoate as well as the simplicity of **2C** where it does not possess any sigma donor group. Additionally, in complex **5e,** the change of the leaving arene from benzene to ethyl benzoate results in a weaker coordination of the ethyl benzoate compared to benzene. To expand the utility

of the transformation, several fluoroarenes have been used to synthesize the corresponding π-arene ruthenium complexes. It was observed that the arene exchange of fluoroarene with the ethyl benzoate ligand is feasible for simple arenes (Scheme 32). At the same time, complex fluoroarenes appeared to be challenging and led to side reactions where the desired product was not obtained. For more challenging substrates, including small drug molecules, such as Sulindac **6g**, the synthesis of the desired complexes was unsuccessful. The starting complex **5e** decomposed, leading to the formation of unknown side products through side reactions that were not possible to identify.

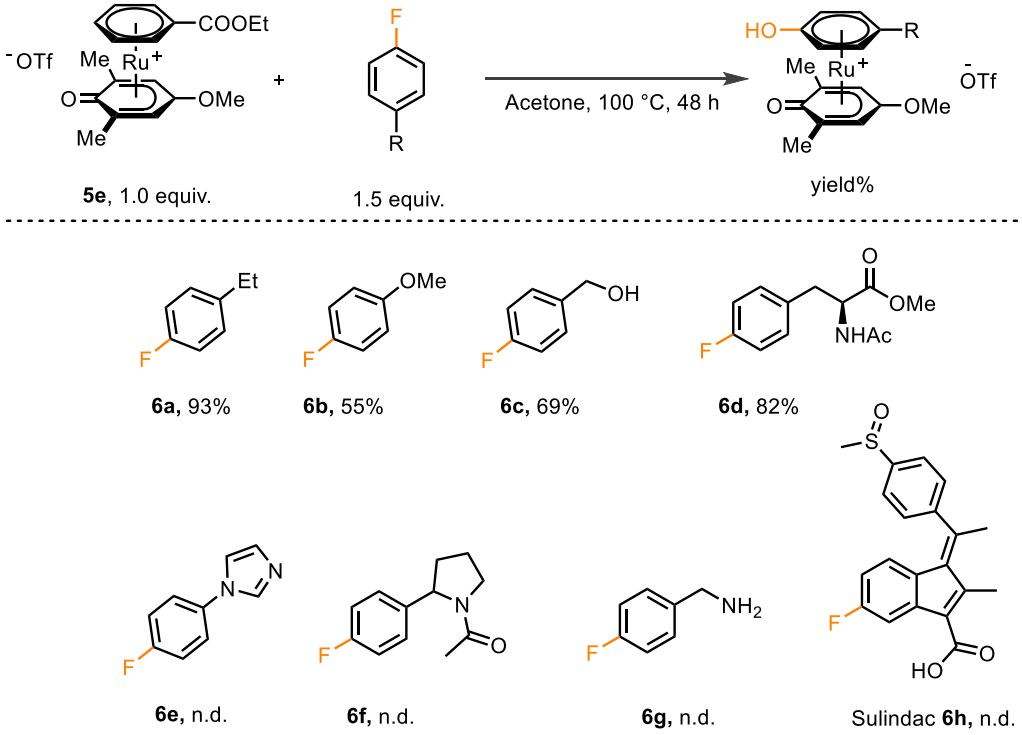

Scheme 32. Substrate scope for the complexation of fluoroarenes and the subsequent hydrolysis using complex **5e**.

The replacement of a hydroxyl substituent with its bioisoesters is an attractive transformation in medicinal chemistry.[164] Therefore, the complexation of phenols to ruthenium phenoxo complexes was evaluated using **5e**. While the coordination of Estrone **8a** proved that the coordination of phenols is possible, the functional group tolerance was notably limited when different phenols were tested. For instance, starting with simple phenols such as paracetamol **8b** and ezetimibe **8e**, it was observed that complex **5e** has decomposed.

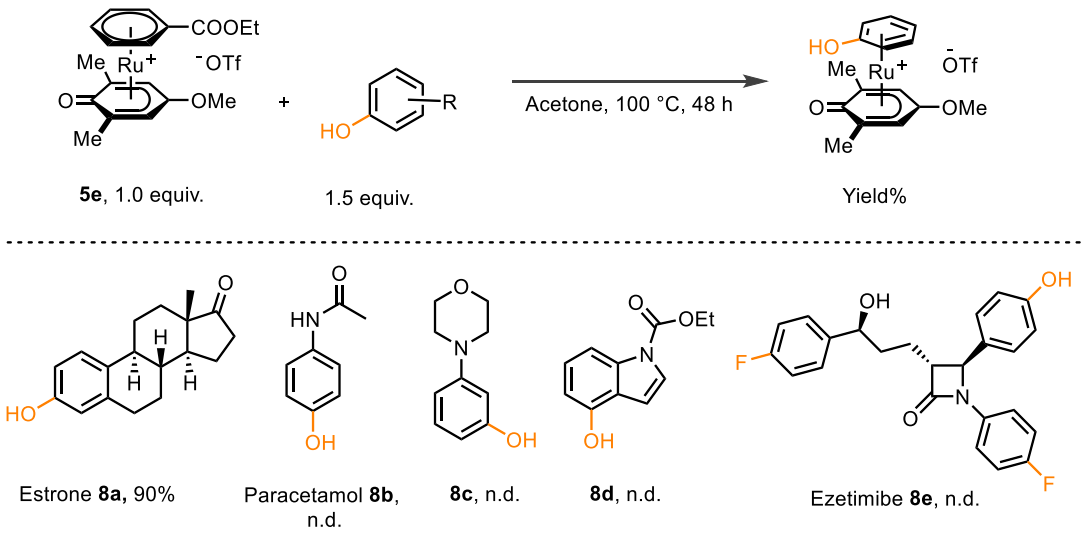

Decomposition of **5e** was observed when substrates **8b-e** were tested and the desired product was not detected

Scheme 33. Substrate scope for the η^6–coordination of phenols to **5e** via arene exchange.

2.3.2 Deoxyfluorination of the η^6–coordinated phenols

The main goal of the project was to synthesize radioactive fluoroarenes starting with non-radioactive fluoroarenes. Therefore, at first, the deoxyfluorination of arene complexes was attempted using non-radioactive fluoride sources to evaluate if the deoxyfluorination reaction of the developed complexes was achievable. For the reaction optimization (table 5), complexes **7a** and **9** were used as model substrates (Scheme 34). It was observed that changing the counter anion of the deoxyfluorinating reagent from triflate to chloride resulted in a noticeable decrease in reactivity, possibly due to the ability of chloride anions to coordinate to ruthenium is better than triflate, which may result in an intermediate that inhibits the reaction. Furthermore, substituting CsF with either TMAF or TBAF did not improve the yield. This outcome is likely attributed to the lower lattice energy of these reagents compared to CsF, which may hinder their efficiency in the reaction.

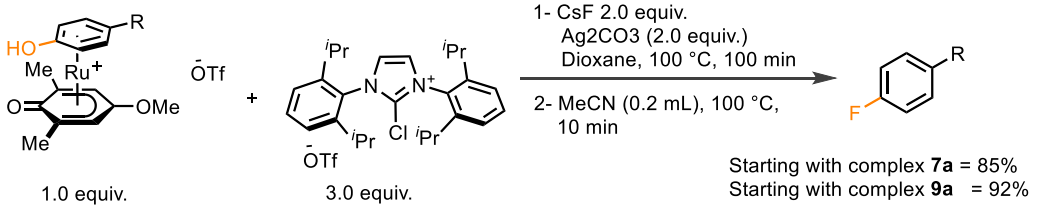

Scheme34. Deoxyfluorination of η^6–coordinated phenols.

Table 5. Optimization of the deoxyfluorination reaction.

Entry	Complex	Change in reaction conditions	Yield [%]
1	**7a**	Acetonitrile instead of Dioxane	30
2	**7a**	Acetone instead of Dioxane	50
3	**7a**	THF instead of Dioxane	23
4	**7a**	DMF instead of Dioxane	80
5	**7a**	No silver carbonate	75
6	**9a**	-	92
7	**9a**	80 °C instead of 100 °C	41
8	**9a**	AgOMs instead of Ag_2CO_3	08
9	**9a**	AgOTf instead of Ag_2CO_3	10
10	**9a**	DMF instead of acetonitrile	47
11	**9a**	Triphenylphosphine instead of acetonitrile	n.d.
12	**9a**	Triethylamine instead of acetonitrile	n.d.
13	**9a**	Pyridine instead of acetonitrile	n.d.
14	**9a**	TMAF instead of CsF	81
15	**9a**	TBAF instead of CsF	87
16	**9a**	Changing the counter anion in ^{iPr}ImCl from OTf to Cl	75

It was observed that by substituting silver carbonated with either silver triflate or silver mesylate, the fluorinated product was not obtained. On the other hand, after the fluorination step, it was observed that the addition of strong sigma donor ligands did not enhance the decomplexation of the arene. The addition of triphenylphosphine to the reaction medium turned it immediately to black where the complex decomposed, and the desired product was not obtained.

2.3.3 Benzylic decarboxylation via π-arene activation

π arene activation via η^6–coordination to transition metals results in the activation of the benzylic position of arenes. During attempts to hydrolyze the η^6–coordinated fluoroarenes to phenols, using 4-fluorophenylacetic acid **6i** as a substrate resulted in stoichiometric decarboxylation (Scheme 35).

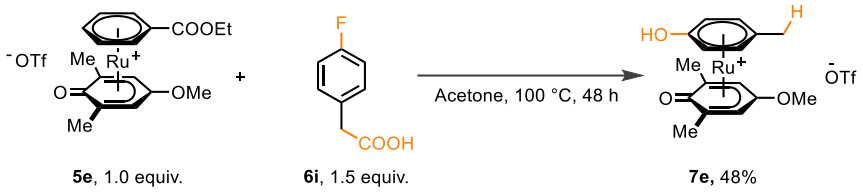

Scheme 35. Simultaneous hydrolysis and decarboxylation of 4-fluorophenylacetic acid via η^6– coordination.

To harness this reactivity, complexes **5a** and **5b**, identified as promising candidates for catalytic arene activation via η^6–coordination,[214] were used to catalyze the benzylic decarboxylation of phenylacetic acid derivatives (Scheme 36). Moreover, ibuprofen, a phenylacetic acid derivative, was employed as a model substrate to optimize the reaction conditions (Table 6) for the potential catalytic decarboxylation at the benzylic position. During the optimization of the reaction, it was observed that switching the catalyst to **5b** resulted in a lower yield. Alternatively, using either **5c** or **5e** led to diminished reactivity, likely due to their limited turnover capability at the given temperature. Additionally, maintaining a catalyst loading of 10 mol% was critical, as reducing the loading resulted in lower yields. This lower yield is presumably attributed to the slow arene exchange, as the starting material is more electron-deficient than the product, which favors the coordination of the product which competes with the substrate. Additionally, changing the additive from TBA-OMS to TBA-NTF led to a lower yield, possibly due to its higher affinity of the latter to coordinate to the ruthenium. The addition of an organic or inorganic base led to a diminished reactivity which indicates that phenylacetic acid cannot be deprotonated prior to the reaction.

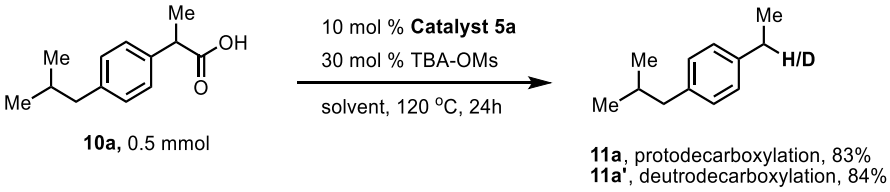

Scheme 36. Catalytic decarboxylation of Ibuprofen via π–arene activation.

Table 6. Optimization of the protodecarboxylation of Ibuprofen via π-arene activation.

Entry	Change in reaction conditions	Yield%
1	DCE as a solvent	83
2	Acetone-*d6* instead of DCE (deuteration)	83
3	Reaction time was 18 h	74
4	DCE as solvent at 1.0 mmol scale	76
5	Catalyst loading lowered to 1.0 mol%	12
6	Catalyst loading lowered to 5.0 mol%	41
7	1.0 equiv. of Cs_2CO_3 was used as an additive	<5
8	2.0 equiv. of DIPEA was used as an additive	<5
9	2.0 equiv. of CsF was used as an additive	<5
10	2.0 equiv. of Ag_2CO_3 was used as an additive	<5
11	2.0 equiv. 2,6-*t*Bu-pyridine was used as an additive	<5
12	Catalyst **5b** instead of **5a** in DCE	62
13	Catalyst **5b** instead of **5a** in Acetone-*d6*	51
14	Catalyst **5c** instead of **5a** in DCE	5
15	Catalyst **5c** instead of **5a** in Acetone-*d6*	15
16	Catalyst **5e** instead of **5a** in DCE	<5
17	Dioxane instead of DCE	26
18	Without adding TBA-OMs	<5
19	TBA-NTf instead of TBA-OMs	37

Various phenylacetic acid derivatives were evaluated for protodecarboxylation (Scheme 37). Additionally, when deuterated acetone was employed, as with substrates **11a** and **11b**, deuterodecarboxylation occurred. Additionally, reactions conducted with substrates **11a** and **11b** in deuterated acetone showed partial benzylic C–H deuteration. Notably, despite the presence of

a second benzylic position in Ibuprofen **11a**, no C–H deuteration was observed, likely due to steric hindrance from the adjacent isopropyl substituent. While efficient decarboxylation was achieved with the substrates mentioned, more complex substrates proved challenging, particularly those containing strong sigma-donor or pi-donor groups. Consequently, the reaction was limited to simple phenylacetic acid derivatives. Protodecarboxylation was successfully achieved when DCE was used as a solvent.

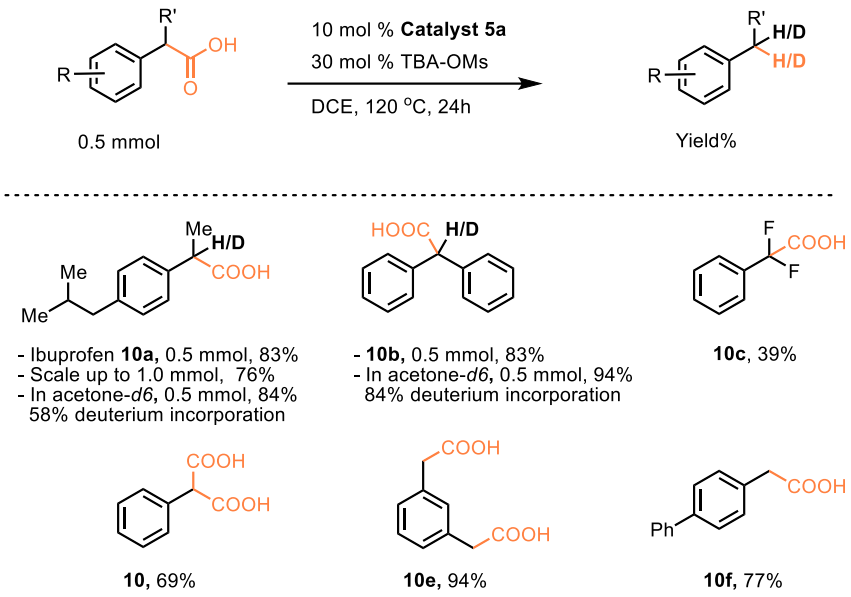

Scheme 37. Substrate scope for benzylic protodecarboxylation via π-arene activation.

2.3.4 Mechanistic investigation

To gain insight into the decarboxylation mechanism and expand the applicability of this reactivity, various experiments were conducted to reveal the reaction mechanism. Therefore, radical trapping reagents were introduced into the standard reaction setup (Table 7). Additionally, the reactions with different radical trapping reagents were performed under blue LED irradiation instead of thermal conditions. However, no product formation was observed, and the original decarboxylation reactivity was suppressed. Efforts to trap a radical intermediate were unsuccessful, suggesting that the reaction proceeds without the involvement of radical intermediates.

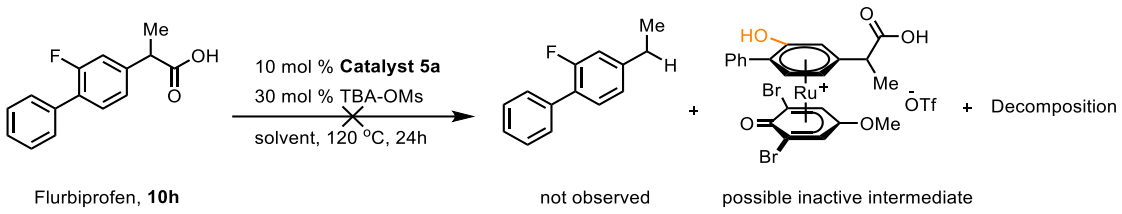

Scheme 38. Unsuccessful protodecarboxylation of flurbiprofen.

To elucidate the reaction mechanism, a series of experiments were performed. Reactions conducted in the absence of **5a**, in the presence of ruthenium chloride instead of **5a**, and with **5e** as an alternative catalyst to **5a**, all failed to yield the desired product. To further probe whether the mechanism involves an η^6–intermediate, flurbiprofen **10h** was chosen as a model substrate. However, the reaction did not result in the target product, likely due to the arene exchange of the electron-rich arene followed by C–F bond hydrolysis. The results obtained using **5e** as a catalyst (Scheme 35), along with the potential formation of a catalytically inactive complex (Scheme 38), suggest that the reaction proceeds via η^6–coordination.

Table7: Radical trapping experiments

Entry	Radical trap	Equivalents	R	Conversion%
1	CCl_4	5.0	Cl	<5
2	CBr_4	5.0	Br	<5
3	Selectfluor	3.0	F	<5
4	1,2-dibromoethane	5.0	Br	<5
5	I_2	3.0	I	<5
6	B_2Pin_2	2.0	BPin	<5
7[a]	Acetone-d_6	1.0	H/D	<5
8[a]	AIBN	1.0	CMe_2CN	<5
9[a]	B_2Pin_2	1.0	BPin	<5

[a] reactions were irradiated with blue LED Kessel lamps in acetone at room temperature for 16 h.

The experimental data provided no evidence for either single-electron transfer (SET) in the reaction mechanism. As an alternative pathway, thermal decarboxylation was proposed, initiated by the η^6–coordination of phenylacetic acid to ruthenium to yield intermediate (**I**). This facial coordination of the phenylacetic acid significantly increases its acidity, facilitating its

deprotonation, which results in a stabilized carboxylate group. Following deprotonation, the negative charge is stabilized by Ru(II) and subsequently, the extrusion of CO_2 leads to the formation of a neutral ruthenium intermediate (**II**), which can subsequently undergo protonation and decomplexation to yield the product. The addition of a base was found to suppress the reaction, possibly due to the coordination of the carboxylate group to ruthenium, forming different undesired complexes that do not undergo further arene exchange. Furthermore, reactions conducted in deuterated solvents yielded exclusively deuterated products, supporting a deprotonation–protonation sequence.

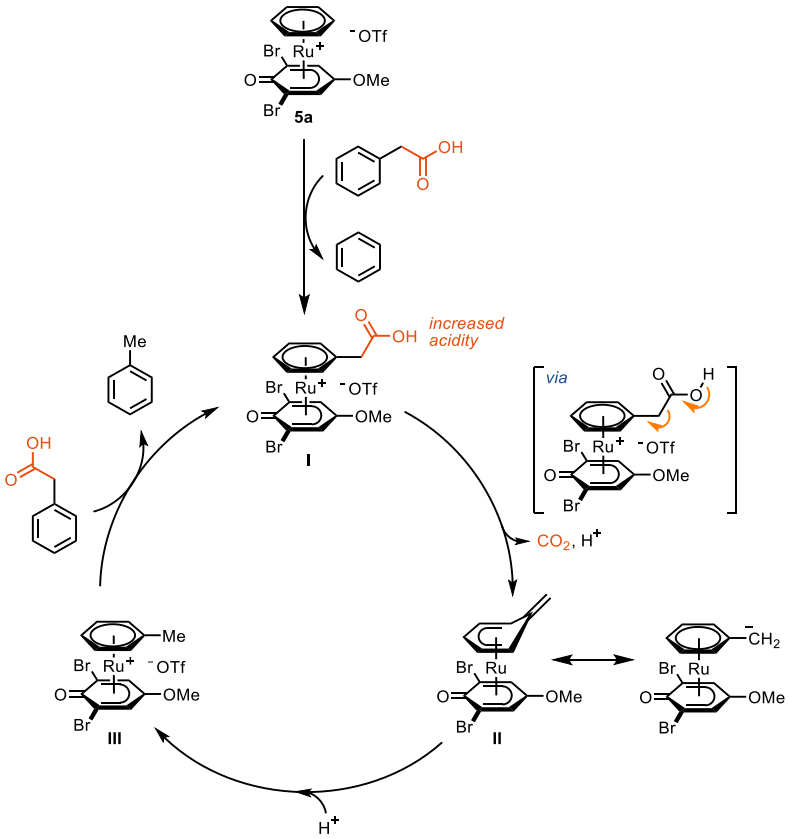

Scheme 39. Proposed catalytic cycle for the protodecarboxylation of phenylacetic acids with **5a**.

Additionally, to explore the reactivity based on the proposed intermediate (**II**), 1,1-bis(phenylsulfonyl)ethylene was employed as a reagent to attempt a 1,3-dipolar cycloaddition. However, no product formation was observed, possibly because of the lower nucleophilicity of (**II**), which diminishes its ability to react with the alkene.

2.4 Conclusion

In conclusion, ruthenium phenoxo complex **5e** was used in stoichiometric arene exchange with simple aryl fluorides. Catalytic decarboxylation of different phenylacetic acid derivatives was performed using complex **5a**. In ruthenium phenoxo complexes, the structure of the phenoxo ligand is critical in achieving the desired transformations.

The use of [η^6–ethylbenzoate-η^5-(2,6-dimethyl-4-methoxy-1-phenoxo)Ru](OTf) **5e** enabled stoichiometric arene exchange of aryl fluorides, followed by hydrolysis of the fluoroarenes to the corresponding phenols in a one-pot reaction. However, this transformation was limited to simple fluoroarenes and required elevated temperatures and extended reaction times.

The use of [η^6–ethyl benzoate-η^5-(2,6-dimethy-4-methoxy-1-phenoxo)Ru](OTf) **5a** was successfully applied in the catalytic benzylic decarboxylation of various phenylacetic acid derivatives. This reaction proceeded efficiently via π-arene activation but is unsuitable for more complex substrates.

3. Experimental results

3.1.1 Materials and Methods

All reactions were carried out under ambient conditions unless otherwise stated. Concentration under reduced pressure was performed by rotary evaporation at 25–45°C at an appropriate pressure. Purified compounds were further dried under vacuum (10^{-6}–10^{-3} bar). Yields refer to purified and spectroscopically pure compounds or mixtures of constitutional isomers. All air- and moisture-sensitive manipulations were performed using standard *Schlenk* and glove-box techniques under an atmosphere of argon or nitrogen. Initial confirmation tests to determine the product formation were checked by LC–MS and GC–MS. Fully characterized compounds were supported by NMR and HRMS data.

3.1 General

3.1.2 Solvents

Anhydrous solutions, *i.e.* dichloromethane, acetonitrile, toluene, and tetrahydrofuran were obtained from PSDS “Phoenix Solvent Drying Systems”. Deuterated solvents were purchased from Euriso-Top. Organic solvents were purchased from Sigma Aldrich unless otherwise stated.

3.1.3 Chromatography

Thin layer chromatography (TLC) analysis was performed using EMD TLC silica gel 60 F_{254} plates pre-coated with 250 µm thickness silica gel 60 F_{254} and visualized by fluorescence quenching under UV light and $KMnO_4$ stain or cerium ammonium molybdate satin. For column chromatography, flash silica gel (40–63 µm particle size) was purchased from Geduran.

3.1.4 Equipment

High-resolution mass spectra were obtained using *Q Exactive Plus* from *Thermo*. NMR spectra were recorded on a Bruker *Ascend*^{TM} 500 spectrometer operating at 500 MHz, 471 MHz, and 125 MHz, for ^{1}H, ^{19}F, and ^{13}C acquisitions, respectively. Chemical shifts are reported in ppm with the solvent residual peak as the internal standard.[211] For ^{1}H NMR: $CDCl_3$, δ 7.26; CD_3OD, δ 3.31; $(CD_3)_2SO$, δ 2.50; CD_3CN, δ 1.94, CD_2Cl_2, δ 5.32. For ^{13}C NMR: $CDCl_3$, δ 77.16; CD_3OD, δ 49.00; $(CD_3)_2SO$, δ 39.52; CD_3CN, δ 1.32, CD_2Cl_2, δ 53.84. Data is reported as follows: s = singlet, d = doublet, t = triplet, q = quartet, m = multiplet, br = broad; coupling constants in Hz.

3.1.5 Starting materials

All chemical reagents and materials were used as received from commercial suppliers without any further purification unless otherwise stated.

Synthesis of 4-(2-cyanobenzyl)dibenzothiophene (1a)

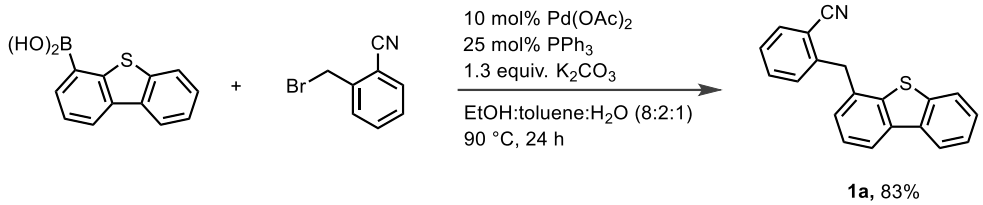

1a, 83%

A 300 mL pressure tube equipped with a Teflon-coated magnetic stirring bar was charged with $Pd(OAc)_2$ (536 mg, 2.34 mmol, 0.10 equiv.), PPh_3 (1.86 g, 7.03 mmol, 0.300 equiv.), dibenzothiophene-4-boronic acid (5.40 g, 23.4 mmol, 1.00 equiv.), 2-cyanobenzyl bromide (6.03 g, 30.5 mmol, 1.30 equiv.) and K_2CO_3 (4.25 g, 30.5 mmol, 1.30 equiv.). The starting materials were suspended in a mixture of EtOH : toluene : H_2O (8:2:1) (100 mL). The reaction mixture was degassed by bubbling argon through the suspension for one minute. The pressure tube was sealed, transferred to a preheated oil bath, and stirred at 90 °C for 24 h. Afterwards, the reaction was allowed to cool down to room temperature and filtered through a short plug of Celite. The filter cake was washed with ethyl acetate (100 mL), and the filtrate was diluted with water (50 mL) and subsequently transferred into a separatory funnel. The layers were separated, and the aqueous layer was extracted with ethyl acetate (3 x 50 mL). The organic layers were combined, dried over anhydrous Na_2SO_4, and concentrated under reduced pressure. The resulting residue was purified by column chromatography on silica gel eluting with a solvent mixture of hexanes / DCM (90:10 gradient to 65:35 (v/v)) to afford 5.85 g (83%) of desired product **1a** as a colorless solid.

R*f* = 0.35 (hexanes/EtOAc, 9:1 (v:v))

NMR Spectroscopy:

^{1}H NMR (500 MHz, $CDCl_3$, 23 ºC, δ): 8.19 – 8.14 (m, 1H), 8.09 (d, *J* = 8.0 Hz, 1H), 7.87 – 7.81 (m, 1H), 7.70 (dd, *J* = 7.8, 1.4 Hz, 1H), 7.50 – 7.43 (m, 4H), 7.36 – 7.25 (m, 3H), 4.50 (s, 2H).

^{13}C NMR (126 MHz, $CDCl_3$, 23 ºC, δ): 144.7, 143.4, 142.7, 140.2, 137.8, 137.2, 133.3, 133.3, 133.2, 132.7, 131.4, 130.7, 129.8, 127.5, 122.2, 120.7, 118.2, 113.1, 36.8.

HRMS-EI (m/z) calc'd for $C_{20}H_{13}N_1S_1$ $[M]^+$, 299.0763; found, 299.0766; deviation: – 0.8 ppm.

Synthesis of 4-(2-cyanobenzyl)dibenzothiophene *S*-oxide (1b)

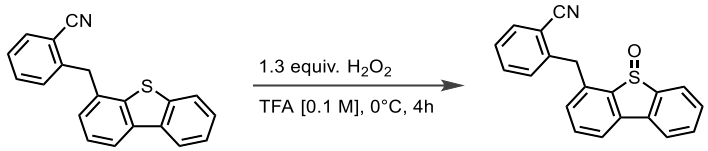

1a **1b,** 99%

In a 100 mL round bottom flask, 4-(2-cyanobenzyl)dibenzothiophene **1a** (5.48 g, 18.1 mmol, 1.00 equiv.) was suspended in trifluoroacetic acid (18 mL) and cooled to 0 °C (water/ice bath). Hydrogen peroxide solution (35 wt. % in H_2O, 2.28 mL, 2.28 g, 23.6 mmol, 1.30 equiv.) was added dropwise to the reaction mixture within 1 min. The reaction mixture was allowed to stir at 0 °C until starting material was consumed. The reaction completion was confirmed by TLC, where a clear solution was observed at this point. The reaction mixture was poured onto a mixture of ice (100 g), saturated aqueous Na_2CO_3 solution (100 mL), and DCM (100 mL). The entire mixture was transferred into a separatory funnel and the layers were separated. The DCM layer was collected, and the aqueous layer was extracted with DCM (4 × 60 mL). The combined organic layer was dried over Na_2SO_4, filtered, and the solvent was removed under reduced pressure. The residue was washed with hexanes (2 × 10 mL) and dried in vacuo to afford 5.75 g (99%) of desired product **1b** as a colorless solid.

$\mathbf{R_f}$ = 0.38 (DCM/MeOH, 98:2 (v:v))

NMR Spectroscopy:

^{1}H NMR (500 MHz, $CDCl_3$, 23 ºC, δ): 7.98 (d, *J* = 7.6 Hz, 1H), 7.80 (d, *J* = 7.6 Hz, 1H), 7.69 (t, *J* = 7.6 Hz, 2H), 7.59 (t, *J* = 7.6 Hz, 1H), 7.57 – 7.47 (m, 4H), 7.35 (t, *J* = 7.4 Hz, 1H), 7.20 (d, *J* = 7.7 Hz, 1H), 4.76 (d, *J* = 15.7 Hz, 1H), 4.62 (d, *J* = 15.7 Hz, 1H).

^{13}C NMR (126 MHz, $CDCl_3$, 23 ºC, δ): 142.9, 139.6, 139.2, 136.2, 136.0, 133.1, 133.0, 130.1, 127.6, 127.3, 127.0, 125.1, 124.7, 123.0, 121.9, 120.5, 118.2, 113.1, 39.3.

HRMS-ESIpos (m/z) calc'd for $C_{20}H_{13}O_1N_1Na_1S_1$ $[M + Na]^+$, 338.0610; found, 338.0611; deviation: – 0.3 ppm.

Synthesis of derived aryl 4-(2-cyanobenzyl)dibenzothiophenium salts

Fluorobenzene derived 4-(2-cyanobenzyl)dibenzothiophenium salt (3a)

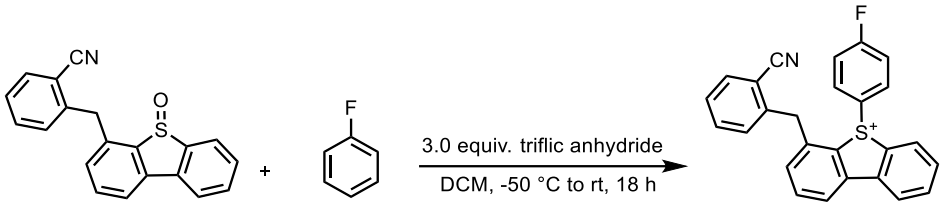

1b, 1 equiv. **2a**, 3.0 equiv. **3a,** 66%

In a flame dried round bottom flask, 4-(2-cyanobenzyl)dibenzothiophene *S*-oxide **1b** (637 mg, 2.00 mmol, 1.00 equiv.) was dissolved in dry DCM (20 mL). The solution was cooled down to -50 °C using dry ice–acetone bath. Subsequently, fluorobenzene **2a** (0.65 mL, 648 mg, 6.00 mmol, 3.00 equiv.) was added followed by dropwise addition of trifluoromethanesulfonic anhydride (1.00 mL, 1.69 g, 6.00 mmol, 3.00 equiv.). The reaction mixture was allowed to warm gradually to room temperature over 16 h. Afterwards, the reaction was quenched by the addition of saturated aqueous Na_2CO_3 solution (5.0 mL). The entire mixture was transferred into a separatory funnel and the layers were separated. The DCM layer was collected, and the aqueous layer was further extracted with DCM (4 × ca. 50 mL). The combined organic layer was dried over Na_2SO_4, filtered and the solvent was removed under reduced pressure. The resulting residue was purified by column chromatography on silica gel eluting with a solvent mixture of DCM / MeOH (100:0 gradient to 95:5 (v/v)) to afford 709 mg (65%) of desired product **3a** as an off-white solid.

R_f = 0.33 (DCM/MeOH, 95:5 (v:v))

NMR Spectroscopy:

^{1}H NMR (500 MHz, $CDCl_3$, 23 ºC, δ): 8.26 (d, *J* = 8.1 Hz, 1H), 8.18 (dd, *J* = 14.7, 7.4 Hz, 2H), 7.84 (q, *J* = 7.0 Hz, 2H), 7.74 (dd, *J* = 9.1, 4.7 Hz, 2H), 7.64 – 7.53 (m, 3H), 7.39 (t, *J* = 7.7 Hz, 1H), 7.28 – 7.16 (m, 4H), 4.38 (d, *J* = 16.6 Hz, 1H), 4.15 (d, *J* = 16.5 Hz, 1H)

^{13}C NMR (126 MHz, $CDCl_3$, 23 ºC, δ): 167.7, 165.6, 140.3, 139.6, 139.4, 138.6, 135.7, 134.7, 134.0, 133.9, 133.8, 133.4, 132.5, 132.2, 132.1, 131.0, 130.1, 129.0, 128.6, 124.7, 124.5, 123.4, 122.2, 119.7, 119.6, 119.6, 119.4, 119.4, 117.4, 112.9, 38.1.

^{19}F NMR (471 MHz, $CDCl_3$, 23 ºC, δ): 99.1 (tt, *J* = 8.11, 4.50 Hz, 1F), 78.2 (s, 3F).

HRMS-ESIpos (m/z) calc'd for $C_{26}H_{17}F_1N_1S_1$ $[M - OTf]^+$, 394.1060; found, 394.1062; deviation: –0.4 ppm.

Anisole derived 4-(2-cyanobenzyl)dibenzothiophenium salt (3b)

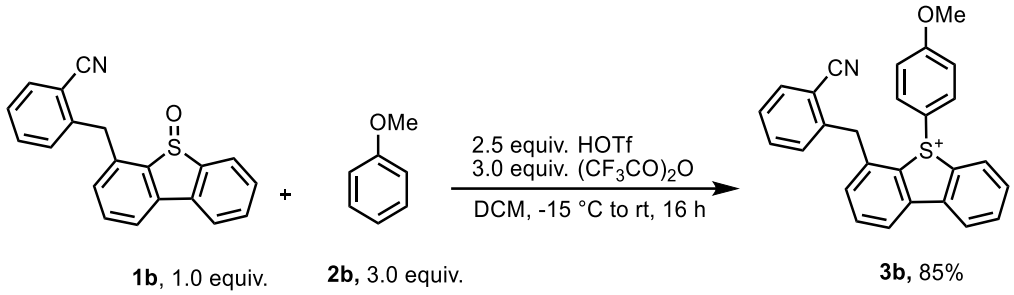

1b, 1.0 equiv. **2b,** 3.0 equiv. **3b,** 85%

In a flame dried round bottom flask, 4-(2-cyanobenzyl)dibenzothiophene *S*-oxide **1b** (637 mg, 2.00 mmol, 1.00 equiv.) was dissolved in dry DCM (20 mL). The solution was cooled down to -15 °C using an ice–brine bath. Subsequently, anisole **2b** (650 µL, 648 mg, 6.00 mmol, 3.00 equiv.) was added followed by dropwise addition of TfOH (440 µL, 750 mg, 5.00 mmol, 2.50 equiv.). After the reaction was stirred at the same temperature for 5 minutes, trifluoroacetic anhydride (840 µL, 1.26 g, 6.00 mmol, 3.00 equiv.) was added dropwise. The reaction mixture was allowed to warm gradually to room temperature over 16 h. Afterwards, the reaction was quenched by the addition of saturated aqueous Na_2CO_3 solution (5.0 mL). The entire mixture was transferred into a separatory funnel, and the layers were separated. The organic layer was collected, and the aqueous layer was further extracted with DCM (4 × ca. 50 mL). The combined organic layers were dried over Na_2SO_4, filtered and the solvent was removed under reduced pressure. The resulting residue was purified by column chromatography on silica gel eluting with a solvent mixture of DCM / MeOH (100:0 gradient to 95:5 (v/v)) to afford 944 mg (85%) of desired product **3b** as an off-white solid.

$\mathbf{R_f}$ = 0.33 (DCM/MeOH, 95:5 (v:v))

NMR Spectroscopy:

^{1}H NMR (600 MHz, $CDCl_3$, 23 ºC, δ): 8.19 – 8.13 (m, 3H), 7.84 – 7.79 (m, 2H), 7.63 – 7.52 (m, 5H), 7.38 (td, *J* = 7.7, 1.2 Hz, 1H), 7.22 (t, *J* = 7.2 Hz, 2H), 6.98 (d, *J* = 9.3 Hz, 2H), 4.35 (d, *J* = 16.5 Hz, 1H), 4.13 (d, *J* = 16.5 Hz, 1H), 3.82 (s, 3H).

^{13}C NMR (151 MHz, $CDCl_3$, 23 ºC, δ): 165.6, 140.2, 139.9, 139.6, 138.7, 135.6, 134.6, 134.2, 133.6, 133.4, 133.2, 132.3, 131.1, 131.0, 128.8, 128.6, 124.6, 123.4, 118.0, 117.8, 113.1, 112.4, 56.5, 38.0.

^{19}F NMR (565 MHz, $CDCl_3$, 23 ºC, δ): – 78.13.

HRMS-ESIpos (m/z) calc'd for $C_{27}H_{20}N_1O_1S_1$ $[M - OTf]^+$, 406.1261; found, 406.1260; deviation:

– 0.2 ppm.

Olefination followed by Sonogashira coupling on derived 4-(2-cyanobenzyl)dibenzothiophenium salt

Synthesis of *n*-Butyl (*E*)-3-(5-(cyclopropylethynyl)-2-fluorophenyl)acrylate (4a)

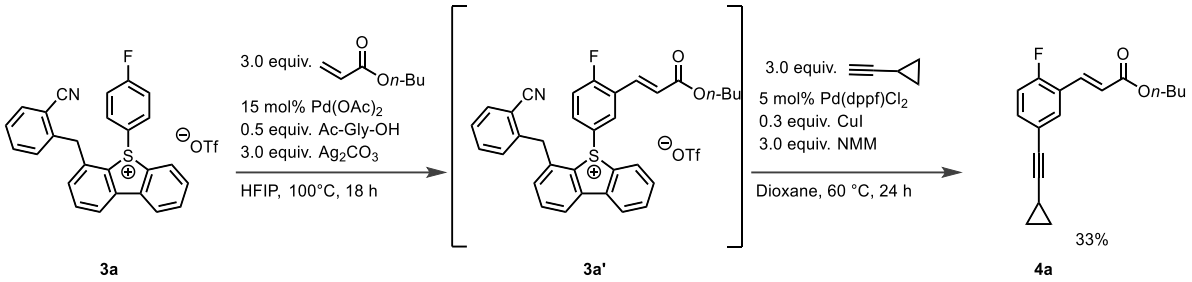

A 20 mL glass vial containing a Teflon-coated magnetic stirring bar equipped with Schlenk-line adapter was charged with fluorobenzene derived 4-(2-cyanobenzyl)dibenzothiophenium salt **3a** (0.30 mg, 0.50 mmol, 1.0 equiv.), $Pd(OAc)_2$ (17 mg, 0.05 mmol, 0.15 equiv.), *N*-acetylglycine (29 mg, 0.25 mmol, 0.50 equiv.) and Ag_2CO_3 (0.41 mg, 1.5 mmol, 3.0 equiv.). The vial was evacuated and backfilled with argon three times. Subsequently, HFIP (10 mL, c = 0.05 M), and *n*-butyl acrylate (0.19 mL, 0.22 mg, 1.5 mmol, 3.0 equiv.) were added to reaction mixture. Subsequently, the vial was closed and transferred directly to a preheated metal block and the reaction mixture was stirred at 100 °C for 18 h. The reaction mixture was allowed to cool down to room temperature, filtered through a short plug of Celite® and the filter cake was washed with DCM (100 mL). To remove black precipitate, the filtrate was filtered again using filter paper which was subsequently washed with an additional amount of DCM (50 mL). The obtained residue containing the olefinated sulfonium salt intermediate **3a'** was concentrated under reduced pressure and then used without further purification.

A 25 mL Schlenk tube containing the obtained crude product **3a'** was charged with CuI (28 mg, 0.15 mmol, 0.3 equiv.) and $Pd(dppf)Cl_2$ (18.3 mg, 0.025 mmol, 0.05 equiv.). The Schlenk tube was evacuated and backfilled with argon three times. Afterwards, dry dioxane (10 mL), N-methylmorpholine (0.17 mL, 0.15 mg, 1.5 mmol, 3.0 equiv.) and ethynylcyclopropane (0.13 mL, 0.10 g,1.5 mmol, 3.0 equiv.) were added to the reaction mixture. After the addition, the tube was sealed and transferred to an oil bath and the reaction was heated to 60°C and stirred at that temperature for 24 h. After cooling down to room temperature the reaction mixture was filtered through a short plug of Celite® and the filter cake was washed with ethyl acetate (50 mL). The filtrate was concentrated under reduced pressure. The resulting residue was purified by column chromatography on silica gel eluting with a solvent mixture of hexanes / EtOAc (90:10 (v/v)) and

fractions with product were collected and combined. Further purification was performed using preparative TLC using solvent mixture of hexanes / EtOAc (90:10 (v/v)) to afford 47 mg (33%, 2 steps) of desired product **4a** as a colorless oil.

$\mathbf{R_f}$ = 0.35 (hexanes/EtOAc, 9:1 (v:v))

NMR Spectroscopy:

^{1}H NMR (600 MHz, $CDCl_3$, 23 ºC, δ): 7.72 (dd, *J* = 16.2, 0.5 Hz, 1H), 7.55 (dd, *J* = 7.1, 2.2 Hz, 1H), 7.33 (ddd, *J* = 8.5, 4.9, 2.1 Hz, 1H), 7.00 (dd, *J* = 10, 3.8 Hz, 1H), 6.51 (d, *J* = 16.2 Hz, 1H), 4.21 (t, *J* = 6.7 Hz, 2H), 1.72 – 1.65 (m, 2H), 1.47 – 1.40 (m, 3H), 0.96 (t, *J* = 7.4 Hz, 3H), 0.89 – 0.86 (m, 2H), 0.82 – 0.78 (m, 2H).

^{13}C NMR (151 MHz, $CDCl_3$, 23 ºC, δ): 166.9, 161.4, 159.7, 136.5 (d, J = 2.8 Hz), 134.7 (d, J = 8.9 Hz), 132.2 (d, J = 3.2 Hz), 122.7 (d, J = 12.6 Hz), 121.6 (d, J = 6.3 Hz), 120.7 (d, J = 3.7), 116.4 (d, J = 23 Hz), 94.0 (d, J = 1.4 Hz), 74.2, 64.7, 30.9, 19.3, 13.9, 8.7, 0.2.

^{19}F NMR (565 MHz, $CDCl_3$, 23 ºC, δ): – 114.3 (ddd, *J* = 10.6, 7.0, 5.0 Hz).

HRMS-ESIpos (m/z) calc'd for $C_{18}H_{19}O_2F_1Na_1$ $[M + Na]^+$, 309.1262; found, 309.1259; deviation: 0.8 ppm.

Synthesis of *n*-Butyl (*E*)-3-(5-(cyclopropylethynyl)-2-methoxyphenyl)acrylate (4b)

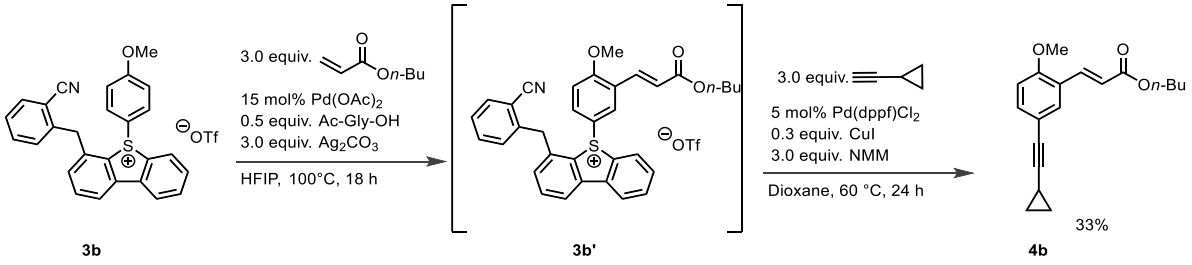

A 20 mL glass vial equipped with Teflon-coated magnetic stirring bar and Schlenk-line adapter was charged with anisole derived 4-(2-cyanobenzyl)dibenzothiophenium salt **3b** (0.29 g, 0.50 mmol, 1.0 equiv.), Pd(OAc)2 (17 mg, 0.05 mmol, 0.15 equiv.), N-acetylglycine (29 mg, 0.25 mmol, 0.50 equiv.), Ag2CO3 (0.41 g, 1.5 mmol, 3.0 equiv.). The vial was evacuated and backfilled with argon three times. Subsequently, HFIP (10 mL, c = 0.05 M), and *n*-butyl acrylate (0.19 mL, 0.22 g, 1.5 mmol, 3.0 equiv.) were added into the vial and the vial was closed and was directly placed into a preheated metal block at 100 °C. and stirred at this temperature for 18h. Afterwards, the reaction mixture was allowed to cool down to room temperature and was subsequently filtered through a short plug of Celite® and the filter cake was washed with DCM (100 mL). In order to

remove black precipitate, the filtrate was filtered again using filter paper which was washed with additional amount of DCM (50 mL). The obtained residue containing the olefinated sulfonium salt intermediate 10a was concentrated under reduced pressure and then used without further purification.

A 25 mL Schlenk tube containing the obtained crude product **3b'** was charged with CuI (28 mg, 0.15 mmol, 0.30 equiv.) and Pd(dppf)Cl2 (18 mg, 25 µmol, 0.05 equiv.). The Schlenk tube was evacuated and backfilled with argon three times. Afterwards, dry dioxane (10 mL), N-methylmorpholine (0.17 mL, 0.15 mg, 1.5 mmol, 3.0 equiv.) and ethynylcyclopropane (0.13 mL, 0.10 g, 1.5 mmol, 3.0 equiv.) were added to the reaction mixture. After the addition, the tube was sealed and transferred to an oil bath and the reaction was heated to 60°C and stirred at that temperature for 24 h. After cooling down to room temperature the reaction mixture was filtered through a short plug of Celite® and the filter cake was washed with ethyl acetate (50 mL). The filtrate was concentrated under reduced pressure and the residue was purified using pre*para*tive HPLC (YMC Actus Pro C18 (150 x 30 mm, 5 µm), MeCN / 0.1% TFA in H2O = 60:40 gradient to 80:20 (v/v), flow rate 42,5 mL/min, 35°C) to afford **4b** (58 mg, 39%, 2 steps) of desired product 11 as a colorless oil.

$\mathbf{R_f}$ = 0.36 (hexanes/EtOAc, 9:1 (v:v))

NMR Spectroscopy:

^{1}H NMR (600 MHz, CDCl3, 23 ºC, δ): 7.90 (d, J = 16.2 Hz, 1H), 7.54 (d, J = 2.1 Hz, 1H), 7.35 (dd, J = 8.5, 2.1 Hz, 1H), 6.81 (d, J = 8.6 Hz, 1H), 6.50 (d, J = 16.2 Hz, 1H), 4.20 (t, J = 6.7 Hz, 2H), 3.87 (s, 3H), 1.71 – 1.65 (m, 2H), 1.49 – 1.37 (m, 3H), 0.96 (t, J = 7.4 Hz, 3H), 0.88 – 0.82 (m, 2H), 0.81 – 0.76 (m, 2H).

^{13}C NMR (151 MHz, CDCl3, 23 ºC, δ): 167.6, 157.8, 139.3, 134.6, 132.2, 123.6, 119.6, 116.4, 111.2, 92.5, 75.0, 64.5, 55.8, 30.9, 19.4, 13.9, 8.7, 0.2.

HRMS-ESIpos (m/z) calc'd for C19H22O3Na $[M + Na]^+$, 321.1461; found, 321.1459; deviation: 0.7 ppm

Synthesis of (ethyl benzoate)ruthenium dichloride dimer (12)

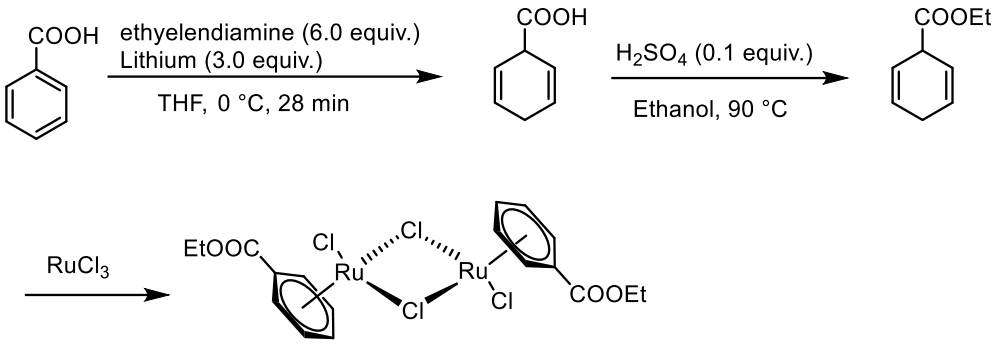

12

(a) Reduction of benzoic acid to 1,4-dihydrobenzoic acid:

A 500-mL round-bottom flask equipped with a Teflon-coated magnetic stir bar and a septum equipped with a needle connected to a bubbler as a gas outlet was charged with benzoic acid (5.00 g, 40.9 mmol), THF (140 mL), and ethylenediamine (16.4 mL, 246 mmol, 6.0 equiv.). The resulting mixture was cooled to 0 °C while stirring, and subsequently, lithium wire (852 mg, 123 mmol, 3.0 equiv.) was added to the solution. The reaction mixture was stirred at 0 °C until the reaction completion was confirmed via TLC (28 min). Afterwards, cold water (50 mL) was added to the reaction mixture, and the resulting mixture was stirred until the remaining lithium was quenched. The reaction mixture was transferred to an ice bath and subsequently acidified with concentrated HCl until pH = 2. After acidification, the reaction mixture was concentrated under reduced pressure with a rotary evaporator until most THF was removed. The resulting mixture was poured into a 125-mL separatory funnel, and the product was extracted with ether (50 mL × 3). The organic layers were combined, dried over Na_2SO_4, filtered through cotton, and concentrated under reduced pressure to give 1,4-dihydrobenzoic acid as a pale-yellow oil (4.82 g, 95% yield).

NMR Spectroscopy:

^{1}H NMR (300 MHz, CDCl3, 298K): δ 11.51 (br s, 1 H), 5.94 (m, 2 H), 5.82 (m, 2 H), 3.78 (m, 1 H), 2.70 (m, 2 H). These data match those in the literature.[212]

(b) Esterification of 1,4-dihydrobenzoic acid:

Under nitrogen atmosphere, a 100 mL round bottom flask equipped with a Teflon coated stir bar was charged with 1,4-dihydrobenzoic acid and ethanol (50 mL). Subsequently, sulfuric acid (0.5

mL) was added dropwise to the reaction mixture. The reaction was stirred and heated to reflux for 16 h and subsequently ethanol was removed under reduced pressure. The crude product was purified by vacuum distillation (temperature = 140 °C, Pressure = 0.01 mbar) and was directly used without further purification.

(c) Complexation with ruthenium chloride:

Under nitrogen atmosphere, a 100 mL round bottom flask equipped with a Teflon coated magnetic stir bar was charged with ruthenium chloride (2.0 g, 9.6 mmol, 1.0 equiv.) and ethanol (50 mL). The flask was attached to a reflux condenser and was closed with a glass stopper. Subsequently, the flask was evacuated and backfilled with nitrogen 3 times. Afterwards, 1,4-dihydrobenzoic acid (4.9 g, 31.0 mmol, 3.2 equiv.) was added to the reaction mixture via a syringe. The reaction mixture was transferred to an oil bath and was heated to 90 °C for 18 h with a bubbler attached to it to eliminate air contamination and ensure an inert atmosphere. After the reaction was cooled down to room temperature, the product was collected by filtration and was subsequently washed with diethylether (30 mL) to afford **12** as a brick red solid (4.9 g, 7.6 mmol, 82%).

NMR Spectroscopy:

^{1}H NMR (600 MHz, Methanol-d_4, 298 K, δ): 7.98 – 7.95 (m, 2H), 7.67 – 7.63 (m, 1H), 7.53 (ddt, *J* = 8.4, 6.6, 1.0 Hz, 2H), 6.68 (dd, *J* = 6.6, 0.7 Hz, 2H), 6.31 – 6.26 (m, 1H), 6.06 – 6.02 (m, 2H), 4.35 – 4.29 (m, 4H), 1.31 (td, *J* = 7.1, 5.5 Hz, 6H).

^{13}C NMR (151 MHz, Methanol-d_4, 298 K, δ): 165.7, 163.9, 133.2, 129.9, 129.1, 128.7, 92.5, 91.8, 85.2, 82.5, 62.1, 60.7, 14.24, 14.2.

Synthesis of 4-Methoxy-2,6-dimethylphenol (13)

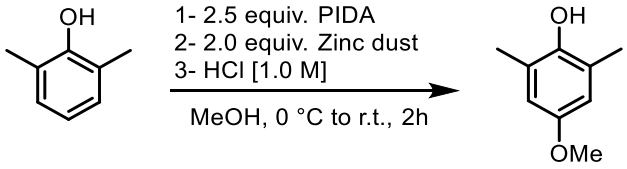

13, 64%

A 250 mL round bottom flask was PIDA (5.4 g, 17 mmol, 2.1 equiv.) was dissolved in methanol (70 mL) and cooled on an ice bath. Subsequently, 2,6-Dimethylphenol (0.98 g, 8.0 mmol, 1 equiv.) was dissolved in methanol (10 mL) and added dropwise over 2 min with vigorous stirring. Afterwards, the reaction mixture was taken out from the ice bath and stirred at room temperature for an additional 30 min. The reaction mixture was cooled on an ice bath and zinc powder (0.79

g, 12 mmol, 1.5 eq) was added in two portions. After the addition, the reaction mixture was taken off from the ice bath and stirred at room temperature for 1 h. The solvent was removed under reduced pressure and Et_2O (50 mL) and HCl (1 M, 50 mL) were added to the crude. The solution was transferred into a separatory funnel, and the layers se*para*ted. The aqueous layer was further extracted with Et_2O (2 x 50 mL). The organic layers were combined and extracted with NaOH solution (1 M, 2 x 25 mL). The basic aqueous layers were combined, acidified with HCl (1 M, 75 mL), and extracted with DCM (3 x 50 mL). The organic layers were combined, dried over Na_2SO_4, filtered, and the solvent removed. The residue was subjected to flash column chromatography (Hexane:EtOAc, 15:1 to 9:1) to afford the desired product (0.78 g, 64%) as an orange solid. The spectral data matched that of literature reported data.[213]

$\mathbf{R_f}$ = 0.23 (Hexane:EtOAc, 9:1)

NMR Spectroscopy:

^{1}H NMR (600 MHz, $CDCl_3$, 298 K, δ): 6.55 (s, 2 H), 4.28 (br. s, 1 H), 3.74 (s, 3 H), 2.23 (s, 6 H).

^{13}C NMR (151 MHz, $CDCl_3$, 298 K, δ): 153.1, 146.3, 124.3, 113.9, 55.8, 16.4.

Synthesis of [η^6–ethyl benzoate-η^5-(2,6-dimethyl-4-methoxy-1-phenoxo)Ru](OTf) (5e)

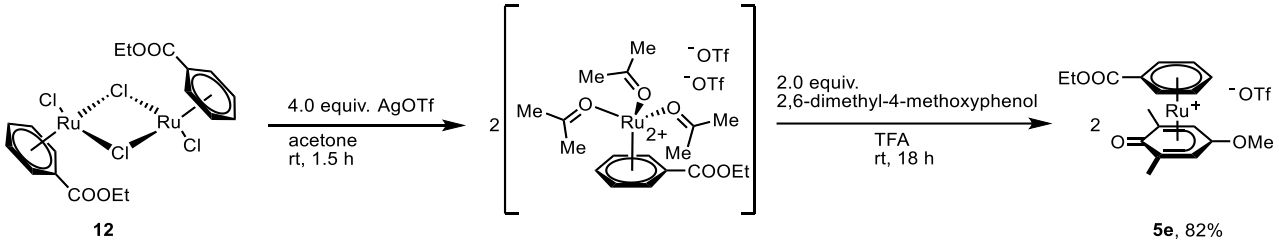

A 20.0 mL borosilicate vial equipped with a Teflon-coated magnetic stirring bar was charged with (ethylbenzenoate)ruthenium dichloride dimer **12** (128 mg, 0.200 mmol, 1.00 equiv.) and AgOTf (206 mg, 0.800 mmol, 4.00 equiv.). The vial was connected via a vial adapter to a Schlenk line and was evacuated and purged with argon three times. Anhydrous acetone (5.0 mL, *c* = 40 mM) was added, the vial covered with aluminum foil and the suspension stirred at room temperature for 1.5 h under an argon atmosphere. Subsequently, the stirring bar was removed, the vial closed with a Teflon-lined screw cap and centrifuged for 5 min at 720 g. 2,6-dimethyl-4-methoxypheol **13** (61 mg, 0.400 mmol, 2.00 equiv.) was added to a second 20.0 mL borosilicate vial equipped with a Teflon-coated magnetic stirring bar and a vial adapter. The latter was evacuated and purged with argon three times, after which the supernatant from the first vial was added. The solvent was

evaporated under reduced pressure and TFA (5.0 mL, *c* = 80 mM) added under an argon atmosphere. The resulting solution was stirred at room temperature overnight. The vial was then cooled in an ice bath and diethyl ether (15.0 mL) added to precipitate a colorless solid. The solid was filtered off, washed with diethyl ether (3 × 10.0 mL), and dried under high vacuum. Recrystallization from diethyl ether and methanol at 50 °C afforded **5e** (93 mg, 0.17 mmol, 84%) as orange solid.

NMR Spectroscopy:

^{1}H NMR (600 MHz, DMSO-d_6, 298 K, δ): 6.94 – 6.91 (m, 2H), 6.85 – 6.79 (m, 3H), 6.57 (s, 2H), 4.49 (q, *J* = 7.1 Hz, 2H), 3.92 (s, 3H), 1.99 (s, 6H), 1.44 (t, *J* = 7.1 Hz, 3H).

^{13}C NMR (151 MHz, DMSO-d_6, 298 K, δ): 162.5, 131.6, 122.9 (q, *J* = 317.6 Hz), 92.9, 92.6, 92.2, 91.5, 82.7, 63.9, 58.3, 16.0, 14.4.

^{19}F NMR (565 MHz, DMSO-d_6, 298 K, δ): -78.7.

Synthesis of [η^6–ethyl benzoate-η^5-(2,6-dichloro-1-phenoxo)Ru](OTf) (5f)

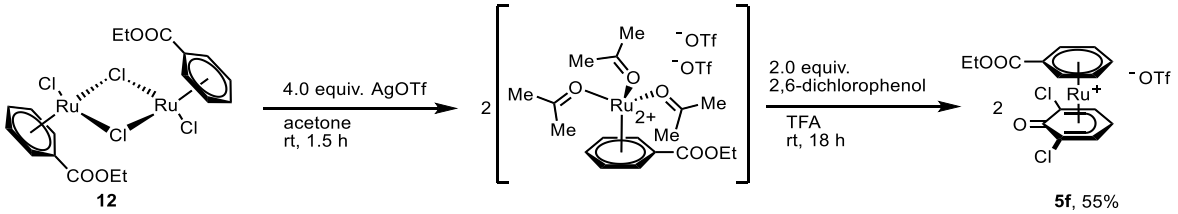

A 20.0 mL borosilicate vial equipped with a Teflon-coated magnetic stirring bar was charged with (ethylbenzenoate)ruthenium dichloride dimer (128 mg, 0.200 mmol, 1.00 equiv.) and AgOTf (206 mg, 0.800 mmol, 4.00 equiv.). The vial was connected via a vial adapter to a Schlenk line and was evacuated and purged with argon three times. Anhydrous acetone (5.0 mL, *c* = 40 mM) was added, the vial covered with aluminum foil and the suspension stirred at room temperature for 1.5 h under an argon atmosphere. Subsequently, the stirring bar was removed, the vial closed with a Teflon-lined screw cap and centrifuged for 5 min at 720 g. 2,6-dichlorophenol (64.2 mg, 0.400 mmol, 2.00 equiv.) was added to a second 20.0 mL borosilicate vial equipped with a Teflon-coated magnetic stirring bar and a vial adapter. The latter was evacuated and purged with argon three times, after which the supernatant from the first vial was added. The solvent was evaporated under reduced pressure and TFA (5.0 mL, *c* = 80 mM) added under an argon atmosphere. The resulting solution was stirred at room temperature overnight. The vial was then cooled in an ice bath and diethyl ether (15.0 mL) was added to precipitate a colorless solid. The solid was filtered

off, washed with diethyl ether (3 × 10.0 mL), and dried under high vacuum. Recrystallization from diethyl ether and methanol at 50 °C afforded **5f** (62 mg, 0.11 mmol, 55%) as an orange solid.

NMR Spectroscopy:

^{1}H NMR (600 MHz, DMSO-d_6, 298 K, δ): 7.16 (dd, J = 6.6, 1.1 Hz, 2H), 7.02 – 6.96 (m, 5H), 6.57 (t, J = 5.6 Hz, 1H), 4.51 (q, J = 7.1 Hz, 2H), 1.46 (t, J = 7.1 Hz, 3H).

^{13}C NMR (151 MHz, DMSO-d_6, 298 K, δ): 162.2, 156.6, 124.8 (q, J = 318.6 Hz), 101.0, 96.5, 96.4, 94.3, 93.9, 82.3, 64.6, 14.5.

^{19}F NMR (565 MHz, DMSO-d_6, 298 K, δ): -78.8.

Hydrolysis of fluoroarenes

Synthesis of [η^6–(4-ethylphenol)-η^5-(2,6-dimethyl-4-methoy-1-phenoxo)Ru](OTf) (7a)

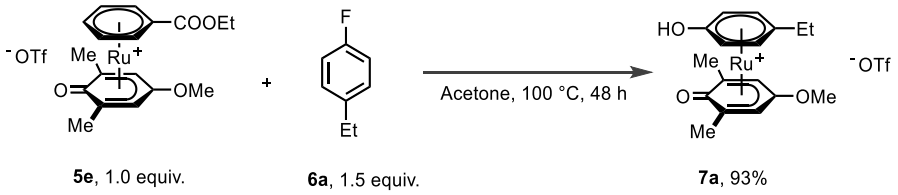

5e, 1.0 equiv. **6a**, 1.5 equiv. **7a**, 93%

A 20 mL borosilicate vial equipped with a Teflon-coated magnetic stirring bar was charged with [η^6–(ethyl benzoate)-η^5-(2,6-dimethyl-4-methoy-1-phenoxo)Ru](OTf) complex (58.7 mg, 0.10 mmol, 1.00 equiv.), 1-Ethyl-4-fluorbenzene **6a** (25.0 µL, 25.3 mg, 0.15 mmol, 1.5 equiv.). The vial was connected to a Schlenk line via a vial adapter and was subsequently evacuated and purged with argon three times. Subsequently, acetone (2.5 mL, c = 40 mM) was added, and the vial was sealed and stirred at 100 °C for 48 h. After cooling down to room temperature, the vial was opened and diethyl ether (15 mL) was added to precipitate the product as a solid. The product was filtered off over a G4 glass frit, washed with diethyl ether (3 × 15 mL), and dried under high vacuum to afford Ru(II) complex **7a** (52 mg, 93 µmol, 93%) as a beige solid.

NMR Spectroscopy:

^{1}H NMR (600 MHz, DMSO-d_6, 298 K, δ): 6.30 (s, 2H), 6.17 (d, J = 6.5 Hz, 2H), 5.94 (d, J = 5.6 Hz, 2H), 3.72 (s, 3H), 2.40 (q, J = 7.5 Hz, 2H), 1.85 (s, 6H), 1.14 (t, J = 7.5 Hz, 3H).

^{13}C NMR (151 MHz, DMSO-d_6, 298 K, δ): 159.2, 137.9, 128.0, 120.7 (q, J = 322.4 Hz), 106.8, 89.92, 87.8, 80.5, 77.9, 57.3, 24.8, 15.4, 14.0.

^{19}F NMR (565 MHz, DMSO-d_6, 298 K, δ): -77.7.

HRMS ESI (m/z) calculated for $C_{14}H_{15}O_3Ru_1$ $[M]^+$, 559.0981; found, 559.0979; deviation: −1.2 ppm.

Synthesis of [η^6–(4-methoxyphenol)-η^5-(2,6-dimethyl-4-methoy-1-phenoxo)Ru](OTf) (7b)

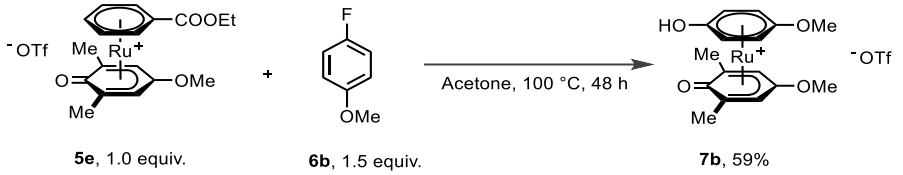

5e, 1.0 equiv. **6b**, 1.5 equiv. **7b**, 59%

A 20 mL borosilicate vial equipped with a Teflon-coated magnetic stirring bar was charged with [η^6–(ethyl benzoate)-η^5-(2,6-dimethyl-4-methoy-1-phenoxo)Ru](OTf) complex (58.7 mg, 0.100 mmol, 1.00 equiv.), 4-fluoroanisole **6b** (16.5 µL, 18.9 mg, 0.150 mmol, 1.5 equiv.). The vial was connected to a Schlenk line via a vial adapter and was subsequently evacuated and purged with argon three times. Subsequently, acetone (2.5 mL, c = 40 mM) was added, and the vial was sealed and stirred at 100 °C for 48 h. After cooling down to room temperature, the vial was opened and diethyl ether (15 mL) was added to precipitate the product as a solid. The solid product was filtered off over a G4 glass frit, washed with diethyl ether (3 × 15 mL), and dried under high vacuum to afford Ru(II) complex **7b** as a (32 mg, 58 µmol, 59%) beige solid.

NMR Spectroscopy:

^{1}H NMR (600 MHz, DMSO-d_6, 298 K, δ): 6.33 (s, 2H), 6.24 (d, J = 6.9 Hz, 2H), 5.89 (d, J = 6.8 Hz, 2H), 3.72 (s, 6H), 1.86 (s, 6H).

^{13}C NMR (151 MHz, DMSO-d_6, 298 K, δ):159.5, 135.8, 132.5, 128.6, 120.7 (q, J = 322 Hz),117.5, 115.7, 114.6, 87.6, 80.2, 76.9, 76.5, 57.7, 57.5, 15.4.

^{19}F NMR (565 MHz, DMSO-d_6, 298 K, δ): -77.8

HRMS ESI (m/z) calculated for $C_{14}H_{15}O_3Ru_1$ $[M]^+$, 545.0821; found, 545.0821; deviation: −0.7 ppm.

Synthesis of [η^6–(4-hydroxyphenylethanol)-η^5-(2,6-dimethyl-4-methoy-1-phenoxo)Ru](OTf) (7c)

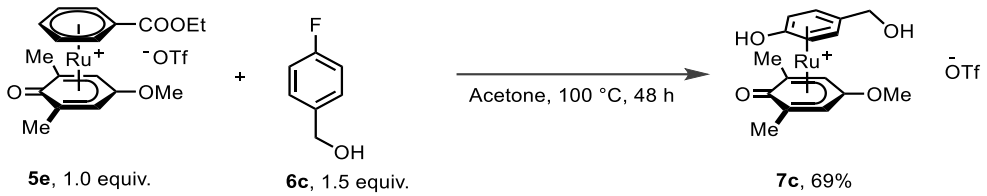

5e, 1.0 equiv. **6c**, 1.5 equiv. **7c**, 69%

A 20.0 mL borosilicate vial equipped with a Teflon-coated magnetic stirring bar was charged with [η^6–(ethyl benzoate)-η^5-(2,6-dimethyl-4-methoy-1-phenoxo)Ru](OTf) Complex **5e** (58.7 mg, 0.10 mmol, 1.00 equiv.), 4-fluorophenylethanol **6c** (24.0 µL, 25.2 mg, 0.15 mmol, 2.0 equiv.). The vial was connected to a Schlenk line via a vial adapter and was subsequently evacuated and purged with argon three times. Subsequently, acetone (2.5 mL, *c* = 40 mM) was added, and the vial was sealed and stirred at 100 °C for 48 h. After cooling down to room temperature, the vial was opened, and diethyl ether (15 mL) was added to precipitate the product as a solid. The solid product was filtered off over a G4 glass frit, washed with diethyl ether (3 × 15 mL), and dried under vacuum to afford Ru(II) complex **7c** (64 mg, 91 µmol, 90%) as a beige solid.

NMR Spectroscopy:

^{1}H NMR (600 MHz, DMSO-d_6, 298 K, δ): 6.30 (s, 2H), 6.18 (d, *J* = 5.5 Hz, 2H), 5.96 (d, *J* = 5.5 Hz, 2H), 3.72 (s, 3H), 2.40 (d, *J* = 7.2 Hz, 2H), 1.85 (s, 6H).

^{13}C NMR (151 MHz, DMSO-d_6, 298 K, δ): 159.2, 128.0, 106.9, 89.9, 87.8, 80.4, 77.8, 57.3, 24.8, 15.4, 14.0.

^{19}F NMR (565 MHz, DMSO-d_6, 298 K, δ): -77.8

HRMS ESI (m/z) calculated for $C_{16}H_{24}O_4Ru_1$ $[M]^+$, 382.0716; found, 707.0715; deviation: -1.4 ppm.

Synthesis of *N*-acetyl tyrosine derived ruthenium complex (7d)

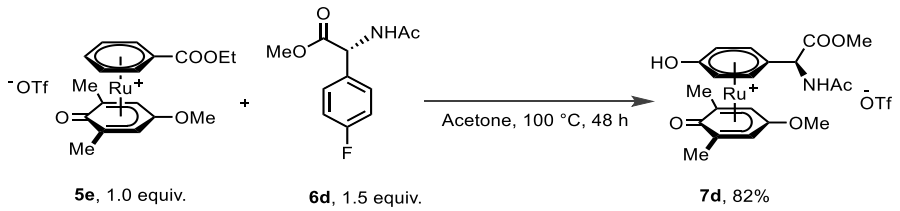

5e, 1.0 equiv. **6d**, 1.5 equiv. **7d**, 82%

A 20.0 mL borosilicate vial equipped with a Teflon-coated magnetic stirring bar was charged with [η^6–(ethyl benzoate)-η^5-(2,6-dimethyl-4-methoy-1-phenoxo)Ru](OTf) complex (58.7 mg, 0.10 mmol, 1.00 equiv.), 4-fluorophenyl-*N*-acetyl alanine methyl carboxylate **6d** (33.8 mg, 0.15 mmol, 1.5 equiv.). The vial was connected to a Schlenk line via a vial adapter and was subsequently evacuated and purged with argon three times. Subsequently, acetone (2.5 mL, *c* = 40 mM) was added and the vial was sealed and stirred at 100 °C for 48 h. After cooling down to room temperature, the vial was opened and diethyl ether (15 mL) was added to precipitate the product as a solid. The solid product was filtered off over a G4 glass frit, washed with diethyl ether (3 × 15 mL), and dried under high vacuum to afford Ru(II) complex **7d** (55 mg, 82 µmol, 82%) as a gray solid.

NMR Spectroscopy:

^{1}H NMR (600 MHz, DMSO-d_6, 298 K, δ): 6.30 – 6.24 (m, 2H), 6.20 (d, *J* = 5.8 Hz, 1H), 6.12 (d, *J* = 5.8 Hz, 1H), 5.93 (t, *J* = 4.8 Hz, 2H), 4.64 (td, *J* = 8.4, 5.4 Hz, 1H), 3.75 (s, 3H), 3.60 (s, 3H), 1.98 (d, *J* = 0.9 Hz, 10H), 1.97 – 1.95 (m, 4H), 1.89 (s, 6H), 1.84 (dd, *J* = 4.4, 2.2 Hz, 1H), 1.79 (s, 3H).

^{13}C NMR (151 MHz, DMSO-d_6, 298 K, δ): 181.4, 180.0, 168.8, 139.6, 131.9 (q, *J* = 321.5 Hz), 110.9, 102.5, 102.3, 99.9, 91.4, 89.3, 67.7, 63.3, 62.5, 45.1, 40.3, 32.3, 25.7.

^{19}F NMR (565 MHz, DMSO-d_6, 298 K, δ): -77.9

HRMS ESI (m/z) calculated for $C_{14}H_{15}O_3Ru_1$ $[M]^+$, 660.1043; found, 660.1043; deviation: +0.7 ppm.

Synthesis of [η^6–(4-hydroxytoluene)-η^5-(2,6-dimethyl-4-methoy-1-phenoxo)Ru](OTf) (7e)

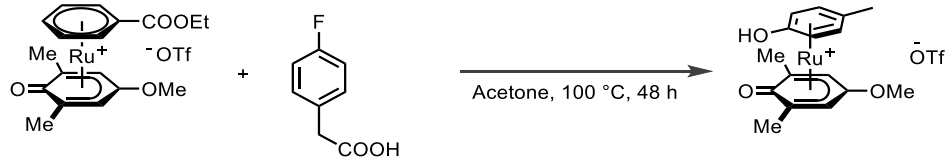

5e, 1.0 equiv. **6i**, 1.5 equiv. **7e**, 48%

A 20.0 mL borosilicate vial equipped with a Teflon-coated magnetic stirring bar was charged with [η^6–(ethyl benzoate)-η^5-(2,6-dimethyl-4-methoy-1-phenoxo)Ru](OTf) complex (58.7 mg, 0.10 mmol, 1.00 equiv.), 4-fluorophenylacetic acid **6i** (23.1 mg, 0.15 mmol, 2.0 equiv.). The vial was connected to a Schlenk line via a vial adapter and was evacuated and purged with argon three times. Subsequently, acetone (2.5 mL, *c* = 40 mM) was added, and the vial was sealed and stirred

at 100 °C for 48 h. After cooling down to room temperature, the vial was opened, and diethyl ether (15 mL) was added to precipitate the product as a solid. The solid product was filtered off over a G4 glass frit, washed with diethyl ether (3 × 15 mL), and dried under vacuum to afford Ru(II) complex **7e** (24.7 mg, 91 µmol, 48%) as an off-white solid.

NMR Spectroscopy:

^{1}H NMR (600 MHz, DMSO-d_6, 298 K, δ): 6.30 (s, 2H), 6.15 (d, J = 6.2 Hz, 2H), 5.97 (d, J = 6.3 Hz, 2H), 3.74 (s, 3H), 2.13 (s, 3H), 1.87 (s, 6H).

^{19}F NMR (565 MHz, DMSO-d_6, 298 K, δ): -77.74

HRMS ESI (m/z) calculated for $C_{16}H_{24}O_3Ru_1$ $[M]^+$, 366.0884; found, 707.0882; deviation: -1.8 ppm

Synthesis of estrone-derived ruthenium complex (9a)

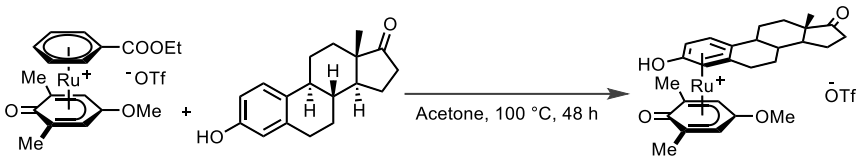

5e, 1.0 equiv. **8a,** 1.5 equiv. **9a**, 90%

A 20.0 mL borosilicate vial equipped with a Teflon-coated magnetic stirring bar was charged with [η^6–(ethyl benzoate)-η^5-(2,6-dimethyl-4-methoy-1-phenoxo)Ru](OTf) complex (58.7 mg, 0.10 mmol, 1.00 equiv.), estrone (32.6 mg, 0.15 mmol, 1.5 equiv.) and was connected via a vial adapter to a Schlenk line and was evacuated and purged with argon three times. Subsequently, acetone (2.5 mL, c = 40 mM) was added, and the vial was sealed and stirred at 100 °C for 48 h. After cooling down to room temperature, the vial was opened and diethyl ether (15 mL) was added to precipitate a solid. The solid was filtered off over a G4 glass frit, washed with diethyl ether (3 × 15 mL), and dried under vacuum to afford Ru(II) complex **9a** (64 mg, 91 µmol, 90%) as a beige solid.

NMR Spectroscopy:

^{1}H NMR (600 MHz, CD_3CN, 298 K, δ): 6.30 – 6.24 (m, 2H), 6.20 (d, J = 5.8 Hz, 1H), 6.12 (d, J = 5.8 Hz, 1H), 5.93 (t, J = 4.8 Hz, 2H), 4.64 (td, J = 8.4, 5.4 Hz, 1H), 3.75 (s, 3H), 3.60 (s, 3H), 1.98 (d, J = 0.9 Hz, 9H), 1.97 – 1.95 (m, 4H), 1.89 (s, 6H), 1.84 (dd, J = 4.4, 2.2 Hz, 1H), 1.79 (s, 3H).

^{19}F NMR (565 MHz, DMSO-d_6, 298 K, δ): -78.9

HRMS ESI (m/z) calculated for $C_{29}H_{44}O_4Ru_1$ $[M]^+$, 707.1817; found, 707.1817; deviation: -0.5 ppm.

Deoxyfluorination of arene complexes

Deoxyfluorination of estrone derived ruthenium complex (9b)

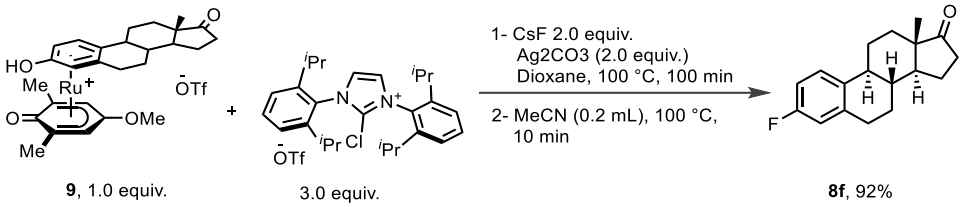

In an argon-filled glove box, a 4 mL borosilicate vial equipped with a Teflon-coated magnetic stirring bar was charged with estrone derived ruthenium complex **9** (57.2 mg, 0.10 mmol, 1.00 equiv.), ^{iPr}ImCl (225 mg, 0.30 mmol, 3.0 equiv.), Ag_2CO_3 (55.1 mg, 0.2 mmol, 2.0 equiv.), CsF (30.4 mg, 0.2 mmol, 2.0 equiv.) and 1,4-dioxane (1 mL). The vial was sealed, and the reaction mixture was stirred at 100 °c for 100 min. Subsequently, the reaction mixture was cooled down in an ice bath for 1 minute, and the vial was carefully opened. Afterwards, dry acetonitrile (0.2 mL) was added to the reaction mixture and the vial was sealed and heated at 100 °C for 10 min. After the reaction was cooled down, the solvent was removed under reduced pressure and the product was obtained by column chromatography on silica gel, eluting with hexane/EtOAc 10:1 (v/v), to afford **8f** (25.1, 92.1 µmol, 92%) as a colorless solid. The spectral data matched that of literature reported data.[215]

R_f = 0.34 (hexane/EtOAc 9:1 (v/v)).

^{1}H NMR (500 MHz, $CDCl_3$, 298 K, δ): 7.22 (dd, *J* = 8.0, 6.1 Hz, 1H), 6.83–6.75 (m, 2H), 2.92–2.87 (m, 2H), 2.53 (dd, *J* = 19.0, 9.1 Hz, 1H), 2.42–2.38 (m, 1H), 2.29–2.23 (m, 1H), 2.17–1.96 (m, 4H), 1.67–1.41 (m, 6H,), 0.92 (s, 3H).

^{13}C NMR (151 MHz, $CDCl_3$, 298 K, δ): 220.4, 161.2 (d, *J* = 243 Hz), 138.9 (d, *J* = 7.3 Hz), 135.4, 127.2 (d, *J* = 7.3 Hz), 115.3 (d, *J* = 20 Hz), 112.5 (d, *J* = 20 Hz), 50.4, 48.2, 44.3, 38.3, 36.1, 31.7, 29.7, 26.5, 26.1, 21.8, 14.1.

^{19}F NMR (375 MHz, $CDCl_3$, 298 K, δ): –118.4.

Deoxyfluorination of 4-ethylphenol derived ruthenium complex (7a)

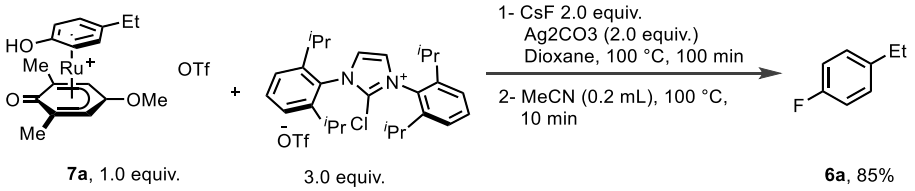

7a, 1.0 equiv. 3.0 equiv. **6a**, 85%

In an argon-filled glove box, a 20 mL borosilicate vial equipped with a Teflon-coated magnetic stirring bar was charged with complex **7a** (159 mg, 0.30 mmol, 1.00 equiv.), ^{iPr}ImCl (675 mg, 0.90 mmol, 3.0 equiv.), Ag_2CO_3 (165 mg, 0.60 mmol, 2.00 equiv.), CsF (91.2 mg, 0.6 mmol, 2.0 equiv.) and 1,4-dioxane (3 mL). The vial was sealed, and the reaction mixture was stirred at 100 °c for 100 min. Subsequently, the reaction mixture was cooled down in an ice bath for 1 min. and the vial was carefully opened. Afterwards, dry acetonitrile (0.6 mL) was added to the reaction mixture, and the vial was sealed and heated at 100 °C for 10 min. After the reaction was cooled down, the solvent was removed under reduced pressure and the product was obtained by flash column chromatography on silica gel to remove the side products, eluting with hexane. The product was obtained by distillation to afford **6a** (31.6, 25.4 µmol, 85%) as a colorless liquid.

^{1}H NMR (500 MHz, $CDCl_3$, 298 K, δ): 7.17 – 7.12 (m, 2H), 6.99 – 6.94 (m, 2H), 2.62 (q, *J* = 7.6 Hz, 2H), 1.23 (t, *J* = 7.6 Hz, 3H).

^{13}C NMR (151 MHz, $CDCl_3$, 298 K, δ): 162.1, 160.5, 139.9, 129.3, 129.2, 115.2, 115.0, 28.2, 15.9.

^{19}F NMR (375 MHz, $CDCl_3$, 298 K, δ): –118.3.

Protodecarboxylation of Phenylacetic Acids catalyzed by 5a

Decarboxylation of Ibuprofen (10a) (1.0 mmol scale)

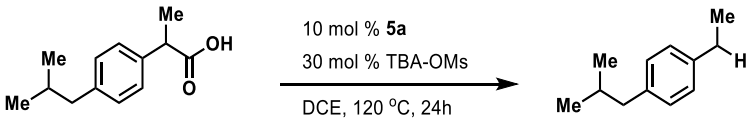

10a **11a,** 76%

A 20.0 mL borosilicate vial equipped with a Teflon-coated magnetic stirring bar was charged with [η^6–benzene-η^5-(2,6-dibromo-4-methoxy-1-phenoxo)Ru](OTf) **5a** (62 mg, 0.10 mmol, 10 mol%), Ibuprofen **11a** (206 mg, 1.00 mmol, 1.00 equiv.) and tetrabutylammonium methylsulfonate (TBA-OMs) (102 mg, 0.300 mmol, 30.0 mol%). The vial was connected via a vial adapter to a Schlenk line and was evacuated and purged with argon three times. DCE (2.0 mL, c = 0.25 M) was then

added, the adapter closed, and the suspension stirred at 120 °C for 24h under an argon atmosphere. Subsequently, the mixture was filtered through a thin layer of Celite loaded on a pipette followed by washing with DCM (3 x 1.0 mL). The volatiles were evaporated under reduced pressure and the residue was purified by column chromatography on silica gel eluting with a solvent mixture of hexanes to afford **11a** (124 mg, 0.760 mmol, 76%) as a colorless oil.

R_f = 0.8 (hexanes)

NMR Spectroscopy:

^{1}H NMR (500 MHz, $CDCl_3$, 298 K, δ): 7.11 (d, *J* = 7.1 Hz, 2H), 7.06 (d, *J* = 7.1 Hz, 2H), 2.63 (q, *J* = 7.6 Hz, 2H), 2.44 (d, *J* = 7.2 Hz, 2H), 1.85 (hept, 1H), 1.23 (t, *J* = 7.6 Hz, 3H), 0.90 (d, *J* = 6.6 Hz, 6H).

^{13}C NMR (126 MHz, $CDCl_3$, 298 K, δ): 141.6, 139.0, 129.2, 45.20, 30.41, 28.58, 22.55, 15.78.

HRMS EI (m/z) calculated for $C_{12}H_{18}$ $[M]^+$, 162.1403; found, 162.1406 deviation: -1.66 ppm.

Decarboxylation of 1,1-diphenylacetic acid (10b)

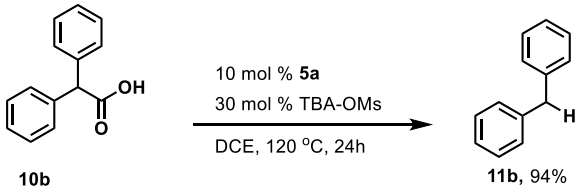

10b **11b,** 94%

A 20.0 mL borosilicate vial equipped with a Teflon-coated magnetic stirring bar was charged with [η^6–benzene-η^5-(2,6-dibromo-4-methoxy-1-phenoxo)Ru](OTf) **5a** (31 mg, 50 µmol, 10 mol%), 1,1-diphenylacetic acid **10b** (106 mg, 0.500 mmol, 1.00 equiv.) and tetrabutylammonium methylsulfonate (TBA-OMs) (51 mg, 0.15 mmol, 30 mol%). The vial was connected via a vial adapter to a Schlenk line and was evacuated and purged with argon three times. DCE (2.0 mL, c = 0.25 M) was then added, the adapter closed, and the suspension stirred at 120 °C for 24h under an argon atmosphere. Afterwards, Silica (ca. 1.0 g) was added to the reaction mixture and the volatiles were removed under reduced pressure. Subsequently, the residue was purified by column chromatography on silica gel eluting with pentane to afford **11b** (80 mg, 0.47 mmol, 94%) as a colorless oil.

R_f = 0.9 (*i*-hexanes, (v:v))

NMR Spectroscopy:

^{1}H NMR (500 MHz, $CDCl_3$, 298 K, δ): 7.34 – 7.28 (m, 4H), 7.25 – 7.18 (m, 5H), 4.01 (s, 2H).

^{13}C NMR (126 MHz, $CDCl_3$, 298 K, δ): 141.3, 129.1, 128.6, 126.2, 42.1.

HRMS EI (m/z) calculated for $C_{13}H_{12}$ $[M]^+$, 168.0934; found, 168.0932, deviation: -1.19 ppm.

Decarboxylation of α,α-difluorophenylacetic acid (10c)

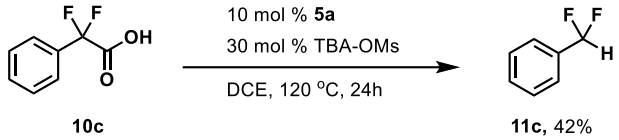

10c **11c,** 42%

A 20.0 mL borosilicate vial equipped with a Teflon-coated magnetic stirring bar was charged with [η^6–benzene-η^5-(2,6-dibromo-4-methoxy-1-phenoxo)Ru](OTf) **5a** (31 mg, 50 μmol, 10 mol%), α,α-difluorophenylacetic acid **10c** (172 mg, 0.500 mmol, 1.00 equiv.) and tetrabutylammonium methylsulfonate (TBA-OMs) (51 mg, 0.15 mmol, 30 mol%). The vial was connected via a vial adapter to a Schlenk line and was evacuated and purged with argon three times. DCE (2.0 mL, c = 0.25 M) was then added, the vial was sealed and the suspension stirred at 120 °C for 24h under an argon atmosphere. Afterwards, the reaction mixture was purified by column chromatography on silica gel eluting with pentane. The fractions containing the product were combined and pentane was removed by distillation at 40 °C to afford **11c** (27 mg, 0.20 mmol, 42%) as a colorless oil.

R_f = 0.9 (hexanes)

NMR Spectroscopy:

^{1}H NMR (500 MHz, $CDCl_3$, 298 K, δ): 7.56 – 7.44 (m, 5H), 6.66 (t, *J* = 56.5 Hz, 1H).

^{13}C NMR (126 MHz, $CDCl_3$, 298 K, δ): 134.5 (t, *J* = 22.3 Hz), 130.9 (t, *J* = 2.1 Hz), 128.8, 125.67 (t, *J* = 6.2 Hz), 116.5, 114.9, 113.3.

^{19}F NMR (565 MHz, $CDCl_3$, 298 K, δ): -110.59 (d, *J* = 56.8 Hz).

HRMS EI (m/z) calculated for $C_7H_6F_2$ $[M]^+$, 128.0432; found, 128.0432, deviation: -0.37 ppm.

Decarboxylation phenylmalonic acid (10d)

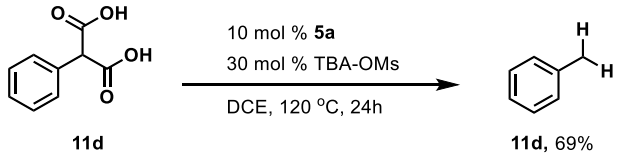

11d **11d,** 69%

A 20.0 mL borosilicate vial equipped with a Teflon-coated magnetic stirring bar was charged with [η^6–benzene-η^5-(2,6-dibromo-4-methoxy-1-phenoxo)Ru](OTf) **5a** (31 mg, 50 µmol, 10 mol%), phenylmalonic acid **10d** (180 mg, 0.500 mmol, 1.00 equiv.) and tetrabutylammonium methylsulfonate (TBA-OMs) (51 mg, 0.15 mmol, 30 mol%). The vial was connected via a vial adapter to a Schlenk line and was evacuated and purged with argon three times. DCE (2.0 mL, c = 0.25 M) was then added, the adapter closed, and the suspension stirred at 120 °C for 24h under an argon atmosphere. Subsequently, Silica (ca. 1.0 g) was added to the reaction mixture and the volatiles were carefully evaporated carefully by rotovap and the residue was purified by column chromatography on silica gel eluting with pentane to afford **11d** (46 mg, 0.44 mmol, 69%) as a colorless oil.

R_f = 0.8 (hexanes)

NMR Spectroscopy:

^{1}H NMR (500 MHz, $CDCl_3$, 298 K, δ): 7.32 – 7.24 (m, 2H), 7.23 – 7.16 (m, 3H), 2.39 (s, 3H).

^{13}C NMR (126 MHz, $CDCl_3$, 298 K, δ): 138.0, 129.2, 128.4, 125.5, 21.60.

HRMS EI (m/z) calculated for C_7H_9 $[M]^+$, 92.0621; found, 92.0620 deviation: -0.22 ppm.

Decarboxylation of 1,3-benzenediacetic acid (10e)

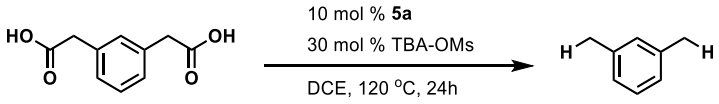

10e **11e**, 94%

A 20 mL borosilicate vial equipped with a Teflon-coated magnetic stirring bar was charged with [η^6–benzene-η^5-(2,6-dibromo-4-methoxy-1-phenoxo)Ru](OTf) **5a** (31 mg, 50 µmol, 10 mol%), 1,3-benzenediacetic acid **10e** (0.19 g, 0.50 mmol, 1.0 equiv.), and tetrabutylammonium methylsulfonate (TBA-OMs) (51 mg, 0.15 mmol, 30 mol%). The vial was connected via a vial adapter to a Schlenk line and was evacuated and purged with argon three times. DCE (2.0 mL, c = 0.25 M) was then added, the adapter closed, and the suspension stirred at 120 °C for 24 h under an argon atmosphere. Afterwards, Silica (ca. 1.0 g) was added to the reaction mixture and the volatiles were removed carefully under reduced pressure. Subsequently, the residue was purified by column chromatography on silica gel eluting with pentane to afford **11e** (53 mg, 0.47 mmol, 94%) as a colorless oil.

R_f = 0.9 (*i*-hexanes, (v:v))

NMR Spectroscopy:

^{1}H NMR (500 MHz, $CDCl_3$, 23 °C, δ): 7.17 (t, J = 7.5 Hz, 1H), 7.04 – 6.97 (m, 3H), 2.34 (s, 6H).

^{13}C NMR (126 MHz, $CDCl_3$, 298 K, δ): 141.3, 129.1, 128.6, 126.2, 42.10.

HRMS EI (m/z) calculated for C7H6F2 [M]+, 106.0778; found, 106.0777 deviation: −0.5 ppm.

Decarboxylation of 4-phenylphenylacetic acid (10f)

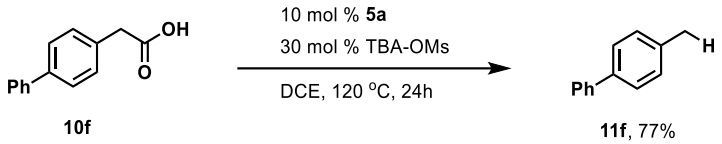

10f **11f**, 77%

A 20.0 mL borosilicate vial equipped with a Teflon-coated magnetic stirring bar was charged with [η^6–benzene-η^5-(2,6-dibromo-4-methoxy-1-phenoxo)Ru](OTf) **5a** (31 mg, 50 µmol, 10 mol%), 4-phenylphenylacetic acid **10f** (106 mg, 0.50 mmol, 1.00 equiv.) and tetrabutylammonium methylsulfonate (TBA-OMs) (51 mg, 0.15 mmol, 30 mol%). The vial was connected via a vial adapter to a Schlenk line and was evacuated and purged with argon three times. DCE (2.0 mL, c = 0.25 M) was then added and the suspension stirred at 120 °C for 24h under an argon atmosphere. Subsequently, the mixture was filtered through a thin celite layer loaded on a pipette followed by washing with DCM (3 x 1.0 mL). Subsequently, volatiles were removed under reduced pressure and the residue was purified by column chromatography on silica gel eluting with hexanes to afford **11f** (65 mg, 0.39 mmol, 77%) as a colorless oil.

R_f = 0.7 (hexanes)

NMR Spectroscopy:

^{1}H NMR (500 MHz, $CDCl_3$, 298 K, δ): 7.63 – 7.61 (m, 2H), 7.56 – 7.51 (m, 2H), 7.56 – 7.51 (m, 2H), 7.39 – 7.33 (m, 1H), 7.32 – 7.26 (m, 2H), 2.44 (s, 3H).

^{13}C NMR (126 MHz, $CDCl_3$, 298 K, δ): 141.3, 138.5, 137.2, 129.6, 128.9, 127.1 (m), 21.23.

HRMS EI (m/z) calculated for $C_{13}H_{12}$ $[M]^+$, 168.0936; found, 168.0934 deviation: -1.55 ppm.

<u>Decaroxylative deuteration of Ibuprofen</u>

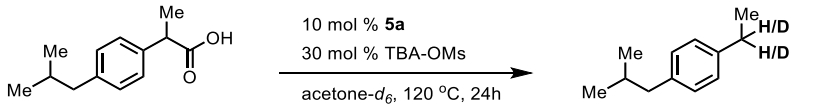

10a **11a'**,84% yield
58% deuterium incorporation

A 20 mL borosilicate vial equipped with a Teflon-coated magnetic stirring bar was charged with **5a** (58 mg, 0.10 mmol, 10 mol%), Ibuprofen **10a** (0.21 g, 1.0 mmol, 1.0 equiv.), and tetrabutylammonium methylsulfonate (0.10 g, 0.30 mmol, 30 mol%). The vial was connected via a vial adapter to a Schlenk line and was evacuated and purged with argon three times. Acetone-d_6 (4.0 mL, c = 0.25 M) was then added, the adapter closed, and the suspension stirred at 120 °C for 18h under an argon atmosphere. Subsequently, the mixture was cooled to 25 °C and the solvent was evaporated. The mixture was filtered through a thin layer of Celite loaded on a pipette followed by washing with DCM (3 x 1 mL). The volatiles were evaporated under reduced pressure and the residue was purified by column chromatography on silica gel eluting with hexanes to afford the desired product (0.14 g, 0.84 mmol, 84%) as a colorless oil.

Note: The signal at 2.63 ppm refers to the benzylic position on which deuteration is observed. The integral of 0.85 refers to the average deuterium incorporation. As the benzylic position bears two hydrogens, a maximum integral of 2.0 would be possible. An integral of 0.85 thus shows a ratio of 0.85:1.15 proton:deuterium (or 0.425:0.575), which translates to 58% deuterium incorporation. A deuterium incorporation of >50% shows that partially double deuteration is obtained, caused by benzylic C–H-deuteration. Therefore, the result demonstrates that partially benzylic C–H-deuteration is obtained.

The substrate **10a** bears two benzylic positions. No deuteration is observed on the second benzylic position possible due to the higher sterical hindrance due to the adjacent isopropyl group.

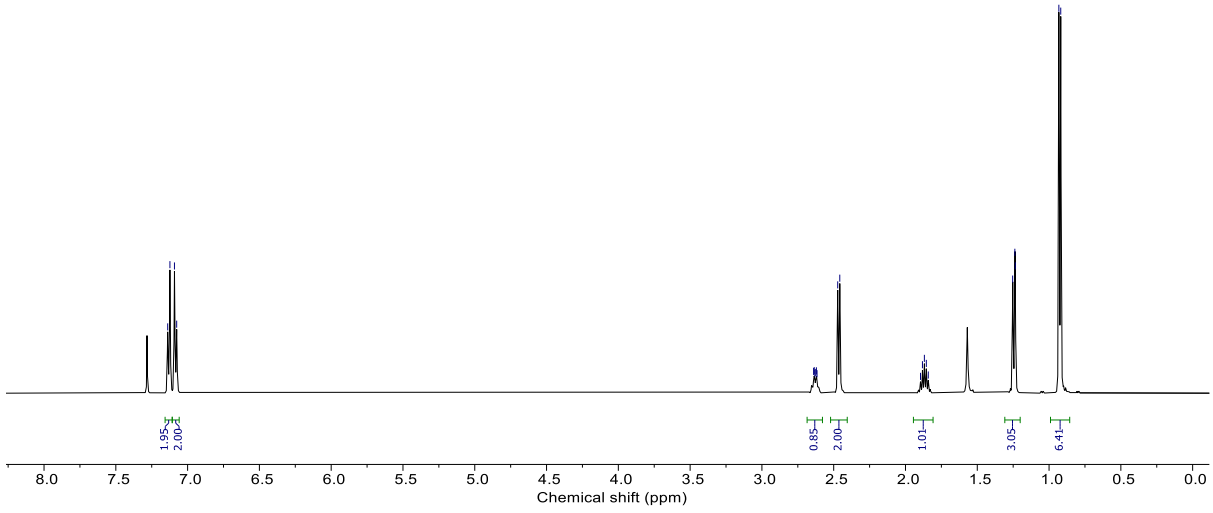

^{1}H-NMR of isolated product; 500 MHz, 298 K, $CDCl_3$; orange diamond: signal of benzylic position on which deuteration is observed, integral: 0.85.

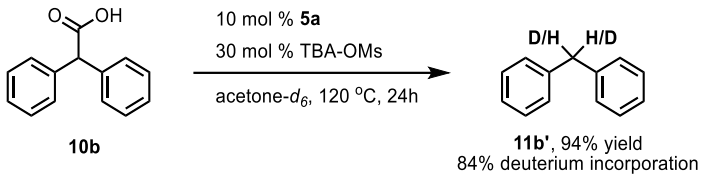

A 20 mL borosilicate vial equipped with a Teflon-coated magnetic stirring bar was charged with **5a** (29 mg, 0.05 mmol, 10 mol%), 1,1-diphenylacetic acid **10b** (0.11 g, 0.5 mmol, 1.0 equiv.), and tetrabutylammonium methanesulfonate (50 mg, 0.15 mmol, 30 mol%). The vial was connected via a vial adapter to a Schlenk line and was evacuated and purged with argon three times. Acetone-d_6 (4.0 mL, c = 0.25 M) was then added, the adapter closed, and the suspension stirred at 120 °C for 18h under an argon atmosphere. Subsequently, the mixture was cooled to 25 °C and the solvent was evaporated. The mixture was filtered through a thin layer of Celite loaded on a pipette followed by washing with DCM (3 x 1 mL). The volatiles were evaporated under reduced pressure and the residue was purified by column chromatography on silica gel eluting with hexanes to afford the desired product (80 mg, 0.47 mmol, 94%) as a colorless oil.

Note: The signal at 4.00 ppm refers to the benzylic position on which deuteration is observed. The integral of 0.32 refers to the average deuterium incorporation. As the benzylic position bears two hydrogens, a maximum integral of 2.0 would be possible. An integral of 0.32 thus shows a ratio of 0.32:1.68 proton:deuterium (or 0.16:0.84), which translates to 84% deuterium incorporation. A deuterium incorporation of >50% shows that partially double C–H deuteration is obtained, caused by benzylic C–H-deuteration. Therefore, the result demonstrates that partially benzylic C–H-deuteration is obtained.

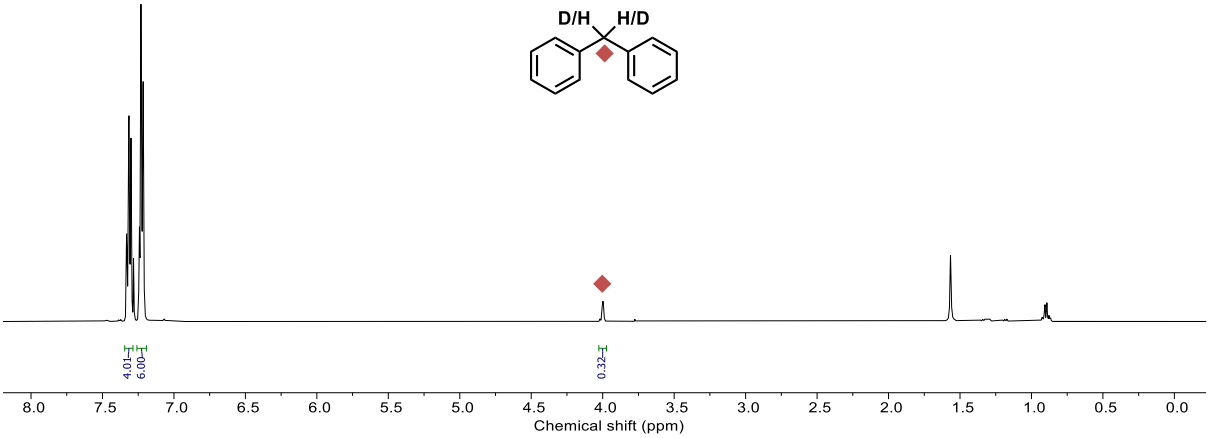

^{1}H-NMR of isolated product; 500 MHz, 298 K, $CDCl_3$; orange diamond: signal of benzylic position on which deuteration is observed, integral: 0.32.

4. Spectroscopic Data

^{1}H NMR of 4-(2-cyanobenzyl)dibenzothiophene (**1a**)

$CDCl_3$, 600 MHz, 298 K

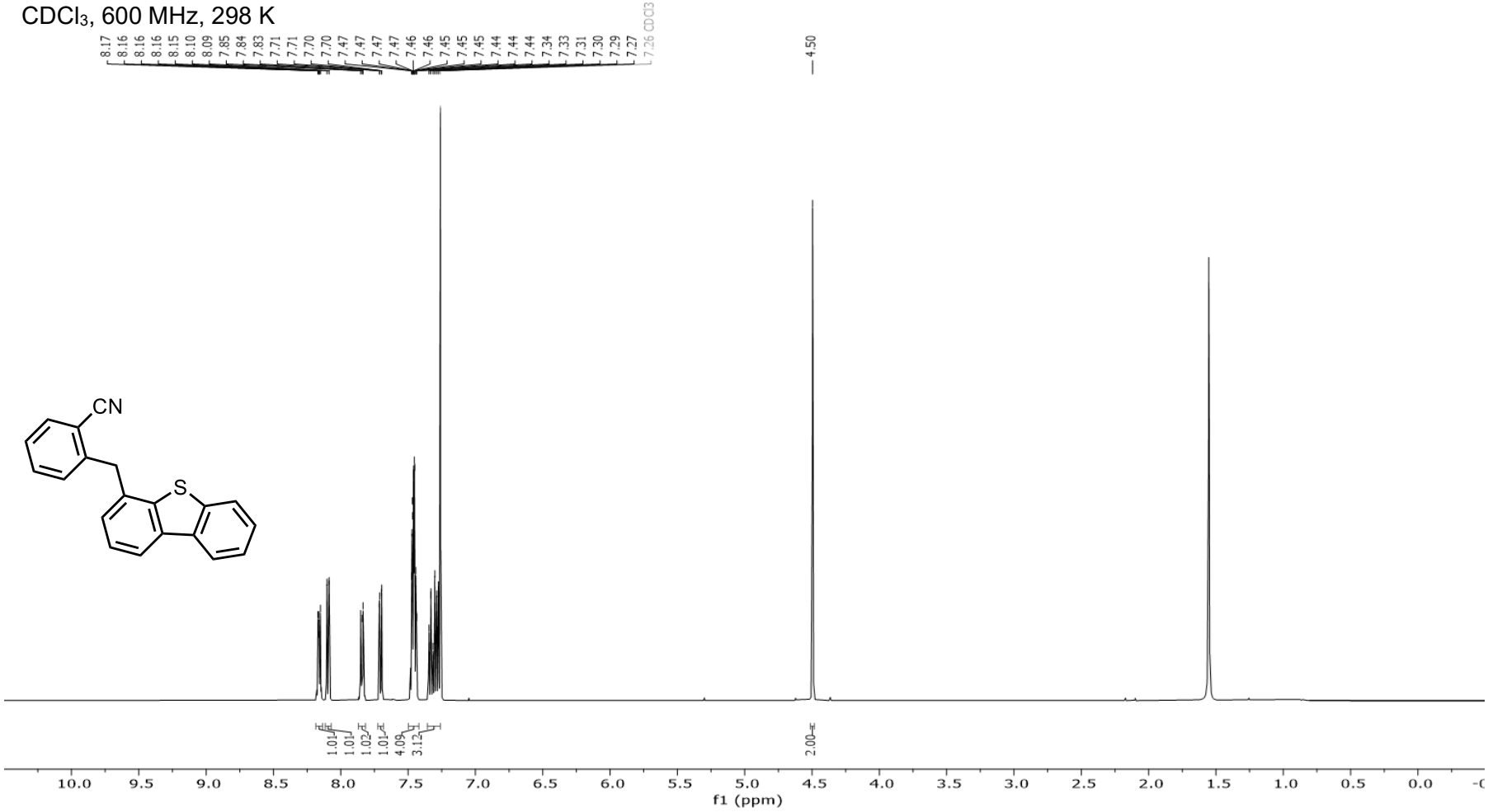

^{13}C NMR of 4-(2-cyanobenzyl)dibenzothiophene (**1a**)

$CDCl_3$, 151 MHz, 298 K

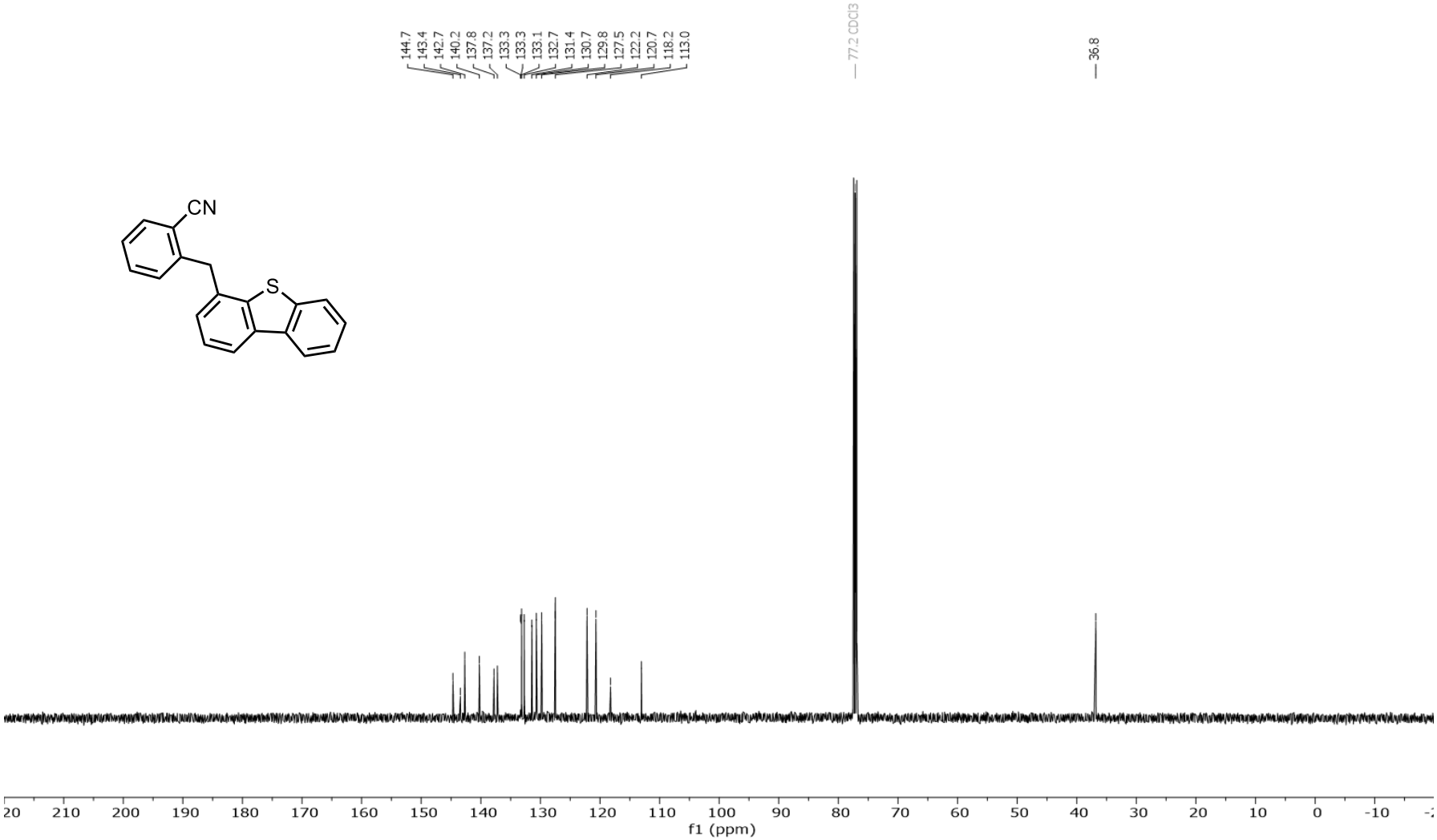

^{1}H NMR of 4-(2-cyanobenzyl)dibenzothiophene (**1b**)

$CDCl_3$, 600 MHz, 298 K

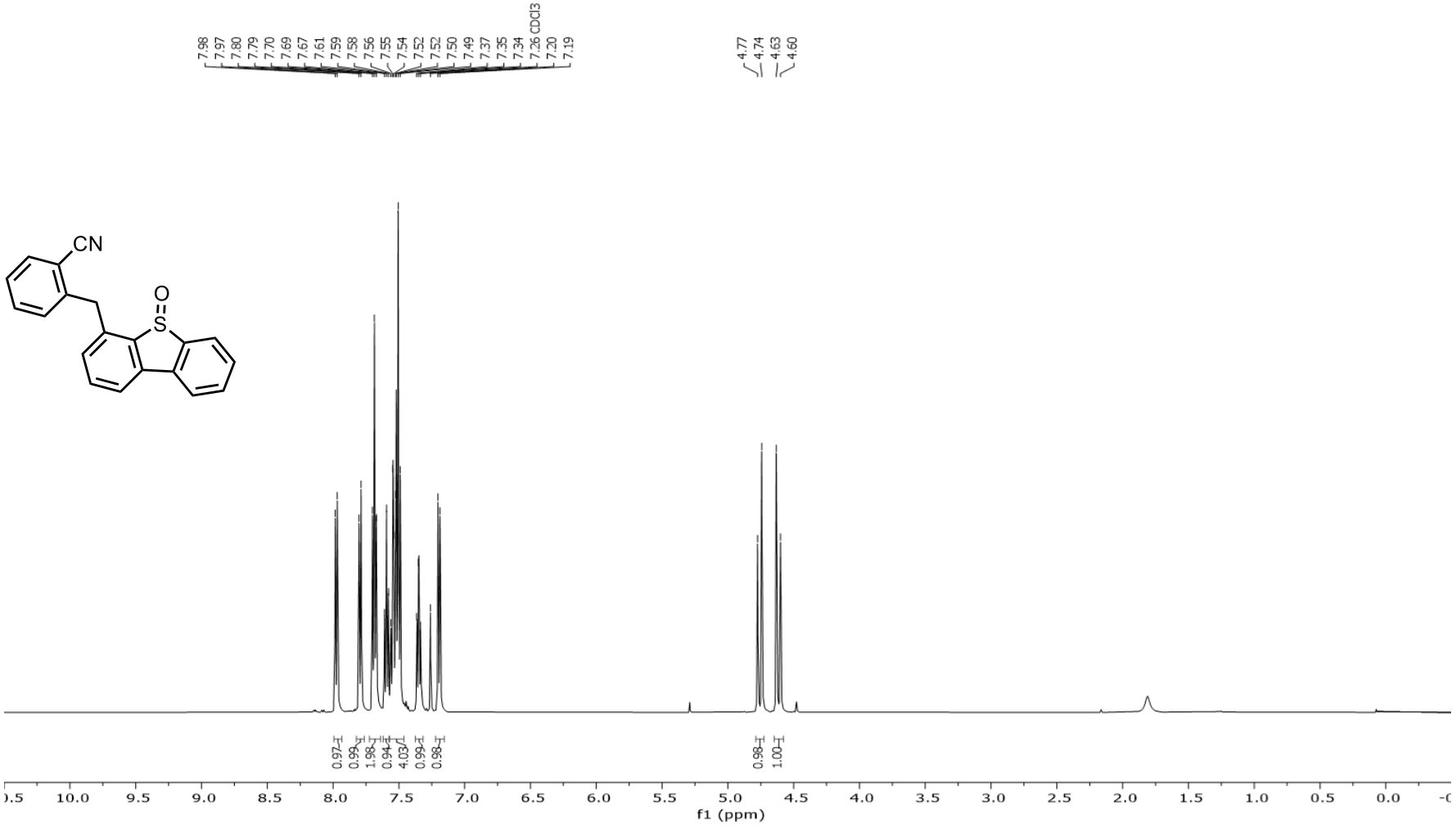

^{13}C NMR of 4-(2-cyanobenzyl)dibenzothiophene (**1b**)

$CDCl_3$, 151 MHz, 298 K

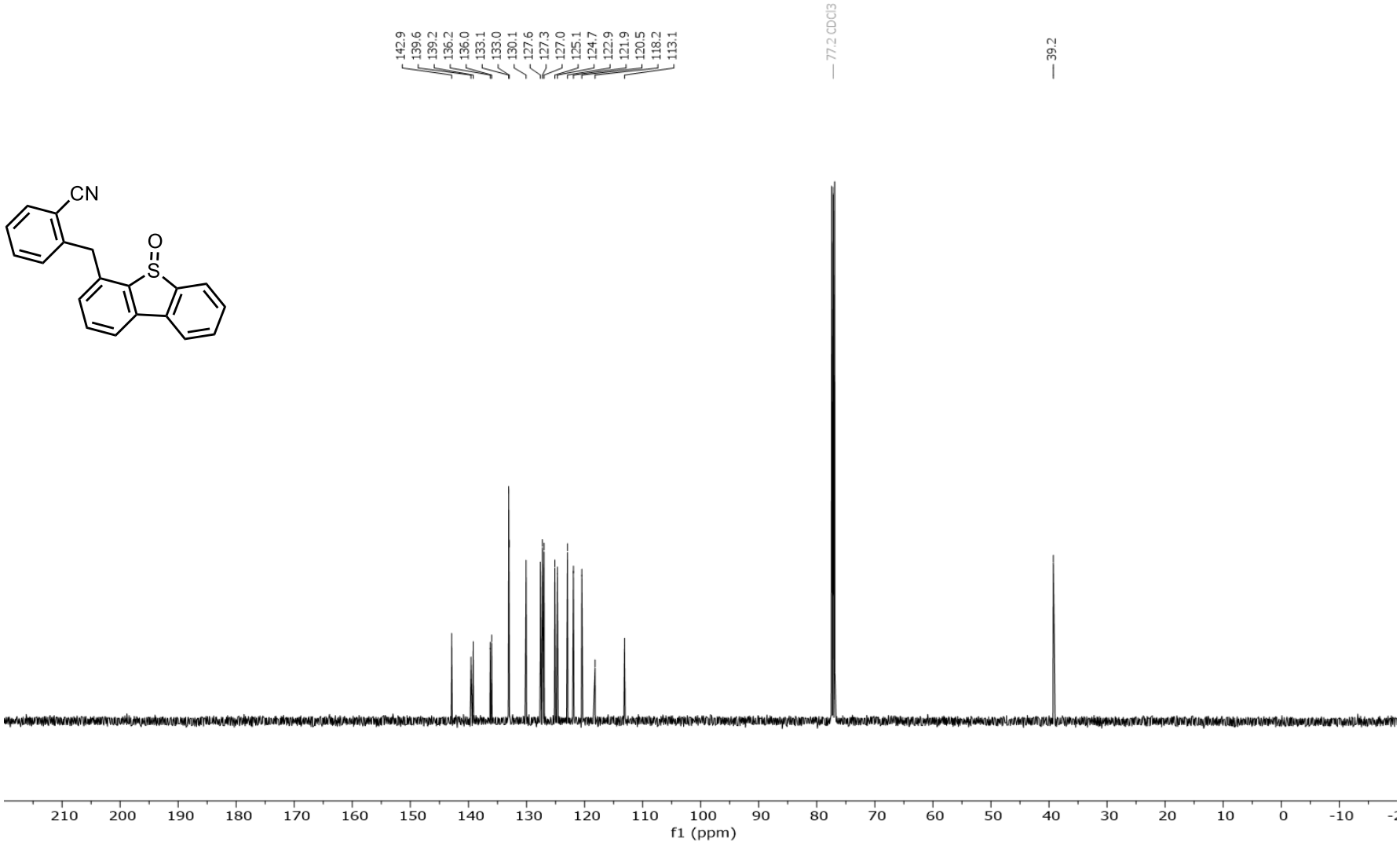

^{1}H NMR of 4 fluorobenzene derived dibenzothiophenium salt (**3a**)

$CDCl_3$, 600 MHz, 298 K

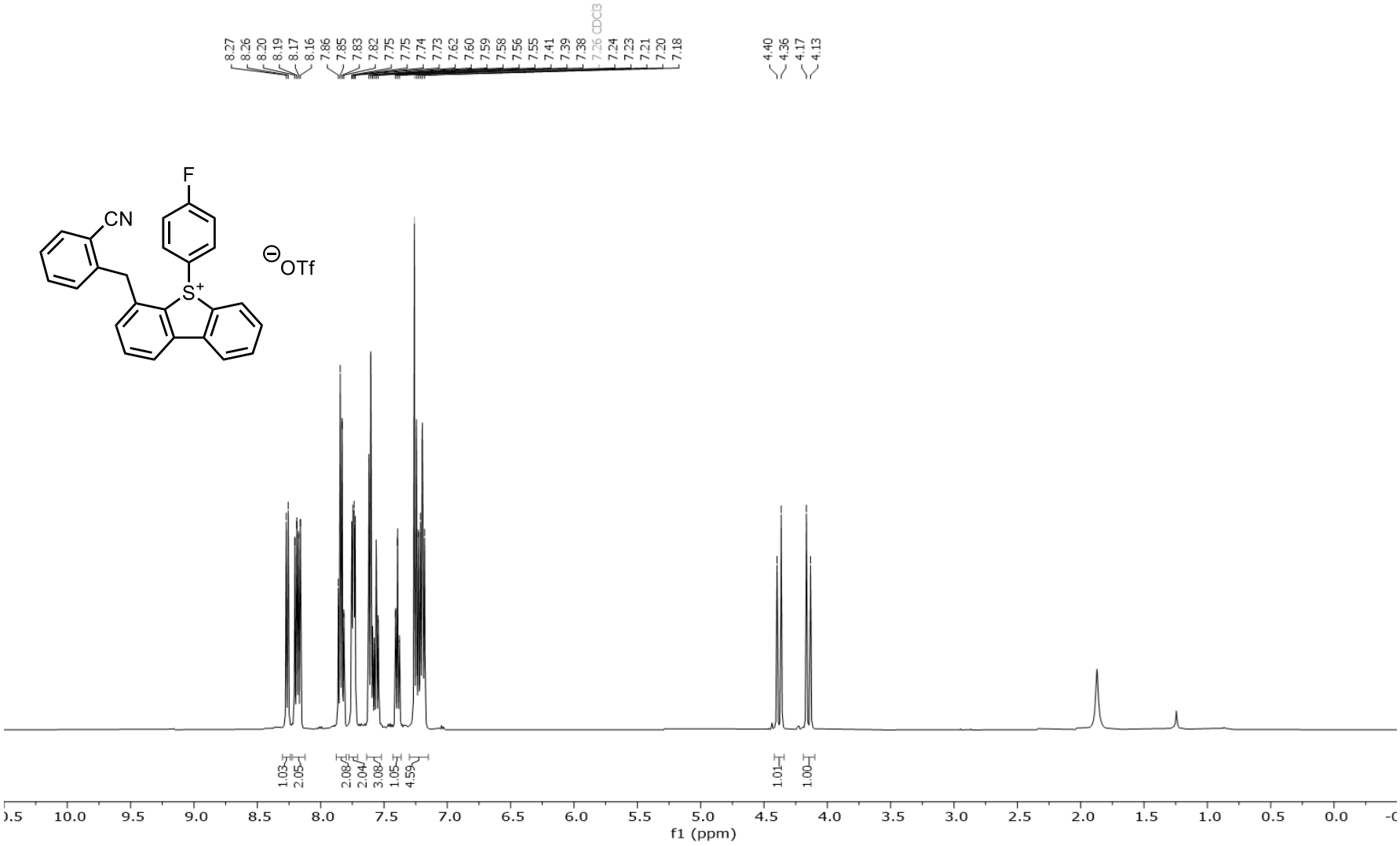

^{13}C NMR of fluorobenzene derived dibenzothiophenium salt (**3a**)

$CDCl_3$, 151 MHz, 298 K

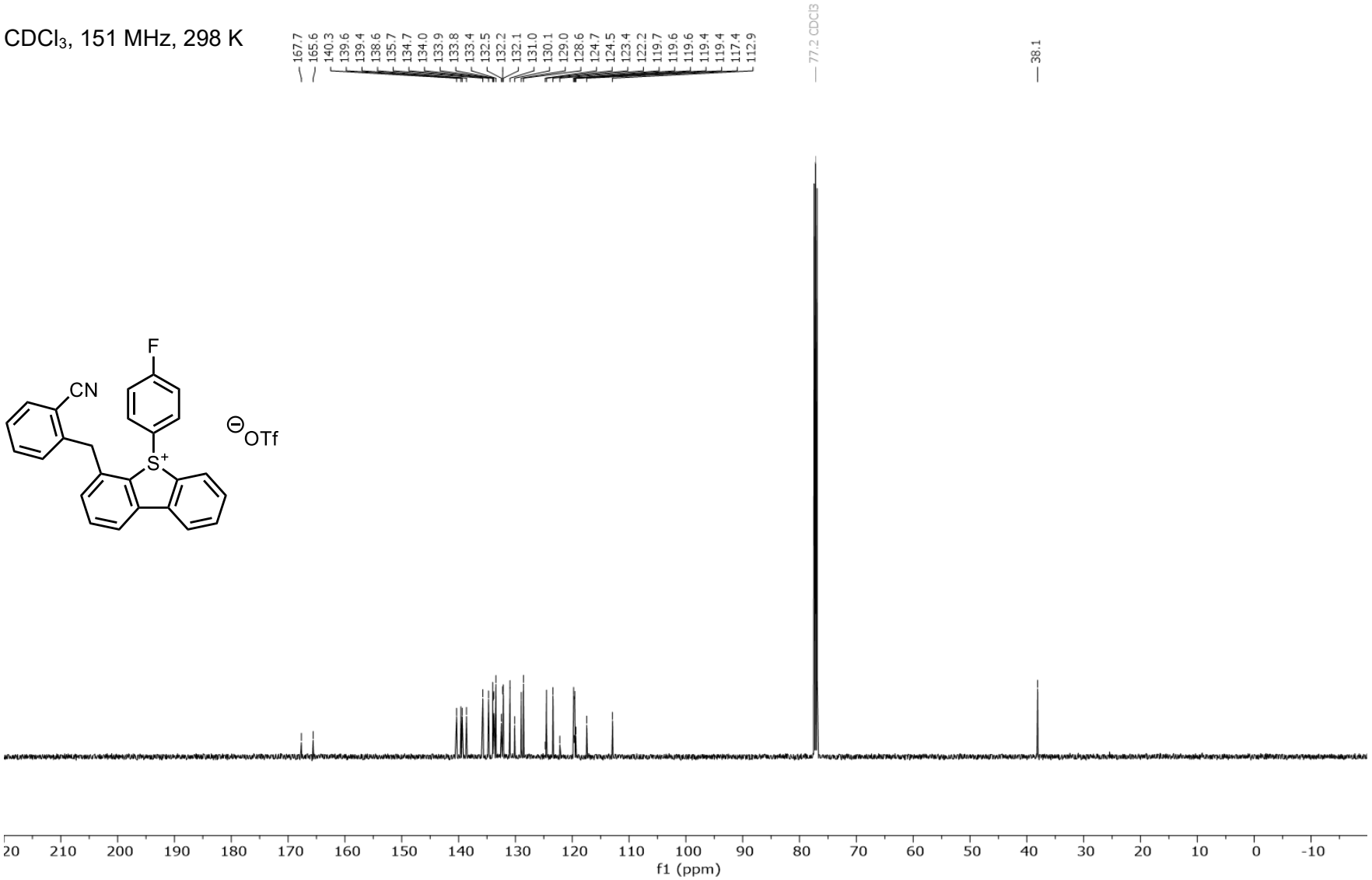

^{19}F NMR of fluorobenzene derived dibenzothiophenium salt (**3a**)

$CDCl_3$, 565 MHz, 298 K

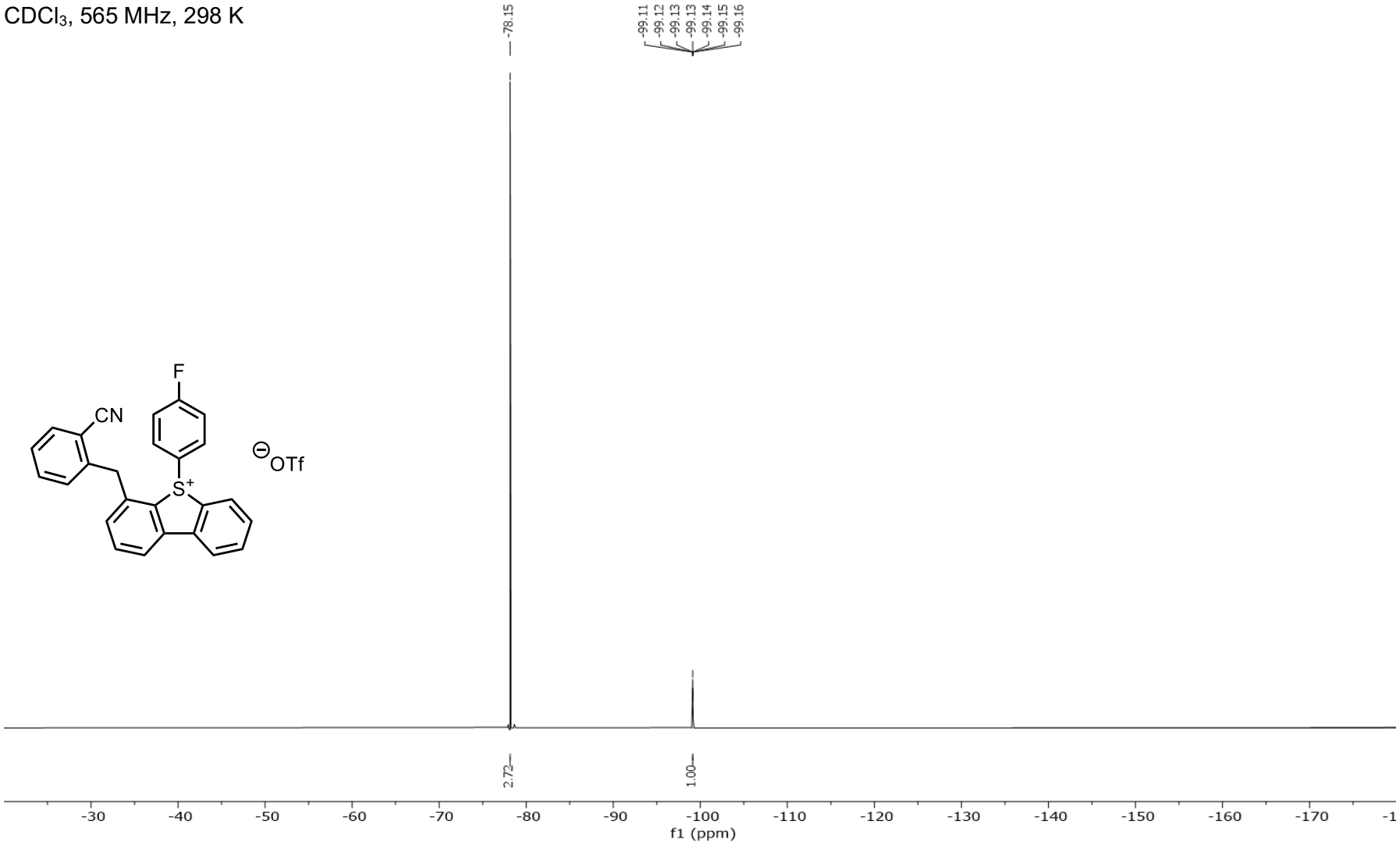

^{1}H NMR of anisole derived dibenzothiophenium salt (**3b**)

$CDCl_3$, 600 MHz, 298 K

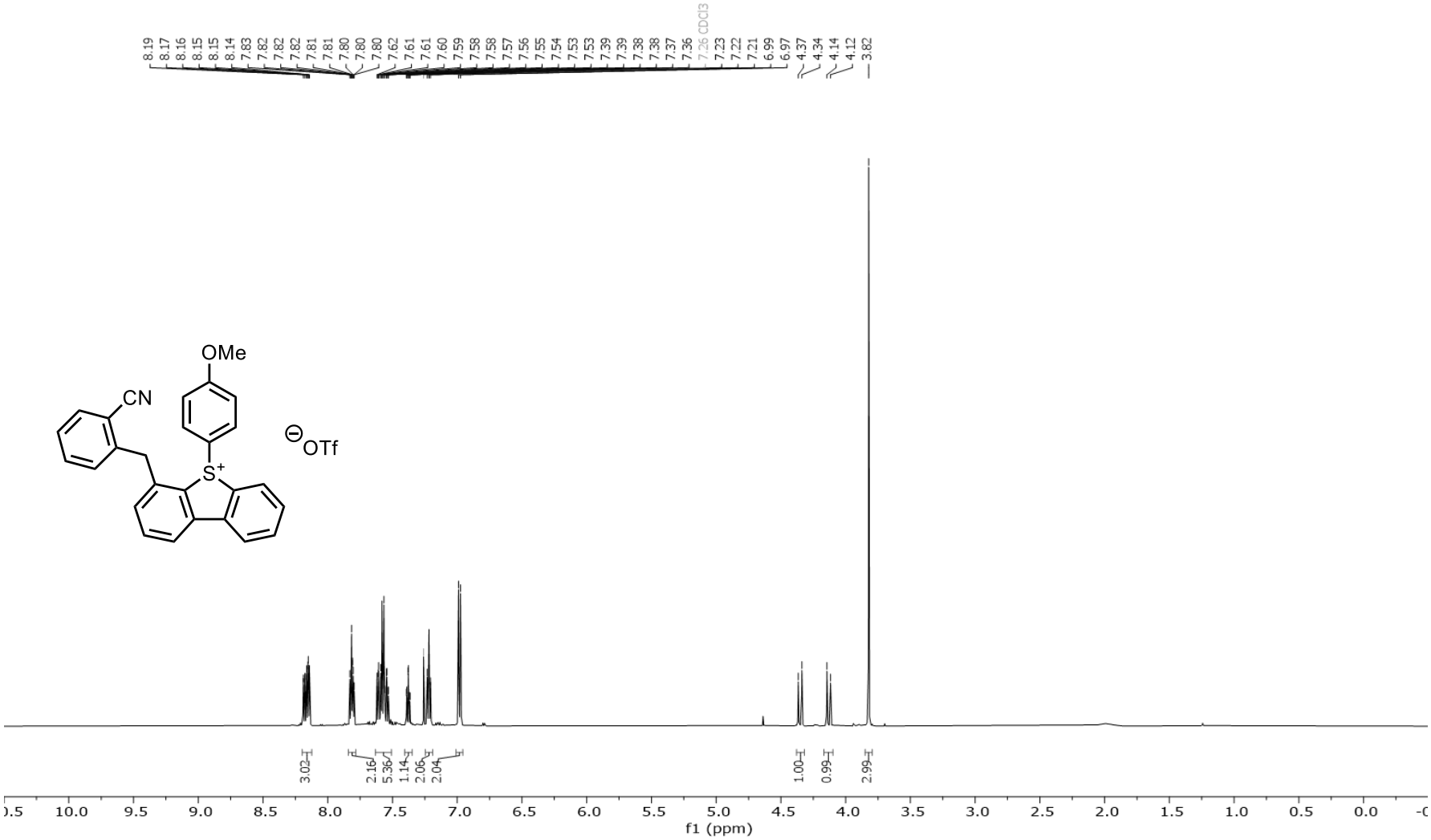

^{13}C NMR of anisole derived dibenzothiophenium salt (**3b**)

$CDCl_3$, 151 MHz, 298 K

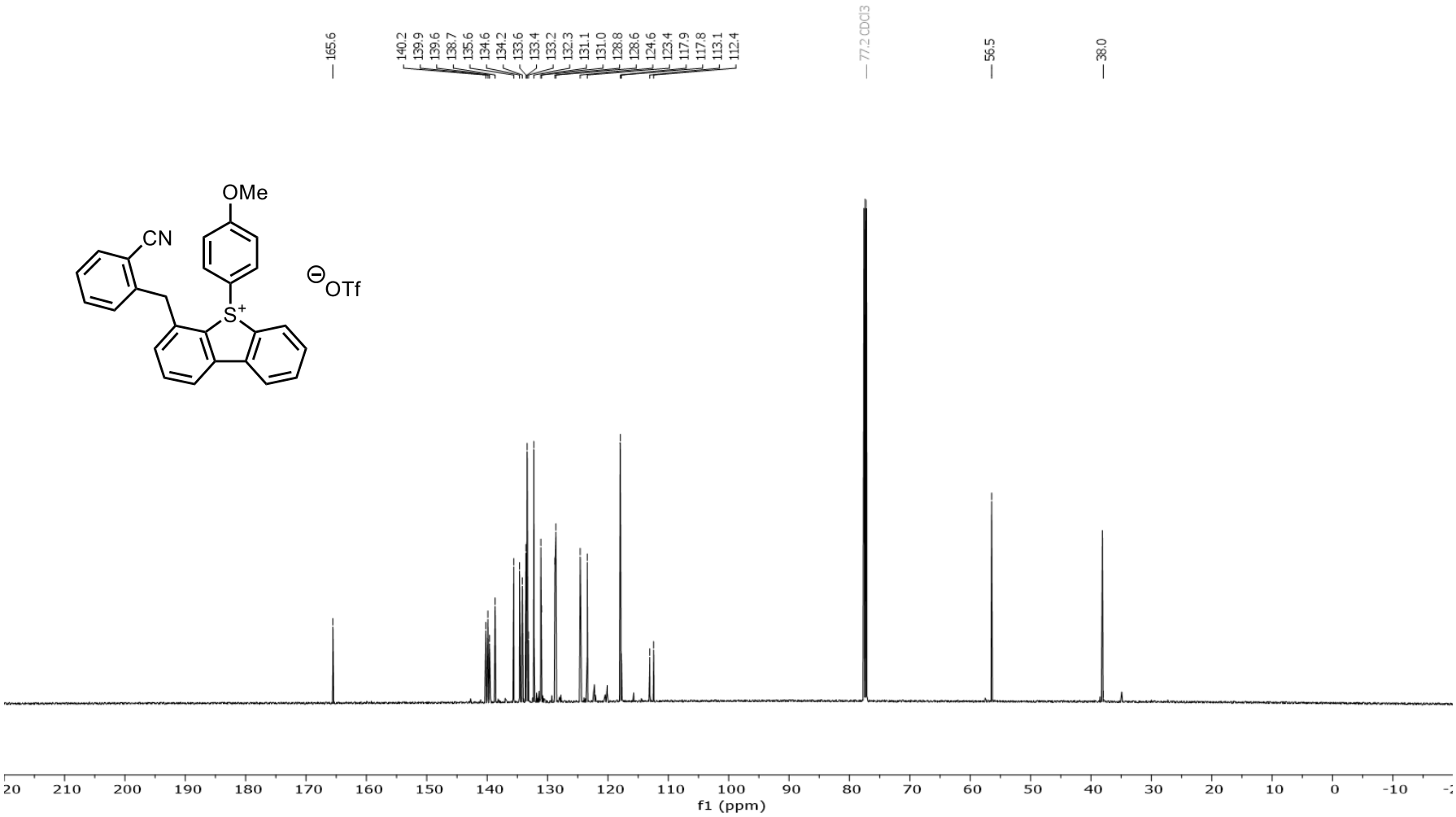

^{19}FNMR of anisole derived dibenzothiophenium salt (**3b**)

$CDCl_3$, 565 MHz, 298 K

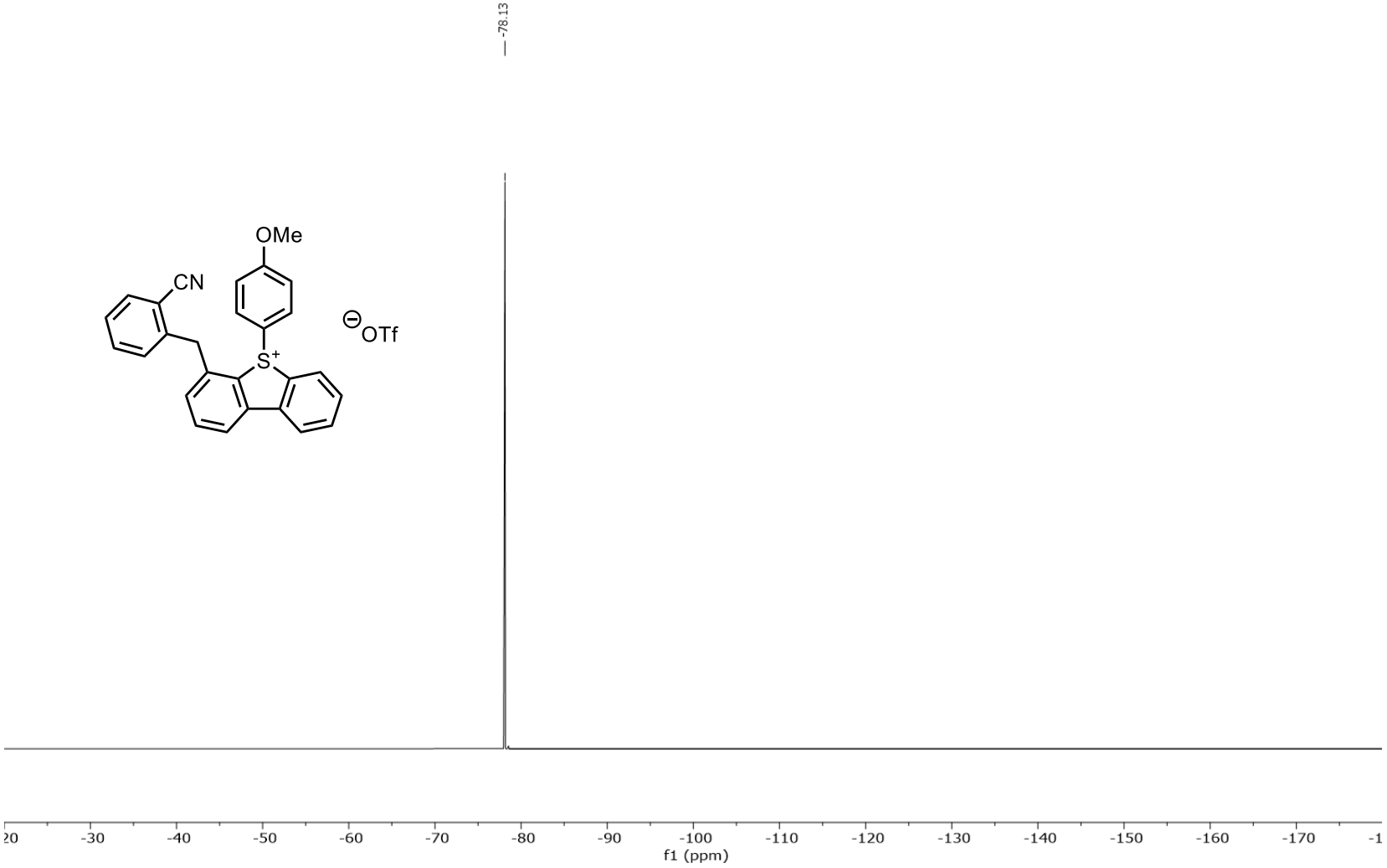

^{1}H NMR of butyl (*E*)-3-(5-(cyclopropylethynyl)-2-fluorophenyl)acrylate (**4a**)

$CDCl_3$, 600 MHz, 298 K

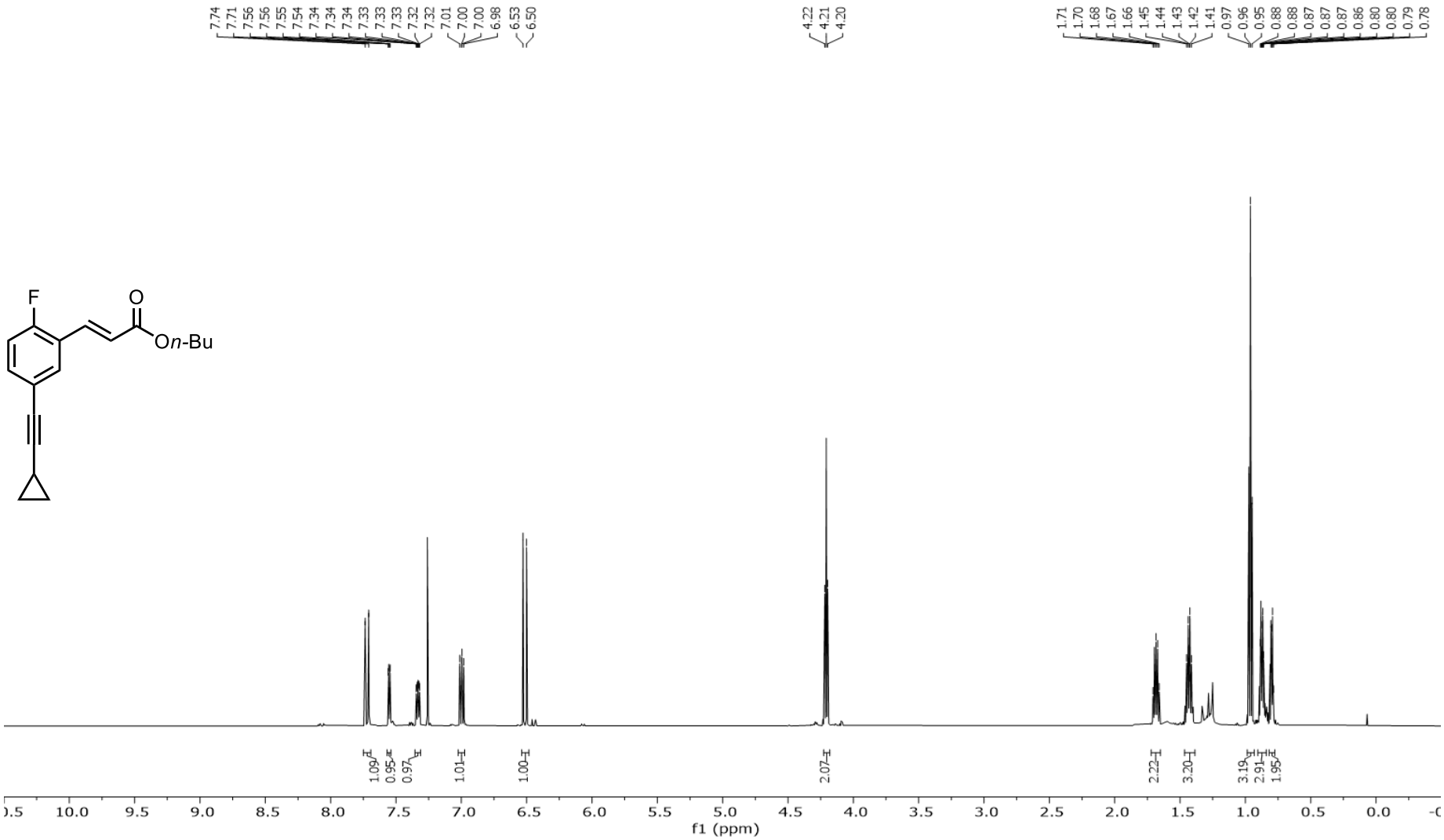

^{13}C NMR of butyl (*E*)-3-(5-(cyclopropylethynyl)-2-fluorophenyl)acrylate (**4a**)

$CDCl_3$, 151 MHz, 298 K

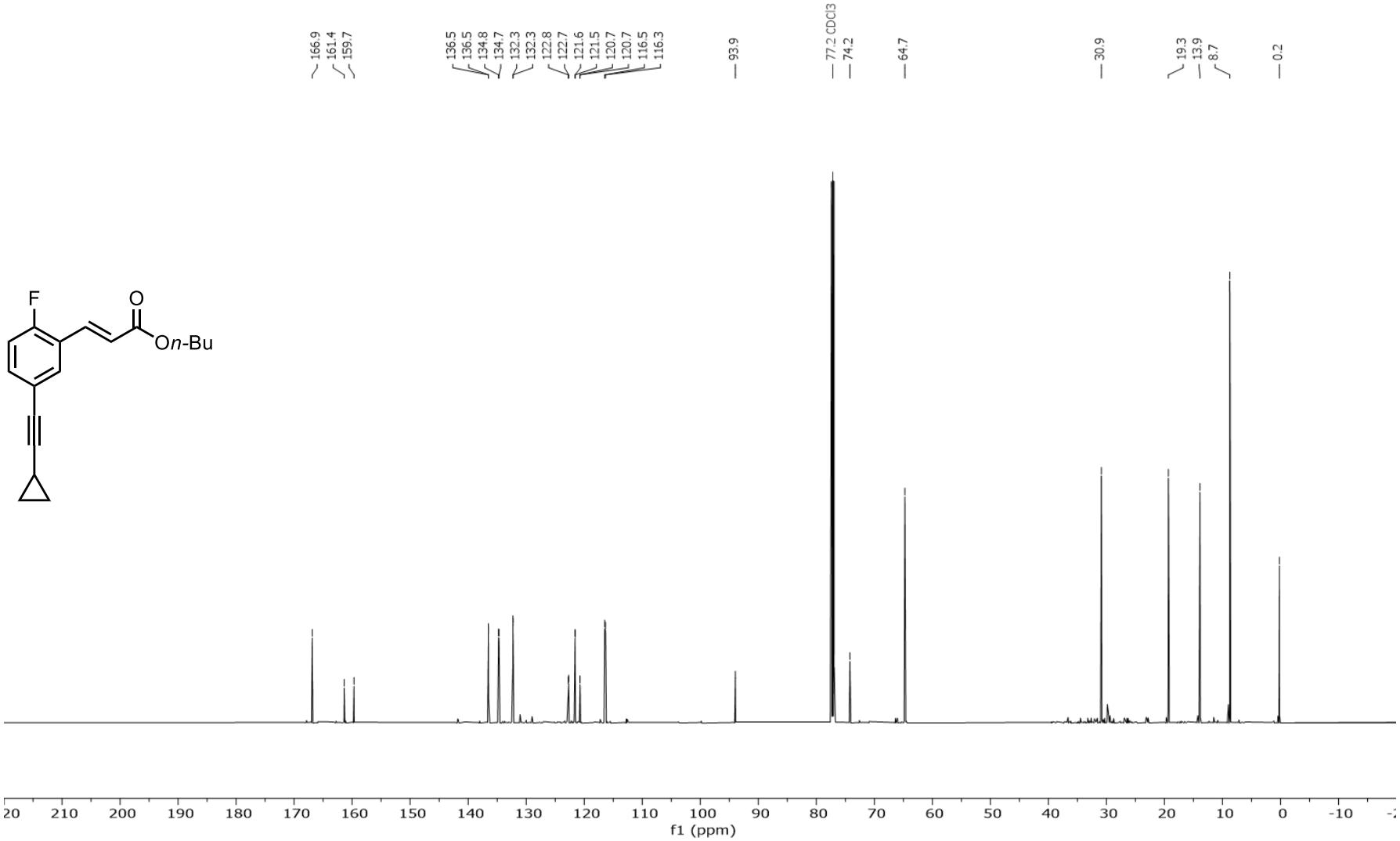

^{19}F NMR of butyl (*E*)-3-(5-(cyclopropylethynyl)-2-fluorophenyl)acrylate (**4a**)

$CDCl_3$, 565 MHz, 298 K

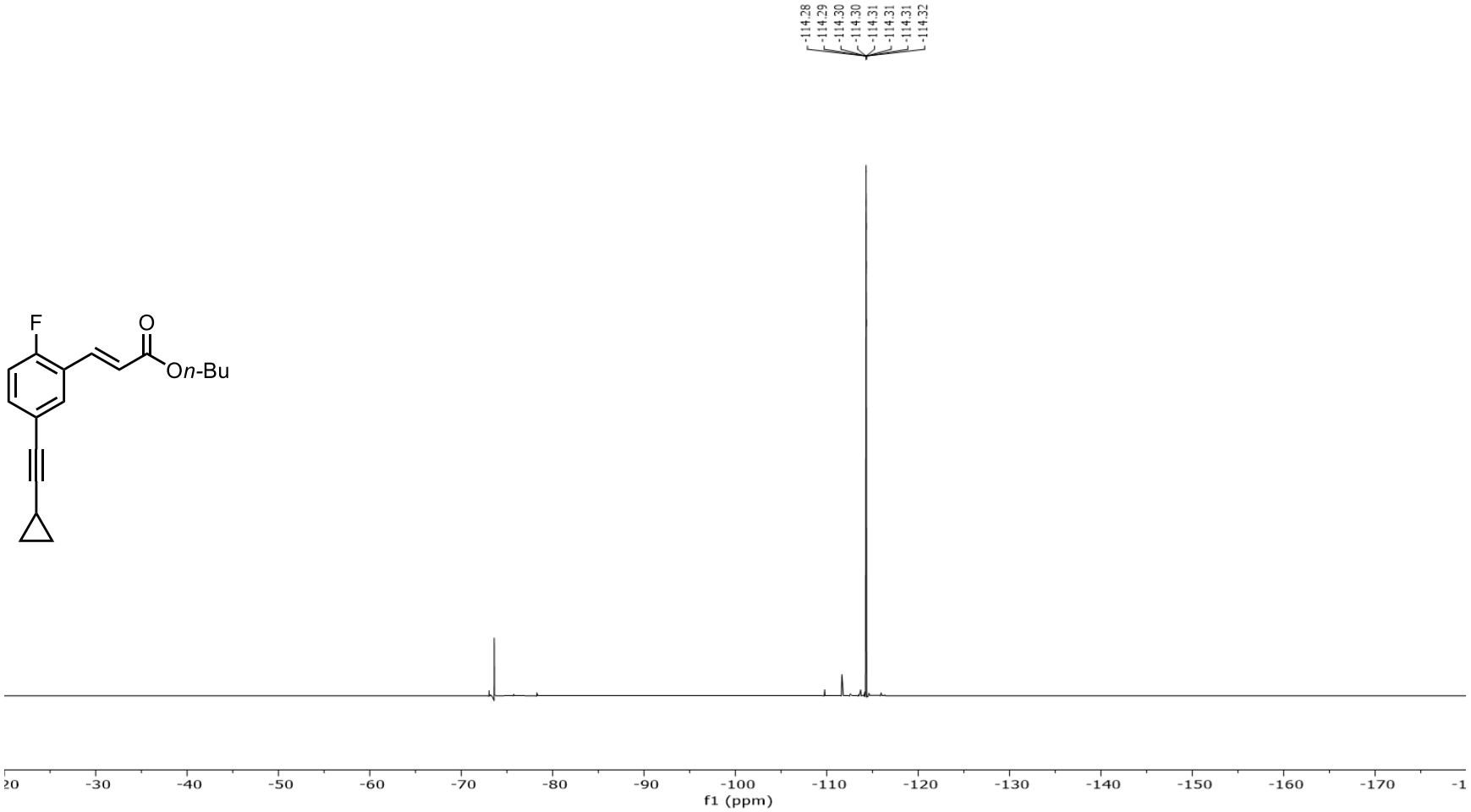

^{1}H – ^{1}H COSY NMR of n-butyl (*E*)-3-(5-(cyclopropylethynyl)-2-fluorophenyl)acrylate (**4a**)

$CDCl_3$, 298 K

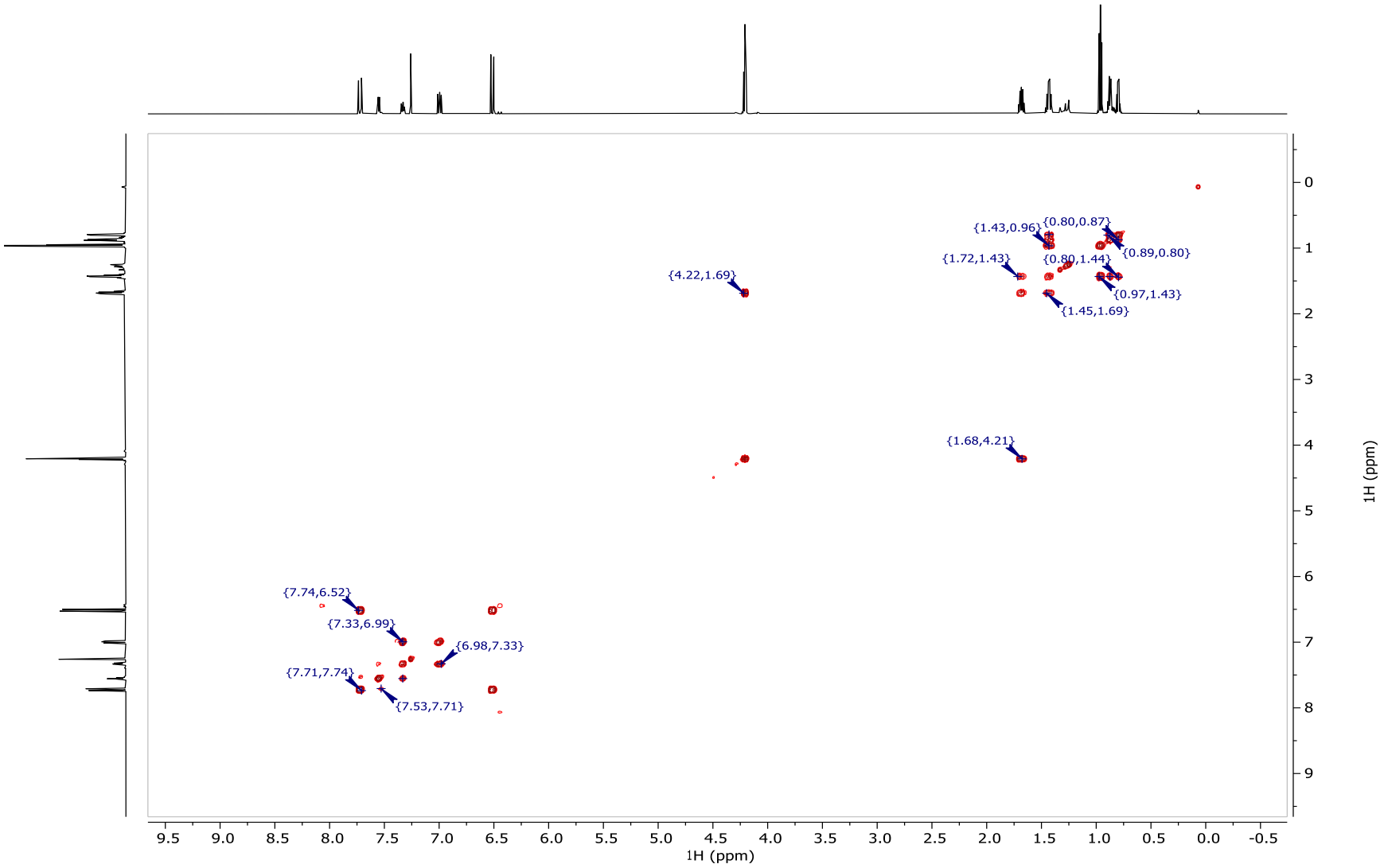

^{1}H – ^{13}C HSQC NMR of *n*-butyl (*E*)-3-(5-(cyclopropylethynyl)-2-fluorophenyl)acrylate (**4a**)

$CDCl_3$, 298 K

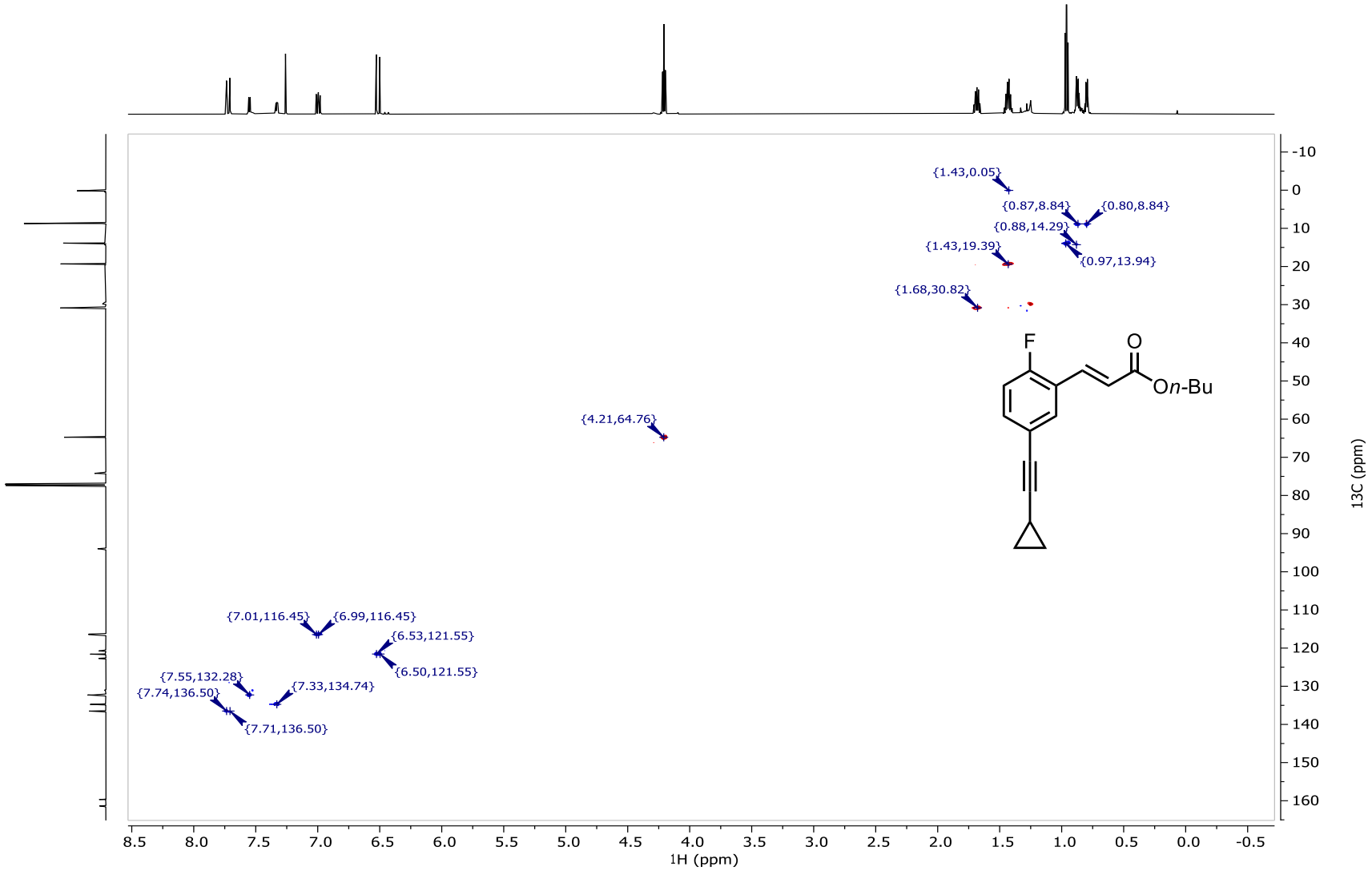

^{1}H – ^{13}C HMBC NMR of *n*-butyl (*E*)-3-(5-(cyclopropylethynyl)-2-fluorophenyl)acrylate (**4a**)

$CDCl_3$, 298 K

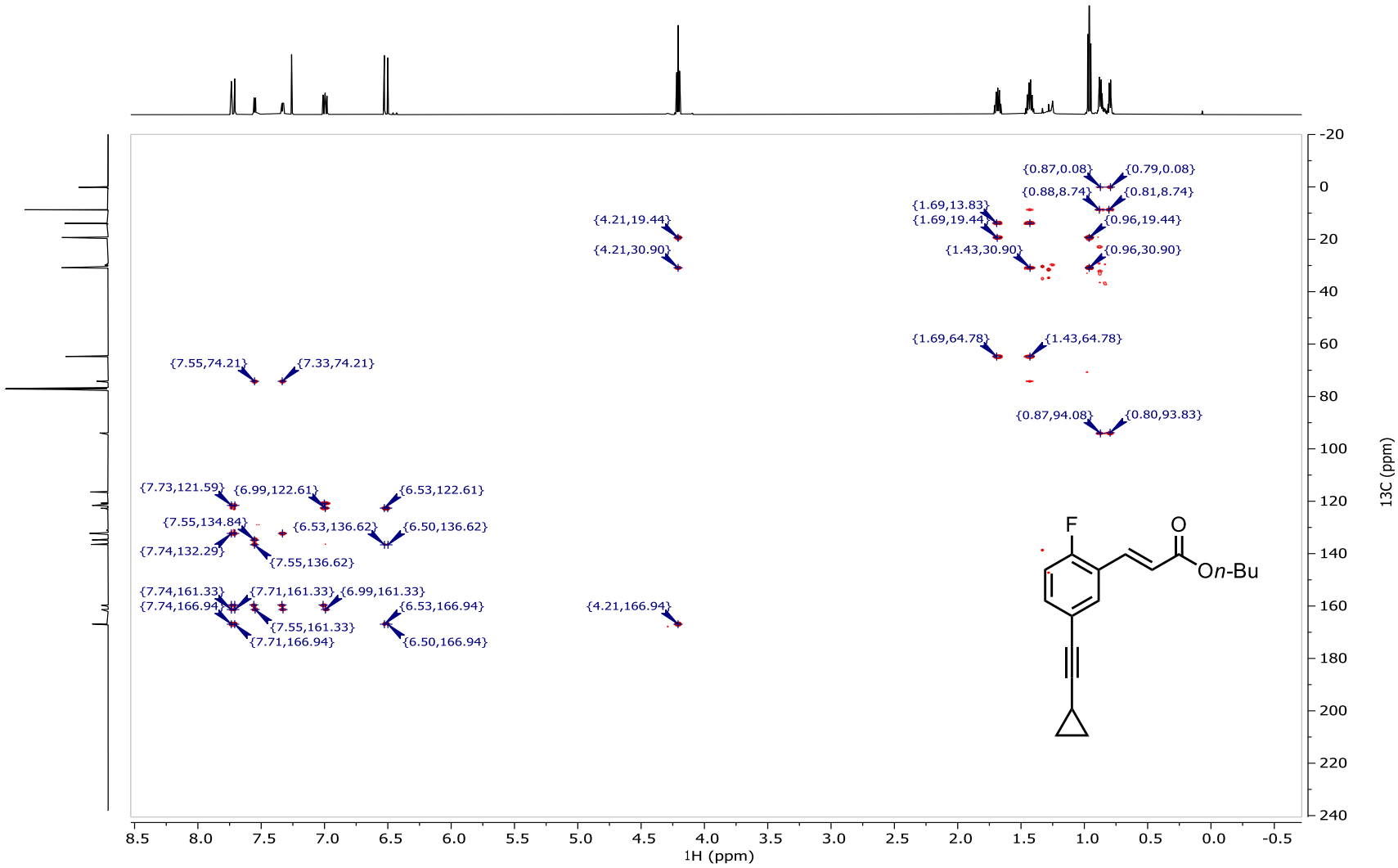

^{1}H – ^{1}H NOESY NMR of *n*-butyl (*E*)-3-(5-(cyclopropylethynyl)-2-fluorophenyl)acrylate (**4a**)

$CDCl_3$, 298 K

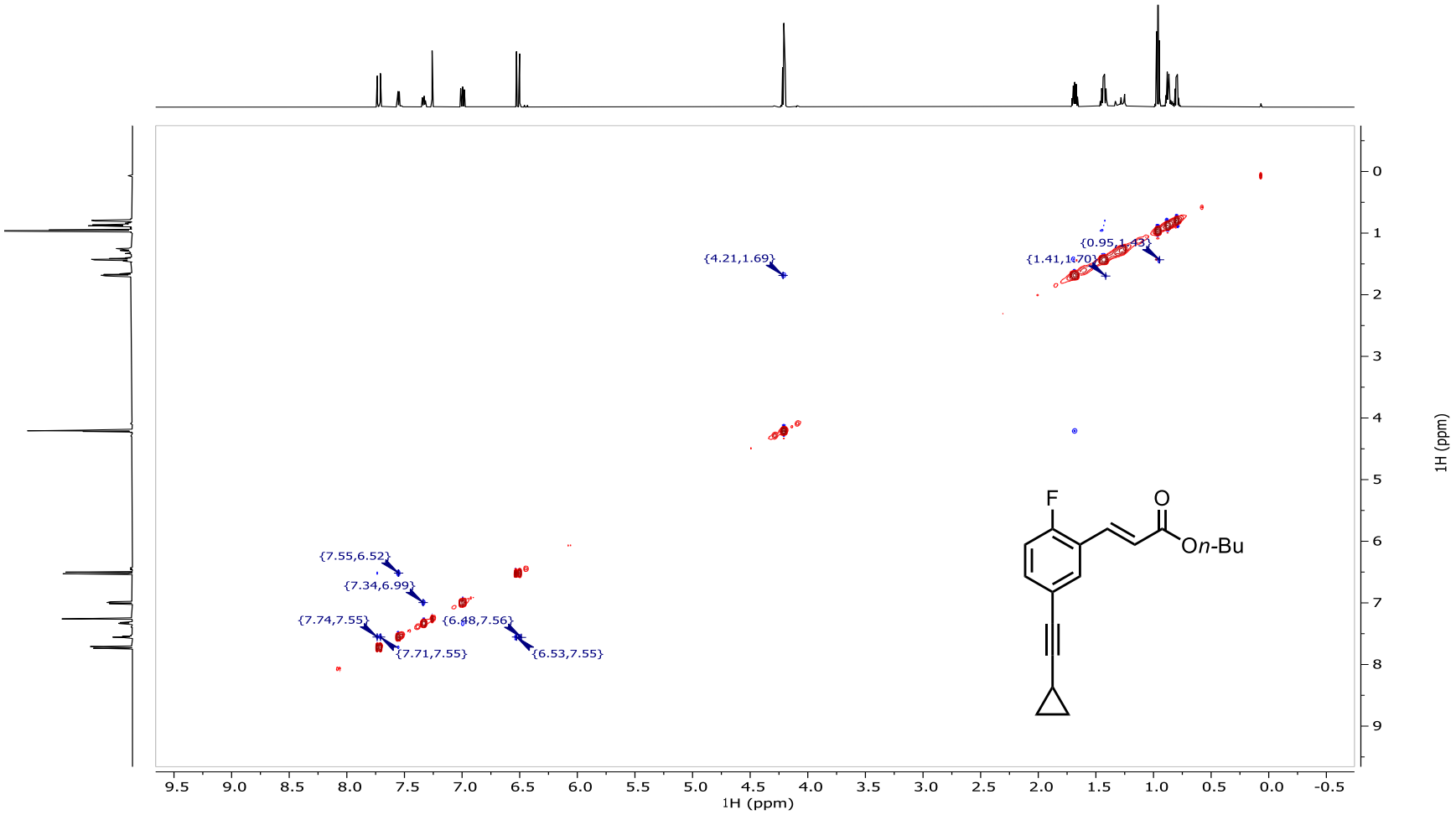

^{1}H NMR of butyl (*E*)-3-(5-(cyclopropylethynyl)-2-methoxyphenyl)acrylate (**4b**)

$CDCl_3$, 600 MHz, 298 K

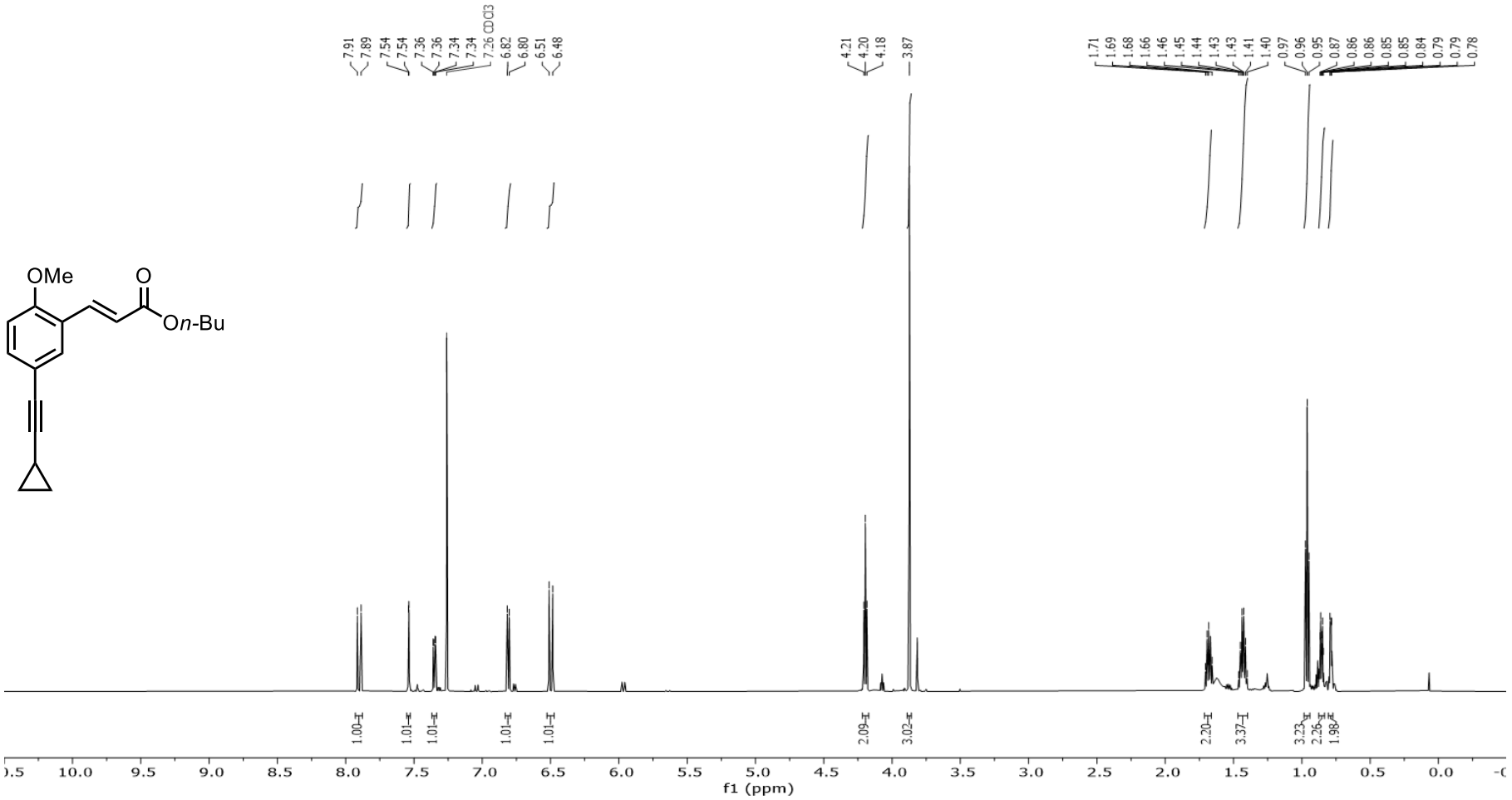

^{13}C NMR of butyl (*E*)-3-(5-(cyclopropylethynyl)-2-methoxyphenyl)acrylate (**4b**)

$CDCl_3$, 151 MHz, 298 K

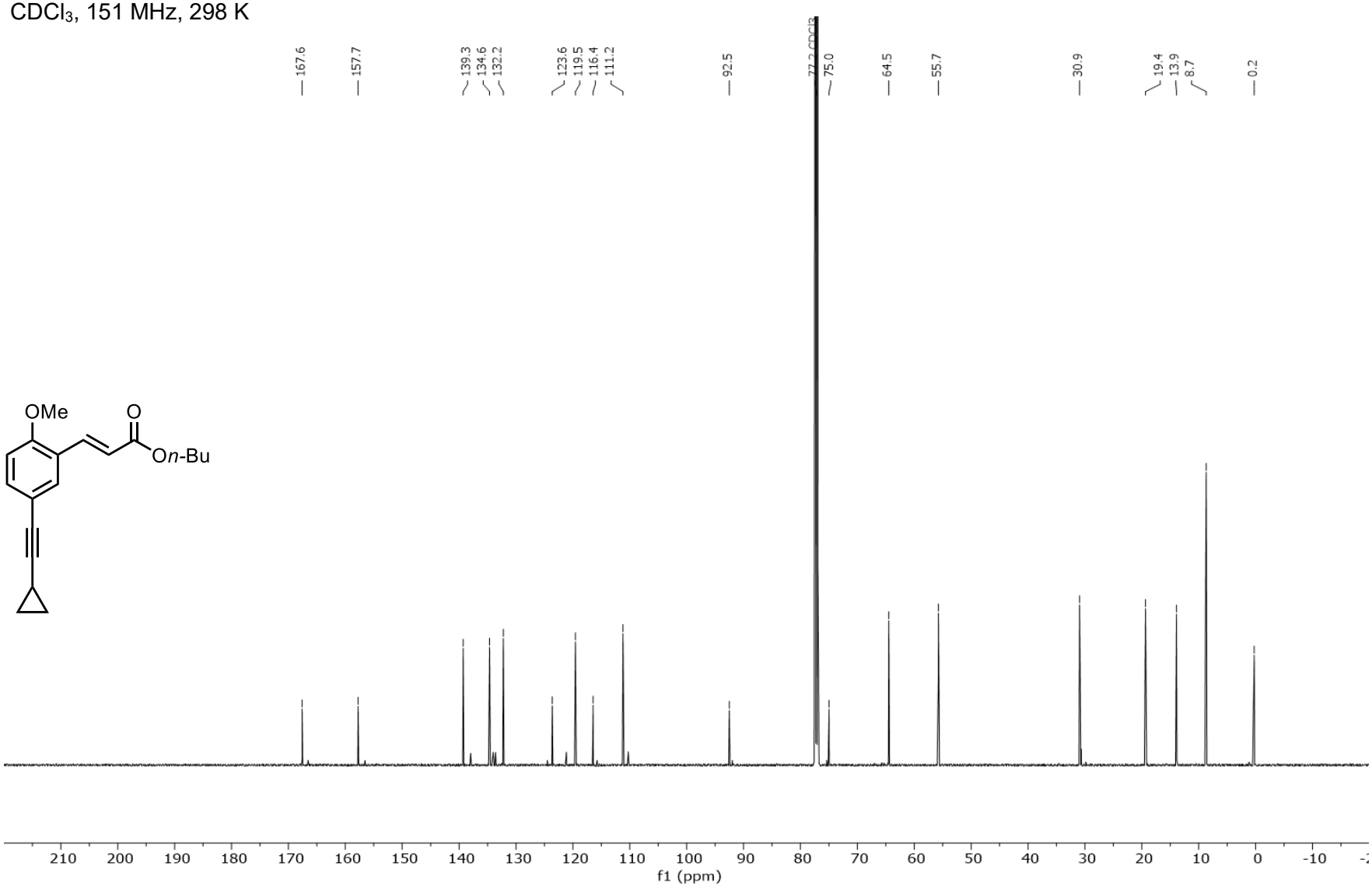

^{1}H NMR of [η^6–ethyl benzoate-η^5-(2,6-dimethyl-4-methoxy -1-phenoxo)Ru](OTf) **(5e)**

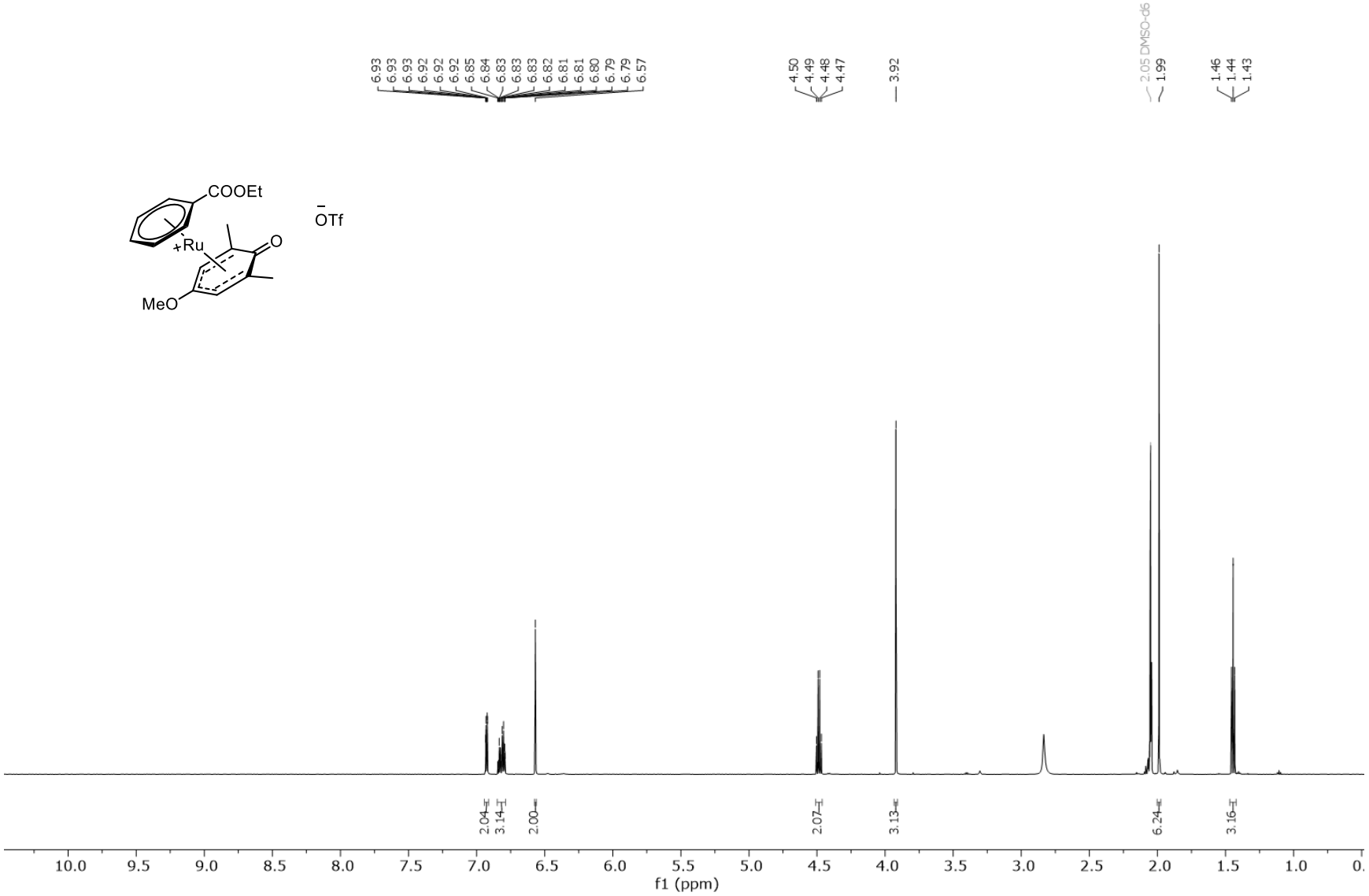

^{13}C NMR of [η^6–ethyl benzoate-η^5-(2,6-dimethyl-4-methoxy -1-phenoxo)Ru](OTf) **(5e)**

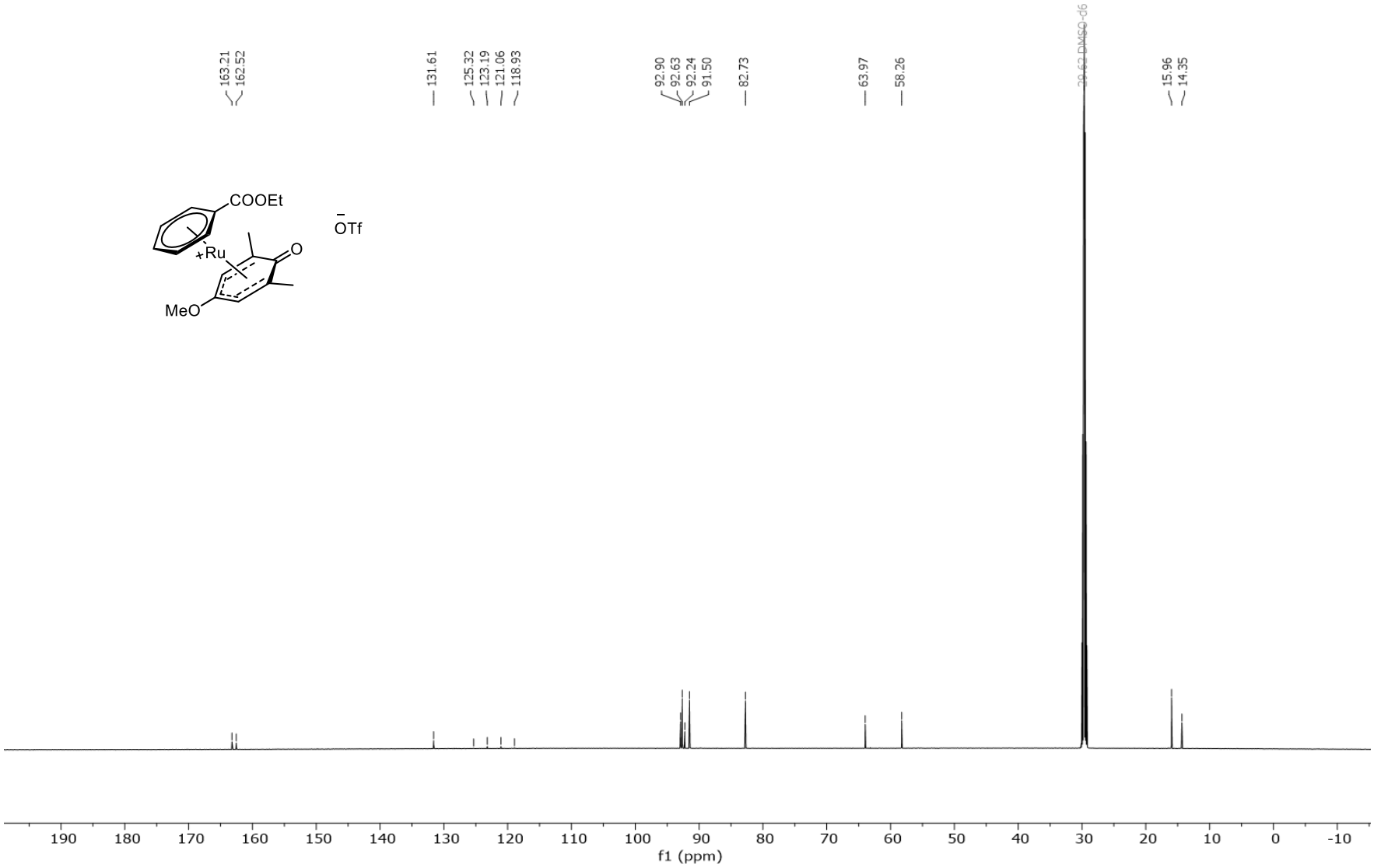

^{19}F NMR of [η^6–ethyl benzoate-η^5-(2,6-dimethyl-4-methoxy -1-phenoxo)Ru](OTf) **(5e)**

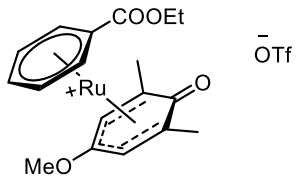

^{1}HNMR of [η^{6}–ethyl benzoate-η^{5}-(2,6-dichloro -1-phenoxo)Ru](OTf) **(5f)**

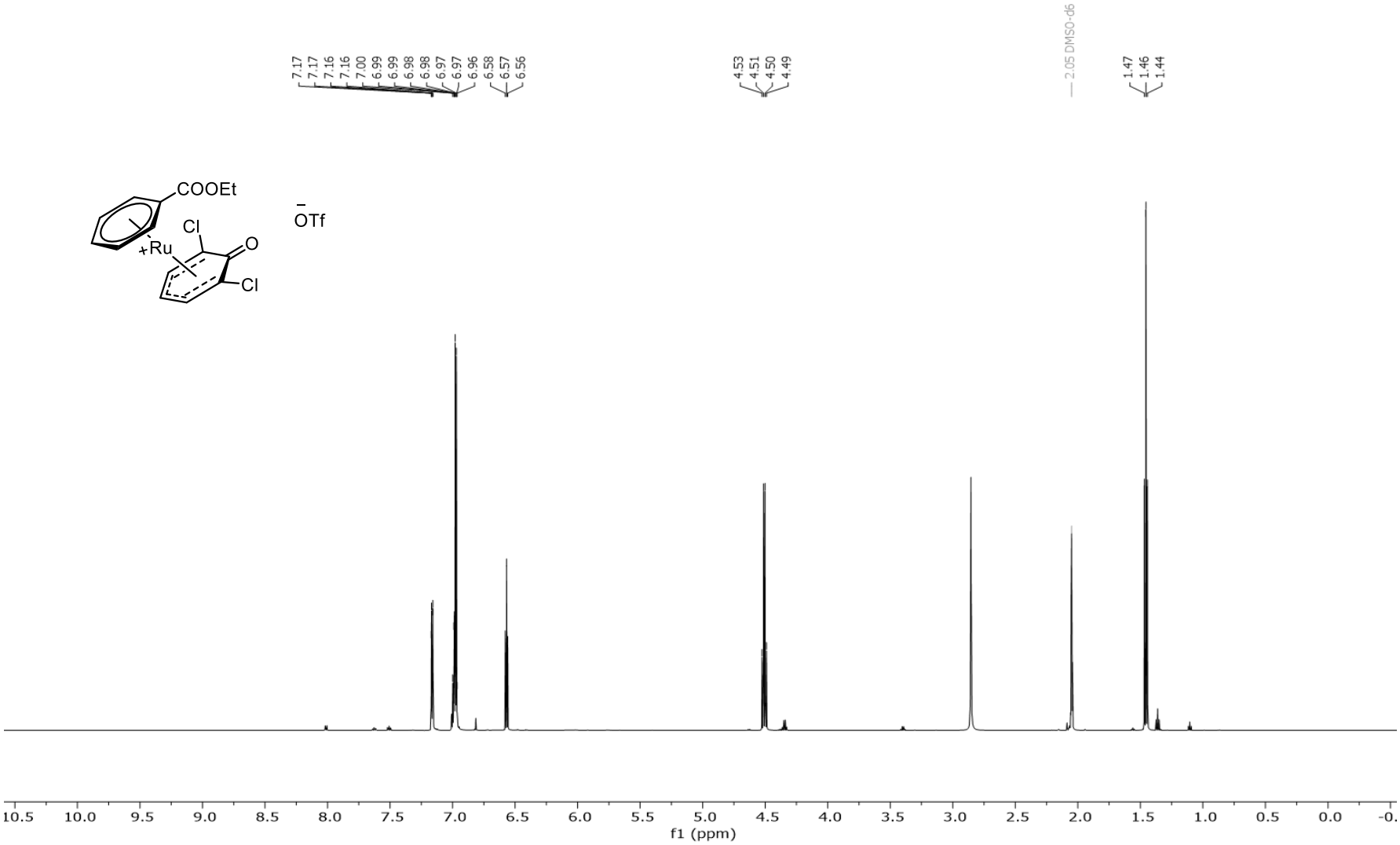

^{13}CNMR of [*η6*–-ethyl benzoate-η^5-(2,6-dichloro -1-phenoxo)Ru](OTf) **(5f)**

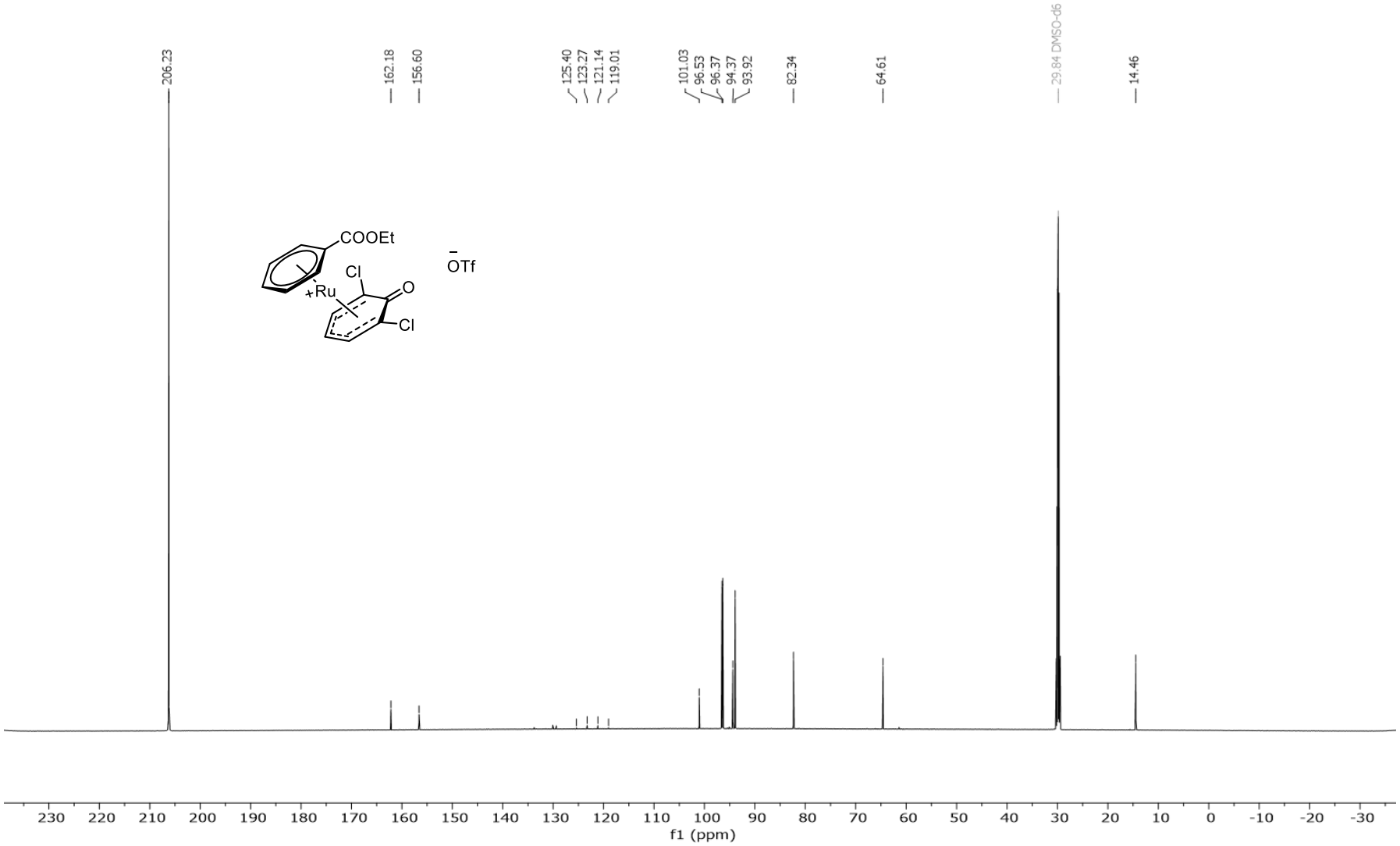

^{19}F NMR of [*η6*–-ethyl benzoate-η^5-(2,6-dichloro -1-phenoxo)Ru](OTf) **(5f)**

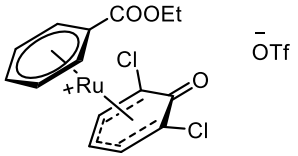

H NMR [*η6*–-(4-methoxyphenol)-η^5-(2,6-dimethyl-4-methoy-1-phenoxo)Ru](OTf) (**7b**)

DMSO-d_6, 600 MHz, 298 K

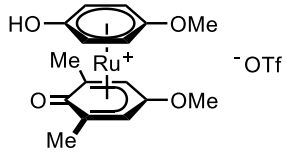

^{13}C NMR of [*η6*–-(4-methoxyphenol)-η^5-(2,6-dimethyl-4-methoy-1-phenoxo)Ru](OTf) (**7b**)

DMSO-d_6, 151 MHz, 298 K

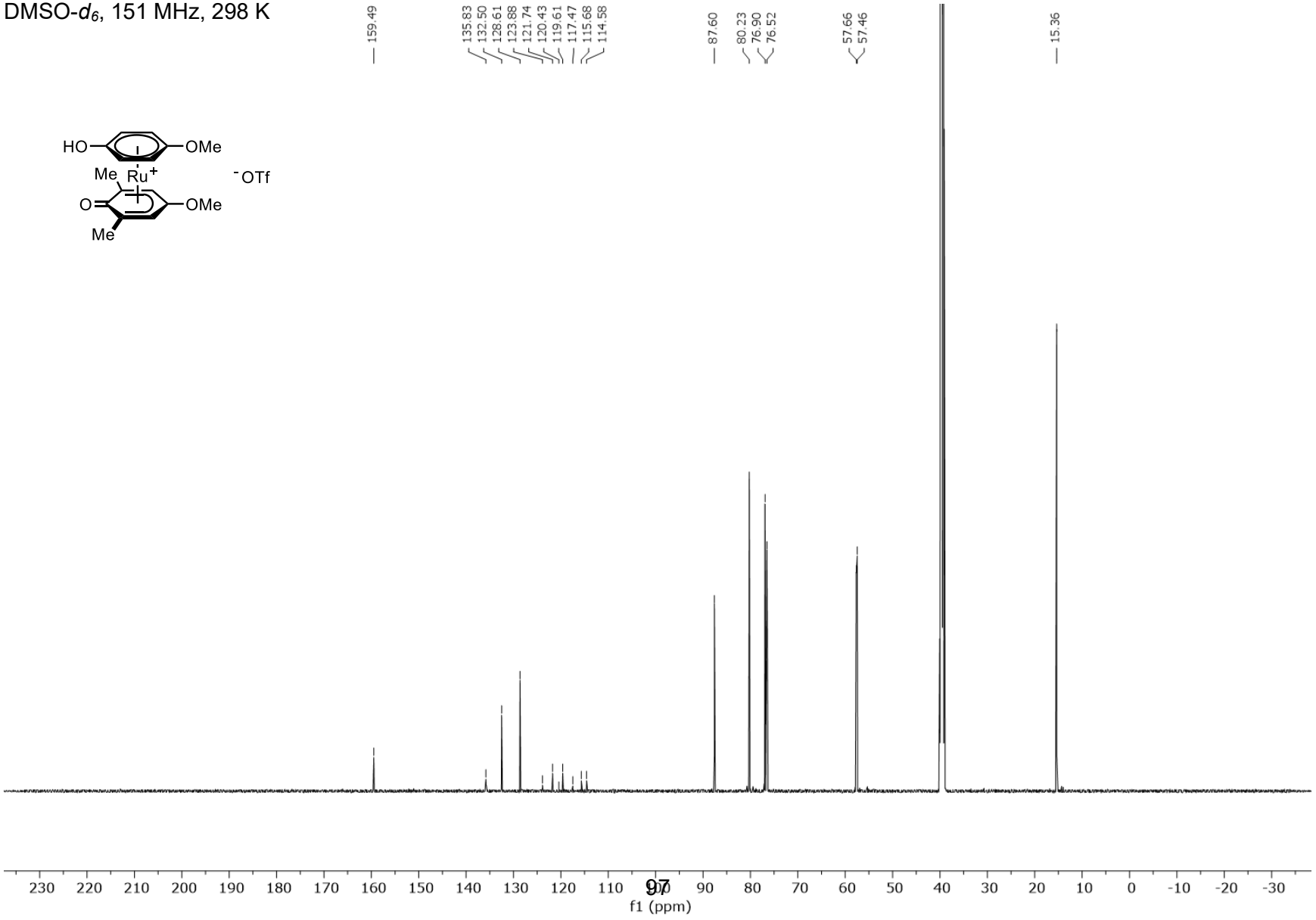

^{19}F NMR of [*η6*–-(4-methoxyphenol)-η^5-(2,6-dimethyl-4-methoy-1-phenoxo)Ru](OTf) (**7b**)

DMSO-d_6, 565 MHz, 298 K

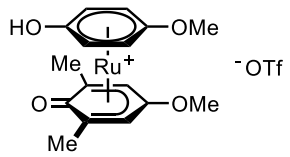

^{1}H NMR [*η6*–-(4-ethylphenol)-*η*^{5}-(2,6-dimethyl-4-methoy-1-phenoxo)Ru](OTf) (**7a**)

DMSO-d_6, 600 MHz, 298 K

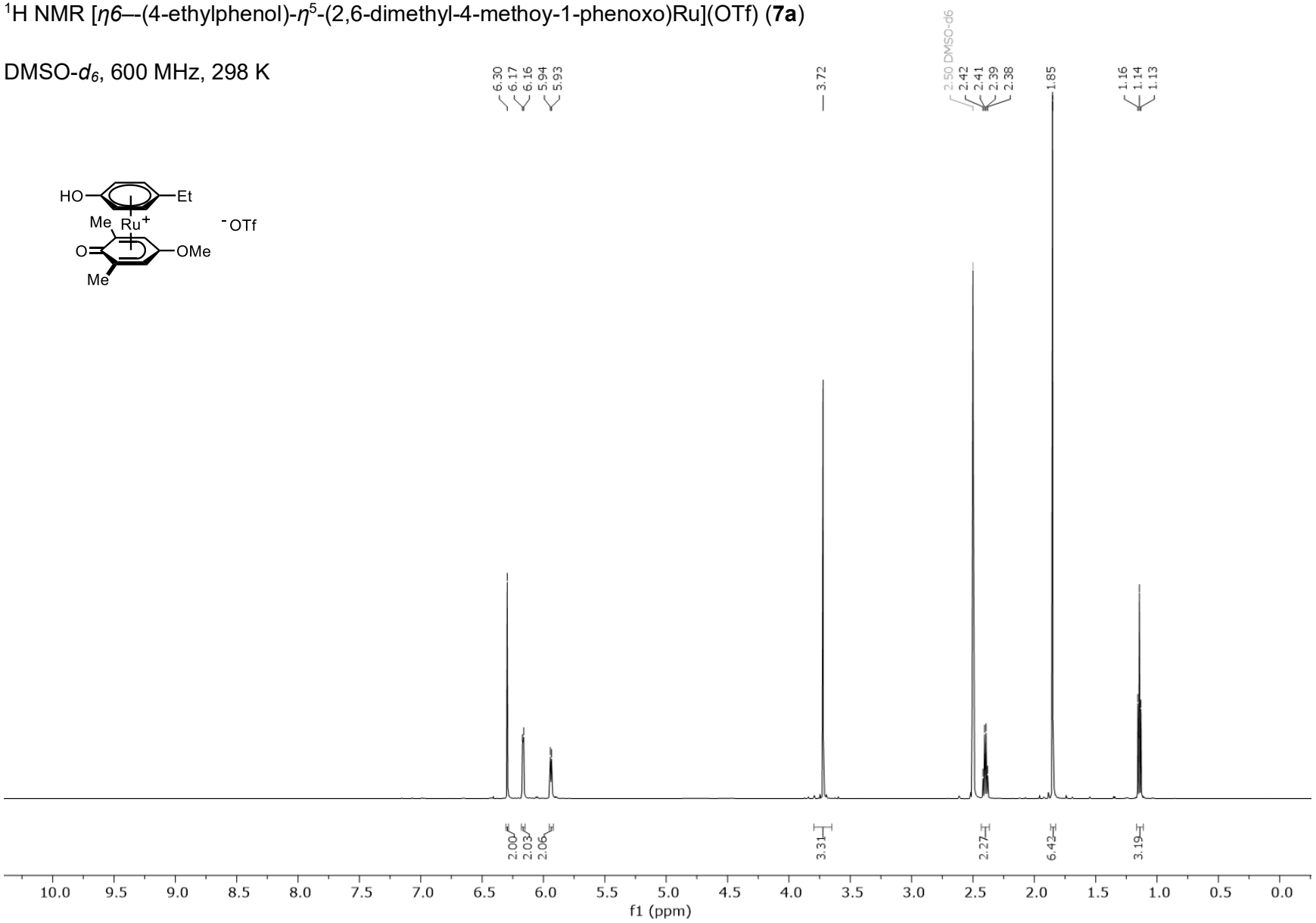

^{13}C NMR of [*η6*–-(4-ethylphenol)-*η*^{5}-(2,6-dimethyl-4-methoy-1-phenoxo)Ru](OTf) (**7a**)

DMSO-d_6, 151 MHz, 298 K

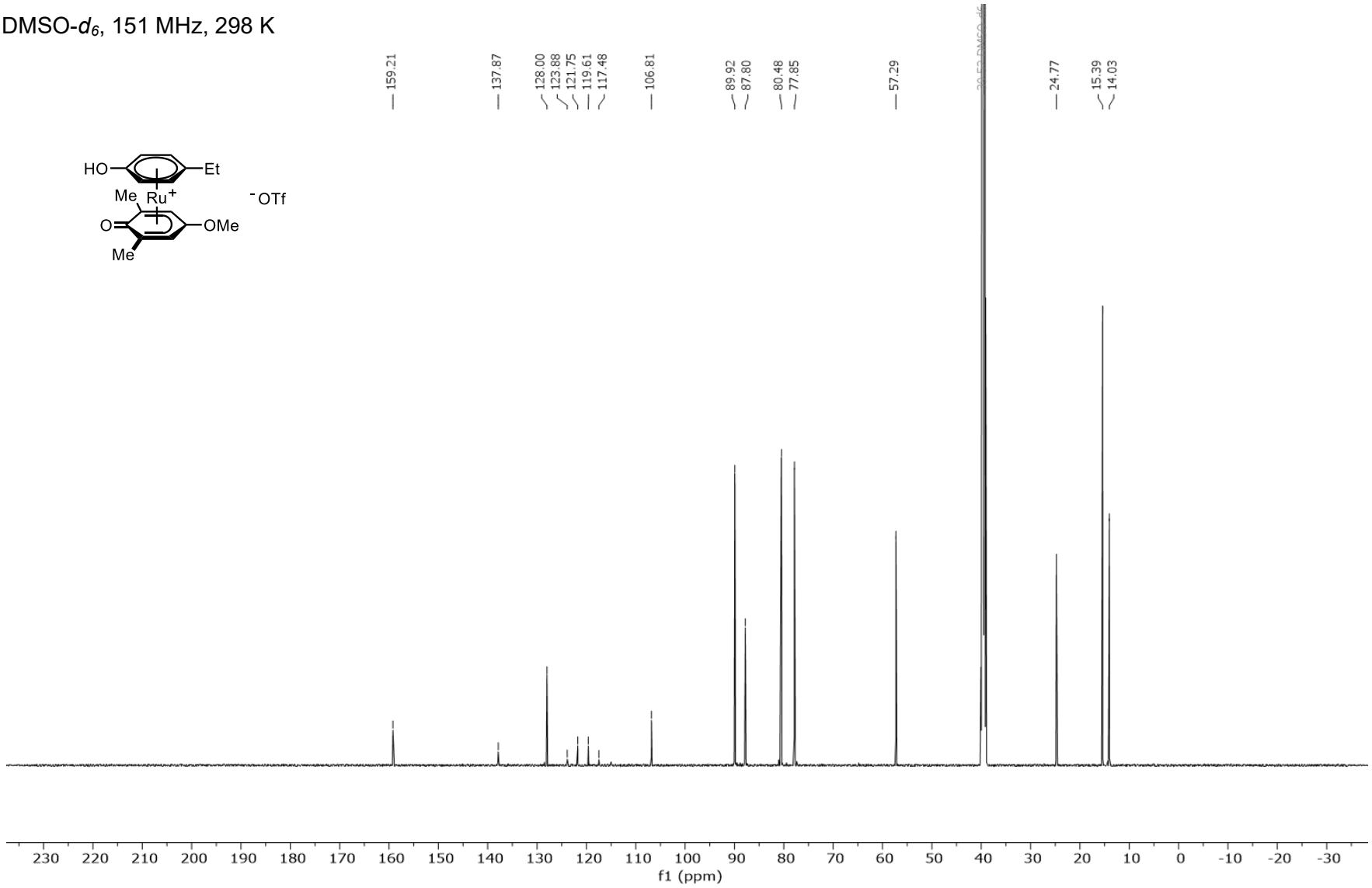

^{19}F NMR of [*η6*–-(4-ethylphenol)-η^5-(2,6-dimethyl-4-methoy-1-phenoxo)Ru](OTf) (**7a**)

DMSO-d_6, 565 MHz, 298 K

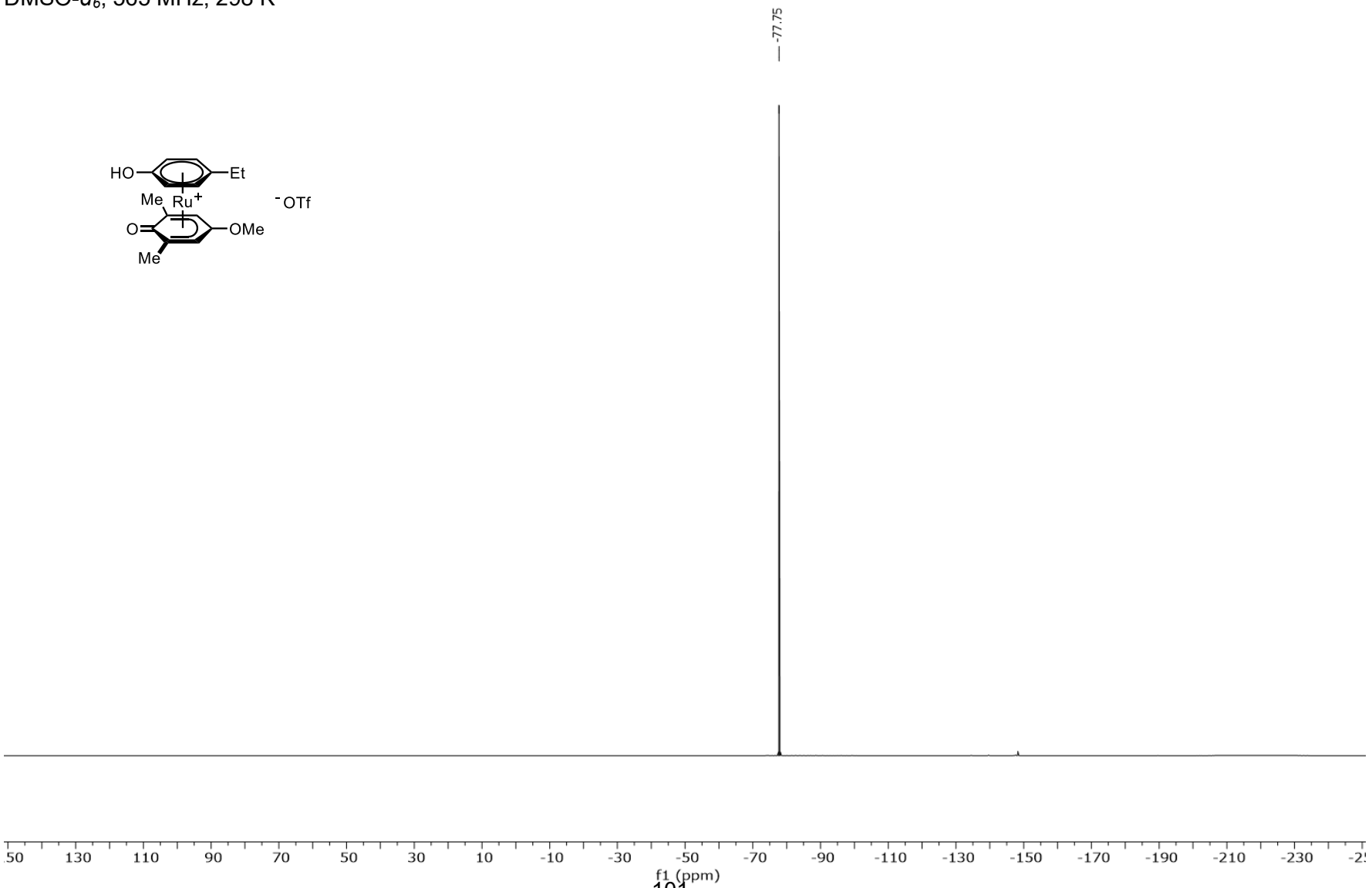

^{1}H NMR *N*-acetyl tyrosine derived ruthenium complex (**7d**)

DMSO-d_6, 600 MHz, 298 K

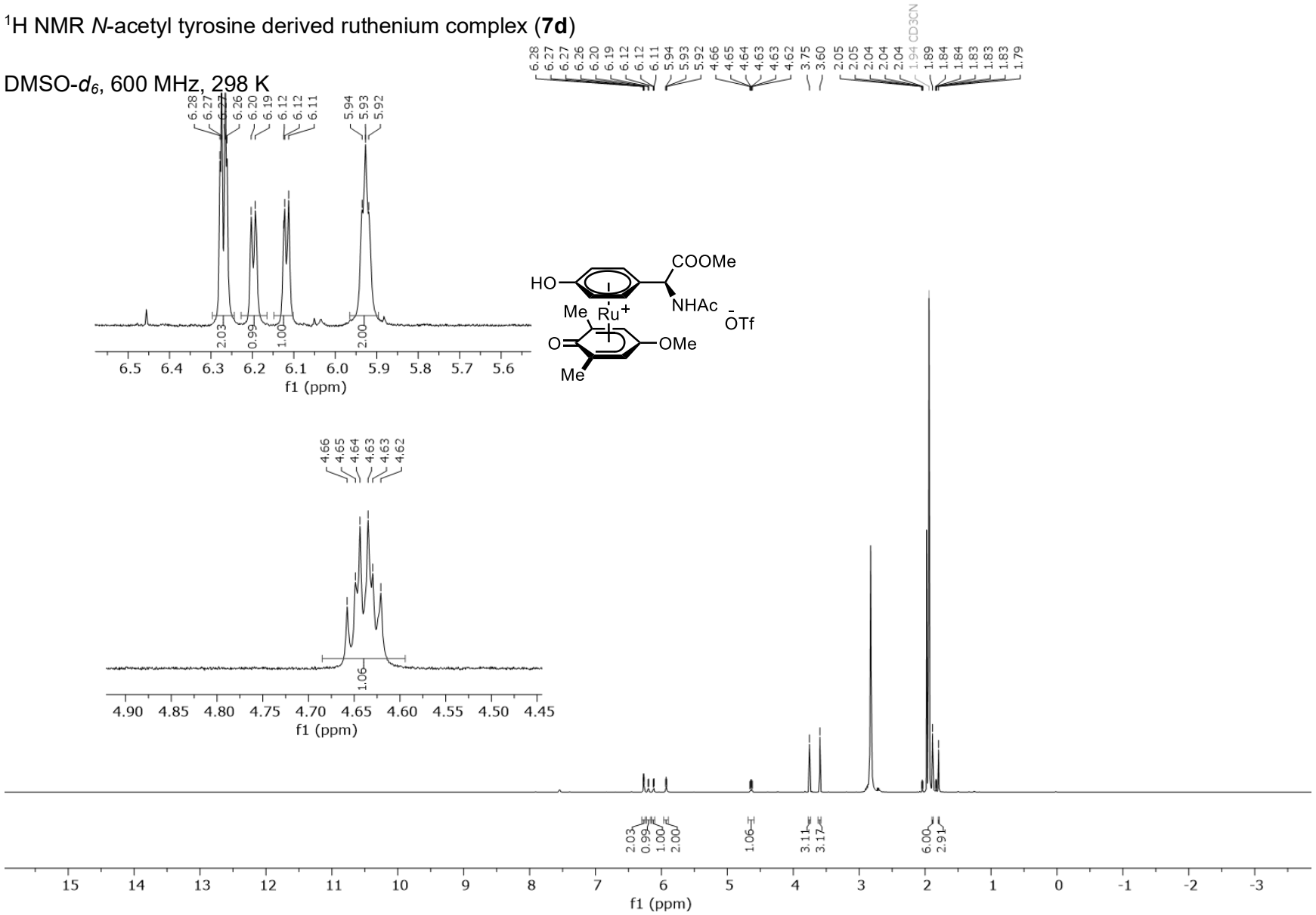

^{13}C NMR of *N*-acetyl tyrosine derived ruthenium complex (**7d**)

DMSO-d_6, 151 MHz, 298 K

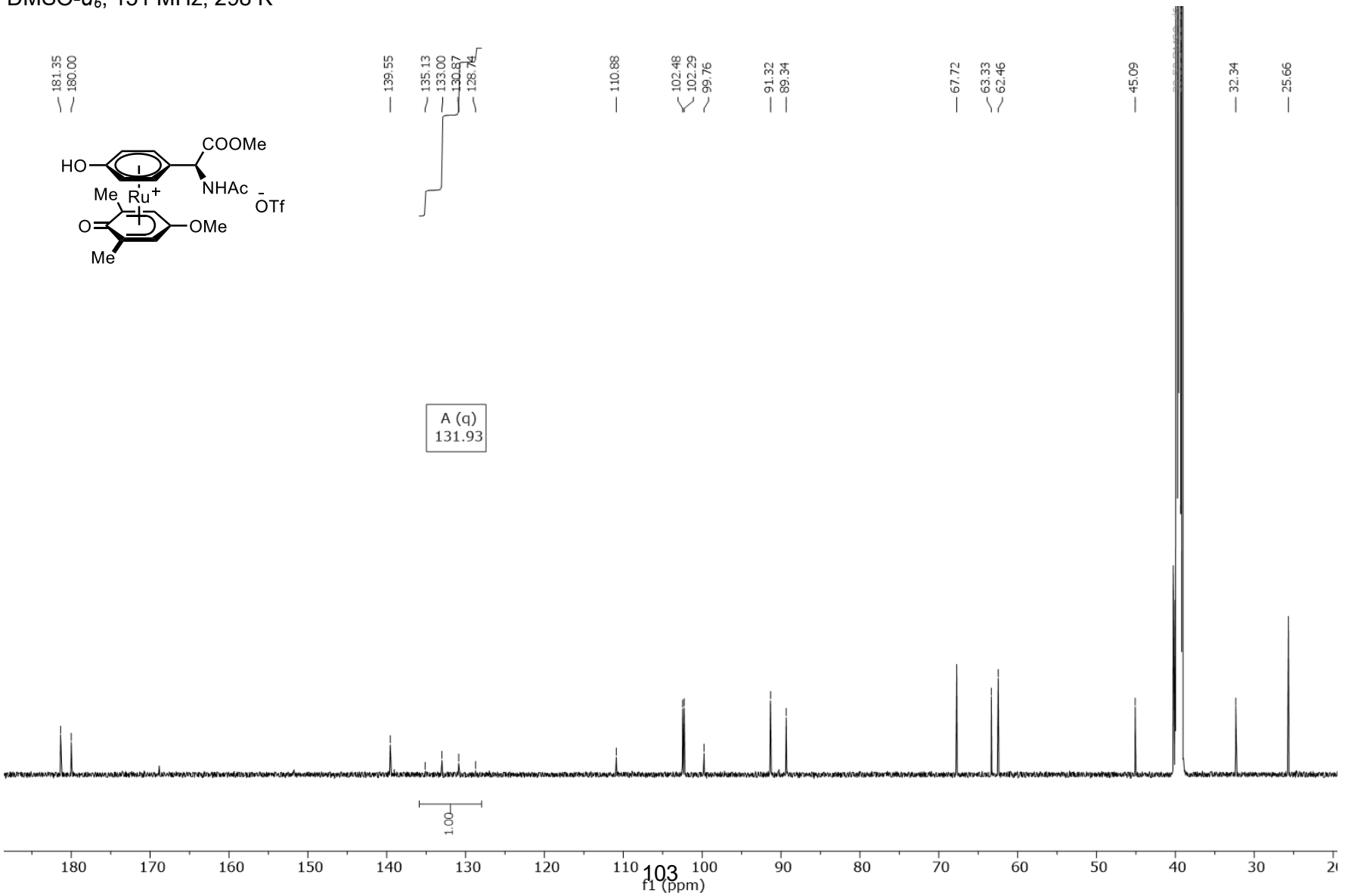

^{19}F NMR of [*N*-acetyl tyrosine derived ruthenium complex (**7d**)

DMSO-d_6, 565 MHz, 298 K

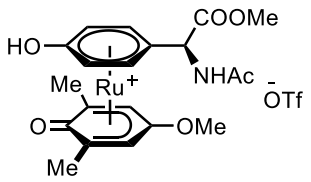

^{1}H NMR Estrone derived ruthenium complex **9**

CD_3CN, 500 MHz, 298 K

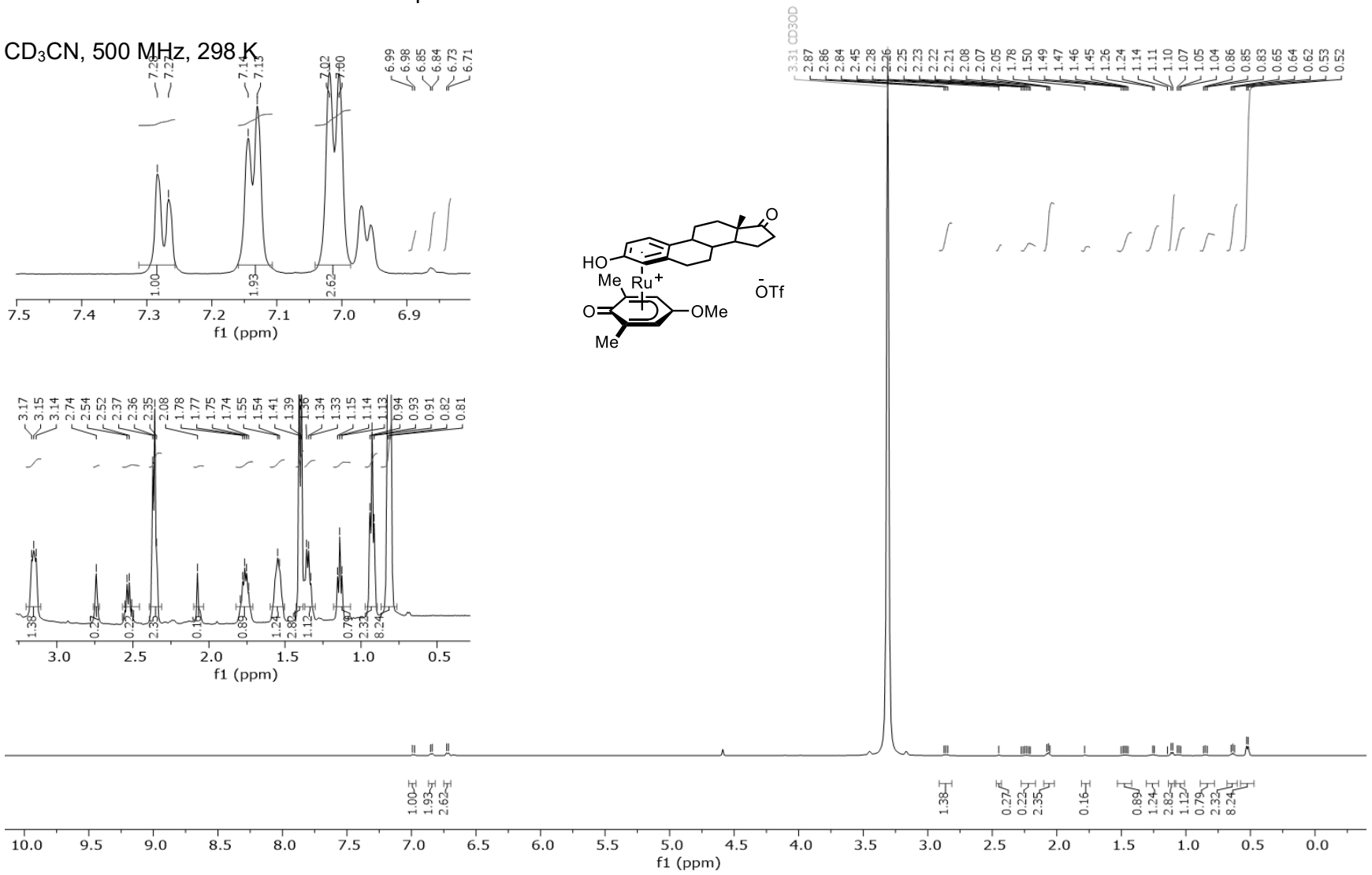

^{1}H NMR of [*η6*–(4-hydroxyphenylethanol)-η^{5}-(2,6-dimethyl-4-methoy-1-phenoxo)Ru](OTf) (**7c**)

DMSO-d_6, 600 MHz, 298 K

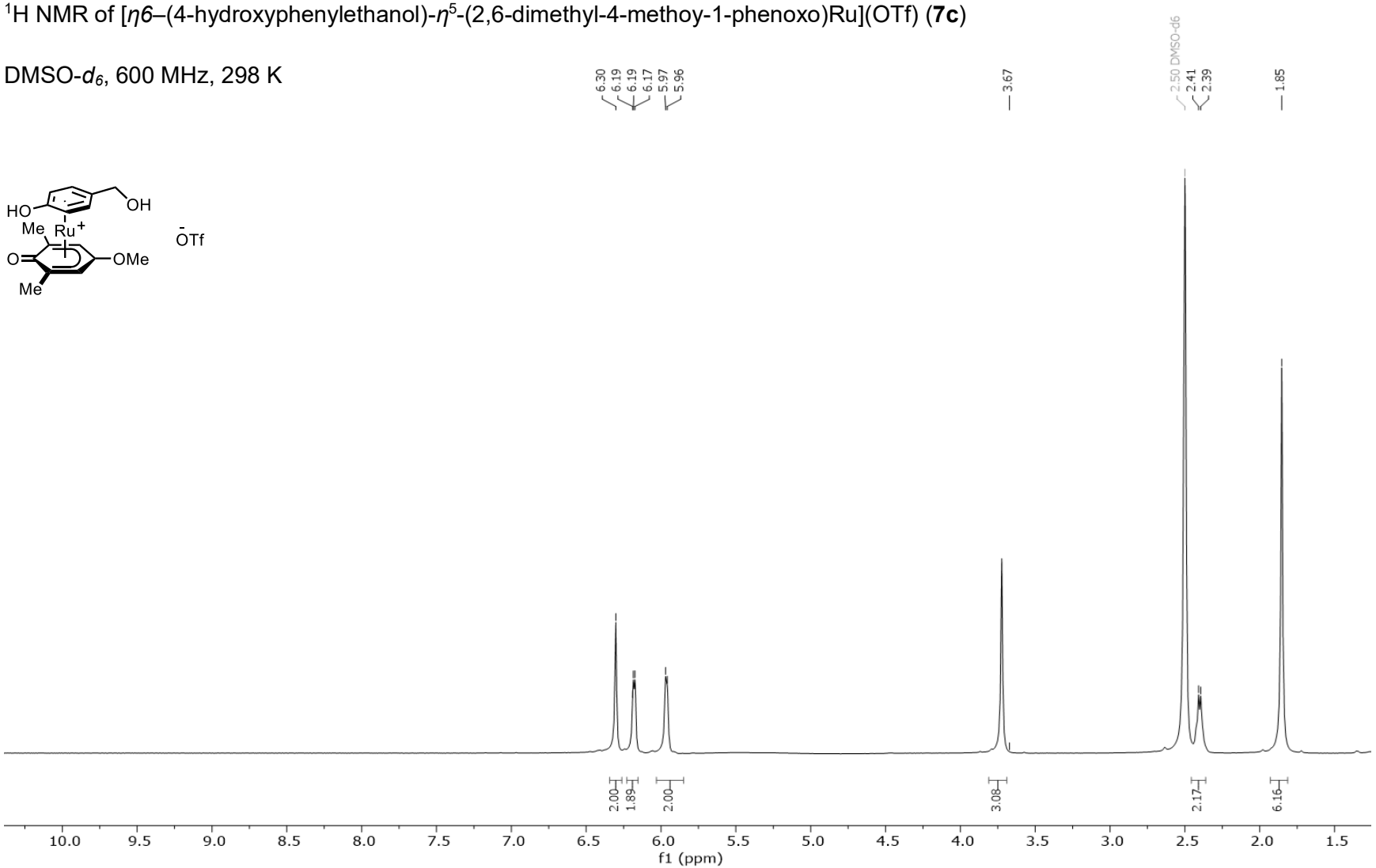

^{19}C NMR of [*η6*–-(4-hydroxyphenylethanol)-η^5-(2,6-dimethyl-4-methoy-1-phenoxo)Ru](OTf) (**7c**)

DMSO-d_6, 565 MHz, 298 K

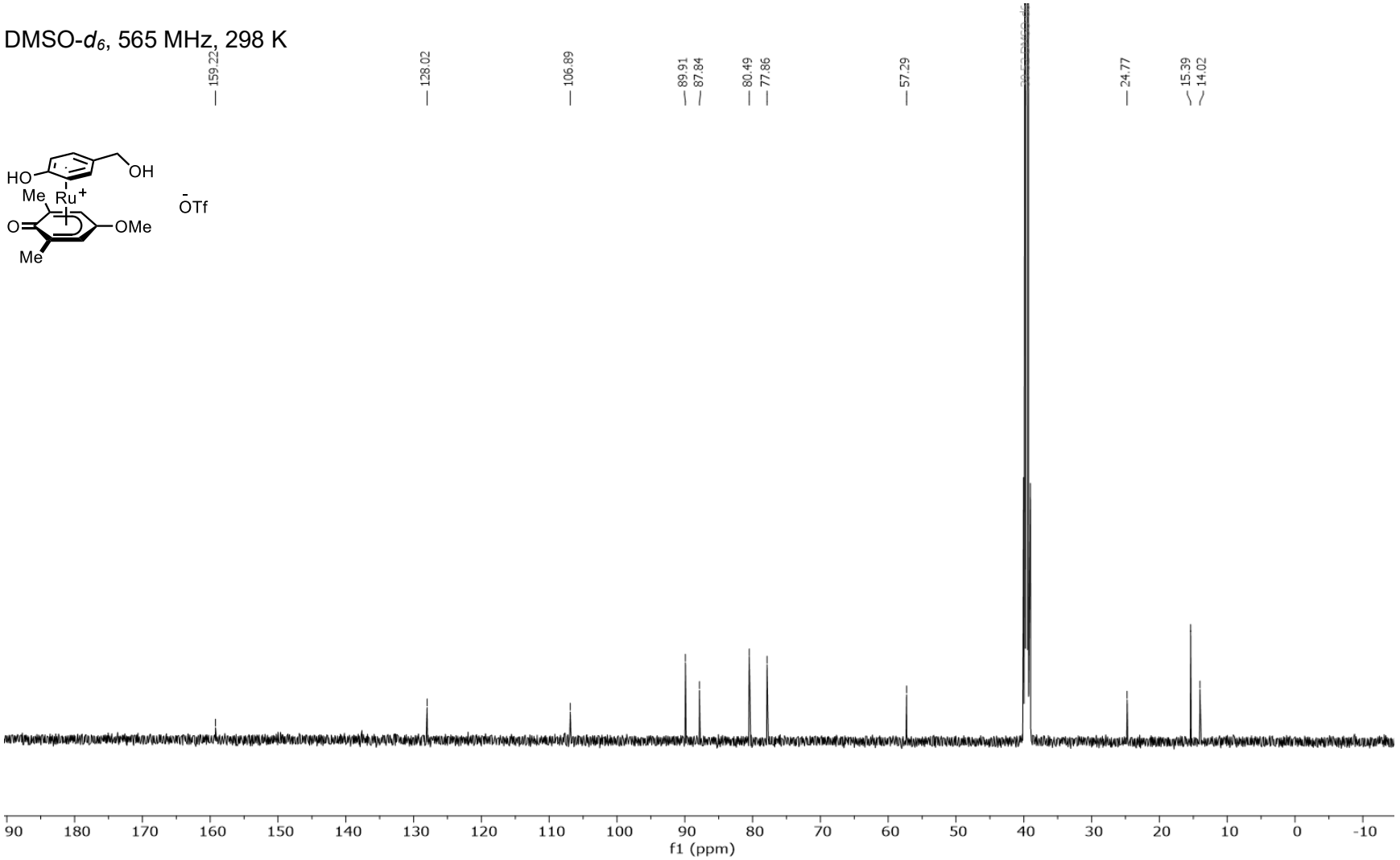

^{19}F NMR of [*η6*–-(4-hydroxyphenylethanol)-η^5-(2,6-dimethyl-4-methoy-1-phenoxo)Ru](OTf) (**7c**)

DMSO-d_6, 565 MHz, 298 K

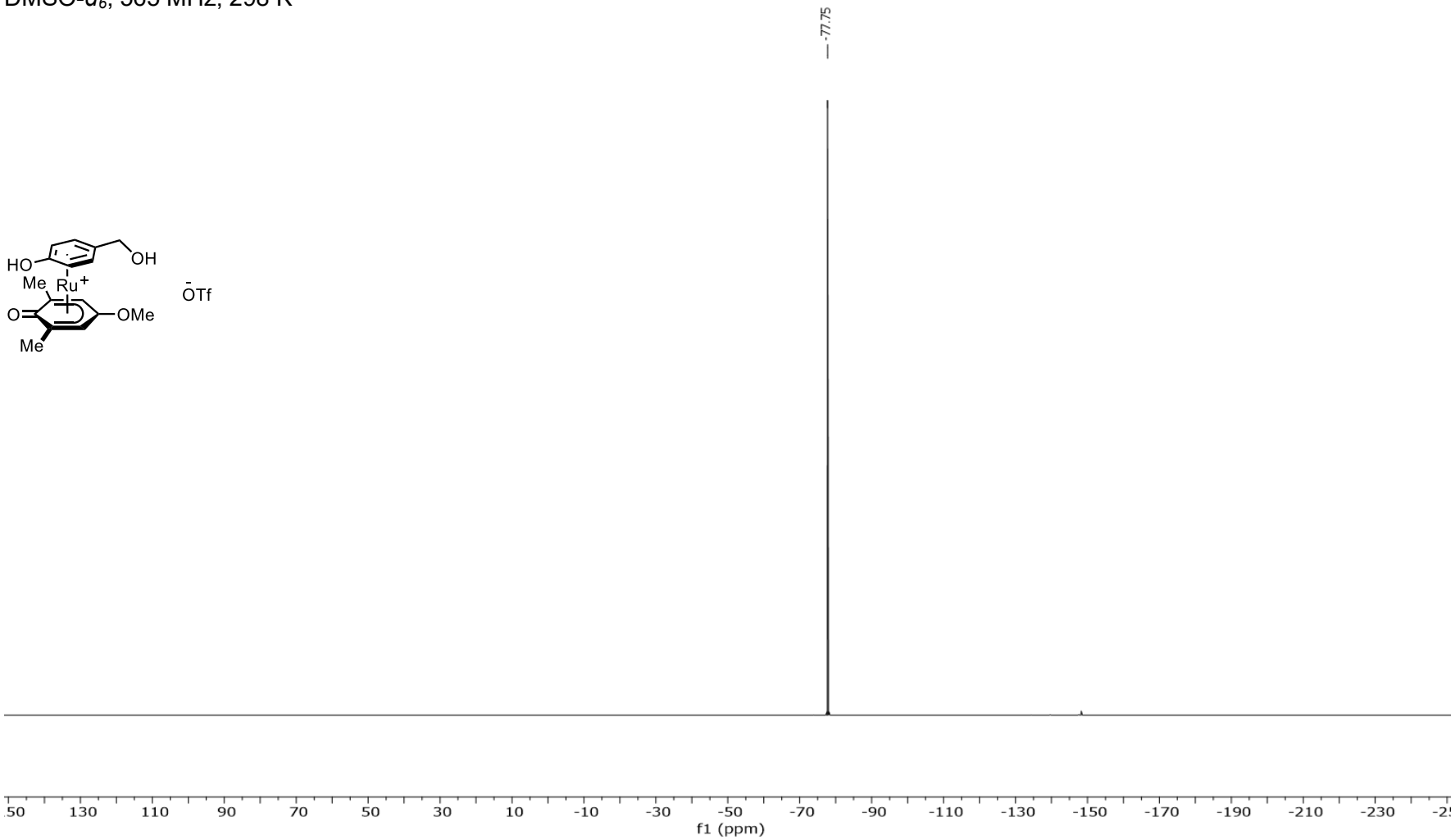

^{19}H NMR of [η^6–(4-hydroxytoluene)-η^5-(2,6-dimethyl-4-methoy-1-phenoxo)Ru](OTf) (**7e**)

DMSO-d_6, 565 MHz, 298 K

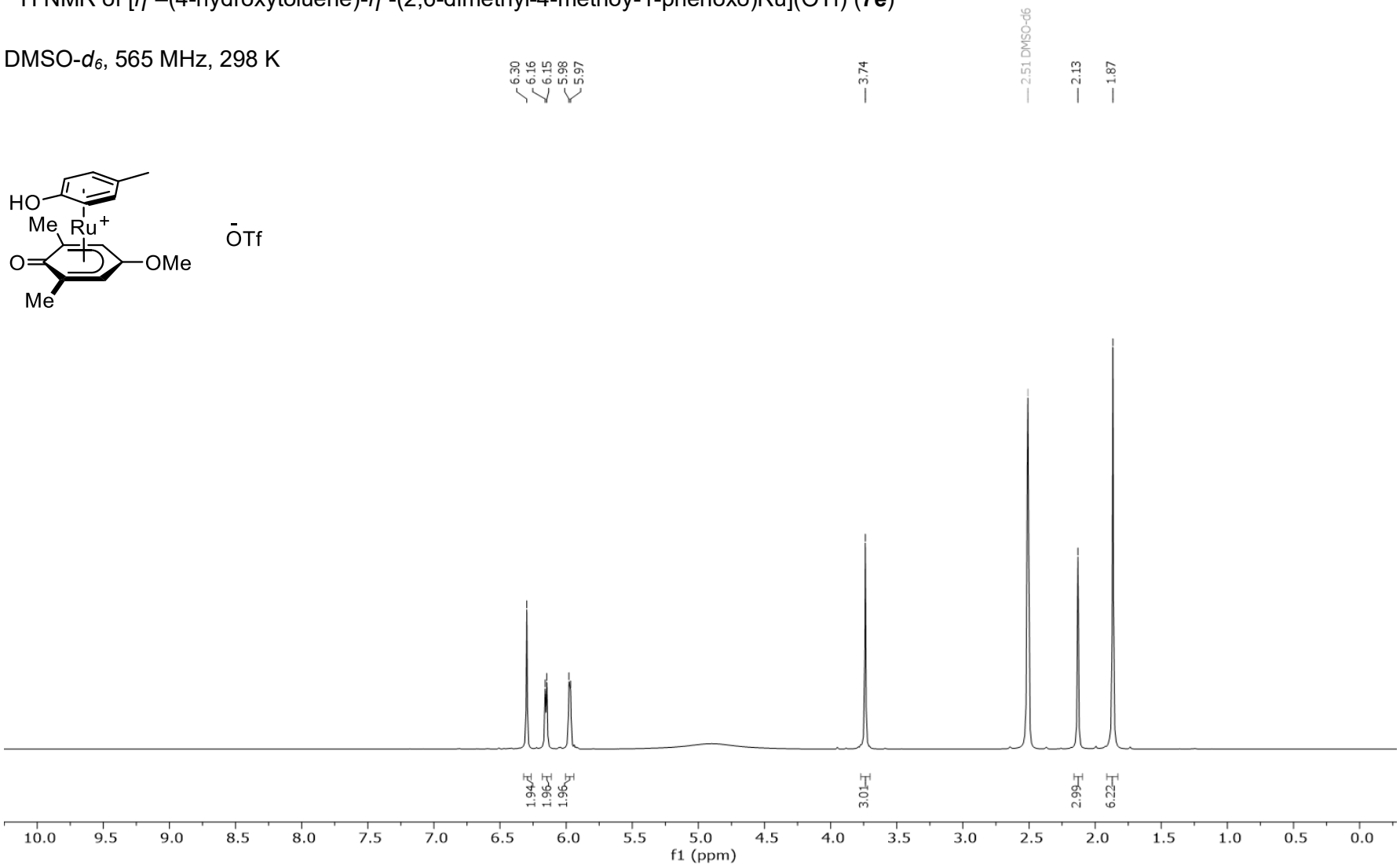

^{19}F NMR of [η^6–(4- hydroxytoluene)-η^5-(2,6-dimethyl-4-methoy-1-phenoxo)Ru](OTf) (**7e**)

DMSO-d_6, 565 MHz, 298 K

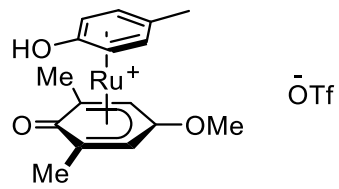

^{1}H NMR of 4-ethylfluorobenzene (**6a**)

$CDCl_3$, 600 MHz, 298 K

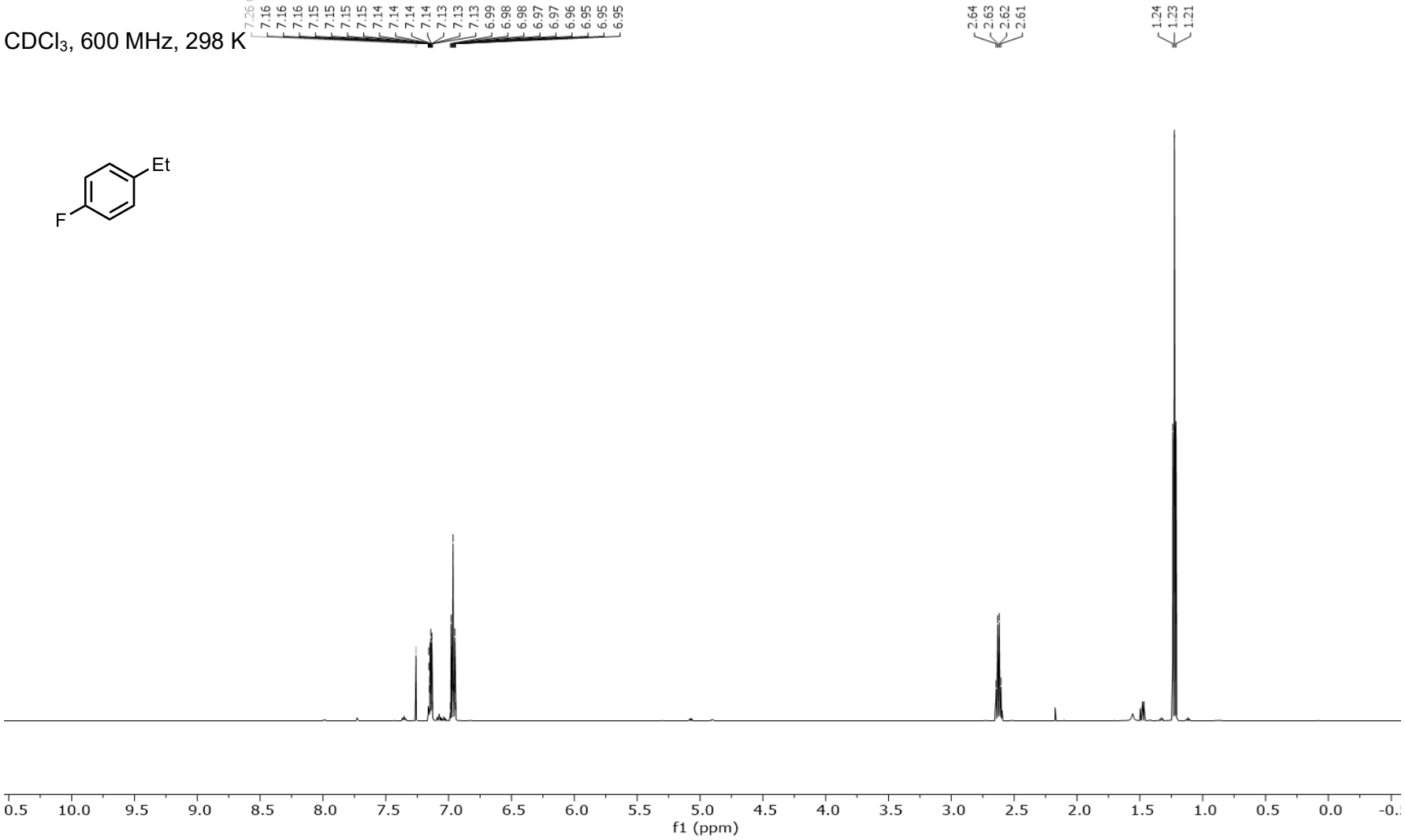

^{13}C NMR of 4-ethylfluorobenzene (**6a**)

$CDCl_3$, 151 MHz, 298 K

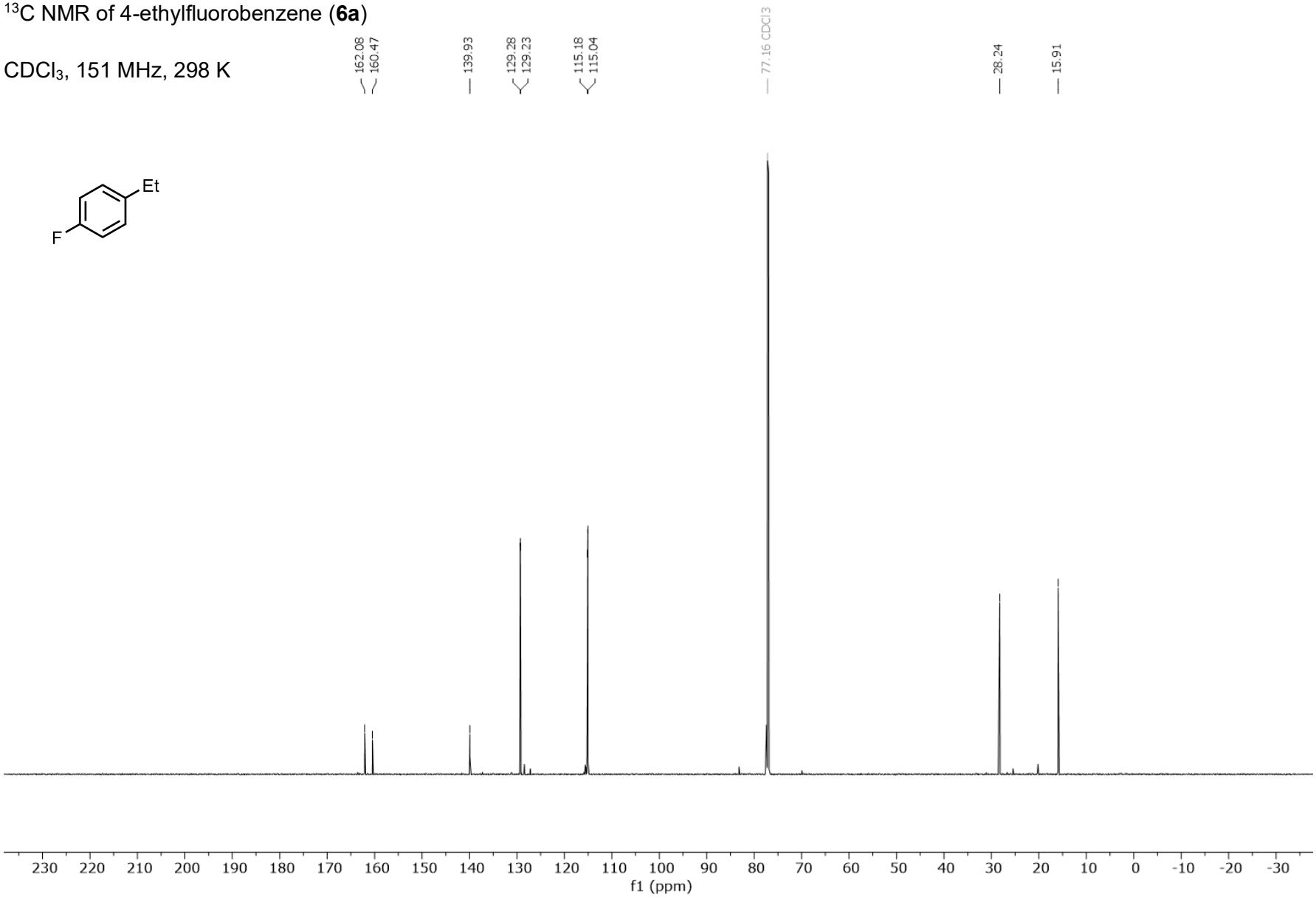

^{19}F NMR of 4-ethylfluorobenzene (**6a**)

$CDCl_3$, 565 MHz, 298 K

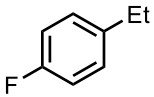

^{1}H NMR of protodecarboxylated Ibuprofen (**11a**)

$CDCl_3$, 500 MHz, 298 K

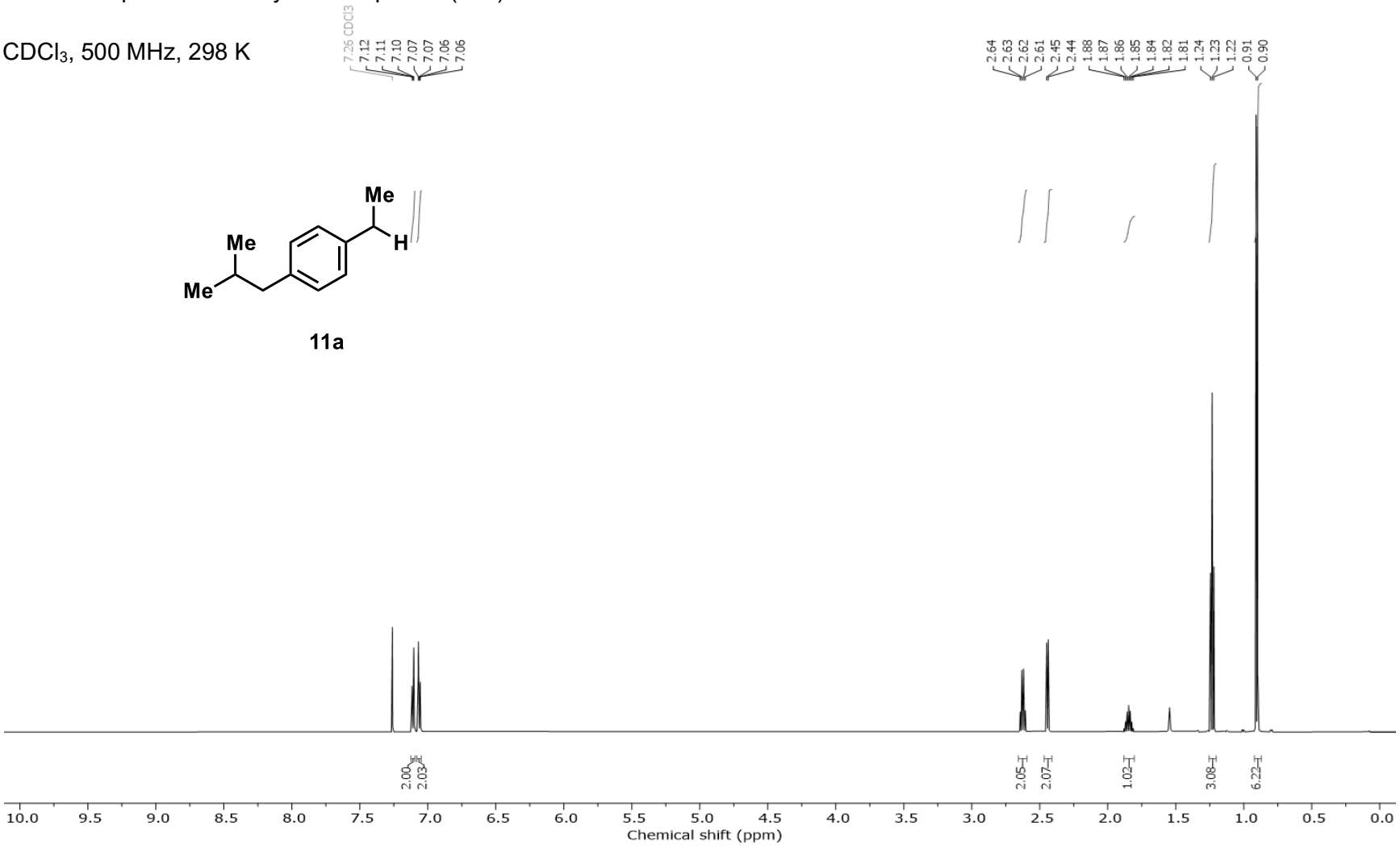

^{1}H NMR of protodecarboxylated Ibuprofen(**11a**)

$CDCl_3$, 500 MHz, 298 K

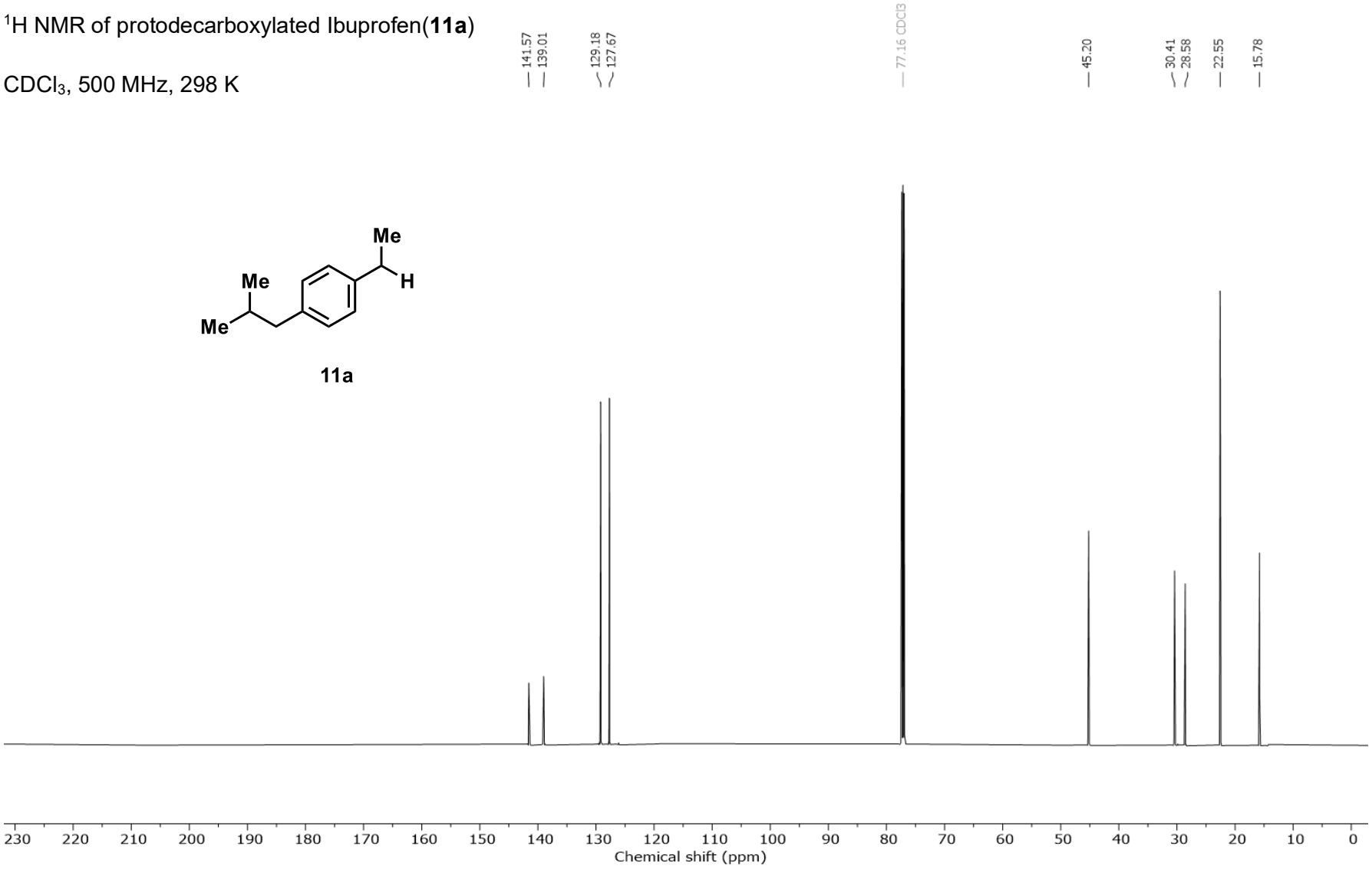

^{1}H NMR of 1,1-diphenylmethane (**11b**)

$CDCl_3$, 500 MHz, 298 K

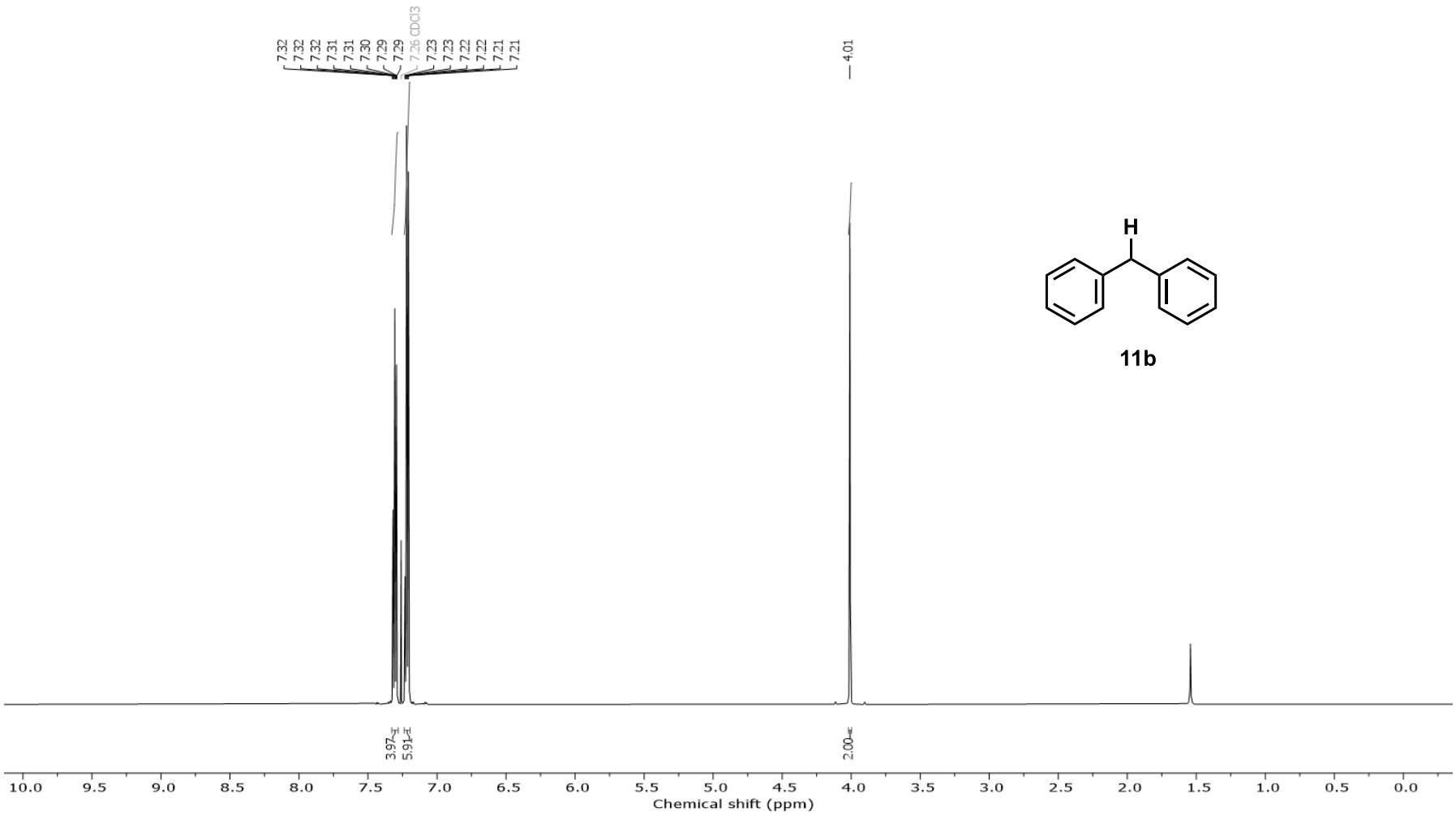

^{13}C NMR of 1,1-diphenylmethane (**11b**)

$CDCl_3$, 125 MHz, 298 K

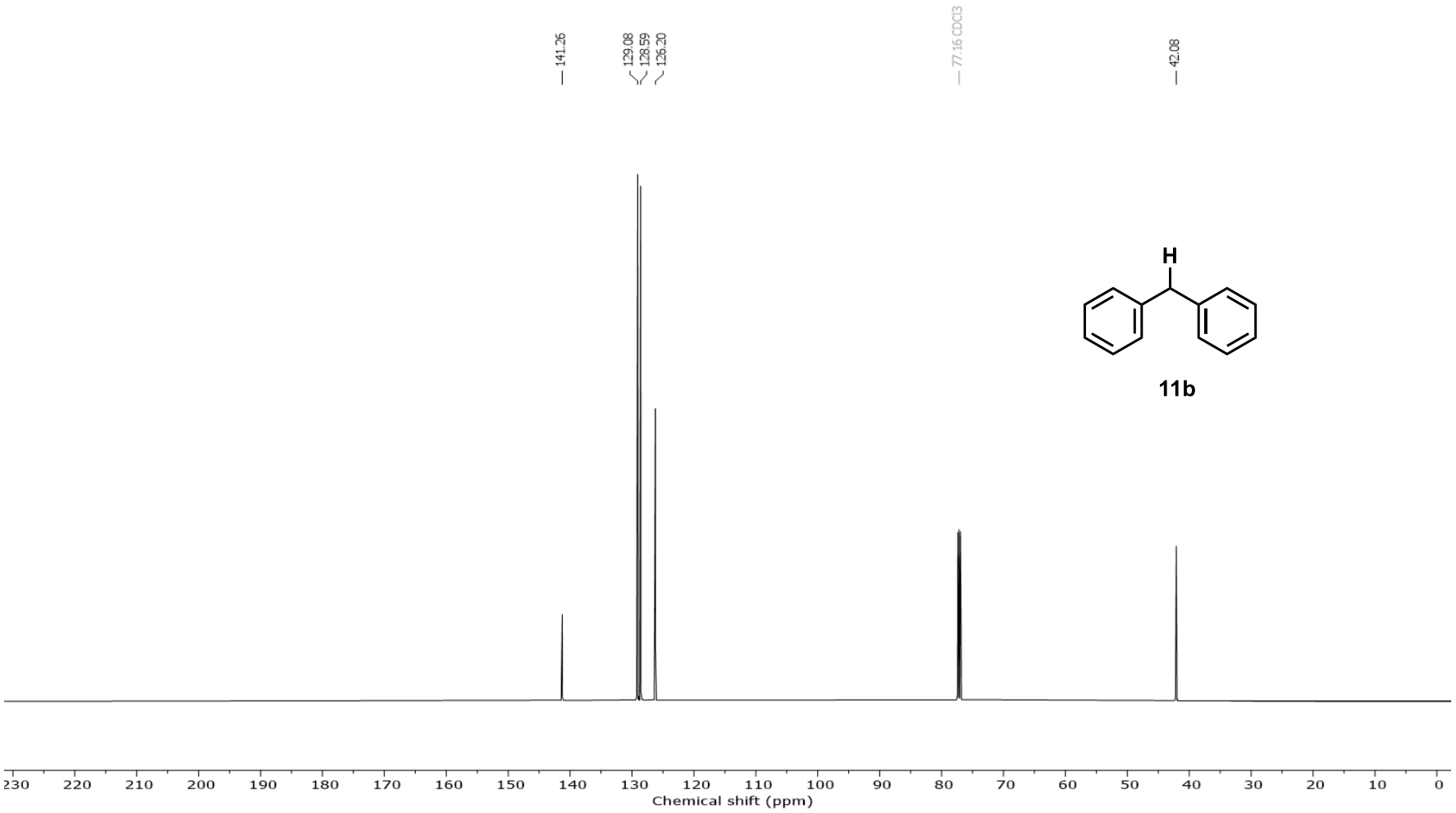

^{1}H NMR of difluoromethylbenzene (**11c**)

$CDCl_3$, 500, MHz 298 K

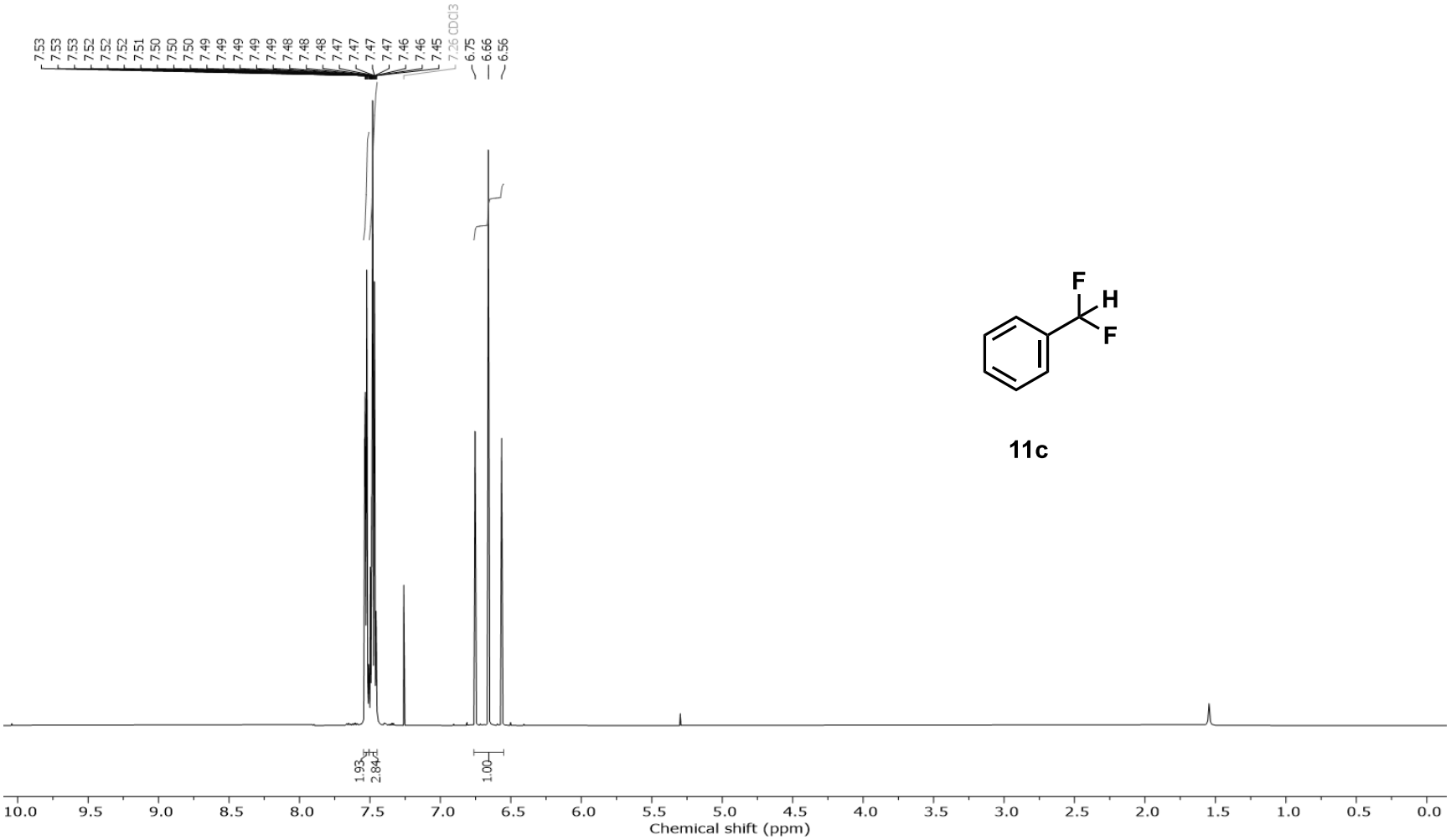

11c

^{13}C NMR of difluoromethylbenzene (**11c**)

$CDCl_3$, 125 MHz, 298 K

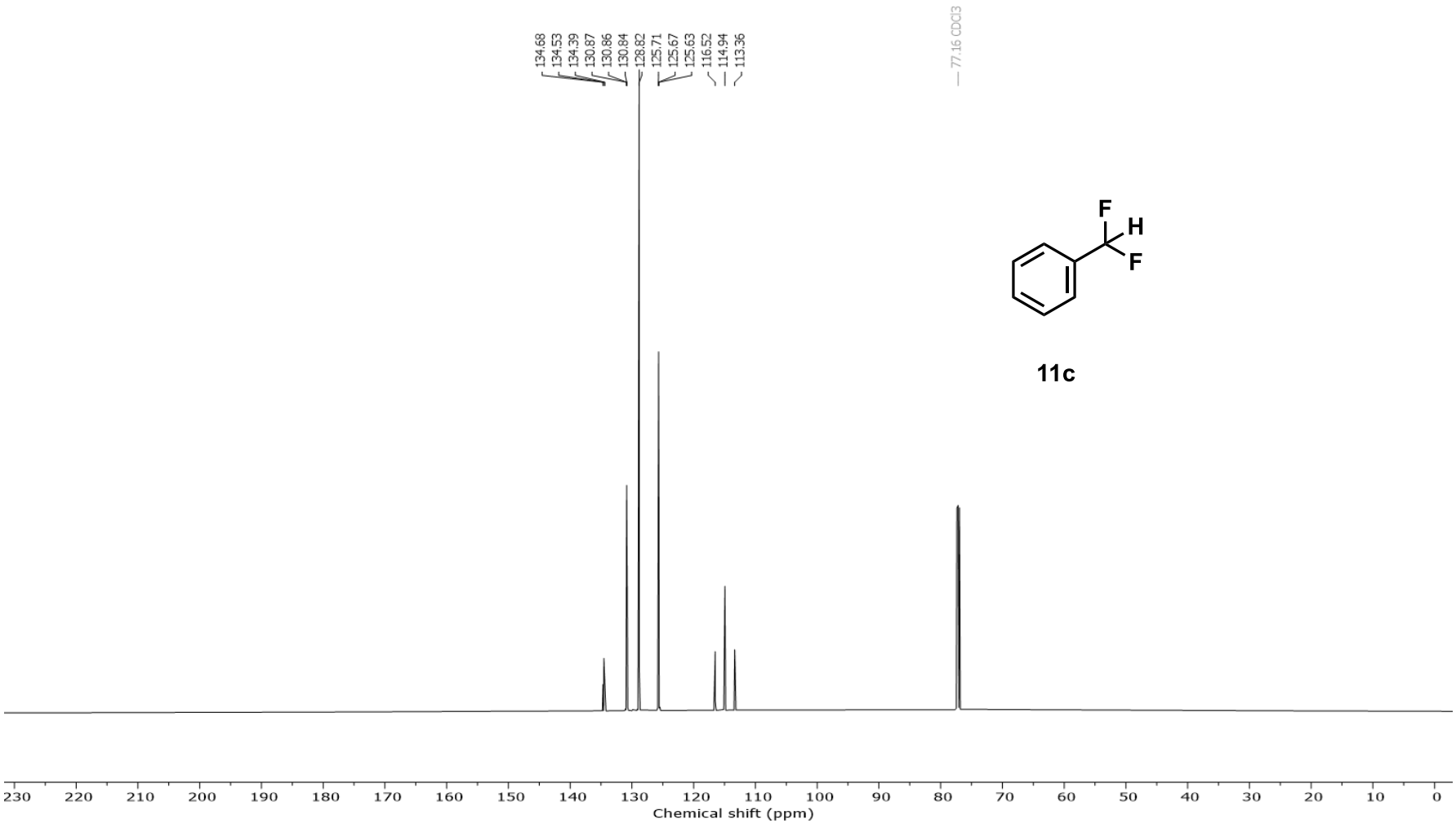

^{19}F NMR of difluoromethylbenzene (**11c**)

$CDCl_3$, 565 MHz, 298 K

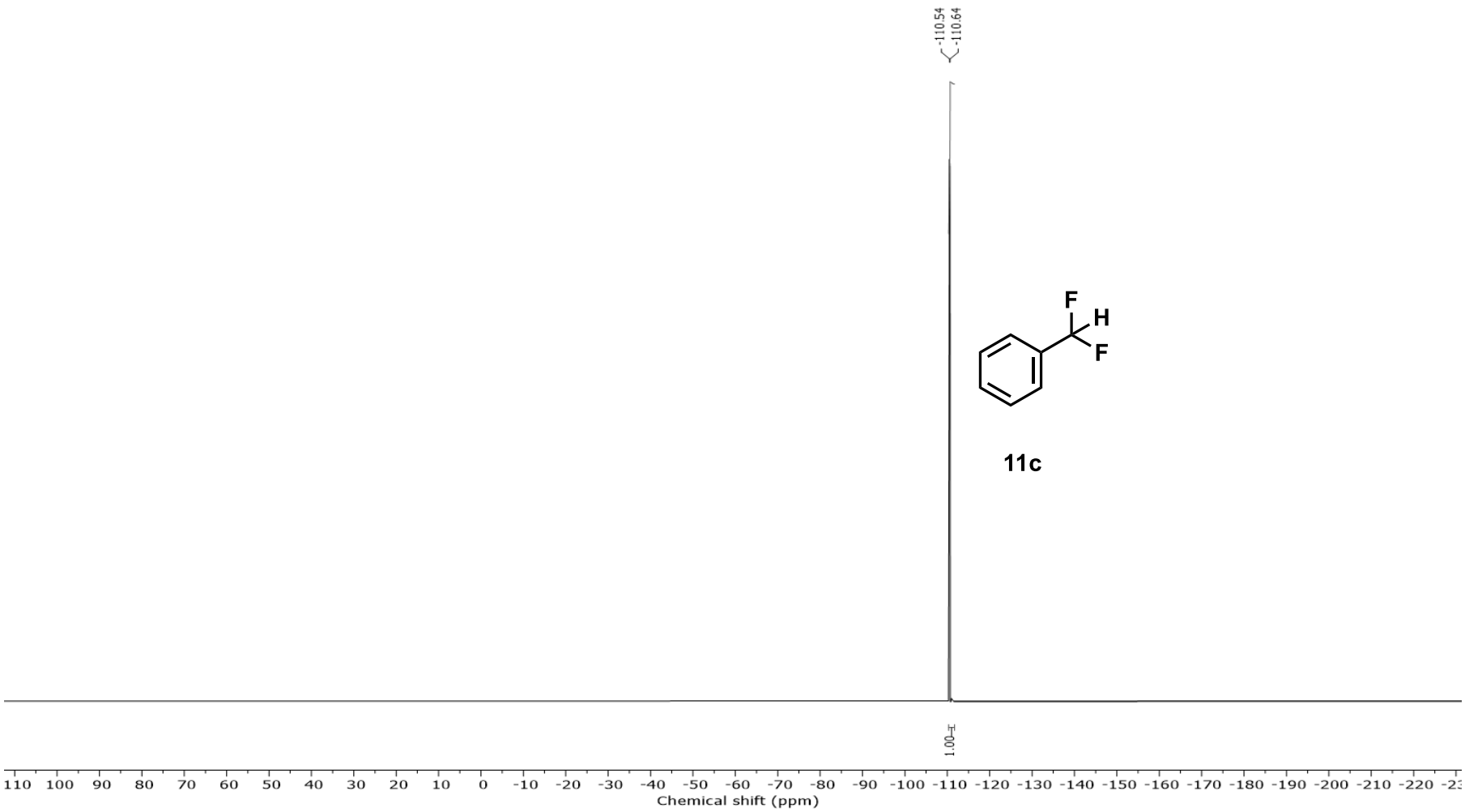

^{1}H NMR of protodecarboxylated phenylmalonic acid (**11d**)

$CDCl_3$, 500 MHz, 298 K

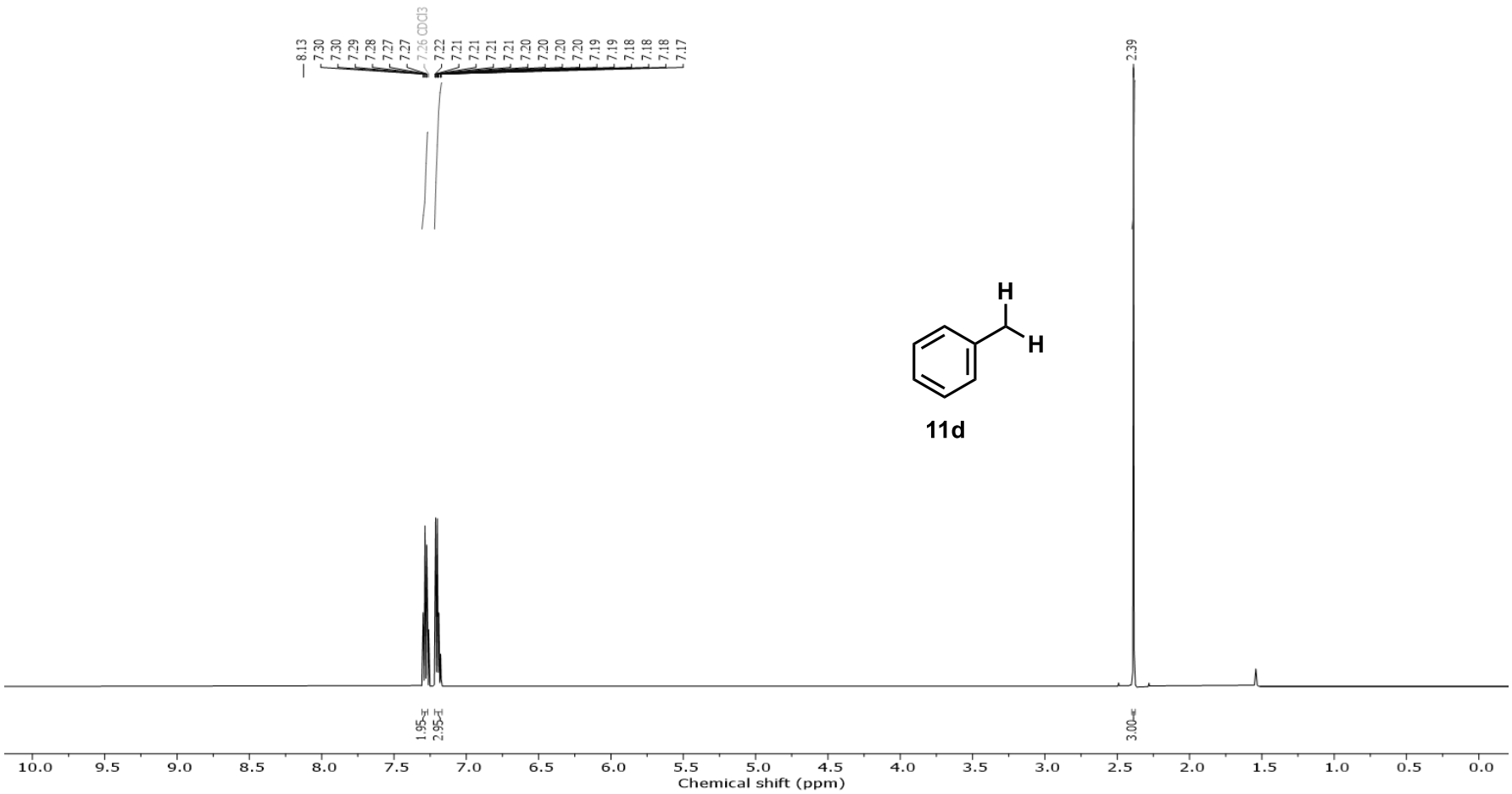

^{13}C NMR of protodecarboxylated phenylmalonic acid (**11d**)

$CDCl_3$, 125 MHz, 298 K

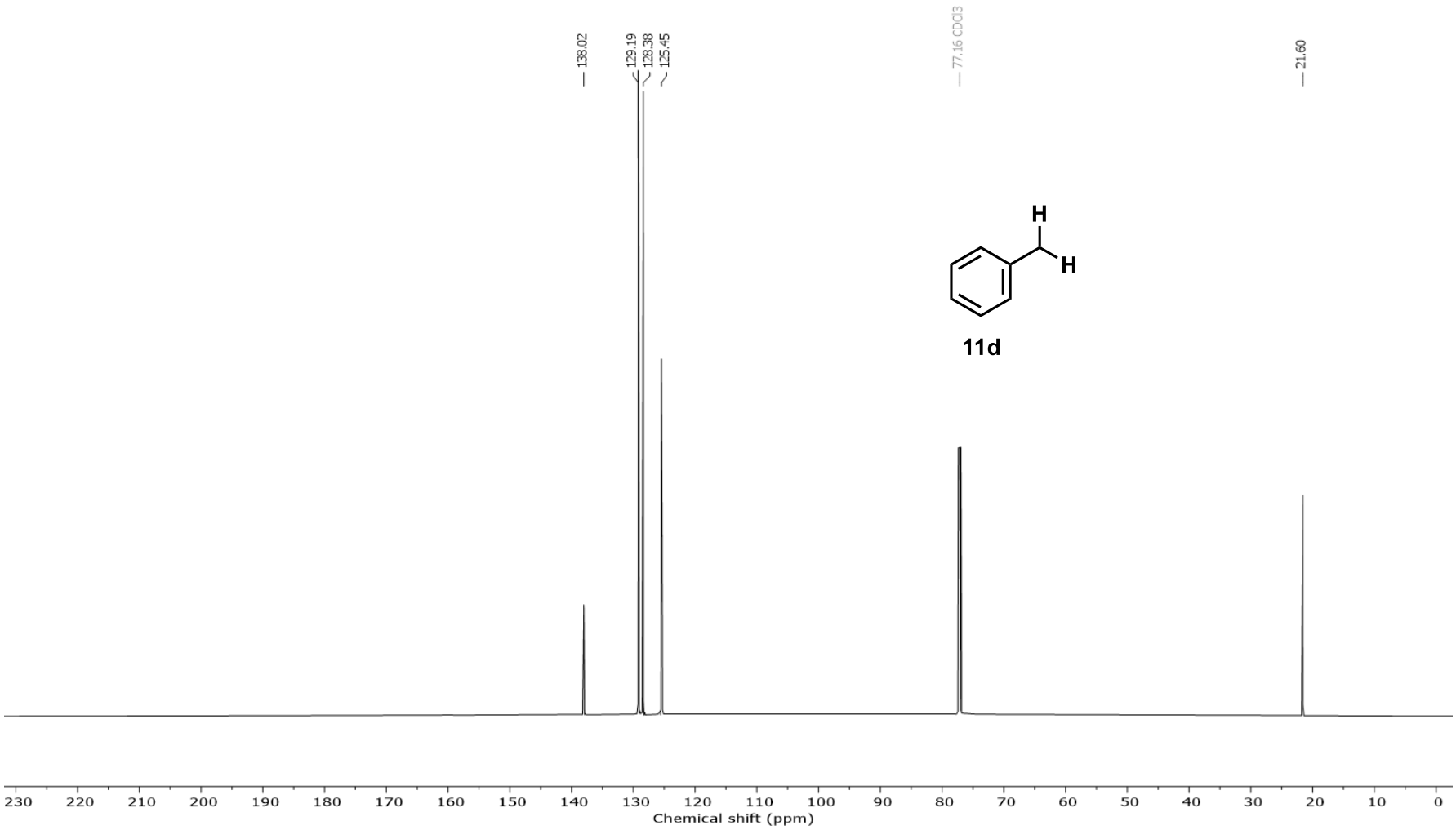

^{1}H NMR of 1,3-dimethylbenzene (**11e**)

$CDCl_3$, 500 MHz, 298 K

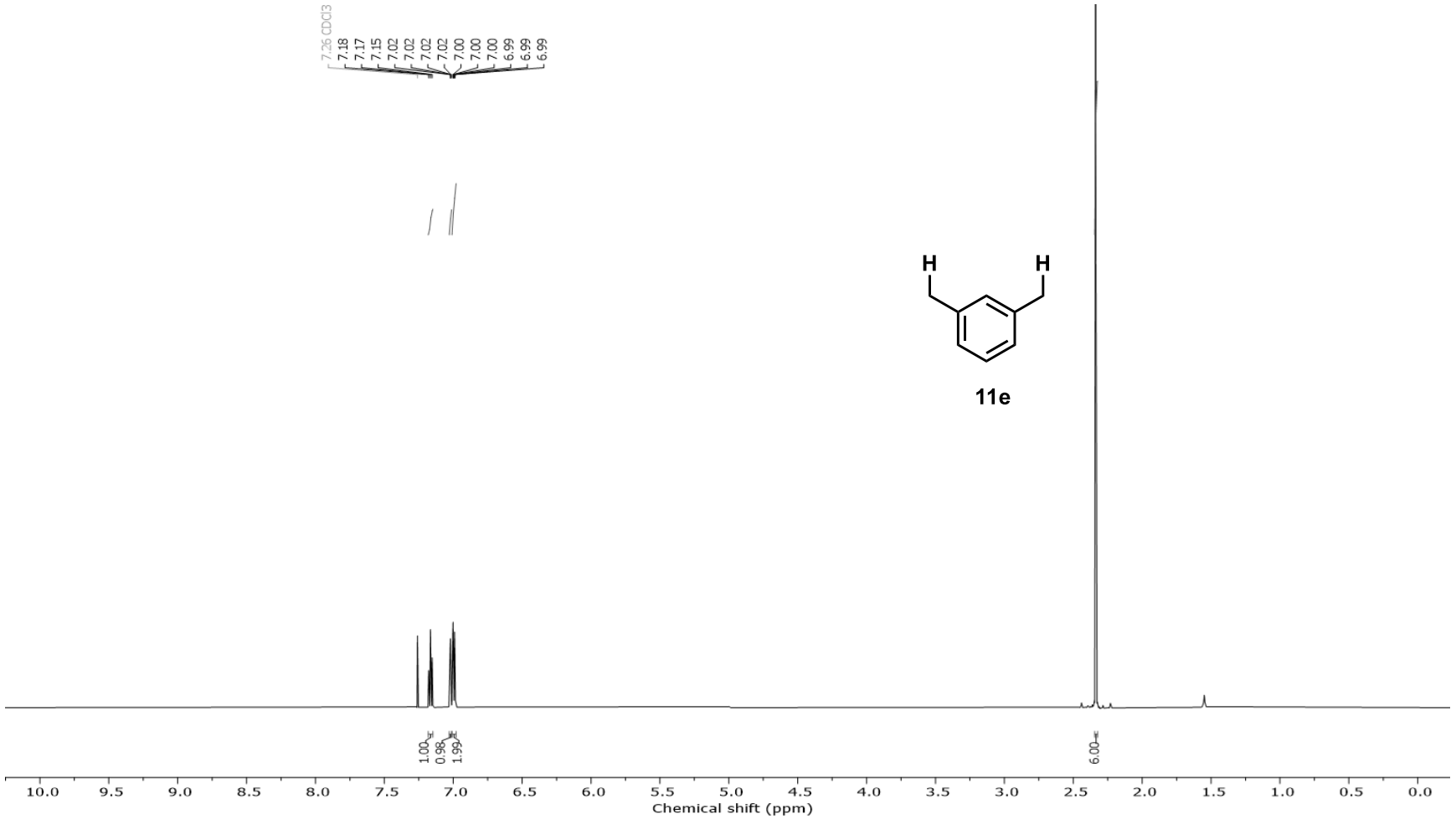

^{13}C NMR of 1,3-dimethylbenzene (**11e**)

$CDCl_3$, 125 MHz, 298 K

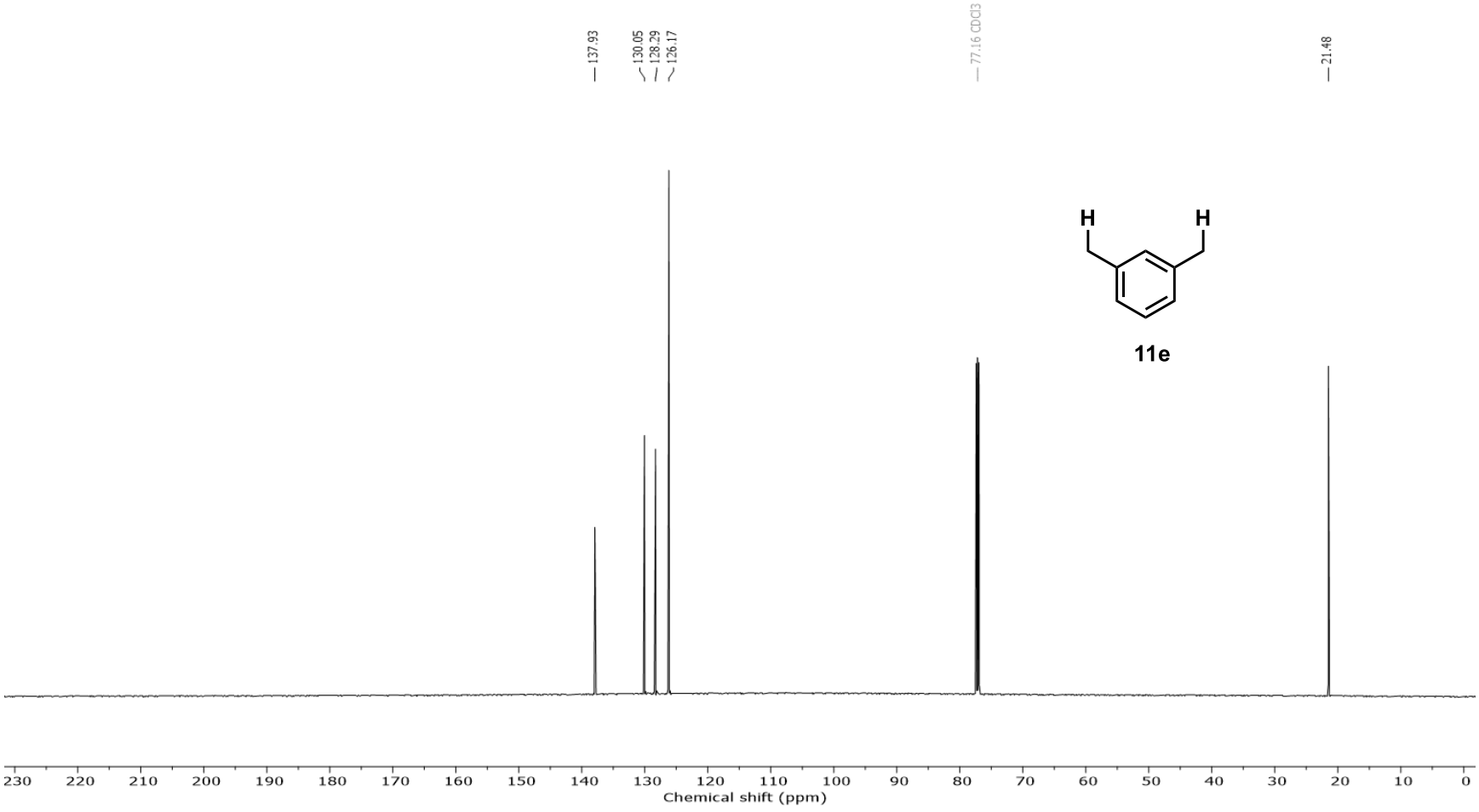

^{1}H NMR of 1-methyl-4-phenylbenzene (**11f**)

$CDCl_3$, 500 MHz, 298 K

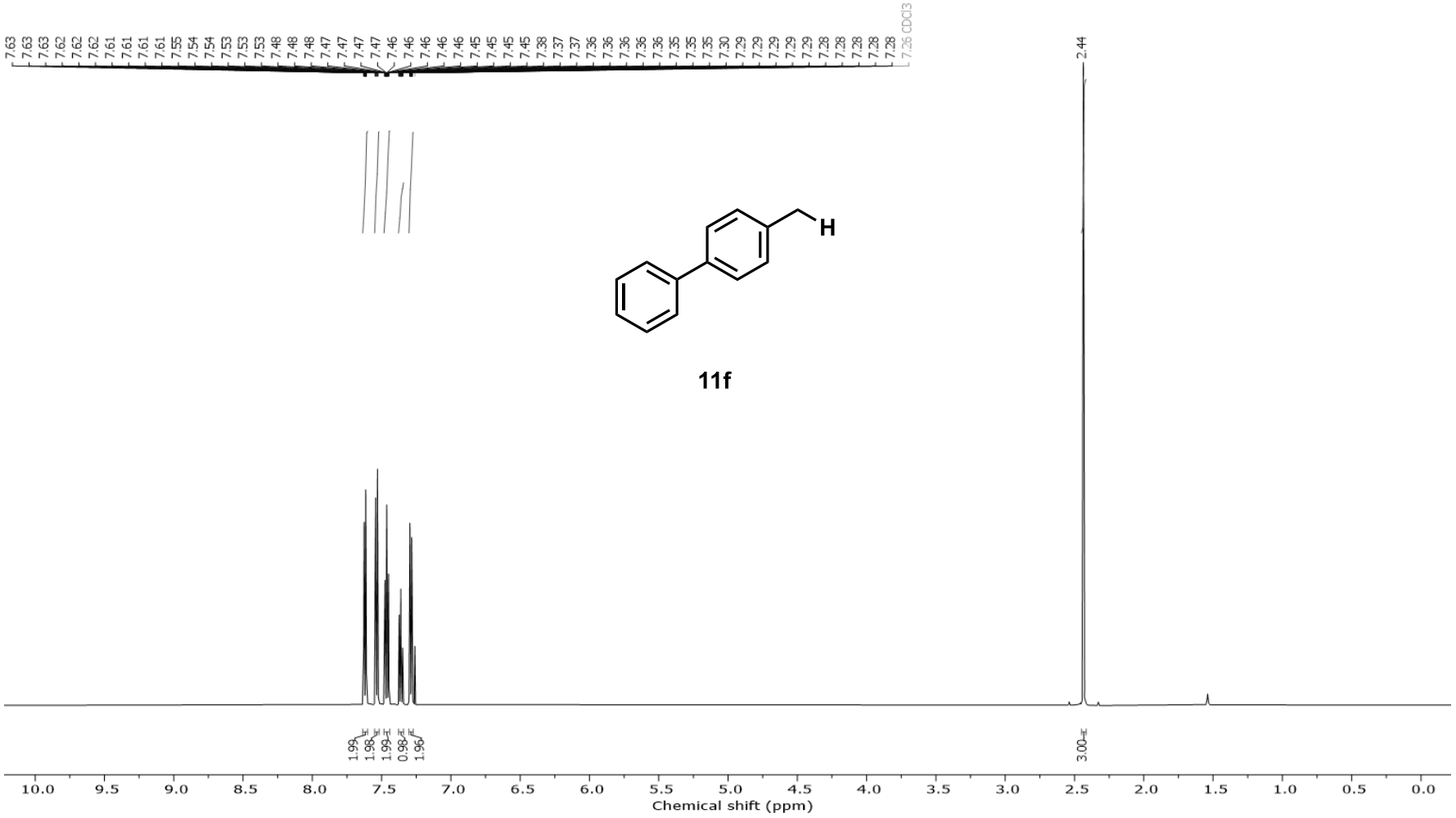

^{13}C NMR of 1-methyl-4-phenylbenzene (**11f**)

$CDCl_3$, 125 MHz, 298 K

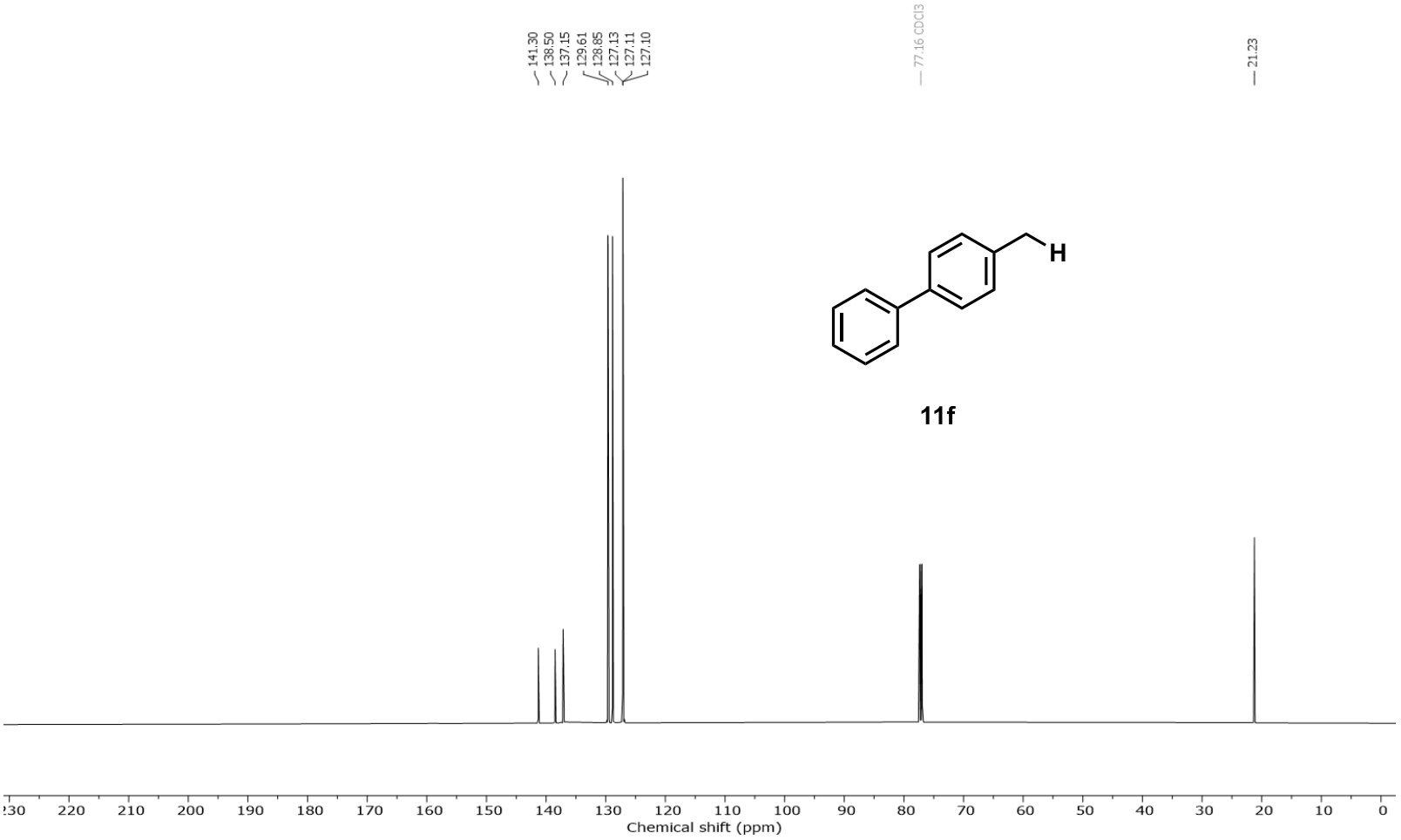

[1]HNMR of (Ethyl benzoate)ruthenium dichloride dimer **(12)**

DMSO, 600 MHz, 298 K

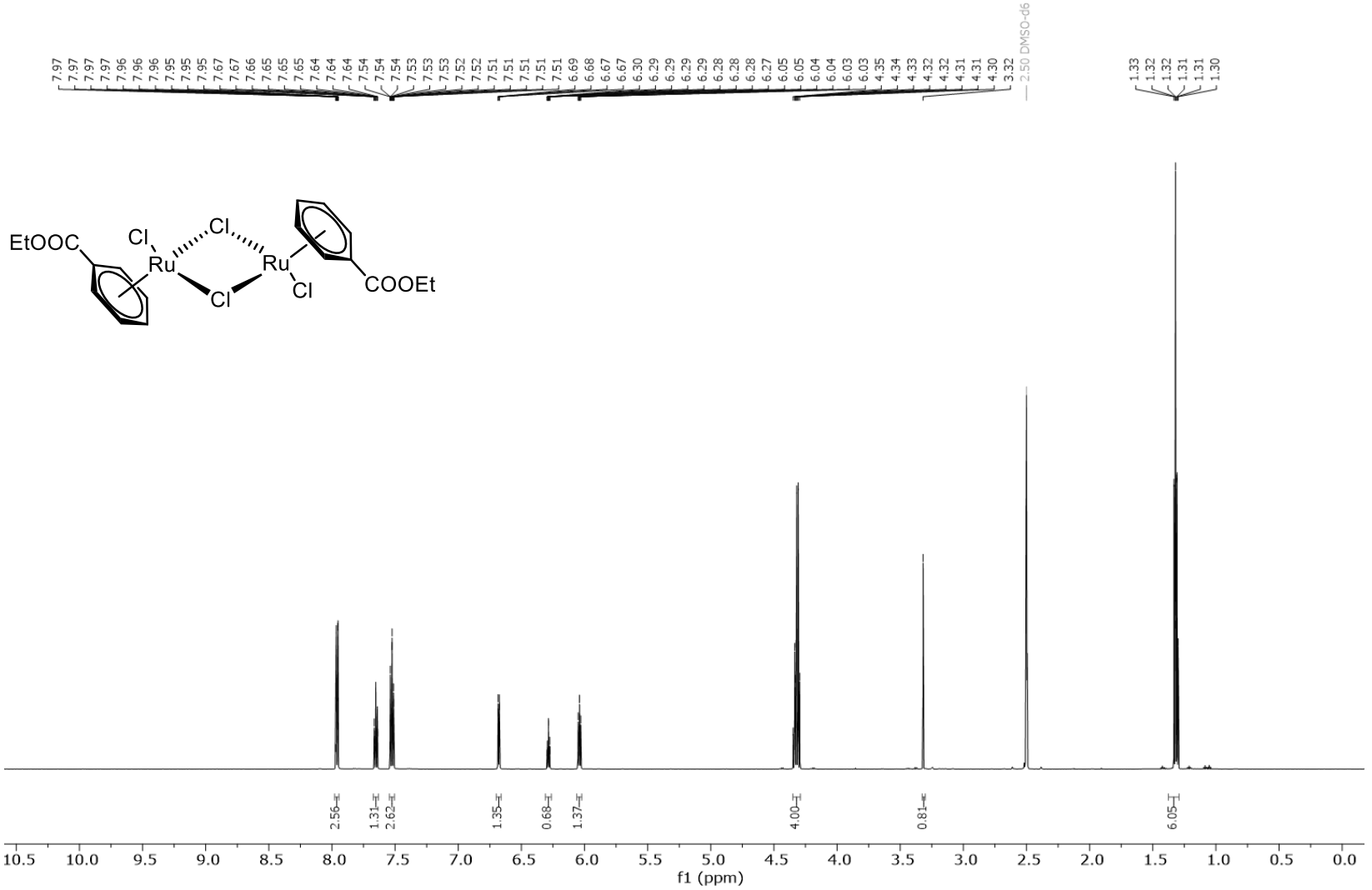

^{13}C NMR of (Ethyl benzoate)ruthenium dichloride dimer **(12)**

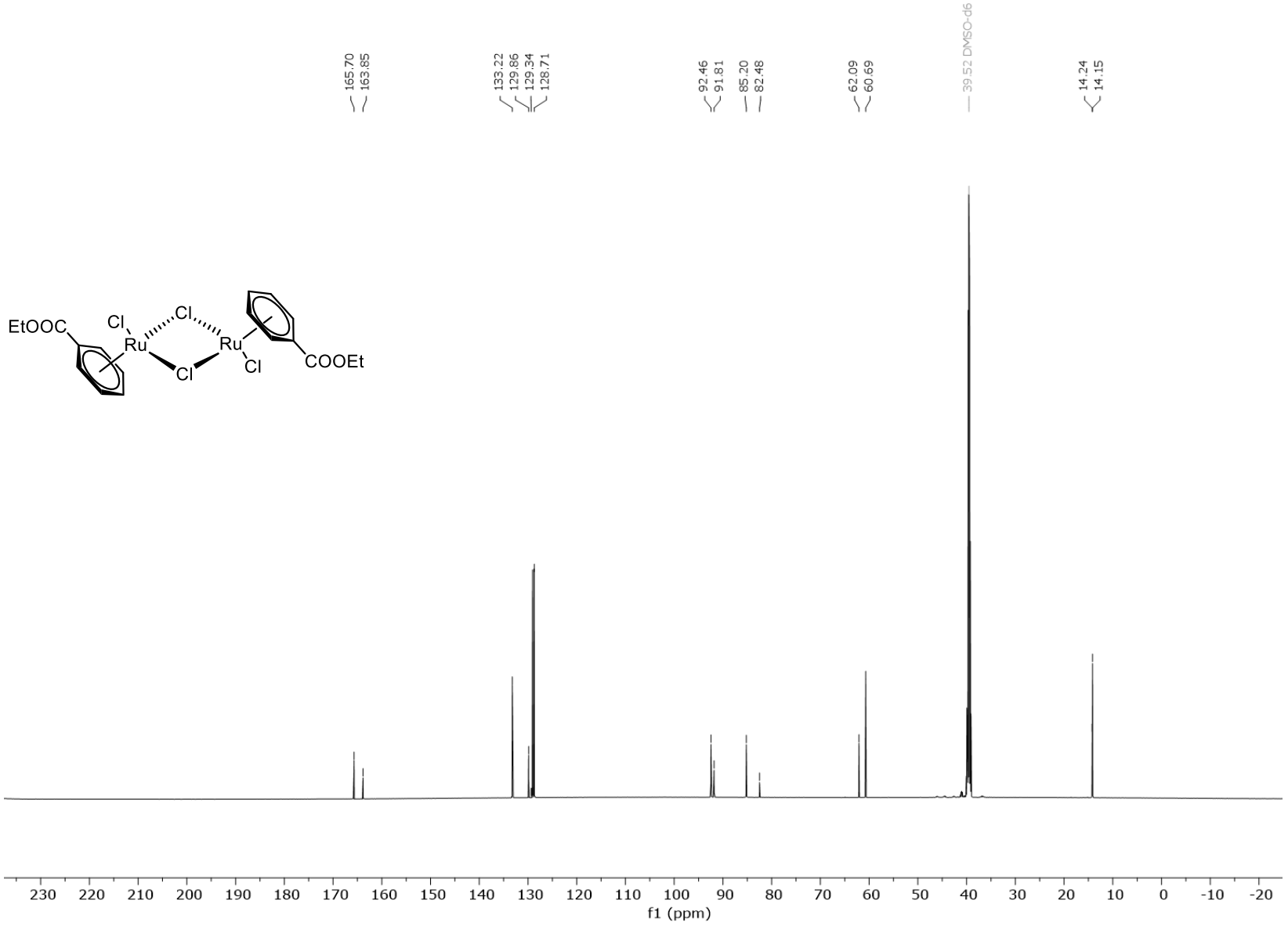

^{1}H NMR of 4-Methoxy-2,6-dimethylphenol (**13**)

$CDCl_3$, 500 MHz, 298 K

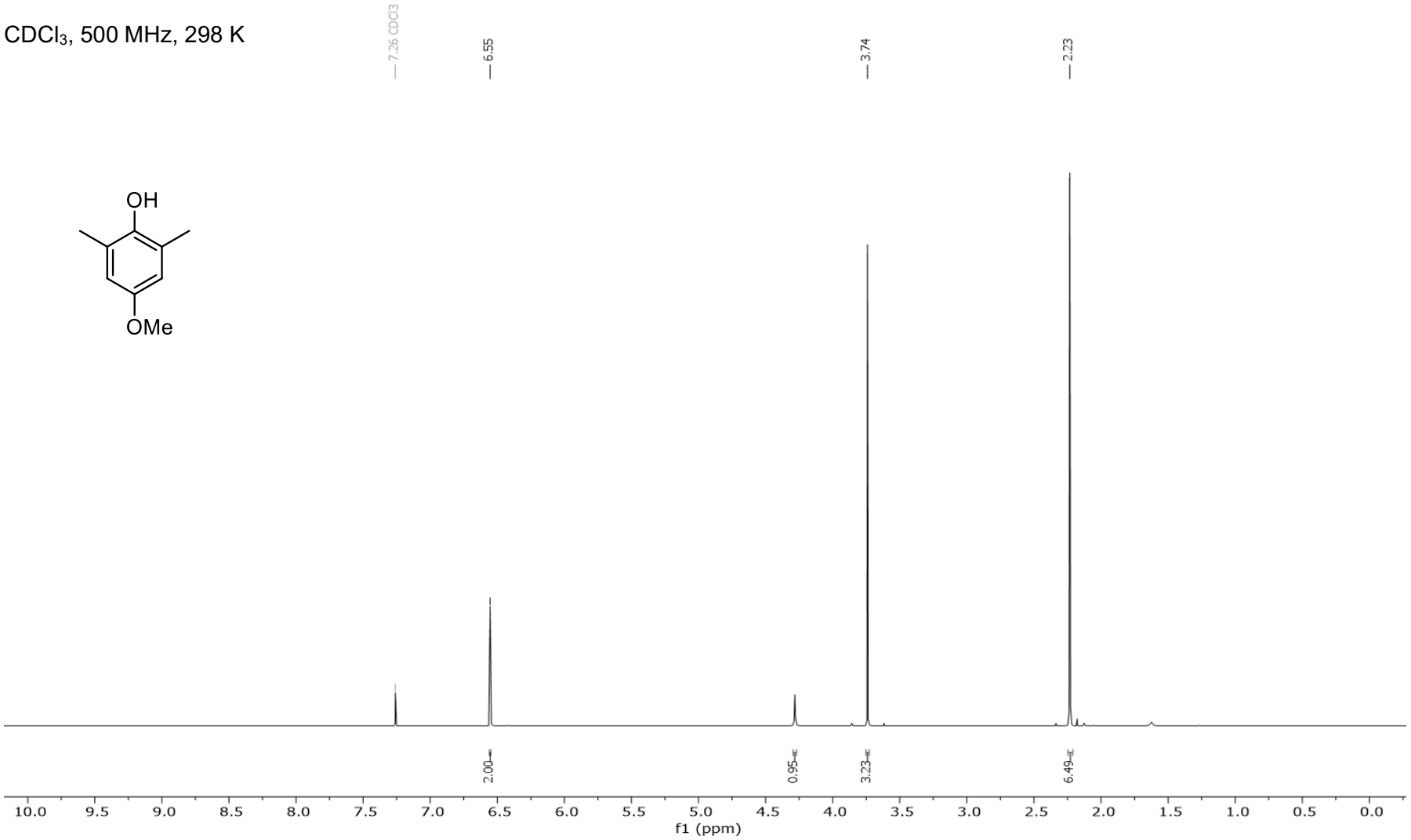

^{13}C NMR of 4-Methoxy-2,6-dimethylphenol (**13**)

$CDCl_3$, 125 MHz, 298 K

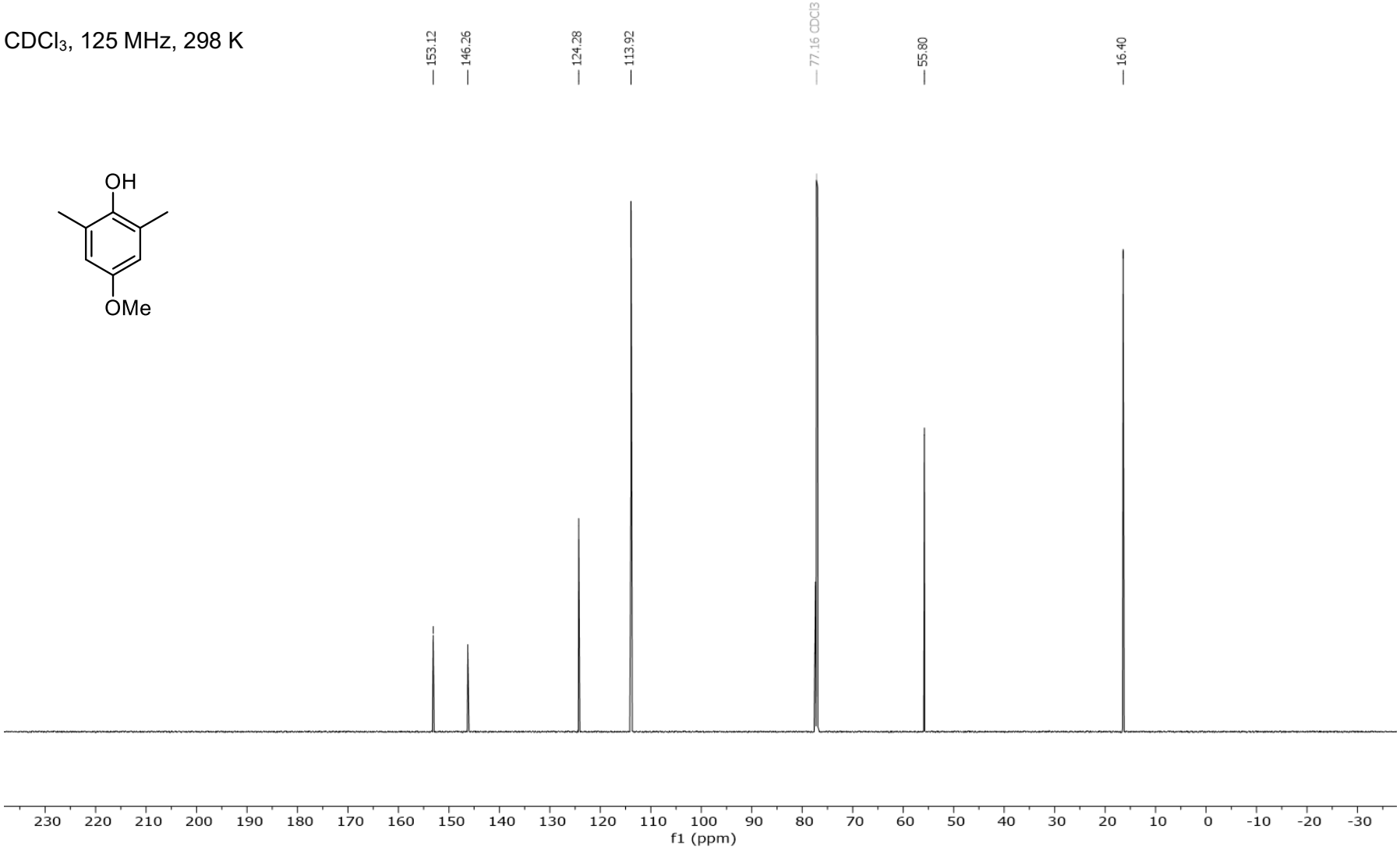

5. References

[1] G. Meng, N. Y. S. Lam, E. L. Lucas, T. G. Saint-Denis, P. Verma, N. Chekshin, J.-Q. Yu, *J. Am. Chem. Soc.* **2020**, *142*, 10571–10591.

[2] G. B. Boursalian, W. S. Ham, A. R. Mazzotti, T. Ritter, *Nat. Chem.* **2016**, *8*, 810–815.

[3] F. Berger, M. B. Plutschack, J. Riegger, W. Yu, S. Speicher, M. Ho, N. Frank, T. Ritter, *Nature* **2019**, *567*, 223–228.

[4] G. A. Olah, *Acc. Chem. Res.* **1971**, *4*, 240–248.

[5] C. Sambiagio, D. Schönbauer, R. Blieck, T. Dao-Huy, G. Pototschnig, P. Schaaf, T. Wiesinger, M. Farooq Zia, J. Wencel-Delord, T. Besset, B. U. W. Maes, M. Schnürch, *Chem. Soc. Rev.* **2018**, *47*, 6603–6743.

[6] I. A. I. Mkhalid, J. H. Barnard, T. B. Marder, J. M. Murphy, J. F. Hartwig, *Chem. Rev.* **2010**, *110*, 890–931.

[7] L. Zhang, T. Ritter, *J. Am. Chem. Soc.* **2022**, *144*, 2399–2414.

[8] D. F. Nippa, R. Hohler, A. F. Stepan, U. Grether, D. B. Konrad, R. E. Martin, *CHIMIA* **2022**, *76*, 258–260.

[9] P. Xu, D. Zhao, F. Berger, A. Hamad, J. Rickmeier, R. Petzold, M. Kondratiuk, K. Bohdan, T. Ritter, *Angew. Chem. Int. Ed.* **2020**, *132*, 1972–1976.

[10] Y. Saito, Y. Segawa, K. Itami, *J. Am. Chem. Soc.* **2015**, *137*, 5193–5198.

[11] T. Ishiyama, J. Takagi, K. Ishida, N. Miyaura, N. R. Anastasi, J. F. Hartwig, *J. Am. Chem. Soc.* **2002**, *124*, 390–391.

[12] B. E. Haines, Y. Saito, Y. Segawa, K. Itami, D. G. Musaev, *ACS Catal.* **2016**, *6*, 7536–7546.

[13] W. Chang, Y. Chen, S. Lu, H. Jiao, Y. Wang, T. Zheng, Z. Shi, Y. Han, Y. Lu, Y. Wang, Y. Pan, J.-Q. Yu, K. N. Houk, F. Liu, Y. Liang, *Chem* **2022**, *8*, 1775–1788.

[14] J. F. Hartwig, *Acc. Chem. Res.* **2012**, *45*, 864–873.

[15] F. A. Carey, R. J. Sundberg, *Advanced Organic Chemistry. Part A: Structure and Mechanisms*, Springer, New York, **2007**.

[16] G.-J. Cheng, Y.-F. Yang, P. Liu, P. Chen, T.-Y. Sun, G. Li, X. Zhang, K. N. Houk, J.-Q. Yu, Y.-D. Wu, *J. Am. Chem. Soc.* **2014**, *136*, 894–897.

[17] T. Rogge, N. Kaplaneris, N. Chatani, J. Kim, S. Chang, B. Punji, L. L. Schafer, D. G. Musaev, J. Wencel-Delord, C. A. Roberts, R. Sarpong, Z. E. Wilson, M. A. Brimble, M. J. Johansson, L. Ackermann, *Nat. Rev. Methods Primers* **2021**, *1*, 1–31.

[18] W. von E. Doering, M. Saunders, H. G. Boyton, H. W. Earhart, E. F. Wadley, W. R. Edwards, G. Laber, *Tetrahedron* **1958**, *4*, 178–185.

[19] B. T. Brooks, *The Chemistry of Petroleum Hydrocarbons,* Reinhold, New York, **1954**.

[20] P. Pfeiffer, R. Wizinger, *Justus Liebigs Ann. Chem.* **1928**, *461*, 132–154.

[21] H. C. Brown, H. W. Pearsall, *J. Am. Chem. Soc.* **1952**, *74*, 191–195.

[22] G. A. Olah, *Acc. Chem. Res.* **1971**, *4*, 240–248.

[23] L. M. Stock, *Aromatic Substitution Reactions*, Prentice-Hall, Englewood Cliffs, N.J., **1968**.

[24] M. J. S. Dewar, *The Electronic Theory of Organic Chemistry.*, Clarendon Press, Oxford, **1949**.

[25] F. Berger, M. B. Plutschack, J. Riegger, W. Yu, S. Speicher, M. Ho, N. Frank, T. Ritter, *Nature* **2019**, *567*, 223–228.

[26] R.-J. Tang, T. Milcent, B. Crousse, *J. Org. Chem.* **2018**, *83*, 930–938.

[27] N. Hofmann, L. Ackermann, *J. Am. Chem. Soc.* **2013**, *135*, 5877–5884.

[28] R. J. Phipps, M. J. Gaunt, *Science* **2009**, *323*, 1593–1597.

[29] D. W. Elrod, G. M. Maggiora, R. G. Ternary, *J. Chem. Inf. Comput. Sci* **1990**, *30*, 477–484.

[30] G. A. Olah, F. Pelizza, S. Kobayashi, J. A. Olah, *J. Am. Chem. Soc.* **1976**, 296–297.

[31] M. Makosza, J. Winiarski, *Acc. Chem. Res.* **1987**, *20*, 282–289.

[32] M. Makosza, *Pure and App. Chem.* **1997**, *69*, 559–564.

[33] N. E. S. Tay, D. A. Nicewicz, *J. Am. Chem. Soc.* **2017**, *139*, 16100–16104.

[34] E. Buncel, A. R. Norris, K. E. Russell, *Q. Rev. Chem. Soc.* **1968**, *22*, 123–146.

[35] M. J. Strauss, *Chem. Rev.* **1970**, *70*, 667–712.

[36] C. R. Allen, A. J. Brook, E. F. Caldin, *J. Chem. Soc.* **1961**, 2171–2180.

[37] K. Tamaru, 1923-, M. Ichikawa, *Catalysis by Electron Donor-Acceptor Complexes, Their General Behavior and Biological Roles*, Kodansha, **1975**.

[38] F. Terrier, *Modern Nucleophilic Aromatic Substitution*, John Wiley & Sons, **2013**.

[39] R. Bacaloglu, C. A. Bunton, G. Cerichelli, *J. Am. Chem. Soc.* **1987**, *109*, 621–623.

[40] J. Burdon, I. W. Parsons, *J. Am. Chem. Soc.* **1977**, *99*, 7445–7447.

[41] F. A. Carey, R. J. Sundberg, *Advanced Organic Chemistry: Part A: Structure and Mechanisms*, Springer Science & Business Media, **2007**.

[42] I. A. I. Mkhalid, J. H. Barnard, T. B. Marder, J. M. Murphy, J. F. Hartwig, *Chem. Rev.* **2010**, *110*, 890–931.

[43] K.-J. Jiao, C.-Q. Zhao, P. Fang, T.-S. Mei, *Tetrahedron Lett.* **2017**, *58*, 797–802.

[44] K. M. Engle, T.-S. Mei, M. Wasa, J.-Q. Yu, *Acc. Chem. Res.* **2012**, *45*, 788–802.

[45] H. M. L. Davies, Y. Lian, *Acc. Chem. Res.* **2012**, *45*, 923–935.

[46] S. R. Neufeldt, M. S. Sanford, *Acc. Chem. Res.* **2012**, *45*, 936–946.

[47] K. Godula, D. Sames, *Science* **2006**, *312*, 67–72.

[48] H. Shi, D. J. Babinski, T. Ritter, *J. Am. Chem. Soc.* **2015**, *137*, 3775–3778.

[49] F. Minisci, R. Bernardi, F. Bertini, R. Galli, M. Perchinummo, *Tetrahedron* **1971**, *27*, 3575–3579.

[50] N. Holmberg-Douglas, D. A. Nicewicz, *Chem. Rev.* **2022**, *122*, 1925–2016.

[51] N. A. Romero, K. A. Margrey, N. E. Tay, D. A. Nicewicz, *Science* **2015**, *349*, 1326–1330.

[52] J. B. McManus, D. A. Nicewicz, *J. Am. Chem. Soc.* **2017**, *139*, 2880–2883.

[53] K. A. Margrey, A. Levens, D. A. Nicewicz, *Angew. Chem. Int. Ed.* **2017**, *56*, 15644–15648.

[54] W. Chen, Z. Huang, N. E. S. Tay, B. Giglio, M. Wang, H. Wang, Z. Wu, D. A. Nicewicz, Z. Li, *Science* **2019**, *364*, 1170–1174.

[55] L. Wang, A. R. White, W. Chen, Z. Wu, D. A. Nicewicz, Z. Li, *Org. Lett.* **2020**, *22*, 7971–7975.

[56] T. W. Lyons, M. S. Sanford, *Chem. Rev.* **2010**, *110*, 1147–1169.

[57] A. R. Dick, K. L. Hull, M. S. Sanford, *J. Am. Chem. Soc.* **2004**, *126*, 2300–2301.

[58] D. Lapointe, K. Fagnou, *Chem. Lett.* **2010**, *39*, 1118–1126.

[59] A. R. Dick, J. W. Kampf, M. S. Sanford, *J. Am. Chem. Soc.* **2005**, *127*, 12790–12791.

[60] D. Leow, G. Li, T.-S. Mei, J.-Q. Yu, *Nature* **2012**, *486*, 518–522.

[61] H. Schwarz, *Acc. Chem. Res.* **1989**, *22*, 282–287.

[62] L. Wan, N. Dastbaravardeh, G. Li, J.-Q. Yu, *J. Am. Chem. Soc.* **2013**, *135*, 18056–18059.

[63] S. Bag, R. Jayarajan, U. Dutta, R. Chowdhury, R. Mondal, D. Maiti, *Angew. Chem. Int. Ed.* **2017**, *56*, 12538–12542.

[64] A. Maji, B. Bhaskararao, S. Singha, R. B. Sunoj, D. Maiti, *Chemical Science* **2016**, *7*, 3147–3153.

[65] A. Modak, T. Patra, R. Chowdhury, S. Raul, D. Maiti, *Organometallics* **2017**, *36*, 2418–2423.

[66] H. Xu, M. Liu, L.-J. Li, Y.-F. Cao, J.-Q. Yu, H.-X. Dai, *Org. Lett.* **2019**, *21*, 4887–4891.

[67] S. Bag, M. Petzold, A. Sur, S. Bhowmick, D. B. Werz, D. Maiti, *Chem. Eur. J.* **2019**, *25*, 9433–9437.

[68] T. K. Achar, X. Zhang, R. Mondal, M. S. Shanavas, S. Maiti, S. Maity, N. Pal, R. S. Paton, D. Maiti, *Angew. Chem. Int. Ed.* **2019**, *131*, 10461–10468.

[69] S. Bag, T. Patra, A. Modak, A. Deb, S. Maity, U. Dutta, A. Dey, R. Kancherla, A. Maji, A. Hazra, M. Bera, D. Maiti, *J. Am. Chem. Soc.* **2015**, *137*, 11888–11891.

[70] M. Li, M. Shang, H. Xu, X. Wang, H.-X. Dai, J.-Q. Yu, *Org. Lett.* **2019**, *21*, 540–544.

[71] B.-F. Shi, Y.-H. Zhang, J. K. Lam, D.-H. Wang, J.-Q. Yu, *J. Am. Chem. Soc.* **2010**, *132*, 460–461.

[72] P. Trillo, A. Baeza, C. Nájera, *J. Org. Chem.* **2012**, *77*, 7344–7354.

[73] H. F. Motiwala, R. H. Vekariya, J. Aubé, *Org. Lett.* **2015**, *17*, 5484–5487.

[74] F.-Z. Zhang, Y. Tian, G.-X. Li, J. Qu, *J. Org. Chem.* **2015**, *80*, 1107–1115.

[75] S. Kumar Sinha, T. Bhattacharya, D. Maiti, *Reaction Chemistry & Engineering* **2019**, *4*, 244–253.

[76] H. F. Motiwala, C. Fehl, S.-W. Li, E. Hirt, P. Porubsky, J. Aubé, *J. Am. Chem. Soc.* **2013**, *135*, 9000–9009.

[77] J. H. Docherty, T. M. Lister, G. Mcarthur, M. T. Findlay, P. Domingo-Legarda, J. Kenyon, S. Choudhary, I. Larrosa, *Chem. Rev.* **2023**, *123*, 7692–7760.

[78] D. Zhao, P. Xu, T. Ritter, *Chem* **2019**, *5*, 97–107.

[79] D. Marcos-Atanes, C. Vidal, C. D. Navo, F. Peccati, G. Jiménez-Osés, J. L. Mascareñas, *Angew. Chem. Int. Ed.* **2023**, *62*, e202214510.

[80] M. T. Mihai, B. D. Williams, R. J. Phipps, *J. Am. Chem. Soc.* **2019**, *141*, 15477–15482.

[81] S. Guria, M. M. M. Hassan, J. Ma, S. Dey, Y. Liang, B. Chattopadhyay, *Nat. Comm.* **2023**, *14*, 6906.

[82] J. R. Montero Bastidas, T. J. Oleskey, S. L. Miller, M. R. I. Smith, R. E. Jr. Maleczka, *J. Am. Chem. Soc.* **2019**, *141*, 15483–15487.

[83] S. R. Shin, H. J. Shine, *J. Org. Chem.* **1992**, *57*, 2706–2710.

[84] H. J. Shine, J. J. Silber, *J. Org. Chem.* **1971**, *36*, 2923–2926.

[85] H. J. Shine, J. J. Silber, R. J. Bussey, Tadashi. Okuyama, *J. Org. Chem.* **1972**, *37*, 2691–2697.

[86] K. Kim, H. J. Shine, *J. Org. Chem.* **1974**, *39*, 2537–2539.

[87] H. J. Shine, W. Yueh, *Tetrahedron Lett.* **1992**, *33*, 6583–6586.

[88] F. Juliá, Q. Shao, M. Duan, M. B. Plutschack, F. Berger, J. Mateos, C. Lu, X.-S. Xue, K. N. Houk, T. Ritter, *J. Am. Chem. Soc.* **2021**, *143*, 16041–16054.

[89] S. Ni, J. Yan, S. Tewari, E. J. Reijerse, T. Ritter, J. Cornella, *J. Am. Chem. Soc.* **2023**, *145*, 9988–9993.

[90] R. Sang, S. E. Korkis, W. Su, F. Ye, P. S. Engl, F. Berger, T. Ritter, *Angew. Chem. Int. Ed.* **2019**, *58*, 16161–16166.

[91] F. Ye, F. Berger, H. Jia, J. Ford, A. Wortman, J. Börgel, C. Genicot, T. Ritter, *Angew. Chem. Int. Ed.* **2019**, *58*, 14615–14619.

[92] J. Li, J. Chen, R. Sang, W.-S. Ham, M. B. Plutschack, F. Berger, S. Chabbra, A. Schnegg, C. Genicot, T. Ritter, *Nat. Chem.* **2020**, *12*, 56–62.

[93] P. S. Engl, A. P. Häring, F. Berger, G. Berger, A. Pérez-Bitrián, T. Ritter, *J. Am. Chem. Soc.* **2019**, *141*, 13346–13351.

[94] S. Ni, R. Halder, D. Ahmadli, E. J. Reijerse, J. Cornella, T. Ritter, *Nat Catal* **2024**, *7*, 733–741.

[95] D. Zhao, R. Petzold, J. Yan, D. Muri, T. Ritter, *Nature* **2021**, *600*, 444–449.

[96] S. Nishimura, *Handbook of Heterogeneous Catalytic Hydrogenation for Organic Synthesis*, John Wiley & Sons, Inc., **2001**.

[97] A. Hamad, M. Mrozowicz, Y. Xie, T. Ritter, Synlett 2023, 35, 1028–1032.

[98] L. J. Williams, Y. Bhonoah, L. A. Wilkinson, J. W. Walton, *Chem. Eur. J.* **2021**, *27*, 3650–3660.

[99] E. O. Fischer, W. Hafner, *Zeitschr. Naturforsch.- Sect. B J. Chem. Sci.* **1955**, *10*, 665–668.

[100] E. P. Kündig, *Transition Metal Arene P-Complexes in Organic Synthesis and Catalysis*, Springer Science & Business Media, **2004**.

[101] A. P. Leon, K. Maguire, *Chem. Rev.* **1984**, *84*, 525–543.

[102] F. Rose-Munch, V. Gagliardini, C. Renard, E. Rose, *Coord. Chem. Rev.* **1998**, *178–180*, 249–268.

[103] R. D. Pike, D. A. Sweigart, *Coord. Chem. Rev.* **1999**, *187*, 183–222.

[104] P. M. Maitlis, *Chem. Soc. Rev.* **1981**, *10*, 1–48.

[105] T. Ohta, S. Nakahara, Y. Shigemura, K. Hattori, I. Furukawa, *App. Organomet. Chem.* **2001**, *15*, 699–709.

[106] R. Noyori, S. Hashiguchi, *Acc. Chem. Res.* **1997**, *30*, 97–102.

[107] L. Ackermann, *Acc. Chem. Res.* **2014**, *47*, 281–295.

[108] P. B. Arockiam, C. Bruneau, P. H. Dixneuf, *Chem. Rev.* **2012**, *112*, 5879–5918.

[109] K. S. Singh, *Catalysts* **2019**, *9*, 173.

[110] B. Çetinkaya, S. Demir, I. Özdemir, L. Toupet, D. Sémeril, C. Bruneau, P. H. Dixneuf, *N. J. Chem.* **2001**, *25*, 519–521.

[111] A. Fürstner, M. Liebl, C. W. Lehmann, M. Picquet, R. Kunz, C. Bruneau, D. Touchard, P. H. Dixneuf, *Chem. Eur. J.* **2000**, *6*, 1847–1857.

[112] D. S. Perekalin, A. R. Kudinov, *Coord. Chem. Rev.* **2014**, *276*, 153–173.

[113] M. Oh, J. A. Reingold, G. B. Carpenter, D. A. Sweigart, *Coord. Chem. Rev.* **2004**, *248*, 561–569.

[114] J. F. Hartwig, *Organotransition Metal Chemistry: From Bonding to Catalysis*, University Science Books, Sausalito (Calif.), **2010**.

[115] K. Ziegler, H.-G. Gellert, E. Holzkamp, G. Wilke, E. W. Duck, W.-R. Kroll, *Justus Liebigs Annalen der Chemie* **1960**, *629*, 172–198.

[116] A. R. Pape, K. P. Kaliappan, E. P. Kündig, *Chem. Rev.* **2000**, *100*, 2917–2940.

[117] M. F. Semmelhack, J. L. Garcia, D. Cortes, R. Farina, R. Hong, B. K. Carpenter, *Organometallics* **1983**, *2*, 467–469.

[118] A. J. Pearson, P. Zhang, K. Lee, *J. Org. Chem.* **1996**, *61*, 6581–6586.

[119] C. C. Lee, U. S. Gill, M. Iqbal, C. I. Azogu, R. G. Sutherland, *J. Organomet. Chem.* **1982**, *231*, 151–159.

[120] A. J. Pearson, G. Bignan, *Tetrahedron Lett.* **1996**, *37*, 735–738.

[121] A. J. Pearson, J. G. Park, *J. Org. Chem.* **1992**, *57*, 1744–1752.

[122] M. F. Semmelhack, A. Chlenov, in *Transition Metal Arene π-Complexes in Organic Synthesis and Catalysis* (Ed.: E.P. Kündig), Springer, Berlin, Heidelberg, **2004**, pp. 43–69.

[123] E. M. D'Amato, C. N. Neumann, T. Ritter, *Organometallics* **2015**, *34*, 4626–4631.

[124] E. P. Kündig, R. Cannas, M. Laxmisha, L. Ronggang, S. Tchertchian, *J. Am. Chem. Soc.* **2003**, *125*, 5642–5643.

[125] E. P. Kündig, A. Quattropani, *Tetrahedron Lett.* **1994**, *35*, 3497–3500.

[126] A. Fretzen, A. Ripa, R. Liu, G. Bernardinelli, E. P. Kündig, *Chem. Eur. J.* **1998**, *4*, 251–259.

[127] D. A. Price, N. S. Simpkins, A. M. MacLeod, A. P. Watt, *Tetrahedron Lett.* **1994**, *35*, 6159–6162.

[128] A. R. Pape, K. P. Kaliappan, E. P. Kündig, *Chem. Rev.* **2000**, *100*, 2917–2940.

[129] D. A. Price, N. S. Simpkins, *J. Org. Chem.* **1994**, *55*, 1961–1962.

[130] N. V. Shvydkiy, D. S. Perekalin, *Coord. Chem. Rev.* **2020**, *411*, 213238.

[131] R. P. Houghton, M. Voyle, R. Price, *J. Chem. Soc., Perkin Transactions 1* **1984**, *0*, 925–931.

[132] J. W. Walton, J. M. J. Williams, *Chem. Comm.* **2015**, *51*, 2786–2789.

[133] Q.-K. Kang, Y. Lin, Y. Li, H. Shi, *J. Am. Chem. Soc.* **2020**, *142*, 3706–3711.

[134] Q.-K. Kang, Y. Lin, Y. Li, L. Xu, K. Li, H. Shi, *Angew. Chem. Int. Ed.* **2021**, *133*, 20554–20562.

[135] J. Su, K. Chen, Q.-K. Kang, H. Shi, *Angew. Chem. Int. Ed.* **2023**, *135*, e202302908.

[136] K. Chen, Q.-K. Kang, Y. Li, W.-Q. Wu, H. Zhu, H. Shi, *J. Am. Chem. Soc.* **2022**, *144*, 1144–1151.

[137] Q.-K. Kang, Y. Li, K. Chen, H. Zhu, W.-Q. Wu, Y. Lin, H. Shi, *Angew. Chem. Int. Ed.* **2022**, *61*, e202117381.

[138] W.-Q. Wu, Y. Lin, Y. Li, H. Shi, *J. Am. Chem. Soc.* **2023**, *145*, 9464–9470.

[139] Y. Li, W.-Q. Wu, H. Zhu, Q.-K. Kang, L. Xu, H. Shi, *Angew. Chem. Int. Ed.* **2022**, *61*, e202207917.

[140] H. Tobita, K. Hasegawa, J. J. Gabrillo Minglana, L.-S. Luh, M. Okazaki, H. Ogino, *Organometallics* **1999**, *18*, 2058–2060.

[141] A. G. Sergeev, J. F. Hartwig, *Science* **2011**, *332*, 439–443.

[142] N. I. Saper, J. F. Hartwig, *J. Am. Chem. Soc.* **2017**, *139*, 17667–17676.

[143] F. Zhu, Z.-X. Wang, *Adv. Syn. Cat.* **2013**, *355*, 3694–3702.

[144] I. Ojima, *Fluorine in Medicinal Chemistry and Chemical Biology*, John Wiley & Sons, **2009**.

[145] K. Müller, C. Faeh, F. Diederich, *Science* **2007**, *317*, 1881–1886.

[146] K. L. Kirk, *Org. Process Res. Dev.* **2008**, *12*, 305–321.

[147] P. W. Miller, N. J. Long, R. Vilar, A. D. Gee, *Angew. Chem. Int. Ed.* **2008**, *47*, 8998–9033.

[148] L. Trump, A. Lemos, B. Lallemand, P. Pasau, J. Mercier, C. Lemaire, A. Luxen, C. Genicot, *Angew. Chem. Int. Ed.* **2019**, *58*, 13149–13154.

[149] W. Chen, Z. Huang, N. E. S. Tay, B. Giglio, M. Wang, H. Wang, Z. Wu, D. A. Nicewicz, Z. Li, *Science* **2019**, *364*, 1170–1174.

[150] S. Preshlock, M. Tredwell, V. Gouverneur, *Chem. Rev.* **2016**, *116*, 719–766.

[151] S. Preshlock, M. Tredwell, V. Gouverneur, *Chem. Rev.* **2016**, *116*, 719–766.

[152] G. J. Kelloff, J. M. Hoffman, B. Johnson, H. I. Scher, B. A. Siegel, E. Y. Cheng, B. D. Cheson, J. O'Shaughnessy, K. Z. Guyton, D. A. Mankoff, L. Shankar, S. M. Larson, C. C. Sigman, R. L. Schilsky, D. C. Sullivan, *Clin. Cancer Res.* **2005**, *11*, 2785–2808.

[153] H. H. Coenen, P. H. Elsinga, R. Iwata, M. R. Kilbourn, M. R. A. Pillai, M. G. R. Rajan, H. N. Wagner, J. J. Zaknun, *Nuc Med Biol* **2010**, *37*, 727–740.

[154] A. Postigo, *Late-Stage Fluorination of Bioactive Molecules and Biologically-Relevant Substrates*, **2019**.

[155] P. Tang, T. Furuya, T. Ritter, *J. Am. Chem. Soc.* **2010**, *132*, 12150–12154.

[156] J. Baudoux, D. Cahard, in *Organic Reactions* (Ed.: John Wiley & Sons, Inc.), John Wiley & Sons, Inc., Hoboken, NJ, USA, **2008**, pp. 1–326.

[157] T. Furuya, C. A. Kuttruff, T. Ritter, *Curr. Opin. Drug Discov. Dev.* **2008**, *11*, 803–819.

[158] T. Furuya, A. E. Strom, T. Ritter, *J. Am. Chem. Soc.* **2009**, *131*, 1662–1663.

[159] C. N. Neumann, J. M. Hooker, T. Ritter, *Nature* **2016**, *534*, 369–373.

[160] E. E. Kwan, Y. Zeng, H. A. Besser, E. N. Jacobsen, *Nat. Chem.* **2018**, *10*, 917–923.

[161] C. N. Neumann, T. Ritter, *Acc. Chem. Res.* **2017**, *50*, 2822–2833.

[162] H. Beyzavi, D. Mandal, M. G. Strebl, C. N. Neumann, E. M. D'Amato, J. Chen, J. M. Hooker, T. Ritter, *ACS Cent. Sci.* **2017**, *3*, 944–948.

[163] J. Rickmeier, T. Ritter, *Angew.Chem. Int. Ed.* **2018**, *57*, 14207–14211.

[164] R. Halder, G. Ma, J. Rickmeier, J. W. McDaniel, R. Petzold, C. N. Neumann, J. M. Murphy, T. Ritter, *Nat. Protoc.* **2023**, *18*, 3614–3651.

[165] D. Morvan, T. B. Rauchfuss, S. R. Wilson, *Organometallics* **2009**, *28*, 3161–3166.

[166] B. T. Loughrey, M. L. Williams, P. G. Parsons, P. C. Healy, *J. Organomet. Chem.* **2016**, *819*, 1–10.

[167] Y. Wei, P. Hu, M. Zhang, W. Su, *Chem. Rev.* **2017**, *117*, 8864–8907.

[168] M. R. F. Ashworth, R. P. Daffern, D. L. Hammick, *J. Chem. Soc.* **1939**, 809–812.

[169] P. Dyson, D. L. Hammick, *J. Chem. Soc.* **1937**, 1724–1725.

[170] E. V. Brown, M. B. Shambhu, *J. Org. Chem.* **1971**, *36*, 2002–2004.

[171] O. Hollóczki, L. Nyulászi, *J. Org. Chem.* **2008**, *73*, 4794–4799.

[172] D. Lavorato, J. K. Terlouw, T. K. Dargel, W. Koch, G. A. McGibbon, H. Schwarz, *J. Am. Chem. Soc.* **1996**, *118*, 11898–11904.

[173] N. H. Cantwell, E. V. Brown, *J. Am. Chem. Soc.* **1953**, *75*, 1489–1490.

[174] Z. Chen, B. Wang, J. Zhang, W. Yu, Z. Liu, Y. Zhang, *Org. Chem. Front.* **2015**, *2*, 1107–1295.

[175] K. M. Engle, T.-S. Mei, M. Wasa, J.-Q. Yu, *Acc. Chem. Res.* **2012**, *45*, 788–802.

[176] J. Das, D. K. Mal, S. Maji, D. Maiti, *ACS Catal.* **2021**, *11*, 4205–4229.

[177] S. Kopf, F. Bourriquen, W. Li, H. Neumann, K. Junge, M. Beller, *Chem. Rev.* **2022**, *122*, 6634–6718.

[178] N. Li, Y. Li, X. Wu, C. Zhu, J. Xie, *Chem. Soc. Rev.* **2022**, *51*, 6291–6306.

[179] G. Prakash, N. Paul, G. A. Oliver, D. B. Werz, D. Maiti, *Chem. Soc. Rev.* **2022**, *51*, 3123–3163.

[180] J. M. Anderson, J. K. Kochi, *J. Org. Chem.* **1970**, *35*, 986–989.

[181] J. M. Anderson, J. K. Kochi, *J. Am. Chem. Soc.* **1970**, *92*, 1651–1659.

[182] S. Seo, J. B. Taylor, M. F. Greaney, *Chem. Comm.* **2012**, *48*, 8270–8272.

[183] L. Xue, W. Su, Z. Lin, *Dalton Trans.* **2011**, *40*, 11926–11936.

[184] L. J. Gooßen, W. R. Thiel, N. Rodríguez, C. Linder, B. Melzer, *Adv. Syn. Cat.* **2007**, *349*, 2241–2246.

[185] M. Rudzki, A. Alcalde-Aragonés, W. I. Dzik, N. Rodríguez, L. J. Gooßen, *Synthesis* **2011**, *44*, 184–193.

[186] Y. Zou, Q. Huang, T. Huang, Q. Ni, E. Zhang, T. Xu, M. Yuan, J. Li, *Org. Biomol. Chem.* **2013**, *11*, 6967–6974.

[187] L. J. Gooßen, N. Rodríguez, C. Linder, P. P. Lange, A. Fromm, *ChemCatChem* **2010**, *2*, 430–442.

[188] L. Xue, W. Su, Z. Lin, *Dalton Trans.* **2010**, *39*, 9815–9822.

[189] J. Cornella, M. Rosillo-Lopez, I. Larrosa, *Adv. Syn. Cat.* **2011**, *353*, 1359–1366.

[190] S. Dupuy, S. P. Nolan, *Chem. Eur. J.* **2013**, *19*, 14034–14038.

[191] S. Dupuy, L. E. Crawford, M. Bühl, S. P. Nolan, *Chem. Eur. J.* **2015**, *21*, 3399–3408.

[192] S. Kubosaki, H. Takeuchi, Y. Iwata, Y. Tanaka, K. Osaka, M. Yamawaki, T. Morita, Y. Yoshimi, *J. Org. Chem.* **2020**, *85*, 5362–5369.

[193] L. Candish, M. Freitag, T. Gensch, F. Glorius, *Chem. Sci.* **2017**, *8*, 3618–3622.

[194] P. Xu, P. López-Rojas, T. Ritter, *J. Am. Chem. Soc.* **2021**, *143*, 5349–5354.

[195] D. H. R. Barton, D. Bridon, I. Fernandaz-Picot, S. Z. Zard, *Tetrahedron* **1987**, *43*, 2733–2740.

[196] D. H. R. Barton, D. Crich, W. B. Motherwell, *Tetrahedron* **1985**, *41*, 3901–3924.

[197] E. J. Ko, G. P. Savage, C. M. Williams, J. Tsanaktsidis, *Org. Lett.* **2011**, *13*, 1944–1947.

[198] T. Qin, L. R. Malins, J. T. Edwards, R. R. Merchant, A. J. E. Novak, J. Z. Zhong, R. B. Mills, M. Yan, C. Yuan, M. D. Eastgate, P. S. Baran, *Angew. Chem. Int. Ed.* **2017**, *56*, 260–265.

[199] T. Itou, Y. Yoshimi, T. Morita, Y. Tokunaga, M. Hatanaka, *Tetrahedron* **2009**, *65*, 263–269.

[200] X. Chen, X. Luo, X. Peng, J. Guo, J. Zai, P. Wang, *Chem. Eur. J.* **2020**, *26*, 3226–3230.

[201] C. Zheng, G.-Z. Wang, R. Shang, *Adv. Syn. Cat.* **2019**, *361*, 4500–4505.

[202] N. Li, Y. Ning, X. Wu, J. Xie, W. Li, C. Zhu, *Chem. Sci.* **2021**, *12*, 5505–5510.

[203] T. Patra, S. Mukherjee, J. Ma, F. Strieth-Kalthoff, F. Glorius, *Angew.Chem. Int. Ed.* **2019**, *131*, 10624–10630.

[204] Z. Li, K.-F. Wang, X. Zhao, H. Ti, X.-G. Liu, H. Wang, *Nat. Commun.* **2020**, *11*, 5036.

[205] J.-M. M. Grandjean, D. A. Nicewicz, *Angew.Chem. Int. Ed.* **2013**, *52*, 3967–3971.

[206] C. Cassani, G. Bergonzini, C.-J. Wallentin, *Org. Lett.* **2014**, *16*, 4228–4231.

[207] J. D. Griffin, M. A. Zeller, D. A. Nicewicz, *J. Am. Chem. Soc.* **2015**, *137*, 11340–11348.

[208] W. Chen, H. Wang, N. E. S. Tay, V. A. Pistritto, K.-P. Li, T. Zhang, Z. Wu, D. A. Nicewicz, Z. Li, *Nat. Chem.* **2022**, *14*, 216–223.

[209] D. S. Hamilton, D. A. Nicewicz, *J. Am. Chem. Soc.* **2012**, *134*, 18577–18580.

[210] Y.-C. Lu, J. G. West, *Angew.Chem. Int. Ed.* **2023**, *62*, e202213055.

[211] G. R. Fulmer, A. J. M. Miller, N. H. Sherden, H. E. Gottlieb, A. Nudelman, B. M. Stoltz, J. E. Bercaw, K. I. Goldberg, *Organometallics* **2010**, *29*, 2176–2179.

[212] K. D. Ashtekar, M. Vetticatt, R. Yousefi, J. E. Jackson, B. Borhan, *J. Am. Chem. Soc.* **2016**, *138*, 8114–8119.

[213] I. Paterson, O. Delgado, G. J. Florence, I. Lyothier, M. O'Brien, J. P. Scott, N. Sereinig, *J. Org. Chem.* **2005**, *70*, 150–160.

[214] T. Schulte, Z. Wang, C.-C. Li, A. Hamad, F. Waldbach, J. Pampel, R. Petzold, M. Leutzsch, F. Bahns, T. Ritter, *J. Am. Chem. Soc.* **2024**, *146*, 15825–15832.

[215] P. Tang, W. Wang, T. Ritter, *J. Am. Chem. Soc.* **2011**, *133*, 11482–11484.

6. Appendix

Declaration of Authorship

I, Aboubakr Hamad,declare that this thesis and the work presented herein are my own and has been generated by me as the result of my own original research.

Hiermit erkläre ich an Eides statt/ I do solemnly swear that:

1. This work was done wholly or mainly while in candidature for the doctoral degree program at this faculty and university;
2. Where any part of this thesis has previously been submitted for a degree or any other qualification at this university or any other institution, this has been clearly stated;
3. Where I have consulted the published work of others or myself, this is always clearly attributed;
4. Where I have quoted from the work of others or myself, the source is always given. This thesis is entirely my own work, with the exception of such quotations;
5. I have acknowledged all major sources of assistance;
6. Where the thesis is based on work done by myself jointly with others, I have made clear exactly what was done by others and what I have contributed myself;
7. Parts of this work have been published before as: see NOTE, p. XII.

Mülheim an der Ruhr,

_____

(Aboubakr Hamad)

7. List Of Publication:

- Ruthenium Phenoxo Complexes: An Isolable Ligand to Cp with Improved Properties.
  J. Am. Chem. Soc. **2024**, 146, 15825−15832. DOI: org/10.1021/jacs.4c02088.

- Regioselective Double C–H Functionalization of Arenes via Aryl Thianthrenium Salt Analogues.
  Synlett **2023**, 35, 1028–1032. DOI: 10.1055/s-0043-1763625.

- Site-Selective Late-Stage Aromatic [18 F] Fluorination via Aryl Sulfonium Salt.
  Angew. Chem. Int. Ed. **2020**, 132, 1972–1976. DOI: 10.1002/anie.201912567.